THE EFFECTS OF MITRAL ANNULAR DYNAMICS, AND THE LACERATION OF THE ANTERIOR LEAFLET WITH TRANSCATHETER MITRAL VALVE REPLACEMENTS

A Dissertation
Presented to
The Academic Faculty

by

Thomas Floyd Easley

In Partial Fulfillment
of the Requirements for the Degree
Doctor of Philosophy in
Bioengineering

Georgia Institute of Technology
August 2019

THE EFFECTS OF MITRAL ANNULAR DYNAMICS, AND THE LACERATION OF THE ANTERIOR LEAFLET WITH TRANSCATHETER MITRAL VALVE REPLACEMENTS

Approved by:

Dr. Ajit P. Yoganathan, Advisor
School of Biomedical Engineering
Georgia Institute of Technology and Emory University

Dr. Vinod H. Thourani
School of Medicine
Georgetown University

Dr. Cyrus K. Aidun
School of Mechanical Engineering
Georgia Institute of Technology

Dr. Joseph H. Gorman
School of Medicine
University of Pennsylvania

Dr. Wei Sun
School of Biomedical Engineering
Georgia Institute of Technology and Emory University

Dr. Vasilis Babaliaros
School of Medicine
Emory University

Date Approved: June 24, 2019

Dedicated to my parents, Mark and Lisa Easley

ACKNOWLEDGEMENTS

To my friends and colleagues near and far: This thesis and my time at Georgia Tech would not have been as successful without you. You kept me sane and continued to show me there was light at the end of the tunnel. I am grateful for the MV group, both past and present for their partnerships and friendships. I would like to specifically thank Vrishank for his guidance, Milan for his ear, and Vahid for his time and effort.

To my undergraduate advisor, Dr. Scott Banks: I have you to thank for helping me get on this combined path of medicine and engineering. You shepherded me into different experiences when I showed desire, taught me to “enjoy” the learning from mistakes, and encouraged me to take the harder road with the higher reward.

To my committee, Drs. Cyrus Aidun, Vasilis Babaliaros, Joe Gorman, Wei Sun, and Vinod Thourani: You each helped shape my thesis work, providing me with clinical and engineering guidance and experience. For that I am extremely grateful and this work’s impact it better for it.

To my advisor, Dr. Ajit Yoganathan: To say that our time together has been eventful would be an understatement. I have learned a lot from our tenure together, and I will carry that knowledge into my career and teachings.

TABLE OF CONTENTS

LIST OF TABLES

LIST OF FIGURES

LIST OF SYMBOLS AND ABBREVIATIONS

AML	Anterior Mitral Leaflet
AS	Aortic Stenosis
AV	Aortic Valve
BHV	Bioprosthetic Heart Valve
HSPIV	High-Speed Particle Image Velocimetry
IMR	Ischemic Mitral Regurgitation
LA	Left Atrium
LV	Left Ventricle
LVOT	Left Ventricular Outflow Tract
LVOTO	Left Ventricular Outflow Tract Obstruction
MA	Mitral Annuloplasty
MR	Mitral Regurgitation
MS	Mitral Stenosis
MV	Mitral Valve
PM	Papillary Muscle
TAV	Transcatheter Aortic Valve
TAVR	Transcatheter Aortic Valve Replacement
TMV	Transcatheter Mitral Valve
TMVR	Transcatheter Mitral Valve Replacement
μCT	Micro-Computed Tomography
VIM	Valve-in-MAC
VIR	Valve-in-Ring

VIV	Valve-in-Valve

SUMMARY

Restrictive annuloplasty rings are a standard mitral valve repair procedure for ischemic mitral regurgitation (MR), however there is a high incidence of recurrent MR. With this recurrent MR, there is a need to understand the restrictive effects from an annuloplasty on the MV leaflets. The first goal of this dissertation is to study the effects of annular dynamics on the mitral leaflets and its restriction. To accomplish this, an MV *in vitro* model with a dynamically contracting annulus will be designed and used to compare leaflet strain between varying contractile states. These, now, high-risk patients with failed MV repairs and replacements created a demand for percutaneous MV interventions. With no dedicated devices currently on the market, clinicians have resorted to placing transcatheter aortic valves (TAV) into mitral annular calcification (valve-in-MAC), failing mitral bioprosthetic valves (valve-in-valve), and failing mitral annuloplasty rings (valve-in-ring). Currently, there are no official clinical guidelines, and no quantitative engineering studies have been conducted to better understand performance and risks. Percutaneous laceration of the anterior mitral leaflet (LAMPOON) is a proposed proactive solution to the risk of left ventricular outflow tract (LVOT) obstruction. The second goal of this dissertation includes designing and performing *in vitro* experiments to evaluate and quantify benefits of LAMPOON on LVOT obstruction and thrombosis. These goals will provide insight into potential causes of recurrent MR with annuloplasty rings, and an in-depth quantitative assessment of the benefits of LAMPOON with transcatheter mitral valve replacements. These will better inform procedural guidelines and medical device design, as well as provide further insight into MV biomechanics and advanced platforms for future

MV *in vitro* studies. In Specific Aim 1, a novel dynamically contracting annulus was developed for *in vitro* studies. It was subsequently found that healthy contraction provided lower strains on the anterior mitral leaflet (AML) than diseased contraction and static conditions. The findings suggested that maintaining annular dynamics during MV repair procedures could improve loading on the AML. In Specific Aim 2, a novel LAMPOON model was incorporated into a modified LV phantom for *in vitro* studies. Results found that LAMPOON can lower velocities in the LVOT, lower maximum VSS in the LV, and increase flow into the anterior neo-sinus during diastole. Combined, the findings suggested that LAMPOON could aid in preventing LVOT obstruction and reduce the risk of thrombosis in the anterior neo-sinus.

CHAPTER 1. INTRODUCTION

The heart is the central part of the cardiovascular system, consisting of a left and right side acting as two pumps in series. Each side has two chambers (atrium and ventricle) and two valves. The smaller right side of the heart receives blood from the body into the right atrium with the right ventricle pumping it to the lungs for reoxygenation. The larger left side receives blood from the lungs into the left atrium and pumps to the body via the left ventricle. Between the left atrium and left ventricle there is a bi-leaflet valve known as the mitral valve. The mitral valve's purpose is to maintain unidirectional flow between the left atrium and ventricle and consists of four major components: annulus, leaflets, chordae tendineae, and papillary muscles. The mitral valve's complex structure allows it to operate under the highest loading in the heart, with any changes in its four major components leading to failure.

Two major endpoints of failure are mitral stenosis (MS) and regurgitation (MR). Stenosis is when the valve cannot completely open during filling (diastole), while regurgitation is when the valve cannot completely close during ejection (systole). Stenosis and regurgitation can be induced through primary/tissue and secondary/structural diseases. Stenosis is usually caused through valvular calcification, but the more prevalent regurgitation is caused by a host of primary and secondary diseases. Primary MR stems from tissue related conditions such as congenital, degenerative, or bacterial diseases creating suboptimal coaptation from changes in the valve itself. Secondary MR is created when the surrounding structures of the otherwise healthy valve are altered creating improper coaptation, e.g. ischemia or a myocardial infarction thinning the left ventricular wall causing the papillary muscles and the annulus to dilate resulting in ischemic mitral regurgitation (IMR).

In order to correct these pathophysiologic conditions, clinicians have developed surgical and interventional, repair and replacement procedures. One surgical repair commonly done to correct mitral regurgitation is the insertion of a mitral annuloplasty ring. The annuloplasty ring attempts to addresses the issue of improper leaflet closure (coaptation) by restructuring the mitral annulus into a shape that would induce better coaptation. For IMR, this is typically done by downsizing the annulus into a smaller orifice using a rigid annuloplasty ring, thus bringing the leaflets closure together and keeping the annulus that new size and shape. Implantation of an annuloplasty ring restricts the motion of the mitral valve throughout the cardiac cycle, with stiffer rings imparting more severe restriction. Although this surgical repair is an effective treatment, studies have shown MR recurrence as high as 30% in patients with IMR within the first 6 months after operation.[1, 2] Assessment of annular dynamics and its effect on the MV leaflets could help in further understanding the incidence of recurrent MR and long-term MV repair outcomes of the annuloplasty procedure.

A surgeon may also opt to replace the mitral valve with a bioprosthetic or mechanical valve. These replacement mitral valves are sutured into the annulus to take over the function of the diseased valve. These surgical repairs and replacements are initially done on low-risk patients,[3] however, these procedures can result in recurrent MR or MS that need further treatment with patients that are likely now at high-risk for surgery. These patient groups created a pertinent demand for percutaneous MV interventions. With no dedicated devices currently on the market for transcatheter mitral valves, clinicians have resorted to placing transcatheter aortic valves (TAV) into mitral annular calcification (valve-in-MAC),[4-7] mitral bioprosthetic valves (valve-in-valve),[7-9] and mitral annuloplasty rings (valve-in-ring).[10-12]

Left ventricular outflow tract (LVOT) obstruction and leaflet thrombosis are potential risks from transcatheter valve replacement in the MV.[13-17]_ENREF_12 This is due to the anterior mitral leaflet (AML) being permanently displaced into the LVOT by the stent of the transcatheter valve. Additionally, the AML also covers the stent frame creating a neo-sinus between the AML and TAV leaflets in danger of flow stasis. One way to proactively relieve these risks is through prior surgical resection of the A2 scallop during placement of a surgical prosthetic MV.[18] Another is through a new percutaneous laceration of the A2 scallop known as LAMPOON.[19] Both the use of transcatheter prosthetic valves in the mitral position and the idea to relieve LVOT obstruction to at risk patients are developing areas. Assessment of how laceration of the AML affects the flow in the LV, LVOT, and neo-sinus with a transcatheter mitral valve could help in further understanding their effects and long-term outcomes.

The overall objectives of the present research were to develop new *in vitro* simulators to better understand the effects of annular dynamics on the AML as well as laceration of the AML with a transcatheter valve replacement on LV flow. Once developed, experiments were conducted to measure how annular contraction plays a role in AML strain and how AML laceration can affect the flow in the LV, LVOT, and neo-sinus with the transcatheter valve. The results from these experiments may help guide annuloplasty ring design and clinical procedure standards, as well as provide a better physiologic understanding of the mitral valve.

CHAPTER 2. BACKGROUND

2.1 The Cardiovascular System and the Heart

2.1.1 The Cardiovascular System

The cardiovascular system is an organ system of the human body. It is designed to circulate blood throughout the body permitting transport of oxygen, hormones, blood cells, and nutrients. This helps maintain the body's homeostasis by providing nourishment, stabilizing temperature and pH, and fighting diseases. The cardiovascular system consists of the heart, blood vessels (arteries, capillaries, and veins), and blood. The heart pumps blood away from it through arteries which exchanges nutrients at capillaries and returns to the heart via veins (Figure 2-1). The blood is reoxygenated by the lungs (pulmonary loop) and sent to the rest of the body (systemic loop).

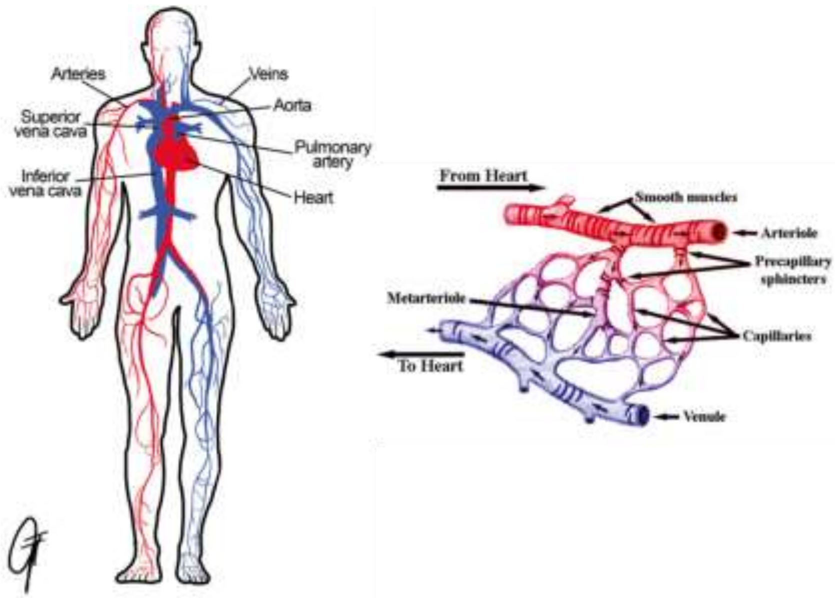

Figure 2-1. Diagram of the circulatory system highlighting the systemic loop and capillary exchange between arteries and veins (modified from Iaizzo et al.[20]).

2.1.2 The Heart

The heart is comprised of four chambers: the right atrium, right ventricle, left atrium, and left ventricle. The chambers are each separated by a valve: tricuspid valve (right atrium/ventricle), pulmonary valve (right ventricle/pulmonary artery), mitral valve (left atrium/ventricle), and aortic valve (left ventricle/aorta). The right and left side of the heart act as two pumps in series. The right side pumps to the lungs (pulmonary loop), returning to the left side, while the left side pumps to the body (systemic loop), returning to the right side (Figure 2-2).

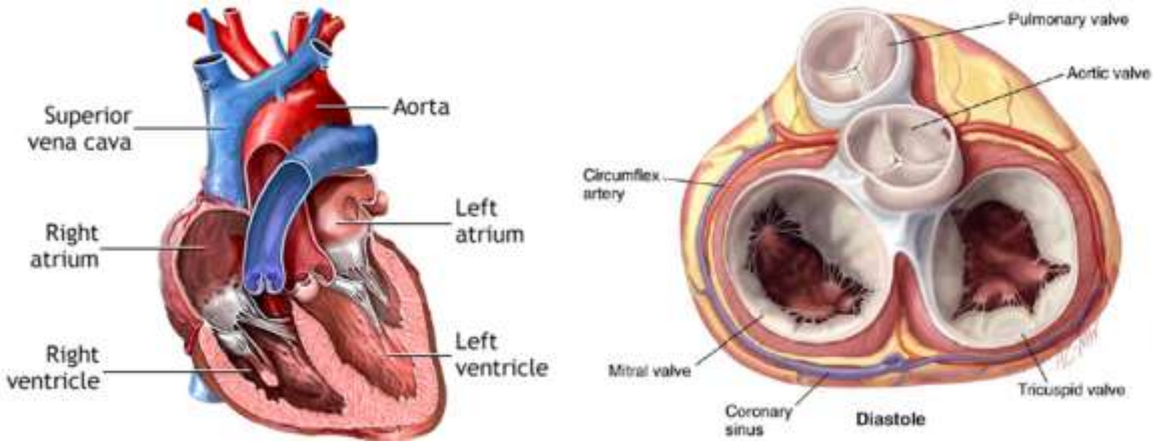

Figure 2-2. Four chamber and four valve anatomical view of the heart (modified from medlineplus.com and Carpentier et al.[21]).

Each valve helps maintain unidirectional flow. The mitral valve opens during diastole to allow the left ventricle to fill with reoxygenated blood and closes during systole as the left ventricle ejects the blood to the body (Figure 2-3).

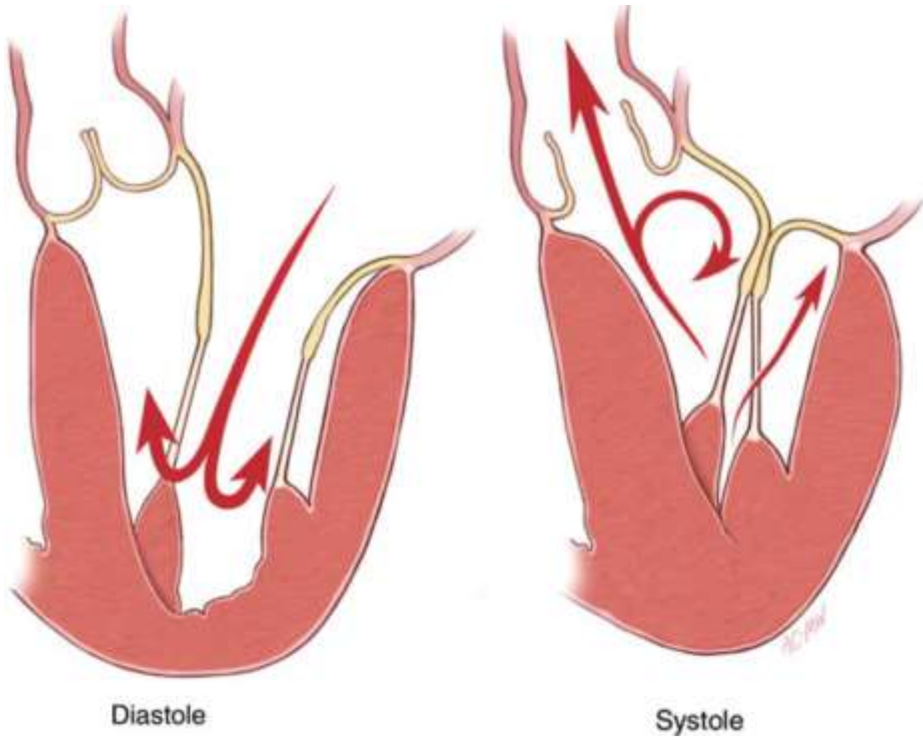

Figure 2-3. Mitral valve open during diastolic filling and closed during systolic ejection of the left ventricle (modified from Carpentier et al.[21]).

In order to pump blood to the whole body, the left ventricle is the largest chamber of the heart with the thickest muscular wall. This creates a powerful contraction resulting in the highest pressures in the heart. Thus, the mitral valve experiences the highest forces and is prone to the highest incidence of disease of any heart valve.[20, 22]

2.2 The Mitral Valve

In order to experience the high systole pressure and open seamlessly during diastole, the mitral valve is comprised of a complex structure of annulus, leaflets, and subvalvular apparatus (chordae tendineae and papillary muscles)(Figure 2-4).

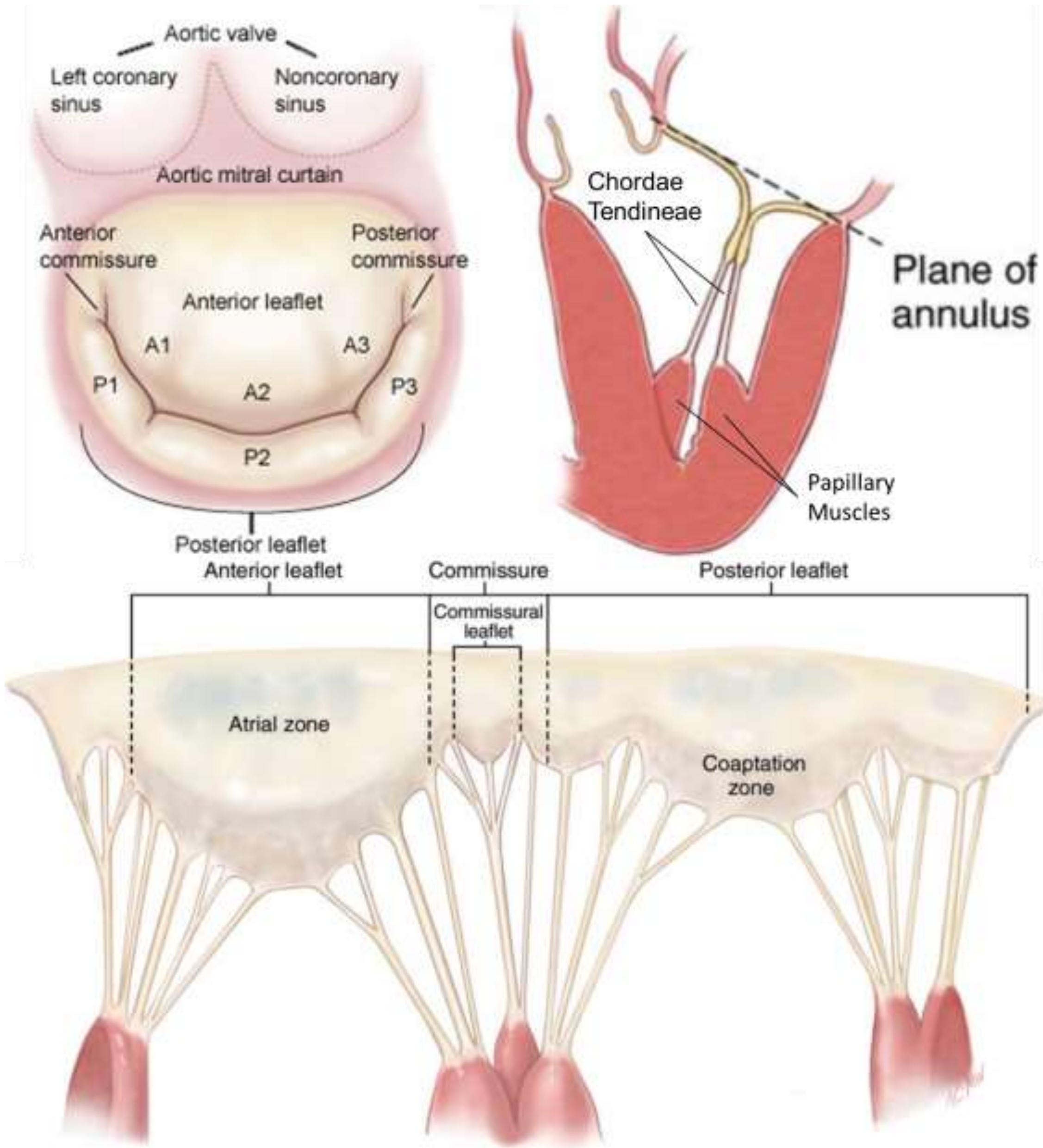

Figure 2-4. Detailed diagram of mitral valve leaflet, annular plane, and subvalvular apparatus (chordae tendineae and papillary muscles) (modified from Carpentier et al.[21]).

2.2.1 The Mitral Leaflets

The MV leaflets are the functioning valve mechanism that opens and closes to provide unidirectional flow between the left atrium and ventricle. The MV is a bicuspid valve consisting of two major leaflets: anterior and posterior (Figure 2-4). The anterior leaflet and posterior leaflet are similar in surface area, but different in size and shape. The surface area of the leaflets is roughly twice that of the orifice area providing redundancy for coaptation during closure.[23] In a healthy valve, it is this coaptation that provides the seal between leaflets and prevents retrograde flow into the left atrium during systole (Mitral Valve Regurgitation).

The MV leaflets share the same free-edge and meet at two points known as commissures. They are attached at the base to the MV annulus (2.2.2) and supported by the subvalvular apparatus along the leaflet surface and edge (2.2.3). The leaflets themselves are made of four layers: atrialis, spongiosa, fibrosa, and ventricularis (in order from atrium to ventricle) (Figure 2-5). The atrialis and ventricularis encompass the leaflet with endothelial cells with the addition of collagen and elastin fibers for structure and elasticity. The fibrosa is the thickest layer of the leaflets and is comprised of densely organized collagen fibers (type I, II, and IV). With most of the collagen content in the leaflet, the fibrosa provides the majority of load-bearing support. The spongiosa is made up of elastin, glycosaminoglycans (GAGs), and proteoglycans and acts as a support layer that helps lubricate and distributes loading.[23]

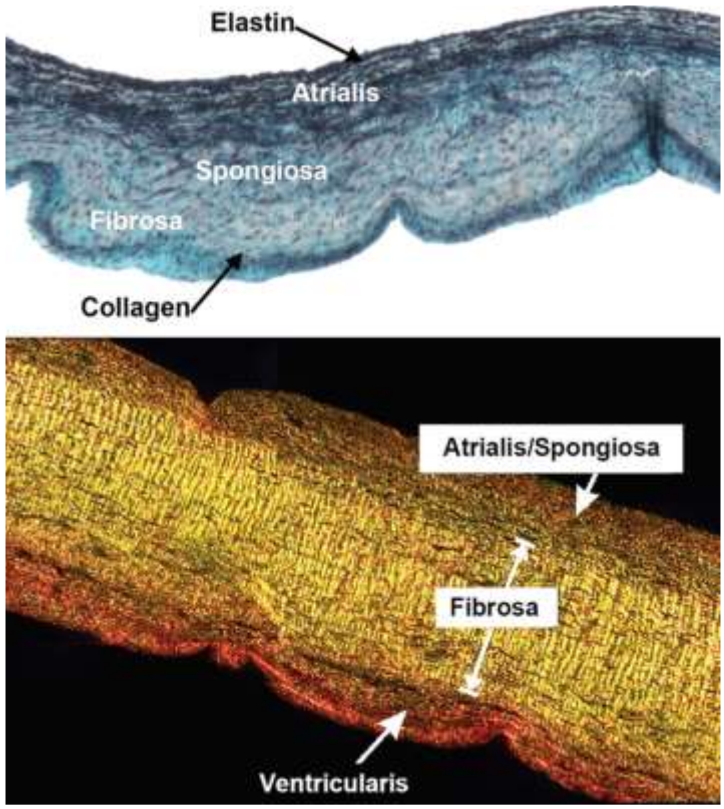

Figure 2-5. Histological cross-section of mitral leaflet.[23]

These combinations of materials give the MV leaflets nonlinear, viscoelastic, anisotropic material properties. The major axis of alignment of leaflet collagen fibers are in the circumferential direction with cross-fiber directionality and heterogeneity changing as you move from the annulus and belly of the leaflet to the commissure and free edge (Figure 2-6).

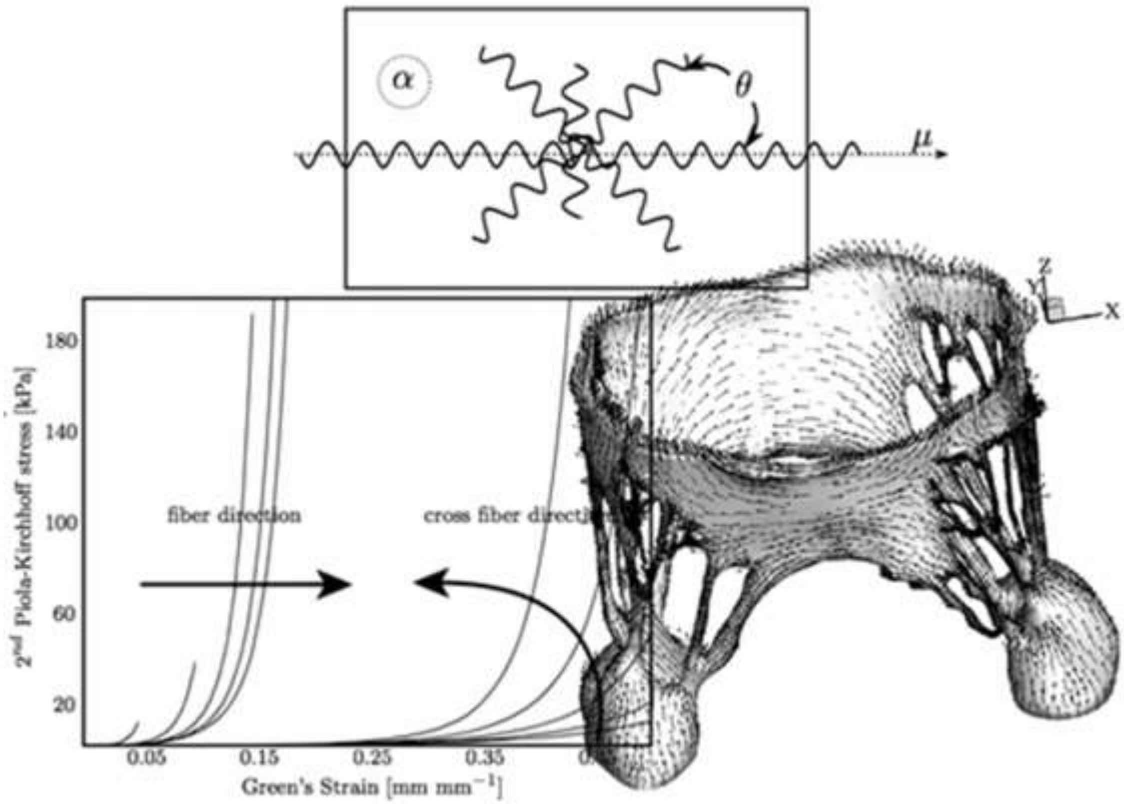

Figure 2-6. Diagram illustrating the stress-strain relationship and fiber orientation of the mitral valve leaflets (modified from Toma et al.[24]).

2.2.2 The Mitral Annulus

The mitral annulus is a region of myocardium between the left atrium and ventricle from which the MV leaflets hinge. The annulus is generally described as having a saddle and D-shape (Figure 2-7) and changes size and shape throughout the cardiac cycle (Figure 2-8).[25-27]

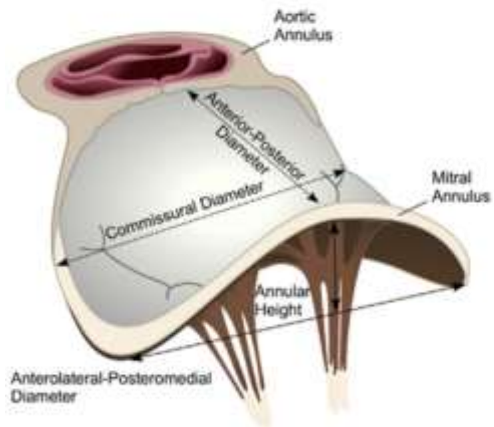

Figure 2-7. Three dimensional representation of the mitral valve annulus (modified from Jolley et al.[27]).

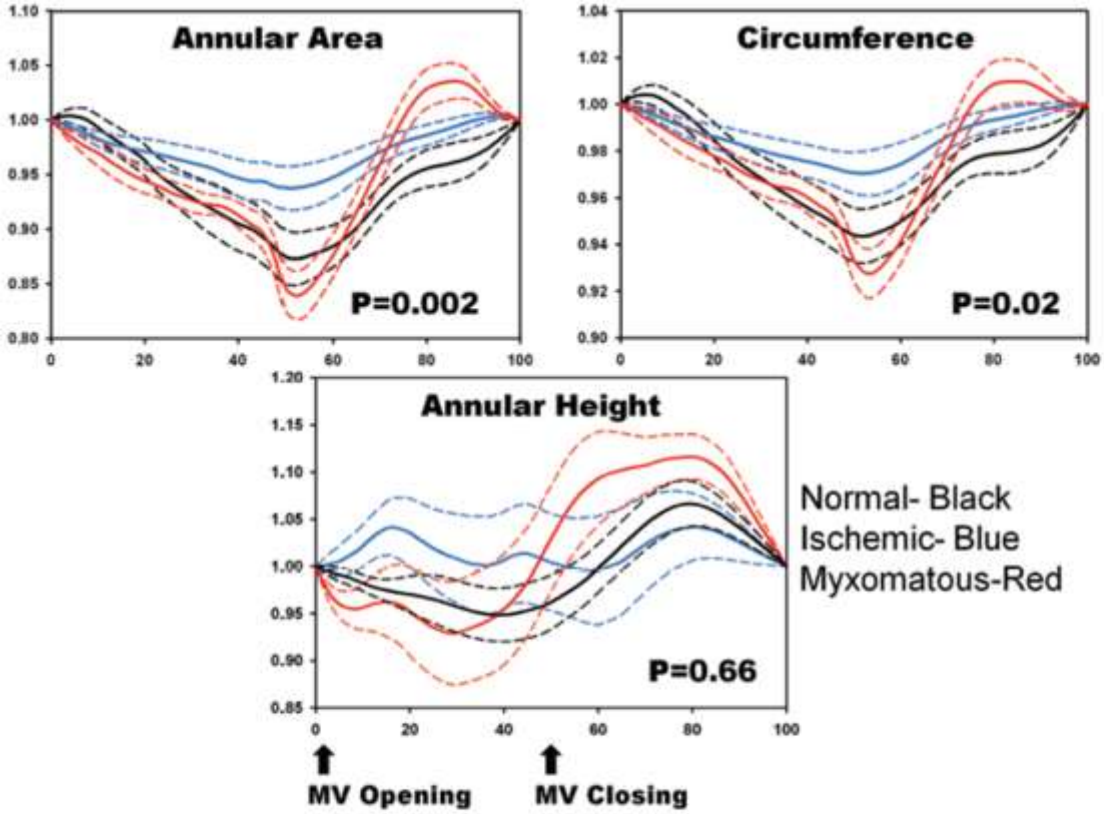

Figure 2-8. Normalized *in vivo* human measurements of annular motion throughout the cardiac cycle (modified from Levack et al.[25]).

The annulus is not well defined and is simply viewed as the ring of tissue that the base of the leaflets attaches to.[28] The material properties of the annulus vary greatly around the perimeter of the annulus and between hearts with different densities of collagen and elastin (Figure 2-9).[29]

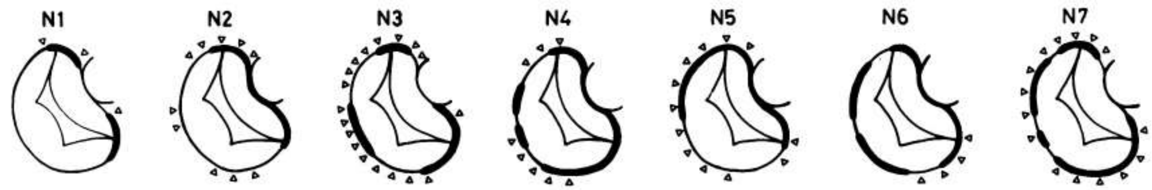

Figure 2-9. Diagram showing variety of annular structure between patients (modified from Angelini et al. [28]).

2.2.3 The Mitral Subvalvular Apparatus

The mitral subvalvular apparatus consists of the chordae tendineae and the papillary muscles (PMs) (Figure 2-4). The chordae insert into both the MV leaflets and PMs and act as tensile pillars for the MV leaflet during systole and help control leaflet mobility throughout the cardiac cycle. There are three classification for chordae: marginal (primary), intermediary (secondary), and basal (tertiary) (Figure 2-10).

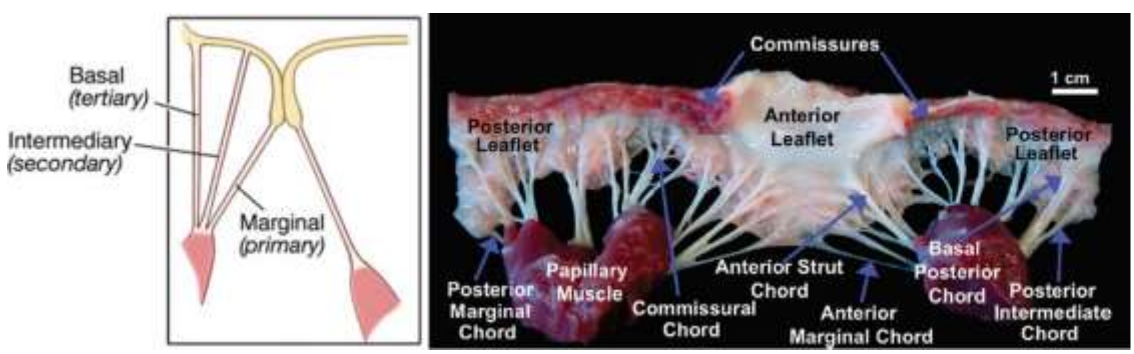

Figure 2-10. Diagram of chordae tendineae classification with papillary muscles: marginal, intermediary, and basal (modified from Carpentier et al.[21] and Rabbah et al.[23]).

Marginal chordae insert into the leaflet free edge, the intermediary chordae insert into the belly of the leaflets, and the basal chordae insert closest to the annulus (furthest away from the apex of the heart). It is worth noting that the there are two larger and distinct intermediary chordae called strut chordae that insert into the belly of the anterior leaflet and carry the majority of the systolic loading. From a biomechanical standpoint, the chordae tendineae are primarily composed of collagen and elastin and show nonlinear viscoelastic behavior under tensile loading.[23]

There are two PMs to which both the anterior and posterior leaflet chordae insert into: anterolateral and posteromedial (Figure 2-10). The PMs are denoted as the anchor point of the chordae into the LV and are distinct myocardial appendages along the LV wall. Their primary role is to help stabilize loading between the chordae and leaflets. This is done through a combination of factors: LV wall motion, chordal insertion pattern, and the material property and structure of the PMs (myocardium) that acts as a foundation for the chordae (Figure 2-11).[21, 23]

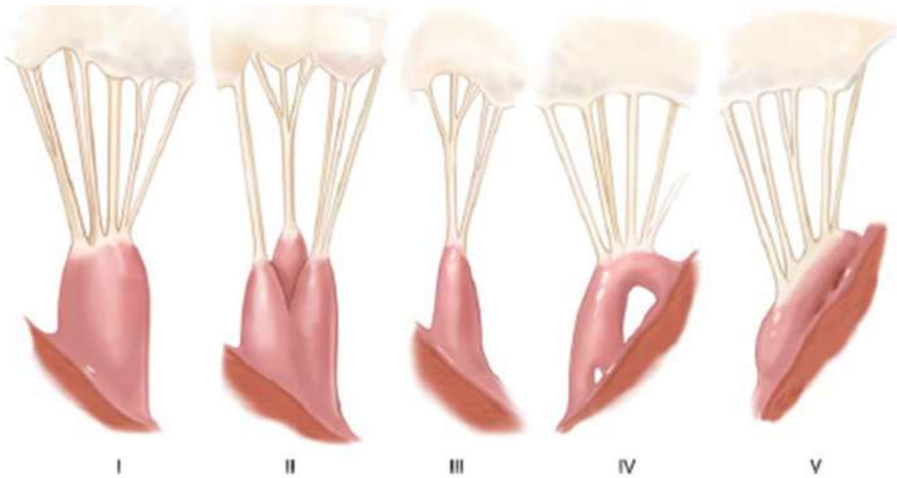

Figure 2-11. Illustration of selected morphologies of papillary muscles and chordal insertions (modified from Carpentier et al.[21]).

2.3 Mitral Valve Pathophysiology

The MV has been identified as the most common heart valve to experience hemodynamically significant disease in the United States of America.[30] This section details the two forms of MV dysfunction: *mitral regurgitation* (MR) and *mitral stenosis* (MS).

2.3.1 Mitral Valve Regurgitation

In MV disease, poor valve geometry or degeneration, creates incomplete valve closure that results in MR (Figure 2-12).[21] This regurgitation creates systolic back flow resulting in a fraction of the oxygenated blood in the ventricle getting returned to the left atrium, rather than being pumped to the body. This flow inefficiency also leads to an increased load on the lungs due to elevated atrial pressure during ventricular systole.

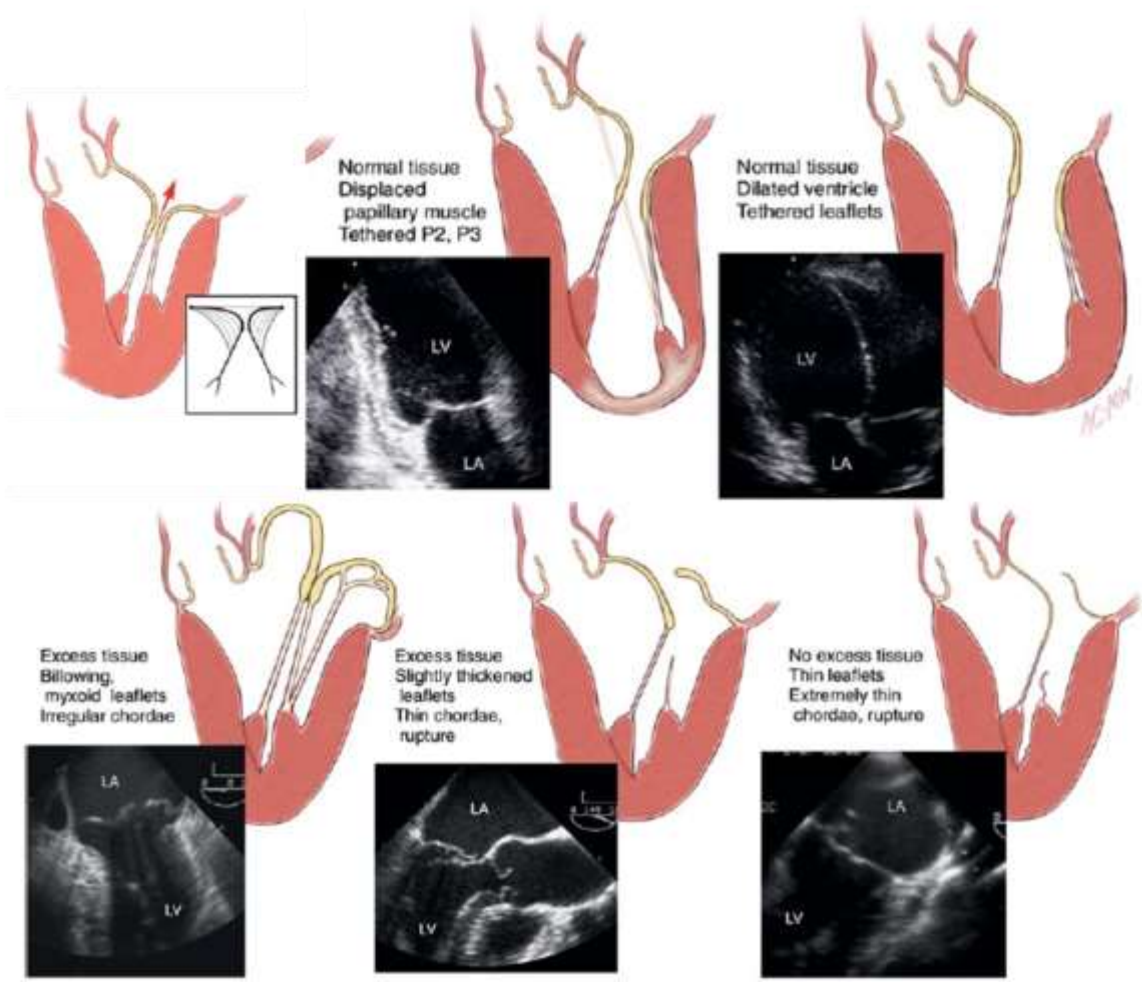

Figure 2-12. Illustrations of mitral regurgitation examples (modified from Carpentier et al.[21]).

There are two types of mitral regurgitation classifications: primary and secondary. Primary MR involves the valvular tissue whereas secondary MR involves the supporting structures, e.g. the ventricle.[21] Common cases of primary MR are congenital malformations, inflammatory or degenerative diseases, bacterial endocarditis, and calcification.[21] Common cases of secondary MR are myocardial infarction, dilated or hypertrophied cardiomyopathies, and endomyocardial fibrosis.[21] Secondary MR lends itself to *in vitro* and *in vivo* studies, because of the ability to manipulate MV geometry with a disease having healthy tissue. In contrast, it is hard to control for the differences in diseased tissue of primary MR as well as acquire the samples for experimental studies.

If left untreated, mitral regurgitation can lead to patient death.[31] With at least moderate MR occurring at a frequency of 1.7% in US adult population,[22] there is a demand for treatment. MR is most commonly treated with mitral valve repair (2.4.1, 2.5.1), but is also treated with mitral valve replacement (2.4.2, 2.5.2).

2.3.2 Mitral Valve Stenosis

In MV disease, valve dysfunction can prevent the valve from opening completely, resulting in mitral stenosis (MS). This stenosis creates an increased pressured gradient across the MV and leads to poor valve function and ventricular filling and elevated atrial pressure. A few causes include leaflet thickening (calcification, congenital, or degenerative), commissure fusion, and chordae thickening/fusion (Figure 2-13).[21] If left untreated, mitral stenosis can lead to patient death.[32, 33] Although there is a smaller prevalence of only 0.1% in US adult population,[22] it is still a surgically treated disease. MS is most commonly treated with a mitral valve replacement (2.4.2, 2.5.2), but can also be treated with mitral valve repair (2.4.1, 2.5.1).

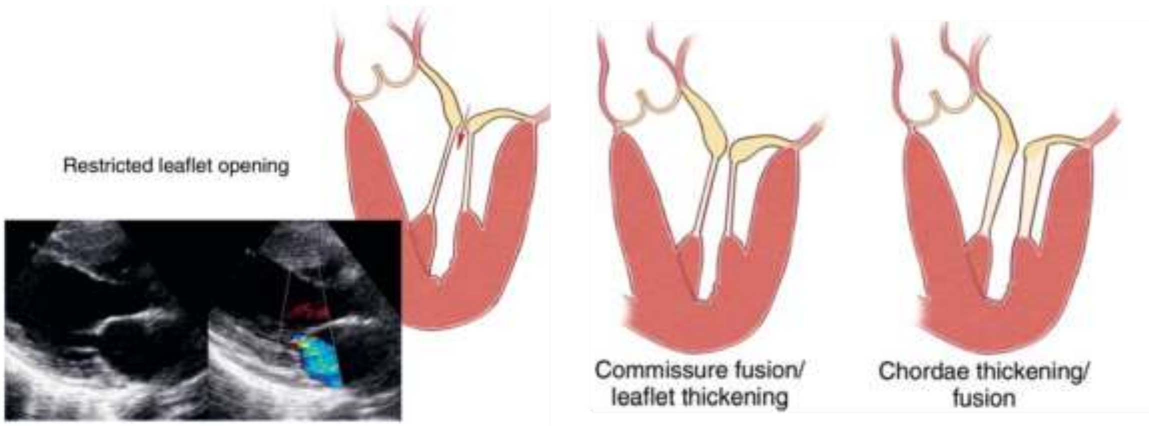

Figure 2-13. Illustration of mitral stenosis examples (modified from Carpentier et al.[21]).

2.4 Mitral Valve Surgical Corrections

In order to help patients with mitral valve disease, clinicians and engineers began making medical devices for surgical treatments. These surgical treatments can be broken down to two major categories: repair or replacement. This section highlights common surgical MV repairs and replacements.

2.4.1 Surgical Repair

Mitral valve surgical repair typically encompasses any procedure that <u>augments the native MV</u> and requires the patient to be on a cardio-pulmonary bypass.

To help treat both primary and secondary MR, implantation of a mitral valve annuloplasty ring (MVAR) is a standard surgical repair.[21, 34, 35] The MVAR is used to restore proper annular geometry and prevent any further changes. MVAR implantation is typically undersized, bringing the leaflets closer together to improve MV leaflet coaptation and reduce MR (Figure 2-14).[35] Additionally, clinicians can attempt to revascularize the left heart for secondary MR, or augment the MV with pseudo-chordae and leaflet resection/modification with primary and secondary MR.[21, 31, 36-40] These are typically done in conjunction with an annuloplasty ring.

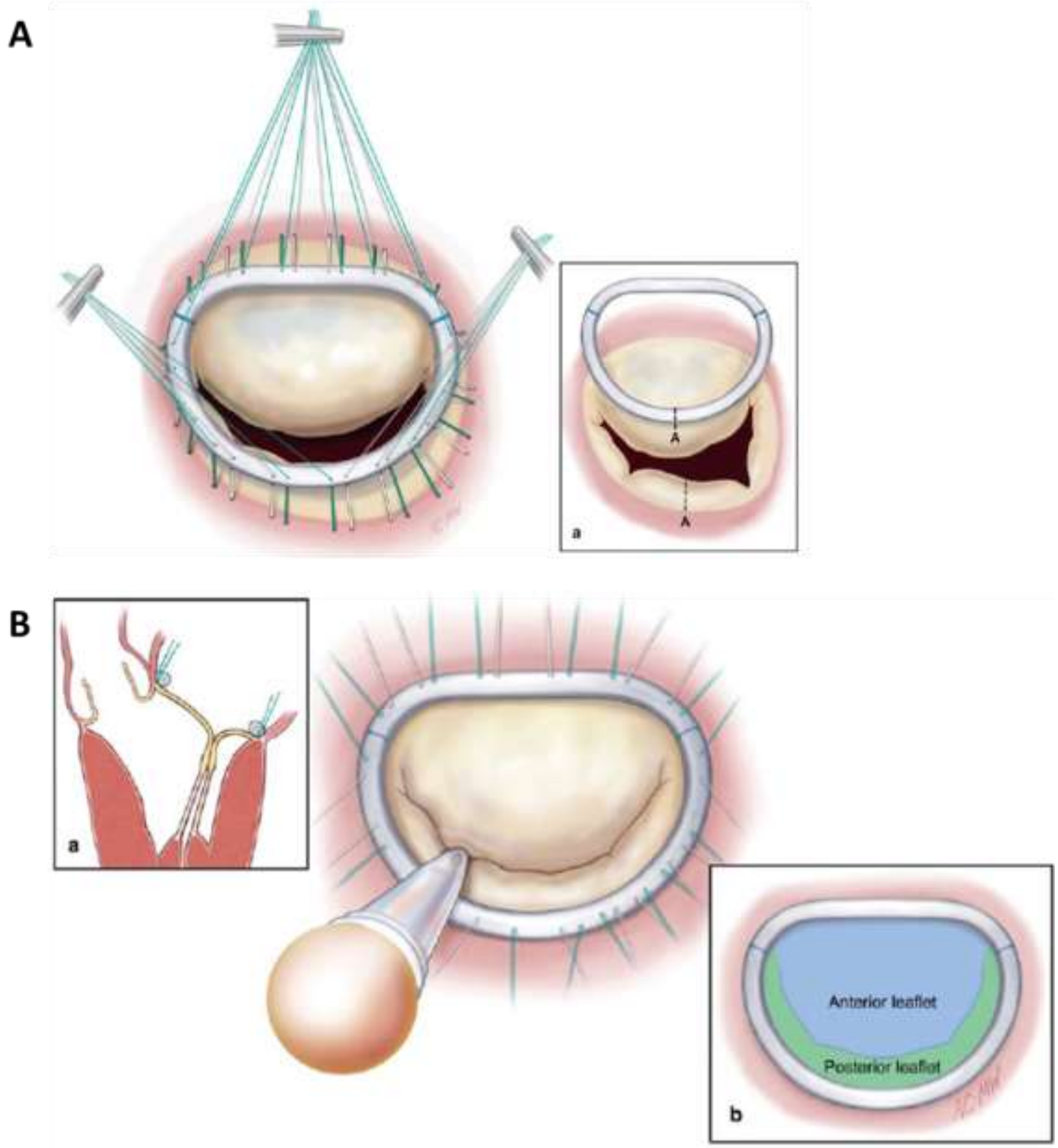

Figure 2-14. Diagram of surgical mitral annuloplasty repair. (A) Suturing rigid ring into a dilated annulus, (B) resulting downsized annulus with proper leaflet coaptation (modified from Carpentier et al.[21]).

Although this surgical repair has been proven to be effective, studies have shown MR recurrence as high as 30% in patients with ischemic MR.[1, 2]

2.4.2 Surgical Replacement

Surgical mitral valve replacements (SMVR) typically encompasses any procedure that replaces the native MV and requires the patient to be on a cardio-pulmonary bypass.

This replacement can either be a bioprosthetic or a mechanical valve (Figure 2-15). Bioprosthetic heart valves (BHV) are made of porcine or bovine pericardium and require less to no anticoagulation therapy, whereas mechanical heart valves (MHV) are made from an assortment of metal polymers and require varying degrees of anticoagulation therapies. BHVs typically have a shorter lifespan of ~10 years and MHVs a longer lifespan of ~30 years.[41]

Figure 2-15. Surgical On-X mechanical heart valve (CryoLife, Atlanta, GA) and Magna Mitral Ease bioprosthetic heart valve (Edwards Lifesciences, Irvine, CA), and diagram of a bioprosthetic mitral valve replacement being sutured into the mitral annulus.

The SMVR is sutured into the mitral annulus replacing the function of the native valve. The native valve can either be spared or resected at the surgeon's discretion.

Resection can encompass the entire MV leaflets and chordae tendineae or as little as the A2 scallop.[18] Chordal sparing is typically done to maintain LV structure and increase ejection performance with SMVR.[42]

2.4.3 Surgical Repair vs Replacement

Mitral repair is the most recommended surgical approach for MR.[43] Mick et al.[43] states that "the well-accepted advantages of mitral valve repair consist of lower operative mortality,[44-48] improved preservation of left ventricular function, and greater freedoms from prosthetic valve-related complications such as thromboembolism, anticoagulant-related hemorrhage and endocarditis.[45, 46, 49-52]" However, patient anatomy and pathophysiology plays the largest role in deciding the optimal correction.[43]

2.5 Mitral Valve Interventional Corrections

Mitral valve intervention is a growing market with only one device, MitraClip repair (Abbott, Lake Bluff, IL), currently approved by the FDA for commercial use. This medical device area stems from the need for minimally invasive approaches for high-risk surgical patients with new or recurrent disease and the desire to treat all patients as minimally invasive as possible. This section details emerging therapies in both intervention mitral valve repairs and replacements.

2.5.1 Interventional Repair

Most MV interventional repair devices are for patients with MR and aim to recreate a similar surgical repair procedure, but with a minimally invasive approach. Three main anatomical targets of transcatheter mitral valve repairs (TMVr) are the mitral leaflets, mitral annulus, and chordal apparatus. Currently, the mitral leaflet approaches recreate the edge-to-edge repair clipping leaflet edges together, the mitral annulus approaches recreate an annuloplasty repair by adjusting the annular shape and size, and the chordal approaches recreate the insertion of a pseudo-chordae to fix leaflet motion. Patient indications and current approval statuses vary widely in this growing market; Figure 2-16 summarizes leading interventional MV repair therapies that have been CE marked for European use.[53]

Anatomic Target	Device Name	Manufacturer	Description	Main indications	Strengths	Weakness
Mitral Leaflets	Mitraclip	Abbott Vascular, Abbott Park, IL	Edge-to-Edge technique	DMR and FMR	Minimal invasiveness	Lack of annuloplasty
	Pascal	Edwards Lifesciences, Irvine, CA	Edge-to-Edge techinique	DMR and FMR	Longer paddles, independent grippers, advanced steerable system	Lack of annuloplasty
Chordal apparatus	NeoChord DS 1000 System	NeoChord Inc, Eden Prairie, MN	Off-pump TA artificial chordal implantation	Mono and multisegmental Posterior leaflet flail/prolapse	Solid surgical background	TA approach
	TSD-5 Harpoon	Harpoon Medical, Baltimore, MD	Off-pump TA artificial chordal implantation	Mono segmental posterior leaflet prolapse	Solid surgical background	TA approach
	Chordart	Coremedic AG, Biel, CH	TF chordal implantation (from leaflet to papillary muscle)	Chordal rupture and elongation	Mini invasiveness, strong surgical background	Demanding procedure
Mitral annulus	Carillon	Cardiac Dimension Inc, Kirkland, WI	Coronary sinus cinching (indirect annuloplasty)	FMR	Simplicity	Limited efficacy, unpredictable results
	Cardioband	Edwards Lifesciences, Irvine, CA	Transcatheter surgical-like annuloplasty	FMR	Solid surgical background	Complexity, advanced imaging
	Bident Mitralign	Mitralign Inc, Tewksbury, MA	Annular plication (direct annuloplasty)	FMR	Simpler than other direct annuloplasty	Limited efficacy

Figure 2-16. Overview of current transcatheter mitral valve repair (TMVr) devices that have been CE marked (modified from Saccocci et al.[53]).

2.5.2 Interventional Replacement

Stemming from the success of transcatheter aortic valve replacement (TAVR) as a minimally invasive alternative to surgical aortic valve replacement (SAVR),[54-60] medical professionals have been exploring the possibilities of transcatheter mitral valve replacement (TMVR).[53] These TMVs are dedicated devices for the MV and are designed to meet the complexity of the MV anatomy and physiology (2.2). Patient indications and current approval statuses vary widely in this growing market; Figure 2-17 summarizes leading interventional MV replacement therapies that have been implanted in human.[53]

	Valve name	Manufacturer	Anchoring mechanism	Strength	Weakness
	Tiara	NeoVasc Inc.– Vancouver, BC	Fibrous trigone capture with native leaflet engagement	D-Shape	Size, fractures
	Tendyne	Abbot Vascular – St Paul MN	Apical tether	Simplicity, versatility, several sizes	TA only
	Intrepid	Medtronic, Menlo Park, CA	Radial force and subanular cleats	Simple design	Sealing?, durability?
	Fortis	Edwards Lifesciences, Irvine , CA	Leaflet Clipping	Simple design	Sealing?
	CardiAQ	Edwards Lifesciences, Irvine , CA	Mitral annulus capture with leaflet engagement	TA and TF approach	Atrial Protrusion, Thrombosis
	Caisson	Caisson Interventional LLC, Minneapolis, MN	External anchor; mitral annulus capture with engagement fibrous groove	Trans-septal approach	2 step procedure
	High-Life	High-Life SAS, Paris, France	External subanular ring; Valve-in-ring	TA and Trans-septal	2 step procedure
	Mvalve/Lotus	MValve technologies ; Boston Scientific, MA, US	Docking fixation systems + self-expandable valves	Adaptability to different transcatheter prosthesis	-
	NCSI Navigate	NCIS Inc. , CA, US	Annular winglets	TA, trans-atrial, trans-septal	-

Figure 2-17. Overview of current transcatheter mitral valve replacement (TMVR) devices that have been implanted in humans (modified from Saccocci et al.[53]).

2.5.3 Interventional Repair vs Replacement

The MVs complex anatomy and physiology make for a challenging target to treat. Accessibility and ease-of-use limits the capabilities of a transcatheter approach for mitral repair in contrast to an open-heart surgery. This has restricted current TMVr designs to target single objectives (e.g. edge-to-edge clip) in as simple deployment as possible. These restricted designs have also led to the quicker development and implementation of TMVr. In contrast, a TMVR must replace the entire function of the MV without embolizing or migrating due to the high pressures of the LV and address the possibility of paravalvular MR due to the shape of the nonuniform, contracting annulus, among other issues. These design hurdles have led to a slower development and implementation of TMVRs.

As it currently stands, there are no FDA approved TMVR devices and only one FDA approved TMVr device (MitraClip). This is soon to change in the coming years with the more than just the examples of TMVr in Figure 2-16 and TMVR in Figure 2-17 in development and early clinical use. The MitraClip has shown that TMVr can provide good clinical outcomes for patients with MR and has a strong hold on the interventional MV market having been implanted in over 30,000 people.[61-64] However, the Tendyne valve (Abbott, Lake Bluff, IL) and Intrepid valve (Medtronic, Minneapolis, MN) have shown encouraging results for TMVR and both have entered into pivotal randomized trials.[65-67] At the end of the day, safety, efficacy, and patient outcomes/quality of life will have to be weighed between TMVr and TMVR, not just feasibility.

2.6 Transcatheter Aortic Valves in the Mitral Valve

Some patients who undergo MV repair or replacements have recurrent MR or MS over time.[68-71] With these patients having already undergone open-heart surgery and are typically elderly with multiple comorbidities, they are often at high-risk for surgery. In response to this high-risk assessment, a non-surgical solution is necessary. However, some patients are not candidates for transcatheter repair and there are currently no dedicated transcatheter mitral valve replacements on the market.

Due to the need for a minimally invasive replacement solution for people these patients, clinicians have begun implanting transcatheter aortic valves (TAV), off-label, in mitral annular calcification (valve-in-MAC),[4-7] mitral bioprosthetic valves (valve-in-valve),[7-9] and mitral annuloplasty rings (valve-in-ring).[10-12] This can be viewed in Figure 2-18, Figure 2-19, and Figure 2-20.

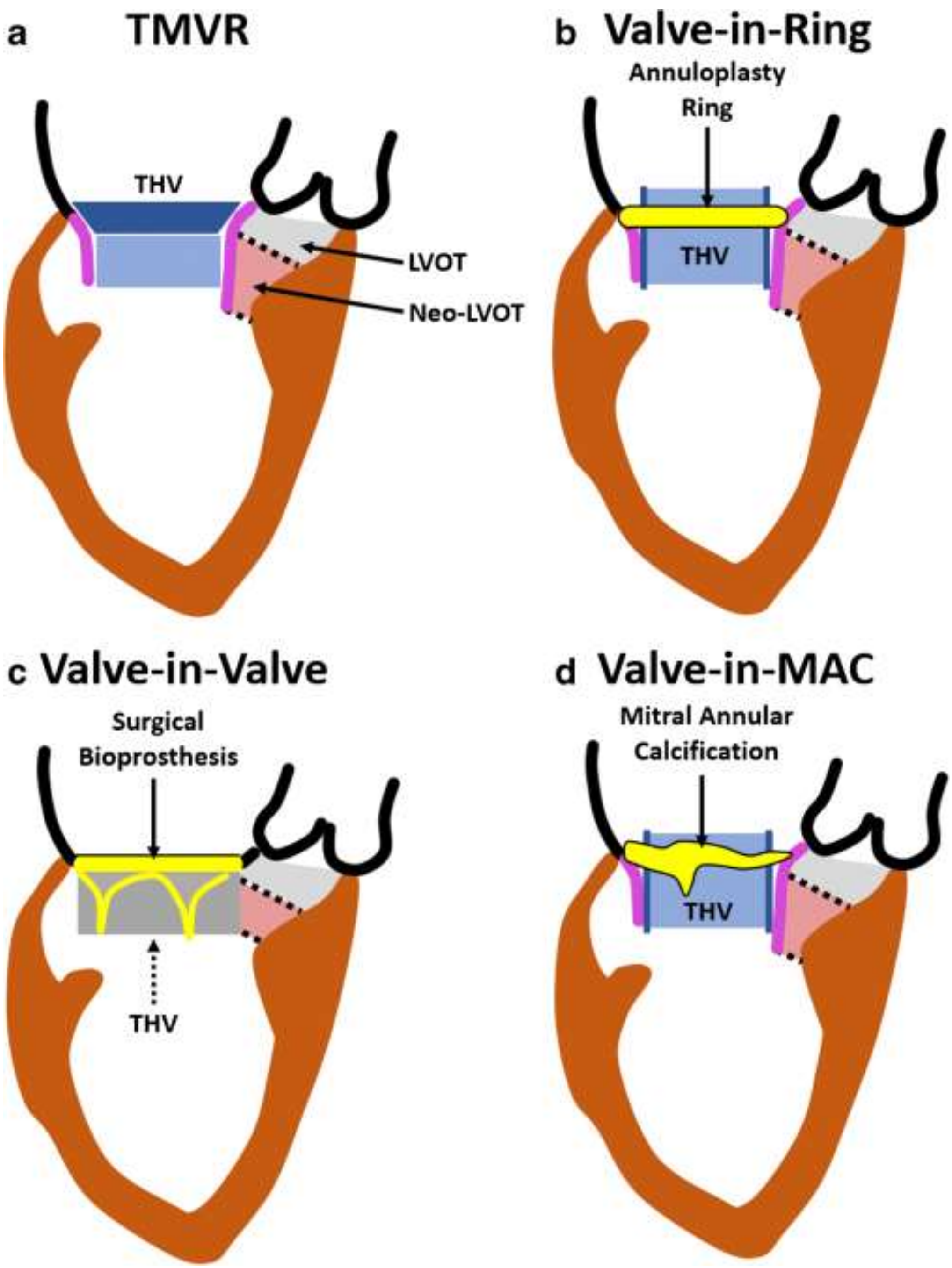

Figure 2-18. Graphical drawings of transcatheter mitral valve approaches.[72]

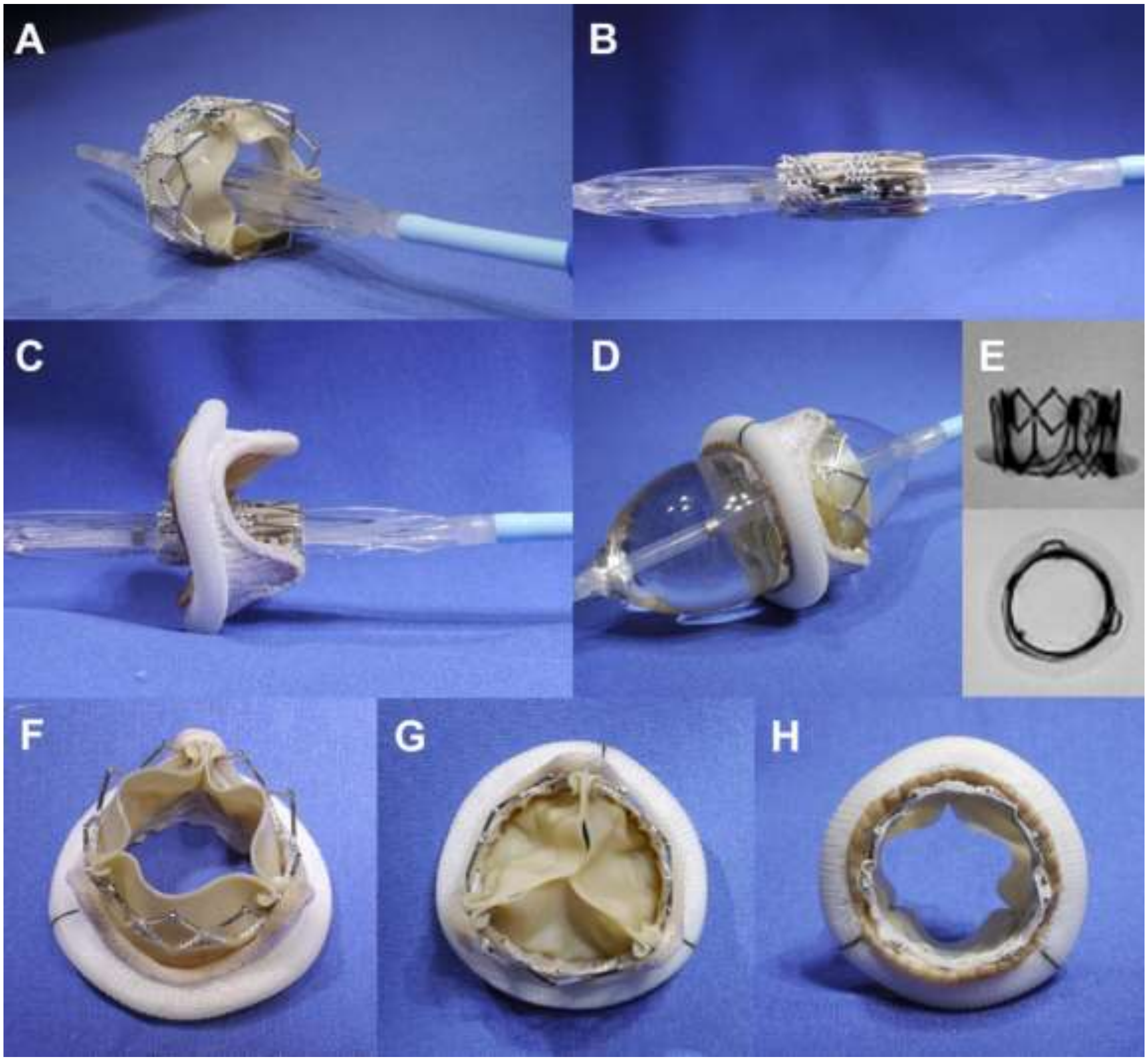

Figure 2-19. Example of mitral valve-in-valve deployment using a Sapien XT transcatheter aortic valve (Edwards Lifesciences, Irvine, California) and Carpentier surgical mitral valve (Edwards Lifesciences).[73]

Figure 2-20. Example of mitral valve-in-ring deployment using a Sapien XT transcatheter aortic valve (Edwards Lifesciences, Irvine, California) and semi-rigid Physio mitral annuloplasty ring (Edwards Lifesciences).

Normally, a TAV would not work in the mitral position, due to the dynamic contraction of the MV annulus and the inability to anchor the TAV in place. However, the MVAR, SMVR, and MAC provide rigid constructs to hold the transcatheter valve in position. Studies have shown successful use of the TAV in the MV;[74-76] however, it is currently not an indicated use of the TAV and companies are still developing dedicated TMVs to be used instead. It is important to note, that the SAPIEN family (Edwards Lifesciences, Irvine, CA) are the only TAVs currently being deployed into the MV due to their low-profile design.

2.7 Transcatheter Mitral Valve Complications

2.7.1 Left Ventricular Outflow Tract Obstruction

A prominent concern with TMVR is the potential obstruction of the left ventricular outflow tract (LVOT) by the TAV and native anterior MV leaflet. Three factors related to TMVR

LVOT obstruction include: device protrusion, aorto-mitral angulation, and septal bulging (Figure 2-21).[13, 14] The TAV protrusion into the LV causes the anterior MV leaflet to be propped open into the LVOT causing obstruction. In addition, compounding with the deployment of the TAV into the MV and LV, the aorto-mitral angulation is a geometric concern that influences the amount of protrusion into the LVOT. The septal bulging can also create an LV that is predisposed to LVOT obstruction due to an already narrowed LVOT.

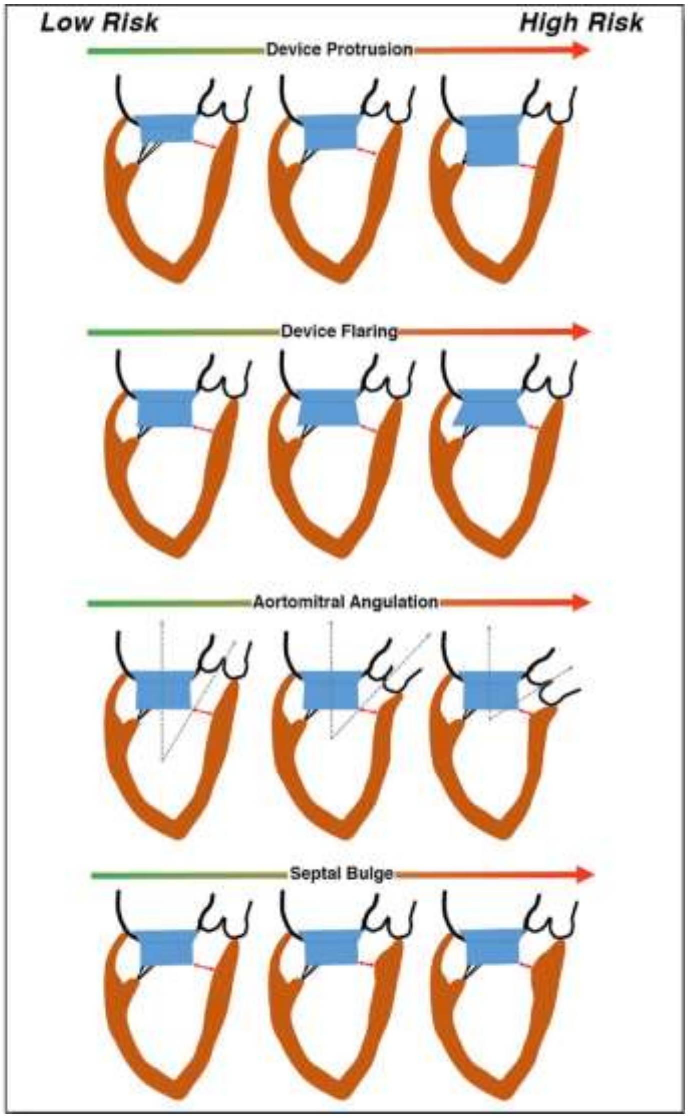

Figure 2-21. Selected risks of LVOT obstruction from Blanke et al.[14] (risk increases from green to red).

2.7.2 Thrombosis

Thrombosis is the formation of a blood clot inside the circulatory system. Thrombosis is a problem for prosthetic heart valves, especially for those in the mitral position.[15, 77, 78] Mechanical prosthetic MVs have a thrombosis prevalence of 0.3% to 1.3% in developed countries and as high as 6.1% in undeveloped countries.[77, 78] In addition, bioprosthetic MVs with native MV leaflets intact have shown to have a thrombosis prevalence as high as 24%.[22] Major factors contributing to thrombosis as outlined by Virchow's Triad are blood coagulability (blood cell damage), prosthetic heart valve surface interactions, and blood flow (stasis and turbulence). In this study we will be investigating thrombosis risk due to the changes in blood flow.

Thrombosis with TAVR has been observed[79-82] with recent studies focusing on the flow stasis in a region known as the *neo-sinus*.[83] The neo-sinus is the region between the native AV leaflets and the TAV leaflets and is formed by the native AV leaflets wrapping around the deployed TAV preventing flow through the open cells of the stent frame.

Additionally, the AML also covers the stent frame creating a neo-sinus in danger of flow stasis between the AML and TAV leaflets. Thrombosis in the mitral position and in TAVs have been independently observed.[16, 17, 84-86] In addition, the major occurrence of thrombosis from patients that underwent a bioprosthetic MV replacement were from those with their native leaflets preserved[22]. It then stands to reason that a TAV in an MV with its native leaflets preserved, would be under similar risks. Overall, these factors need to be considered when performing transcatheter mitral valve replacement.

2.8 Percutaneous Laceration of Anterior Mitral Leaflet (LAMPOON)

In order to proactively prevent LVOT obstruction for TMVR caused by the AML, clinicians have begun intentionally lacerating the AML in a minimally invasive approach known as LAMPOON prior to transcatheter valve deployment (Figure 2-22).[19, 87, 88]

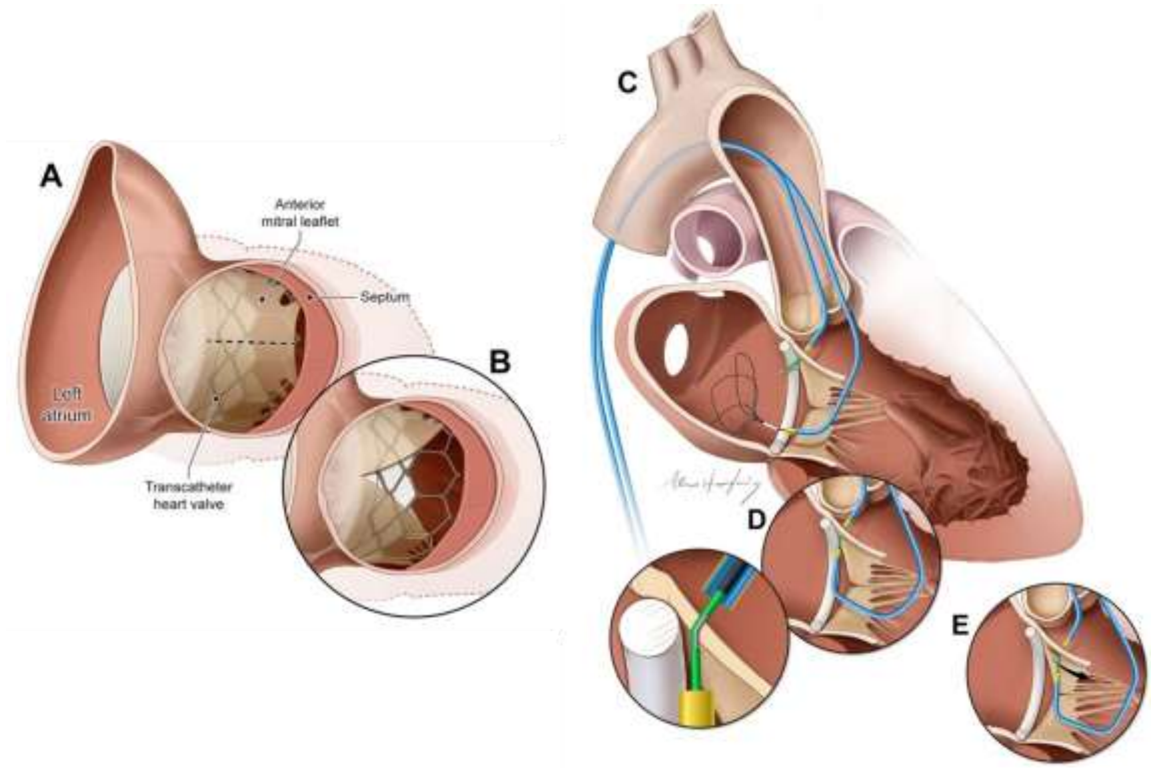

Figure 2-22. Diagram of LAMPOON procedure from Babaliaros et al.: (A) TMV inserted displacing AML, (B) post-LAMPOON AML separation, (C-E) Guidewires inserted into LV via aorta, electrified to puncture AML and ensnared, then electrified and pulled to lacerate AML (modified from Babaliaros et al.[19]).

Guided by fluoroscopy and echocardiography, LAMPOON first involves placing a guidewire at the A2 insertion of the AML and placing a second guidewire with a snare into the atrium via retrograde approach. The first guidewire is electrified to puncture and burn through the AML. The second guidewire the ensnares the first on the other side of the AML. Lastly, the first guidewire is electrified a second time and both wires pulled, burning and lacerating the AML. This effectively creates a larger LVOT by allowing the TMVR stent frame and chordae to spread the AML apart post-LAMPOON. The LVOT is increased even more with open cell stent frame designs, as blood can now flow through the cells of the stent frame that were originally blocked by the AML.

2.9 Mitral Valve In Vitro Modeling

Mitral valve *in vitro* modeling is used to study the MV in a controlled environment with the ability to acquire metrics that are unable to be obtained *in vivo*. In current rigid *in vitro* models, the structural complexity of the excised MV is preserved and can be studied (Figure 2-23).[89]

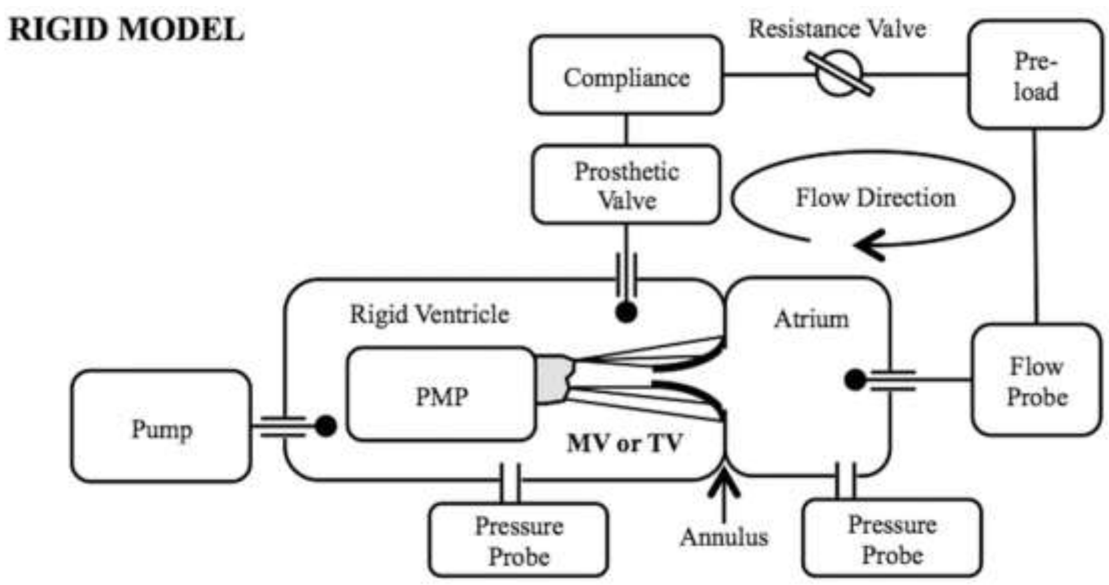

Figure 2-23. Basic schematic of *in vitro* rigid chamber left heart model.[90]

However, these models rely on certain simplifications, one being that the MV is mounted to a static, rigid annulus (leaflet attachment to the myocardium). This simplification of the annulus is justified when looking to control factors that are separate from a study's interest, e.g. investigating chordal forces. However, in order to study, for example, how the motion of the MV annulus affects the biomechanics of the MV (e.g. MV leaflets), a more physiological model with dynamic contraction is needed.

In addition to the rigid wall *in vitro* model, our lab has developed a flexible wall *in vitro* model (Figure 2-24).[90] In current flexible wall models, the LV is made of a deformable material that is able to change shape under pressure. This provides a more anatomic and contractile motion of the LV wall when compared to the rigid wall. This typically used when the interest of study involves LV flow in addition to the aortic or mitral valves.[90-92]

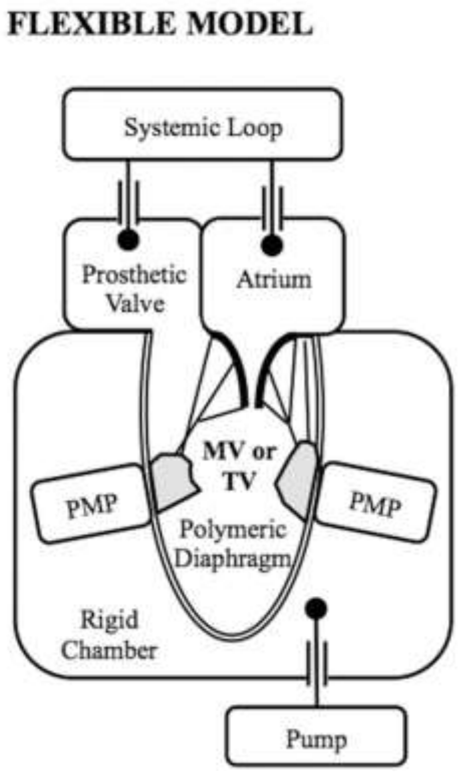

Figure 2-24. Basic schematic of *in vitro* flexible chamber left heart model.[90]

2.10 Significance

There are currently no *in vitro* simulators that incorporate dynamic MV annular contraction. This simplification of MV motion provides a limitation for complete assessment of the MV and its annulus focused medical devices (e.g. annuloplasty ring) in an *in vitro* environment. *Specific Aim 1 will provide an in vitro means of studying the effects of annular contraction to further understand valvular biomechanics.* The new simulator could also help in advancing complex MR quantification techniques, computational simulations, and medical devices by providing a moving boundary condition and a means to exert force on MV devices in a left heart simulator. In addition, there are currently no official guidelines for LAMPOON with TMVR (valve-in-ring, valve-in-valve, and valve-in-MAC) as TMVR is an off-label use of the TAV and LAMPOON is an investigational procedure. Clinicians are relying on personal experience/intuition and selected case reports when making decisions during TMVR and LAMPOON procedures. There have been no quantitative analyses on the performance and safety of TMVR or LAMPOON. Thus, information of this nature could help create new evidence-based guidelines and recommendations for LAMPOON procedures. *The results from Specific Aims 2 will provide insights into the benefits of LAMPOON on LV flow and help create the first evidence-based guidelines for TMVR and LAMPOON procedures*.

CHAPTER 3. OBJECTIVE AND SPECIFIC AIMS

The mitral valve (MV) is an intricate anatomical structure that undergoes complex conformational changes due to its dynamic loading environment. The contractile motion of the annulus has been omitted from previous *in vitro* models due to the added level of complexity that was deemed unnecessary for the studies being pursued at the time. However, with the recent innovations in the MV space[24, 93, 94] a dynamic annulus is necessary to fully understand the interactions between MV anatomy and repair or replacement options.

For patients at high-risk for surgical repair and replacement, transcatheter mitral valve replacement (TMVR) are now being performed. Cardiologists have begun implanting transcatheter aortic valves (TAVs) into mitral annular calcification (valve-in-MAC),[4-7] mitral bioprosthetic valves (valve-in-valve),[7-9] and mitral annuloplasty rings (valve-in-ring)[10-12] in order to correct recurrent mitral regurgitation (MR). With these being new, off-label procedure, no evidence-based deployment guidelines or recommendations exist outside isolated experiences reported in clinical case reports.[95-97] Hence, in order to better guide and inform TMVR, there is a need for quantitative analysis of TMVR efficacy.

The complex geometries of the left ventricle (LV) and MV present significant challenges to TMVR. The most critical periprocedural decision is the TAV position within the MV. In order to maximize expansion of the device, it is generally preferred to implant the TAV further into the LV. However, if implanted too far into the LV, the native anterior mitral leaflet held open by the TAV, could obstruct systolic flow through the aortic valve (AV) via the left ventricular outflow tract (LVOT), thus resulting in a sub-aortic stenosis.[13, [14, 98] In addition, the TAV implantation in the mitral position introduces a new structure into the MV and LV that can disrupt the natural flow of the LV. This can result in an increased risk of thrombosis as seen on the LV side of bioprosthetic valves in the mitral position.[84] One way to proactively relieve these problems is through prior surgical resection of the A2 scallop of the anterior mitral leaflet (AML) during placement of a surgical prosthetic MV[18] or through a new percutaneous laceration of the AML known as LAMPOON.[19, 28, 29]

The main objective for this study is to better understand the biomechanical challenges facing mitral valve repair and intervention replacement procedures. The central hypothesis for Specific Aim 1 is that **healthy mitral valve (MV) annular contraction minimizes MV leaflet strain**. To evaluate leaflet strain, leaflet marker tracking will be measured. The central hypothesis for Specific Aim 2 is that **increasing AML laceration (LAMPOON) will positively impact AV and TMVR performance and safety**. To evaluate TMVR performance, velocity fields of the LV will be acquired. The flow field of the LV and MV will be acquired to assess risk of left ventricular outflow tract (LVOT) obstruction and thrombosis.

Specific Aim 1: Assess the impact of healthy and pathophysiological dynamic MV annulus contraction on MV leaflet strain. Building on an existing *in vitro* left heart simulator[99], a novel dynamically contracting annulus (DCA) will be used to compare how dynamic contraction impacts MV leaflet strain. This will be done by first comparing the healthy contraction with ischemic MV disease condition, and subsequently the healthy with static-systolic and diastolic states. Leaflet strain will be measured via marker tracking from images acquired using stereophotogrammetry.

Specific Aim 2: Evaluate how LAMPOON affects LVOT obstruction and the risk of TAV thrombosis as a function of TAV implantation heights, AML lengths, and LAMPOON lengths. A previously validated *in vitro* left heart phantom[91] will be adapted to provide a more physiologic LVOT geometry for quantitative assessment of TMVR procedures. Rigid MV leaflets with different AML lengths and degrees of LAMPOON will be made for the LV phantom. With the newly modified LV phantom, the aortic transvalvular pressure gradient and LV velocity fields will be studied using pressure transducers and 2-D high-speed particle image velocimetry (HSPIV). Favorable performance will be defined as maximizing AV effective orifice area and minimizing flow obstruction and maximizing neo-sinus washout as seen and quantified by pressure transducers and HSPIV, respectively. In addition, flow in the entire LV will be captured to further study LAMPOON. From the flow velocities we will calculate viscous shear stress (VSS), principal Reynolds shear stress (pRSS), and turbulent kinetic energy (TKE). These metrics have shown to be indicators of flow stagnation and turbulence. Unfavorable results will be increased stagnation, VSS, pRSS, and TKE.

CHAPTER 4. MATERIALS AND METHODS – SPECIFIC AIM 1

4.1 Materials

4.1.1 Pulsatile Left Heat Simulator

The pulsatile left heart simulator (LHS)(Figure 4-1) consists of a left heart chamber for studying the mitral valve, flow probes and pressure transducers to tune to and record left heart hemodynamics, a piston pump to drive fluid, and piping, a reservoir, and compliance/resistance devices to create a flow loop.[100, 101]

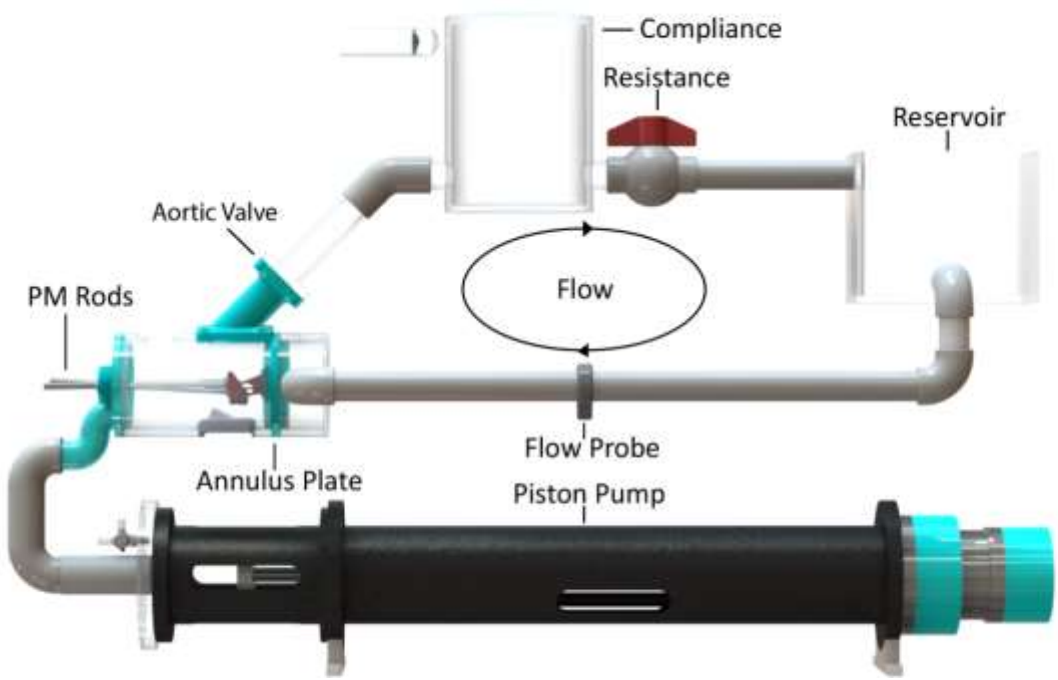

Figure 4-1. Schematic of left heart simulator complete flow loop with cylindrical chamber for ovine valves.

The left heart chamber (Figure 4-2; Figure 4-3) is made of clear acrylic left atrium, ventricle, and aorta sections, an annulus plate (4.1.2) between the atrium and ventricle, and papillary muscle (PM) rods within the left ventricle. The annulus plate is used for mounting the excised MV (4.1.4) with the PM rods securing and positioning the valve's PMs within the left ventricle from the exterior of the left heart chamber. Lastly, a bi-leaflet mechanical valve is placed inside aorta section and used as the working aortic valve for the outlet flow. For SA1, two left heart chambers were used: 1) ovine (Figure 4-2) and 2) porcine (Figure 4-3). These separate chambers were used in order to accommodate the difference in size between ovine and porcine MVs.

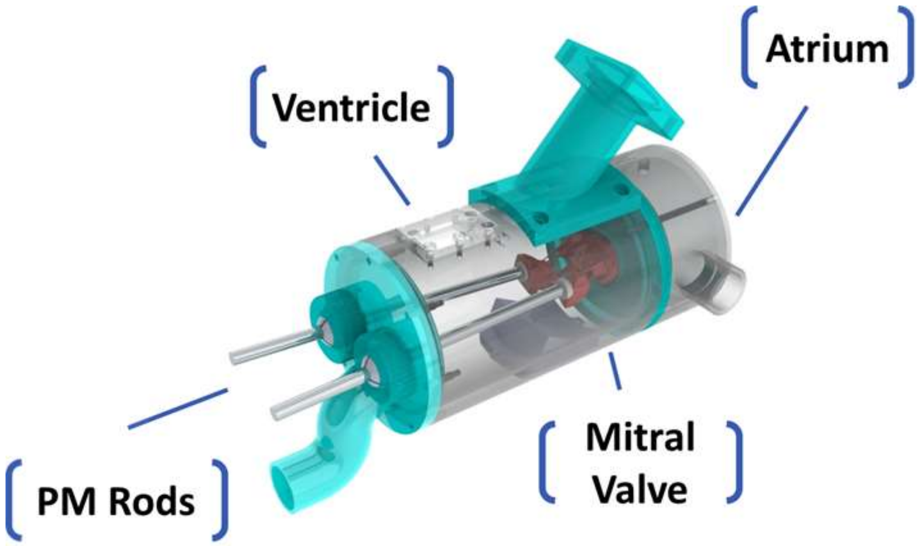

Figure 4-2. Ovine left heart chamber.

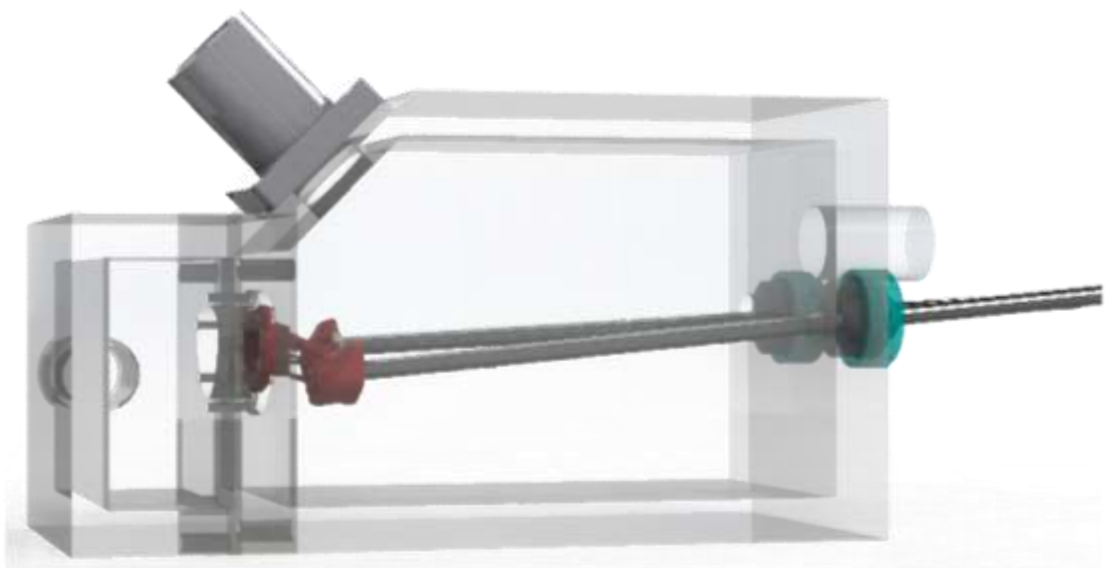

Figure 4-3. Porcine left heart chamber.

4.1.2 Annulus Plates

A dynamically contracting MV annulus (DCA) was designed to fit within an existing modular left heart simulator (4.1.1) to maintain the current imaging capabilities. A spring was embedded within a Dacron cuff to which the MV annulus is sutured. A wire was fed through the center of the spring and attached to the piston heads of two linear actuators (Figure 4-4). The wire facilitated contraction of the annulus using the motors, while the spring provided an improved means for relaxation. Two different annulus plates were fabricated; a larger to better accommodate the size of porcine MVs (porcine DCA) (Figure 4-5) and a smaller for ovine (ovine DCA) (Figure 4-6). Both annulus plates were designed in SolidWorks (Dassault Systemes; France) and 3-D printed (Proto Labs; Maple Plain, MN) using Accura Xtreme White as the material. See APPENDIX H for computer-aided design (CAD) drawings and materials used to assemble.

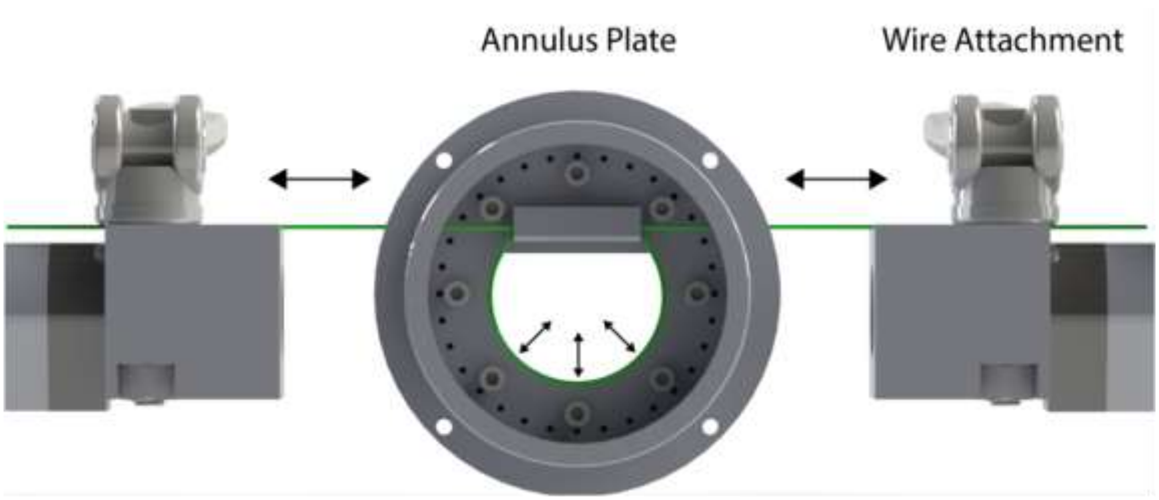

Figure 4-4. Simplified diagram of the ovine dynamically contracting annulus (DCA) setup with the ovine annulus plate centered between the wire attachments at the ends of the linear actuators. Cam levers are used to secure the steel wire imaged in green.

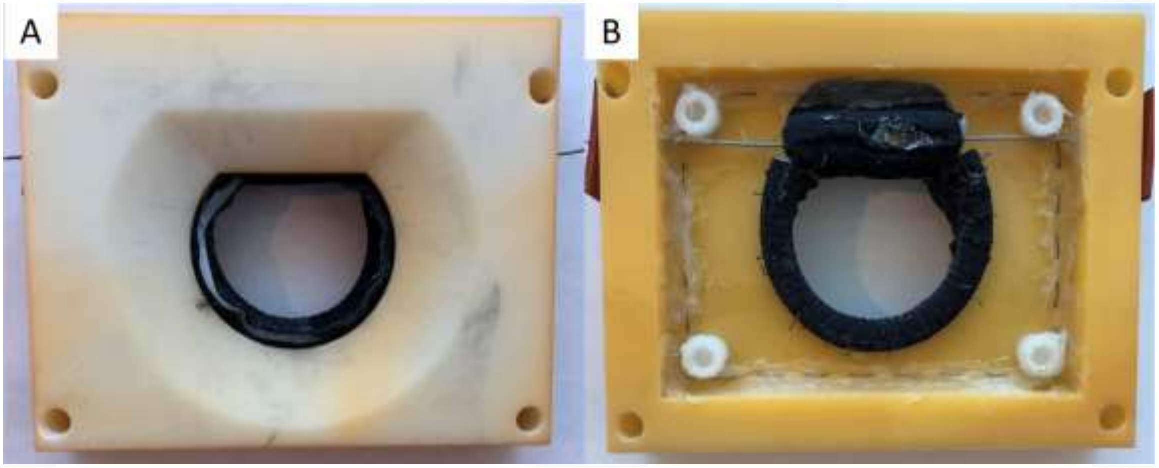

Figure 4-5. Porcine dynamically contracting annulus (DCA) plate. (A) atrial side. (B) ventricular side.

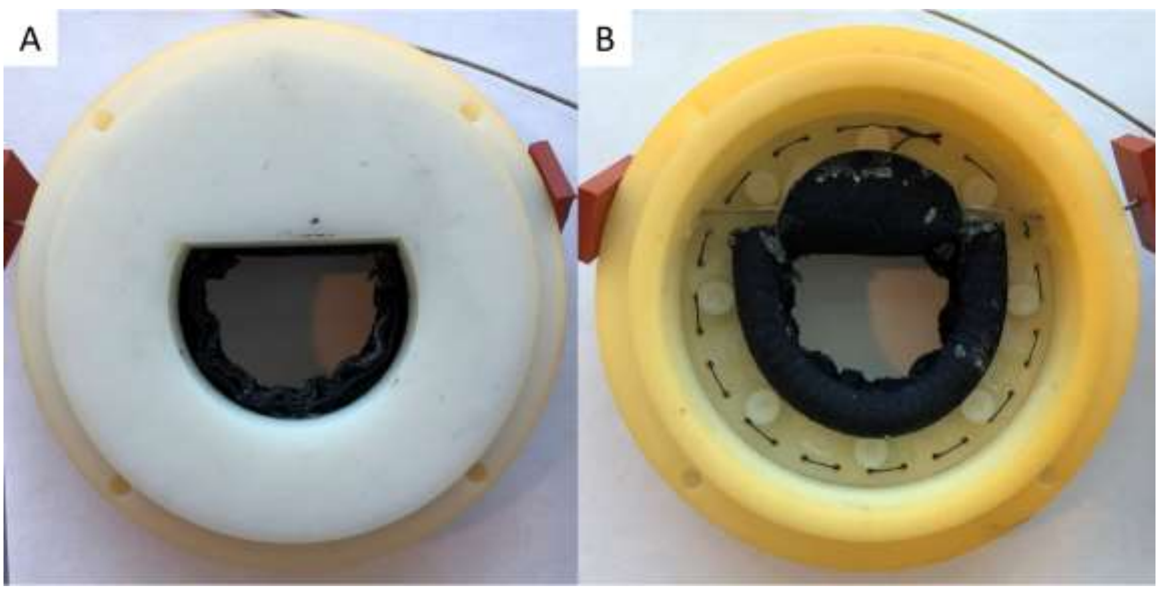

Figure 4-6. Ovine dynamically contracting annulus (DCA) plate. (A) atrial side. (B) ventricular side.

4.1.3 Motors and Controllers

The linear actuators (HAD2-2, RobotZone; Winfield, KS) were displacement driven and controlled individually using a proportional-integral-derivative (PID) controller with the addition of a feed-forward loop written in LabVIEW (2015, National Instruments; Austin, TX). With the LabVIEW controller, H-bridge controllers (1015B, DeviceCraft; Fitchburg, MA) with power supplies (RS-100-12, Meanwell Power Supplies; Taiwan) provided voltage to the motors. The positions of the motors were measured using their built-in potentiometers. A full wiring diagram (A.1), controller settings (A.2), PID tuning methods (A.3), and input waveforms (A.4) can be found in APPENDIX A.

All displacement waveforms used for the motors were derived from the mean MV annular circumference data from prior human, *in vivo* 3-D echocardiography work on mitral annular dynamics.[25] From the raw images from the paper, the figure data was extracted using a custom MATLAB code (APPENDIX K). This data was scaled to match the same mean percent areal change for the different annular area sizes of the DCAs. Tuning of the motors for accuracy and precision of the waveform tracking was done before MV experiments were performed. This was tested in LabVIEW (APPENDIX J) by comparing the actual position of the motors using their potentiometer to the desired position being output by the controller.

4.1.4 Mitral Valves

Healthy mitral valves were excised from fresh, never frozen ovine hearts (Superior Farms; Denver, CO) and porcine hearts (Holifield Farms; Atlanta, GA). The excision left both the valvular (annulus and leaflets) and subvalvular (chordae tendineae and papillary muscles) apparatuses preserved (Figure 4-7).

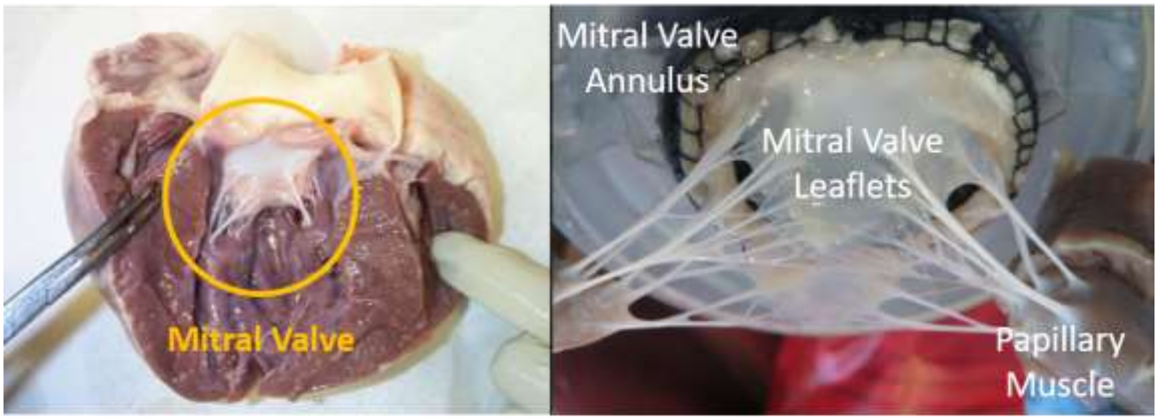

Figure 4-7. Excision and mounting of the full mitral valve apparatus.

Each valve was sized to their respective annulus plate suture cuff dimensions; the inter-trigonal distance and total annular perimeter of the annulus were primary measurements used in selection criteria. In addition, the chordal insertion points were a secondary criterion used in excluding mitral valves. It was necessary for the MV to have distinct grouping of chordal insertions into each papillary muscle with minimal spreading, and no primary chordal insertions into the wall of the ventricle.

4.1.5 Echocardiography

To image the MV in the LHS over the cardiac cycle, 4-D echocardiography via ie33 xMatrix ultrasound system and x7-2 probe (Philips Healthcare; Andover, MA) was used. The echocardiography was then assessed in QLAB (Philips Healthcare; Andover, MA) where the geometry of the MV was measured. Although not used for this study, DICOMs can be exported for 3-D segmentation.

4.1.6 High-Speed Imaging

To image the anterior mitral leaflet over the cardiac cycle, two high-speed A504k cameras (Basler Inc.; Exton, PA) and XCAP video acquisition software (EPIX, Inc.; Buffalo Grove, IL) were used. The cameras were placed as close as possible to the LHS, en face of the MV from the atrial side, and approximately 15° apart. Additional lighting was used to illuminate the MV from the atrial side, and the aperture of the lenses were opened to the minimal amount that provided good visibility with the best possible focal depth.

4.1.7 Instrument Calibration

4.1.7.1 Flow Probe Calibration

A gain value of 1 was given to the channel of the electromagnetic flow probe (Carolina Medical Electronics; East Bend, NC). A reservoir with a controllable valve was attached upstream of the probe with an extended hose attached downstream to orderly flow into a large graduated cylinder. With LabVIEW running and reading the voltage from the flow probe, the reservoir valve was opened, and fluid poured into the graduate cylinder. Next, flow was cut off by closing the valve. In order to calculate the flow rate, the volume of fluid through the probe was measured with the graduated cylinder and the amount of time the valve was opened was measured with LabVIEW or a timer. This was repeated for multiple flow rates by the resistance of the reservoir valve. The time vs voltage plot was exported from LabVIEW and the curve integrated to calculate the flow probe constant necessary to match the volume measure with the graduated cylinder.

4.1.7.2 Pressure Transducer Calibration

A gain value of 1 was given to the channel of the Deltran pressure transducer (Model# DPT-100, Utah Medical Products; Midvale, UT). A Delta-Cal transducer calibration/verification device (Model# 650-950, Utah Medical Products; Midvale, UT) was then attached to the transducer and flow valve opened to its channel. Before acquiring readings, the pinch valve was squeezed to equilibrate the transducer. With LabVIEW running and reading the voltage from the pressure transducer, the Delta-Cal was adjusted to varying pressure values (-50 to 200 mmHg), imposing those known pressure values onto the transducer. The pressure transducer voltage was recorded along with the corresponding pressure from the Delta-Cal to make a plot. The slope of the linear fit line (should be $R^2 = 0.99$) for voltage vs pressure was used as the new gain value, so that the voltage from the transducer was scaled to match the pressure in LabVIEW.

4.2 Methods

4.2.1 Experimental Conditions

Changes in anterior leaflet strain between physiological and pathophysiological annulus conditions were investigated using the porcine DCA plate (Experiment A). Two states of annular function were tested: 1) healthy and 2) diseased. To isolate the effects of the annular contraction on leaflet strain, only the annulus size/motion was changed between healthy and diseased states, and papillary muscles were left in-place. This consisted of increasing its diastolic area from 11.4 cm^2 to 13.0 cm^2 to simulate annular dilation and using a contractile waveform consistent with ischemic MR patients. The percent change of contraction from diastole to systole of averaged healthy and ischemic annular area data[25] was used for scaling (-13.2 ± 2.5% and -5.4 ± 1.9% change, respectively).

Changes in anterior leaflet strain between a rigid annuloplasty (static annulus) and a dynamic annulus were investigated using the ovine DCA plate (Experiment B). Three states of annular function were tested: 1) healthy contractile, 2) static-min, and 3) static-max. The minimum and maximum static states were sized to be the systolic and diastolic annular area (4.5 cm^2 and 5.5 cm^2, respectively) of the healthy dynamic contraction used as the healthy state. Differing from the porcine study, 2-D annular area fraction change as defined by Levack et al.[25] was used for scaling of the healthy contraction (-19.02 ± 4.94% change). This was done to simulate a healthy contraction for a worst-case comparison of differences due to changes made by a rigid annuloplasty. To isolate the effects of the annular contraction on leaflet strain, only the annular variables were changed between states and the papillary muscles remained stationary.

4.2.2 Experimental Protocol

Healthy mitral valves were excised from fresh ovine hearts and porcine hearts (N=8 for each). The valves were sized to match the healthy, diastolic annular area of their respective annulus plate (4.1.4). During excision, the annuli and subvalvular structures (i.e. chordae tendineae and papillary muscles) were preserved. The MVs were then mounted into the left heart chamber by suturing the MV annulus to the annulus cuff and attaching the PMs to the PM positioning rods (Figure 4-2; Figure 4-3).

A marker grid was applied to the MV leaflets using tissue dye (Mark-It Tissue Marking Dye, Fisher Scientific; Hampton, NH). Stereophotogrammetry was used to track a 3x3 grid on the central A2 scallop (Figure 4-8) of the MV using two high-speed cameras at 250 Hz (4.1.6).

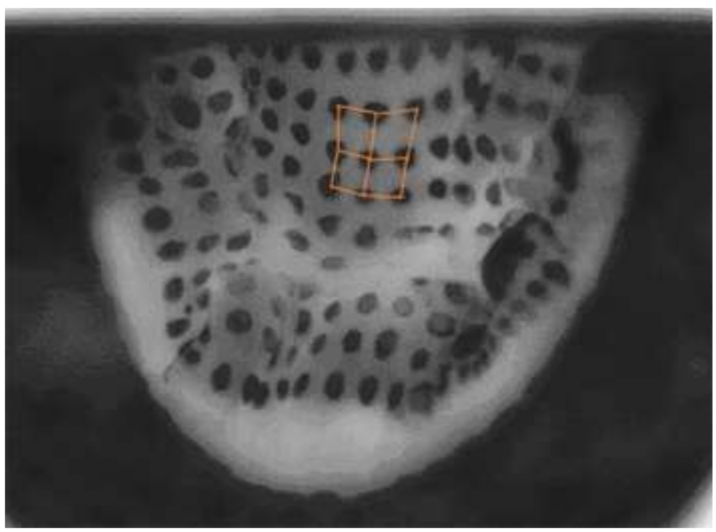

Figure 4-8. Ovine mitral valve leaflet marked with tissue dye for stereophotogrammetry. 3x3 grid used for strain measurements highlighted.

Before camera acquisition, the LHS was run for multiple cardiac cycles to remove any initial transients in the MV dynamics and flow due to start-up. A cube of known side-length (1 cm) was placed in the same field-of-view (FOV) of the cameras where, in the paired 2-D camera frames, the same 7 corners of the cube were in their FOV. Using those

7 corners and the known length and shape of the cube, we defined a 3-D coordinate system between the two cameras using direct linear transformation. 4-D echocardiography was used for measuring annular area and leaflet midline coaptation length (4.1.5).

Normal left heart pressures and flows (5 liters/min, 100 mmHg peak MV gradient, 70 beats/min, 35/65 systole/diastole ratio) were replicated within the simulator. A custom LabVIEW code was used to control the pulsatile pump (Vivitro Labs, Victoria, BC, CA), and record hemodynamics from a flow probe (4.1.7.1) and wall-tapped pressure transducers (4.1.7.2). The pressure transducers were placed in the left atrium and left ventricle with the flow probe placed within the inlet of the left atrium as shown in Figure 4-1.

4.2.3 Data Analysis

Green areal strain between peak systole and diastole for each state of annular function was computed over one cardiac cycle using a custom code written in MATLAB (R2016a, MathWorks, Natick, MA). In preliminary analysis, it was seen that there was minimal cycle to cycle variation in strain measurements, thus one was used to cut down on processing time. Midline leaflet coaptation for each state was measured with QLAB (Philips Healthcare, Andover, MA) using 4-D echocardiography. In addition, annular area change was measured with QLAB to ensure proper annular contraction for each experiment.

The Wilcoxon signed-ranked test was used for paired-group statistics using IBM SPSS Statistics (v24, IBM Corp., Armonk, NY).

CHAPTER 5. MATERIALS AND METHODS – SPECIFIC AIM 2

5.1 Materials

5.1.1 Pulsatile Left Heart Simulator w/ Left Ventricular Phantom

Based on the extensively studied Georgia Tech left heart simulator,[100, 101] a novel and more comprehensive left ventricle simulator was designed by the Cardiovascular Fluid Mechanics Laboratory (Figure 5-1 and Figure 5-2).[91, 102, 103]

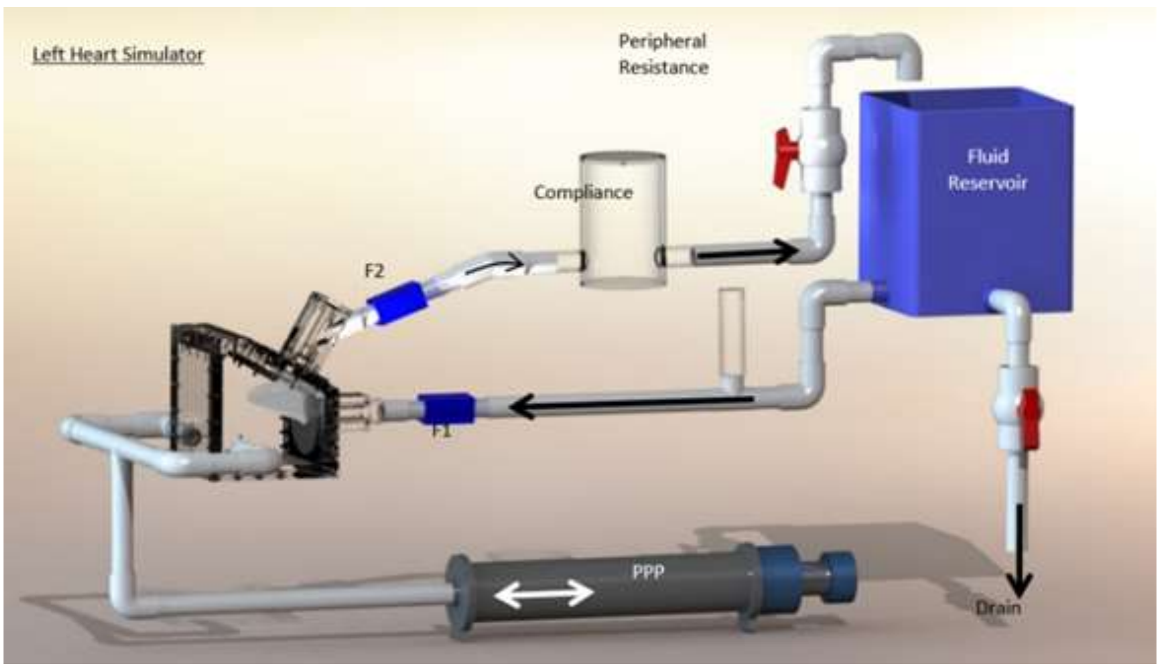

Figure 5-1. Complete realistic left heart simulator (RLHS) flow loop.

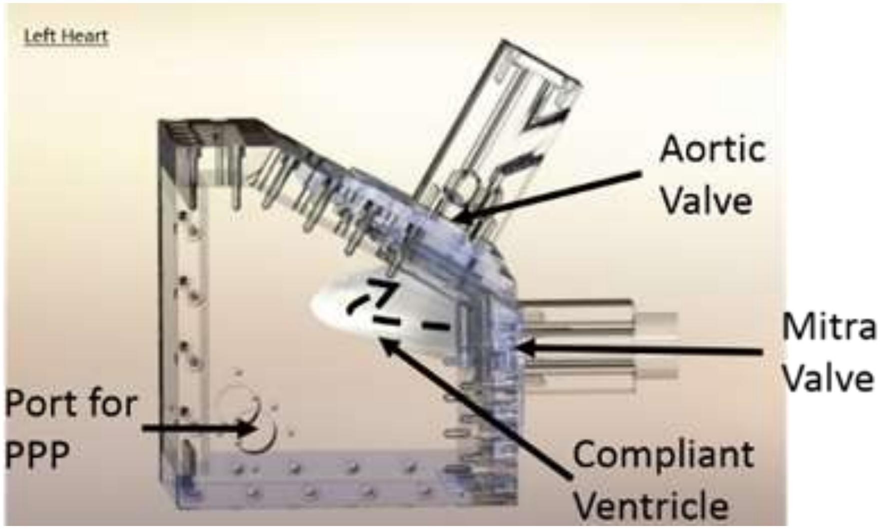

Figure 5-2. Complete LV box chamber assembly with LV phantom.

This realistic left heart simulator (RLHS) was comprised of an LV phantom complete with bioprosthetic aortic and mitral valves. The silicone LV phantom (5.1.2) is compliance-matched (diastolic) to a healthy myocardium and is housed in an acrylic chamber. The pulsatile piston pump (PPP) controls the pressure within the acrylic housing causing expansion and contraction of the LV, resulting in flow through the simulator. The peripheral resistance and compliance were used to help maintain proper hemodynamics of the LV. Wall-tapped pressure transducers were placed in the left atrium, left ventricle, and aorta, while a catheter extension was placed in the LVOT. The flow probes were placed upstream of the MV and downstream of the AV to measure both MV and AV flow curves. A 36% glycerin, 64% water solution was used in the loop in order to match the dynamic viscosity of blood (3.5 cP). LabVIEW was used to control the pulsatile piston pump as well as record and monitor the hemodynamics of the RLHS.

For the purposes of this study (CHAPTER 3) and future studies, the RLHS was redesigned to achieve a more anatomically correct LVOT and the ability to add MV leaflets inside the LV. This was done externally by moving the MV inlet and AV outlet as close together as possible within the LV box chamber, and then further accomplished internally with an LV insert (5.1.3). A 29 mm GT-TAV (5.1.5) was placed inside the MV leaflets (5.1.4), while a 23 mm PERIMOUNT BHV (Edwards Lifesciences; Irvine, CA) will be used as the AV. See APPENDIX B for a detailed assembly guide for the LV box chamber. See APPENDIX I for CAD drawings and materials used in making the LV box chamber.

5.1.2 Left Ventricle Phantom

The silicone LV phantom (Figure 5-3) used for this study was previously studied by Okafor et al.[91, 102] and cast by a third-party company (VenAir; Terrassa, Spain). The healthy LV phantom specifications used in this study were an aorto-mitral angle of 125°, a sphericity index of 0.598 (width of 40 mm), stiffness of 1.169 mmHg/mL, and shore A hardness of 23. The silicone phantom provided the optical clarity necessary for high-speed particle image velocimetry (HSPIV). Details behind the development and design of the LV phantom from patient data can be found in the thesis of Okafor.[103]

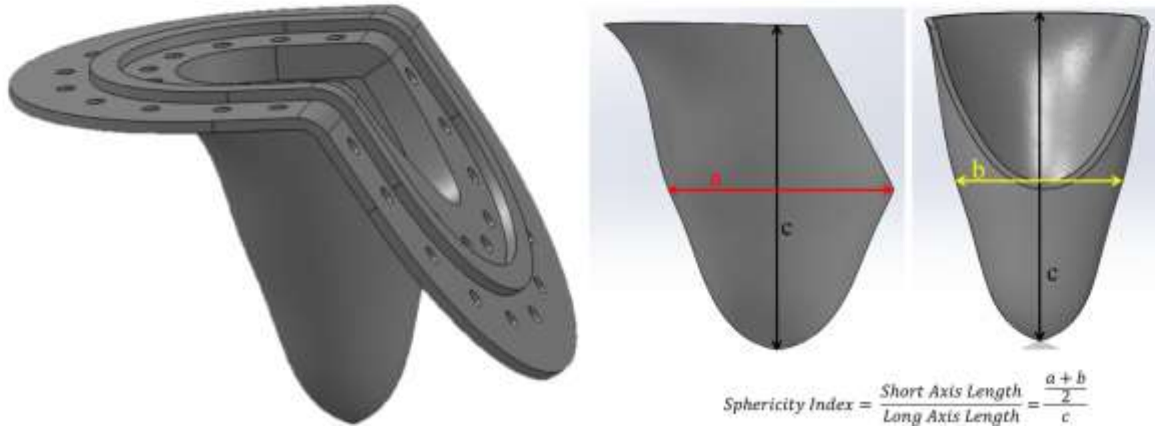

Figure 5-3. Schematic of the LV phantom and dimensionality of the sphericity index (modified from Okafor[103]).

5.1.3 Left Ventricle Insert

The LV insert (Figure 5-4) served three important purposes: 1) provided a modular attachment for different MV leaflet geometries, 2) moved the aorto-mitral plane further into the LV, putting the whole LV in FOV of the high-speed camera, and 3) created an even better LVOT geometry by bringing the AV outlet and MV inlet closer together.

Figure 5-4. 3-D printed LV insert with Long AML, 0% LAMPOON 3-D printed MV glued in place.

The LV insert was designed using SolidWorks and made to fit securely into the MV inlet of the LV box chamber. It was then 3-D printed using stereolithography (SLA) at a resolution of 0.010 in., solid density, and ABS-P430 material. See APPENDIX I for CAD drawings used in the making of the LV insert.

5.1.4 Mitral Valve Leaflets

The transparent MV leaflets (Figure 5-5) were 3-D printed (CIDEAS, Crystal Lake, IL) using SLA at a resolution of 0.0040 in., solid density, and Accura ClearVue material. The MV leaflet geometry was acquired from micro-computed tomography (µCT) images of an excised porcine valve and exported as an .STL file for printing.

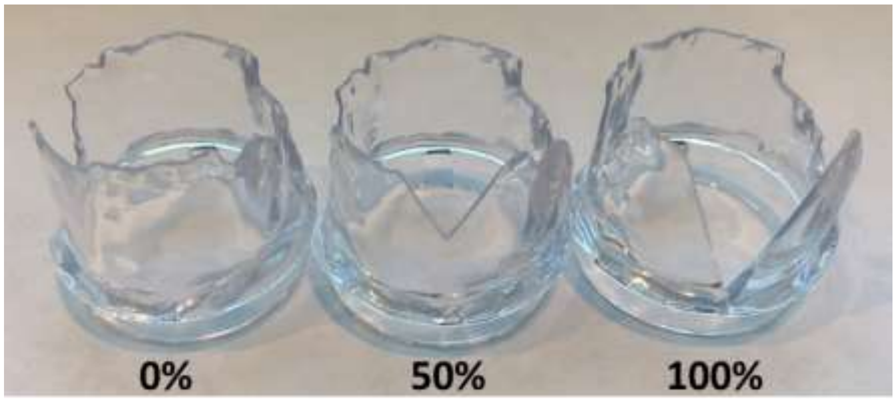

Figure 5-5. 3-D printed, transparent MV leaflets modeling three LAMPOON geometries (0%, 50%, and 100%) with Short AML.

Prior to µCT, a porcine MV was sized for a 29 mm SAPIEN 3 and excised keeping the native valvular anatomy intact. The excised valve was then mounted onto an annulus plate with a circular suture cuff sized to a 29 mm SAPIEN 3. During µCT, a cylinder with the dimensions of a 29 mm SAPIEN 3 was inserted into the valve to provide the correct leaflet geometry for when we place a TAV inside the rigid, printed leaflets of the simulator (FIGURE XXX).

After µCT, the valve and cylinder were segmented using 3D Slicer and the cylinder insert and annulus plate removed in SolidWorks. The chordae and papillary muscles were then removed in Geomagic Studio (3D Systems, Morrisville, NC) leaving just the MV leaflets. The MV leaflet surface was then smoothed in Geomagic Studio/Design X for better optical clarity during printing. Next, simulated AML flail into the LVOT (Long AML) was done in SolidWorks and Geomagic Studio at the hinge point where the TAV stent frame ends and the leaflet would no longer be taut. The Long AML (XXX mm) was within the extreme of human lengths while the Short AMl (XXX mm) was in the norm of human lengths (XXX). Lastly, different size sections of the A2 scallop of the AML were cut away in SolidWorks to mimic the resultant geometry from different lengths of LAMPOON (Figure 5-6).

Figure 5-6. Models of three LAMPOON geometries (0%, 50%, and 100%) with Long AML geometry and an image of 100% LAMPOON with porcine MV and SAPIEN 3 deployed at 80/20 ventricle/atrium ratio. The A2 scallop is lacerated allowing the AML to be pulled open by the TAV stent frame and the AML chordae.

5.1.5 Georgia Tech – Transcatheter Aortic Valve

The TAV model used for this study was made in-house (GT-TAV) to replicate the geometry of a 29 mm SAPIEN 3 (Edwards Lifesciences, Irvine, CA) (Figure 5-7). The GT-TAV has previously been validated for hemodynamic performance in the AV position.[83] The stent frame is made of a clear acrylic sheet that has been laser cut to the SAPIEN 3 internal dimensions and the leaflets are made of bovine pericardium. This provided a transparent stent frame for better optical access into the AML neo-sinus during high-speed particle image velocimetry (HSPIV). A complete manufacturing protocol of the GT-TAV can be found in APPENDIX C. Part drawings and CAD of the GT-TAV can be found in APPENDIX I.

Figure 5-7. Open 29mm GT-TAV without retaining ring alongside closed 29mm SAPIEN 3. The extra length at the bottom of the GT-TAV is for assembly purposes and is accounted for with regards to deployment height.

5.1.6 High-Speed Particle Imaging Velocimetry (HSPIV)

HSPIV was used to measure the 2-D, time-resolved velocity field of the LV and neo-sinus. A 2W, 532nm diode-pumped continuous wave solid-state laser (Shenzhen Optlaser, Shenzhen, China) emitting a 2 mm beam was used as the light source. The laser beam was converted to a high frequency pulsed laser sheet by using a scanning mirror (rotating mirror array) setup provided by LaVision (GmbH, Goettingen, Germany). This frequency was manually controlled and its sensor reading shown in DaVis (by LaVision). The flow was seeded with fluorescent polymeric rhodamine-B particles (Dantec Dynamics; Denmark) with a mean diameter of approximately 10μm. A CMOS camera (Phantom VEO 340L, Vision Research; Wayne, NJ) was used to image the particles in the central long-axis plane of the LV (Figure 5-8).

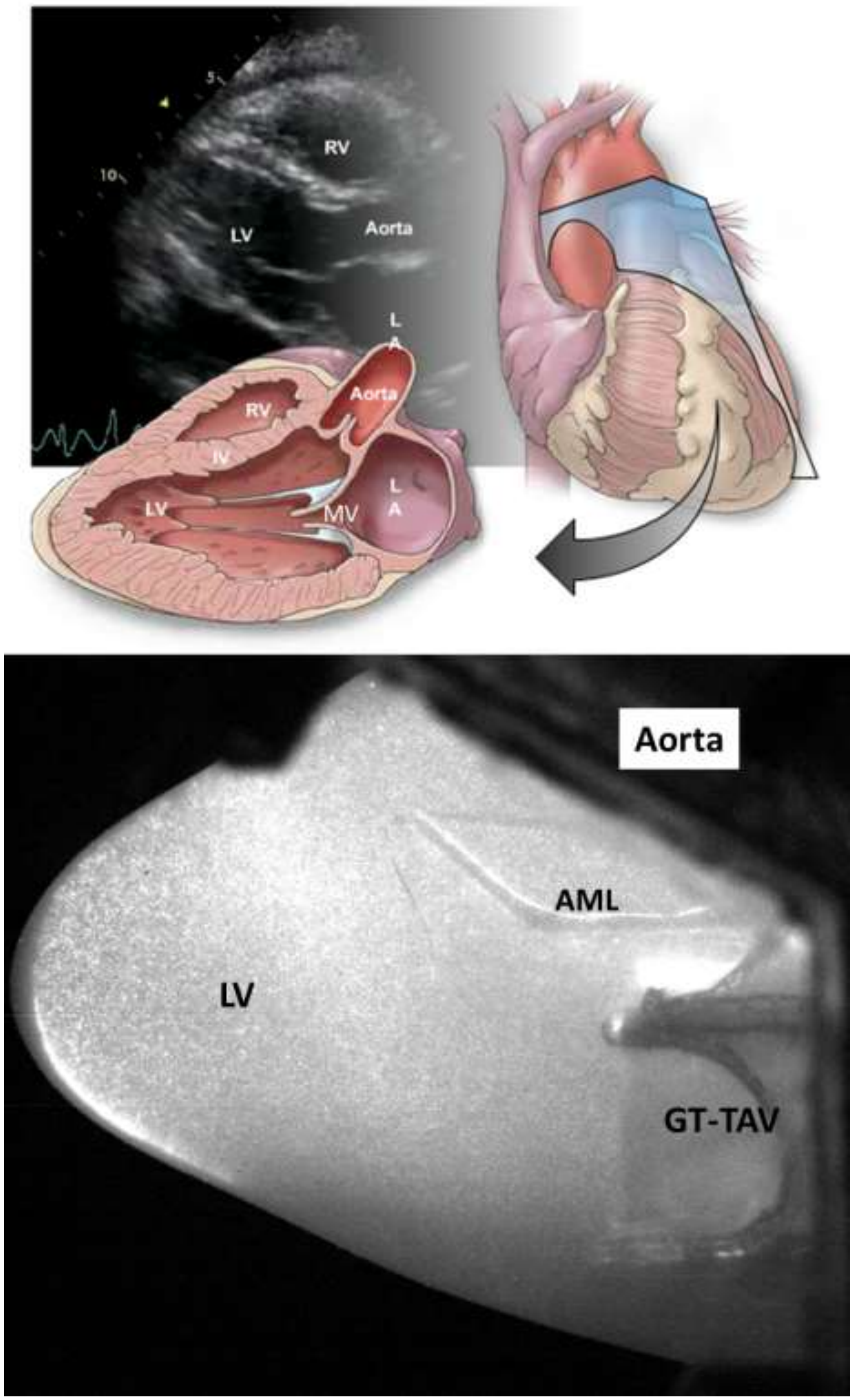

Figure 5-8. Diagram showing anatomical orientation of the PIV image plane. The image plane is the LV central long-axis which slices down from the A2-P2 of the MV.

The particle size in the camera image ranged from 2 to 4 pixels. The camera was fitted with a macro lens system of focal length 60 mm and the aperture was set at f/4. To improve the signal-to-noise ratio of the acquired data, a high-pass lens filter (cut-off wavelength of 580 nm) was used to minimize laser reflections from the sinus region. Detailed hardware configuration protocols can be found in APPENDIX D.

5.1.7 Instrument Calibration

5.1.7.1 Flow Probe Calibration

See Section 4.1.7.1.

5.1.7.2 Pressure Transducer Calibration

See Section 4.1.7.2.

5.1.7.3 Viscosity Tuning

A U-tube viscometer was used to measure the viscosity of the water/glycerin solution (Figure 5-9). This was done by drawing 6.8 mL of fluid to the top red line using a pipette. The amount of time it took to drain from the bulb to the bottom red line was then measured. The drainage time was then used to calculate the viscosity of the 36% glycerin, 64% water solution. For this study, a time of 480 seconds achieved a dynamic viscosity of 3.5 cP.

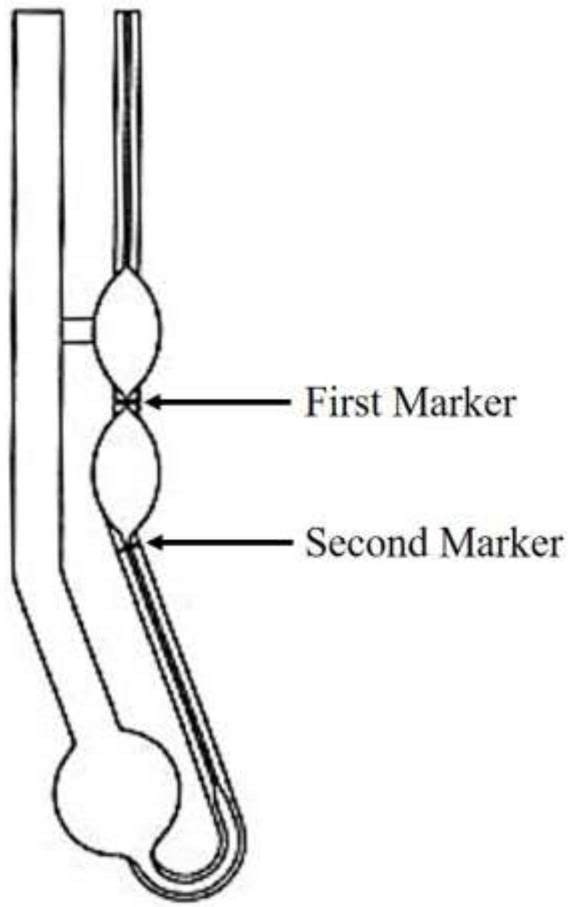

Figure 5-9. Diagram of the U-tube viscometer used to measure viscosity of the water-glycerin solution.

5.2 Methods

5.2.1 Experimental Conditions

For both Specific Aims 2A and 2B, three conditions were varied: 1) AML length, 2) LAMPOON length, and 3) TAV deployment height (Table 5-1).

Table 5-1. Specific Aim 2 Experimental Matrix

Specific Aim	AML Length	LAMPOON Length (%)	TAV Deployment	Flow Rate (L/min)	Total Experiments	
SA2A	Short	3 (0, 50, 100)	1 (50/50)	3 (2.5, 5.0, 6.5)	*9*	**27**
	Long	3 (0, 50, 100)	2 (50/50, 80/20)	3 (2.5, 5.0, 6.5)	*18*	
SA2B	Long	3 (0, 50, 100)	1 (80/20)	3 (2.5, 5.0, 6.5)	*9*	**9**

A Short AML and a Long AML were used to study how different sized AMLs, and by relation LVOTs, affect the flow in the LV (SA2A) and neo-sinus (SA2B). Each AML condition was given three different lengths of LAMPOON: 0%, 50%, and 100% AML length. This was done in order to study the changing effects that an optimal LAMPOON (100%) or suboptimal LAMPOON (50%) would have on the flow in the LV (SA2A) and AML neo-sinus (SA2B) when compared to the intact AML (0%).

For the Short AML condition, a 50/50 ventricular/atrial ratio deployment height was used, and for the Long AML condition, 50/50 and 80/20 deployment heights were used. The 50/50 condition was used to mimic a generic deployment of the TAV in a valve-in-ring or valve-in-MAC case. However, in order to get further expansion of the TAV to provide better hemodynamic performance, clinicians deploy the TAV further into the LV. The 80/20 condition was used to mimic the more optimal TAV deployment in conjunction with the worst-case AML length (Long AML condition). The 50/50 deployment provided a comparative variable between Short and Long AML conditions. For SA2A, a control condition with no MV leaflets and the GT-TAV placed upstream of the MV annular plane was also done to help better characterize native systole.

5.2.2 Experimental Protocol

The LV box chamber was assembled and GT-TAV (5.1.5) placed into the LV insert at its experimental deployment height condition. A different LV insert (5.1.3) was used inside the chamber for each AML length and LAMPOON condition (6 total). Once the LV box chamber was assembled, the RLHS was configured.

The RLHS was tuned and run for multiple cardiac cycles to remove any initial transients in the LV flow due to start-up. Normal left heart hemodynamics (100 mmHg peak MV gradient, 70 beats/min, 35/65 systole/diastole ratio) with varying cardiac output of 2.5, 5.0, and 6.5 liters/min were replicated within the simulator. A previously written custom LabVIEW code was used to trigger the HSPIV controller, control the pulsatile pump (Vivitro Labs, Victoria, BC, CA), and record hemodynamics from a flow probe (4.1.7.1) and pressure transducers (4.1.7.2).

Following the tuning of each cardiac output, HSPIV was performed (5.1.6). The high-speed laser was adjusted to ≈700 Hz for SA2A and ≈400 Hz for SA2B to optimize frame rate and light intensity in the regions of interest (ROI) (Figure 5-10). The camera was initially positioned and focused on the SA2A ROI (the LV). For each LAMPOON length and TAV deployment condition, SA2A HSPIV data was acquired in order of 2.5, 5.0, and 6.5 liters/min cardiac outputs. Immediately following SA2A data acquisition, the camera would be moved closer and focused on the SA2B ROI (the neo-sinus) to maximize image resolution (Figure 5-11). Using the same experimental condition as SA2A, SA2B HSPIV data was then acquired in order of 6.5, 5.0, and 2.5 liters/min cardiac output. For

SA2A and SA2B, images of 20 and 36 sequential cardiac cycles were acquired, respectively.

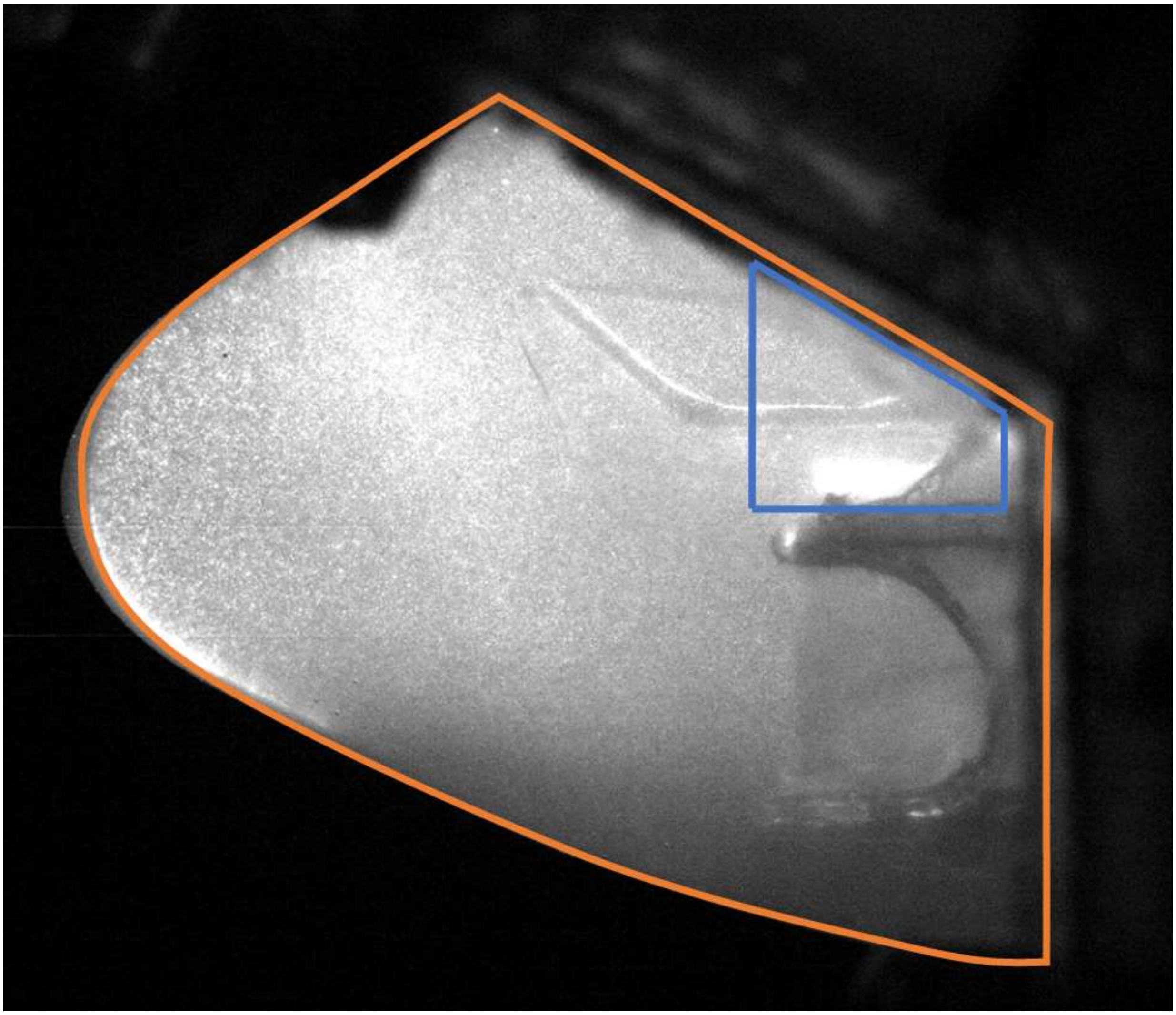

Figure 5-10. Raw camera image from SA2A showing SA2A (orange) and SA2B (blue) regions of interest. SA2A focuses on the whole LV while SA2B focuses on the MV neo-sinus.

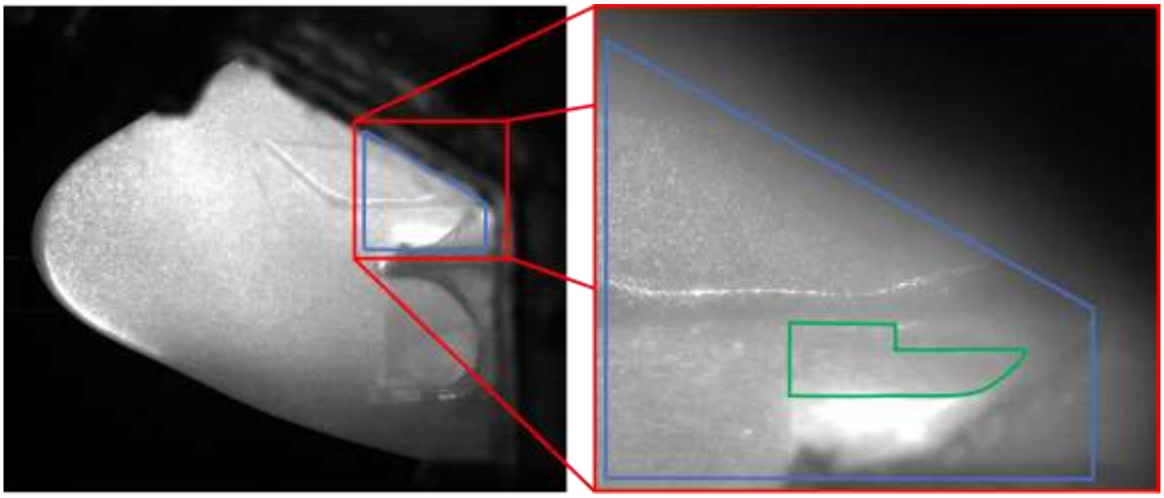

Figure 5-11. Raw camera image from SA2A with raw camera image from SA2B. The camera is moved closer between SA2A and SA2B to focus on the MV neo-sinus (outlined in green) while maximizing resolution.

5.2.3 Data Processing and Analysis

DaVis 8.4 and 10 (LaVision) were used to process HSPIV data for SA2A and SA2B, respectively. In order of operation, a mask was made to isolate the ROI (LV for SA2A or neo-sinus for SA2B) from the raw images, a background subtraction filter was used to remove background noise from the masked images, sequential cross-correlation was used for velocity vector calculation, and vector post-processing was used to remove erroneous vectors and smooth the velocity field.

Once the velocity field was calculated in DaVis, custom MATLAB code was used to bin-average, phase-average, and calculate velocity magnitude. Viscous shear stress (VSS; Equation 5-1), principal Reynolds shear stress (pRSS; Equation 5-2), and turbulent kinetic energy (TKE; Equation 5-3) were subsequently calculated from the phase- averaged velocity fields. Lastly, instantaneous streamlines and pathlines were calculated using Tecplot 360 (Tecplot, Bellevue, WA) and MATLAB was used to better articulate particle tracking in the LV and neo-sinus.

$$VSS = \mu \left(\frac{du}{dy} + \frac{dv}{dx} \right) \quad \left[\frac{N}{m^2} \right] \tag{5-4}$$

$$pRSS = \rho \sqrt{ \left(\frac{\overline{u'u'} - \overline{v'v'}}{2} \right)^2 + \left(\overline{u'v'} \right)^2 } \quad \left[\frac{N}{m^2} \right] \tag{5-5}$$

$$TKE = \frac{1}{2} \left(\overline{u'^2} + \overline{v'^2} \right) \quad \left[\frac{m^2}{s^2} \right] \tag{5-6}$$

For SA2B, the maximum and average velocity magnitudes experienced at each grid location over the cardiac cycle were computed in MATLAB as a means of identifying and comparing regions of flow stasis. Velocity fields during diastole and systole were then investigated to better understand the maximum and average velocity magnitudes. The average velocity as well as the maximum velocity within the neo-sinus was then computed for each velocity field: 1) cycle average 2) cycle maximum, 3) diastole, and 4) systole. Particle tracking was seeded at 200 ms into diastole to calculate washout of the neo-sinus during diastole.

Detailed DaVis, MATLAB, and Tecplot processing settings used for this study can be found in APPENDIX E. All MATLAB and Tecplot processing codes used for this study can be found in APPENDIX L and APPENDIX M, respectively.

CHAPTER 6. RESULTS AND DISCUSSION – SPECIFIC AIM 1

6.1 Specific Aim 1 Results

Raw Specific Aim 1 results can be found in APPENDIX F.

Motor position showed strong agreement with the target waveforms (Figure 6-1; Table 6-1). In addition, tracking annular area showed similar agreement with the desired *in vivo* percent areal change (Figure 6-2; Table 6-2).

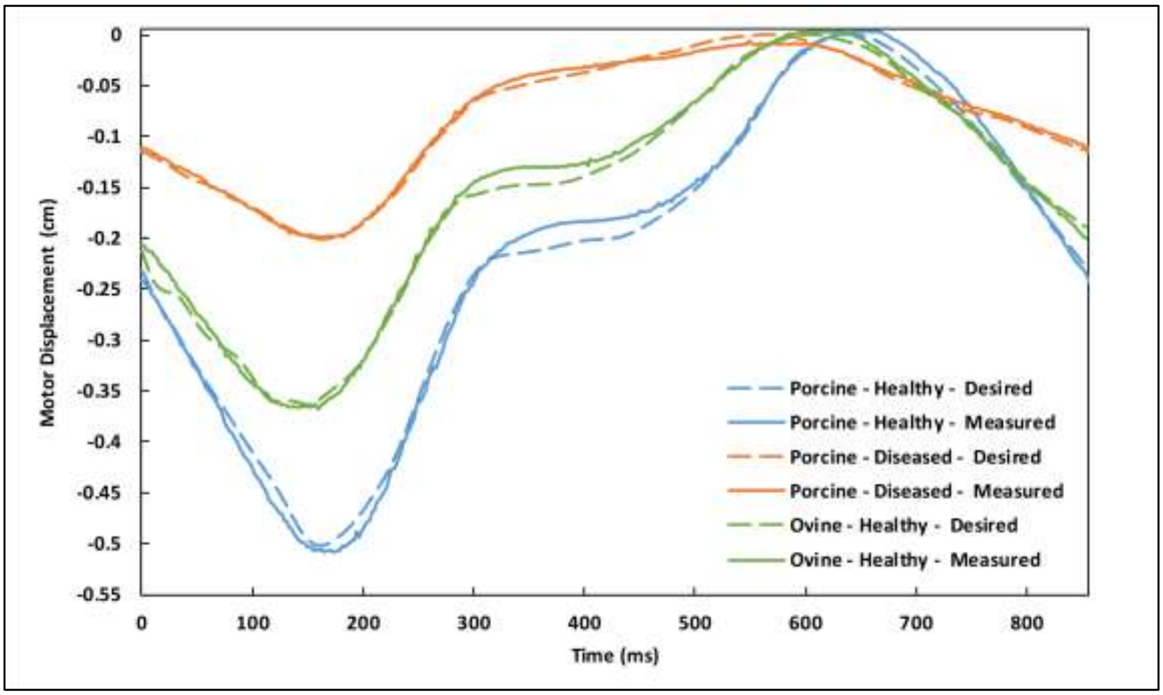

Figure 6-1. Comparison of desired and measured displacements of a single linear actuator starting with systole for plate type - waveform.

Table 6-1. Resultant accuracy of measured motor displacements compared to their desired waveforms.

Plate Type	Contractile Waveform	R^2	RMSE (µm)
Porcine	Healthy	0.99	113.3
	Diseased	0.99	47.3
Ovine	Healthy	0.99	84.2

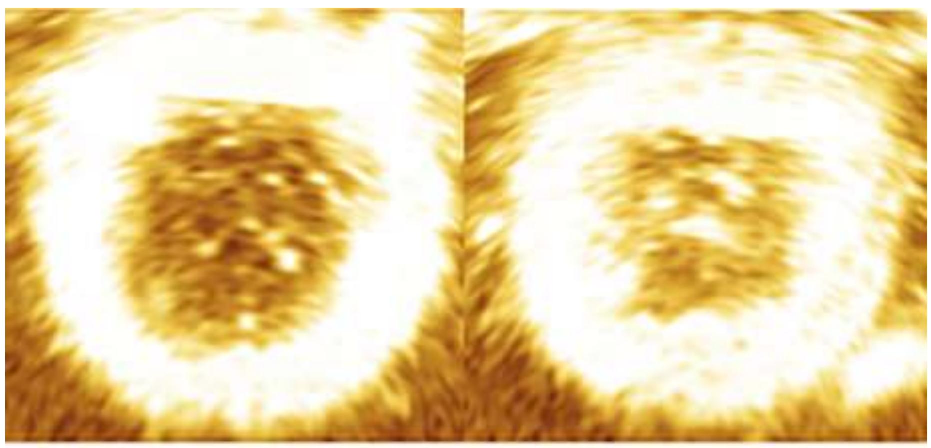

Figure 6-2. Echocardiographic image showing annular contraction from diastole to systole (see Table 6-2 for results).

Table 6-2. Measured mean ± SEM annular area of contractile states from 4-D echocardiography compared to the desired annular area.

		Porcine						Ovine		
		Healthy			Diseased			Healthy		
		Diastole (cm^2)	Systole (cm^2)	Contraction (%)	Diastole (cm^2)	Systole (cm^2)	Contraction (%)	Diastole (cm^2)	Systole (cm^2)	Contraction (%)
Desired		11.4	9.9	-13.2	13.0	12.3	-5.4	5.5	4.5	-19.0
Measured	Mean	11.53	9.97	-13.51	13.09	12.35	-5.64	5.48	4.44	-18.87
	SEM	0.05	0.04	0.39	0.06	0.05	0.24	0.10	0.08	0.61

The mean ± standard error (SEM) anterior leaflet strain of the healthy and diseased states from Experiment A were 0.64 ± 0.06 and 0.70 ± 0.06, respectively (Figure 6-3; Figure 6-4). The healthy state significantly reduced leaflet strain when compared to the diseased state ($p < 0.05$). There was no significant difference in coaptation length between the two states.

The mean ± SEM anterior leaflet strain of the healthy, static-min, and static-max states from Experiment B were 0.32 ± 0.06, 0.37 ± 0.06, and 0.41 ± 0.05, respectively (Figure 6-5; Figure 6-6). The healthy state significantly reduced leaflet strain versus both static states (each $p < 0.05$). There was no significant difference in anterior leaflet strain between static states, or coaptation length between the three states.

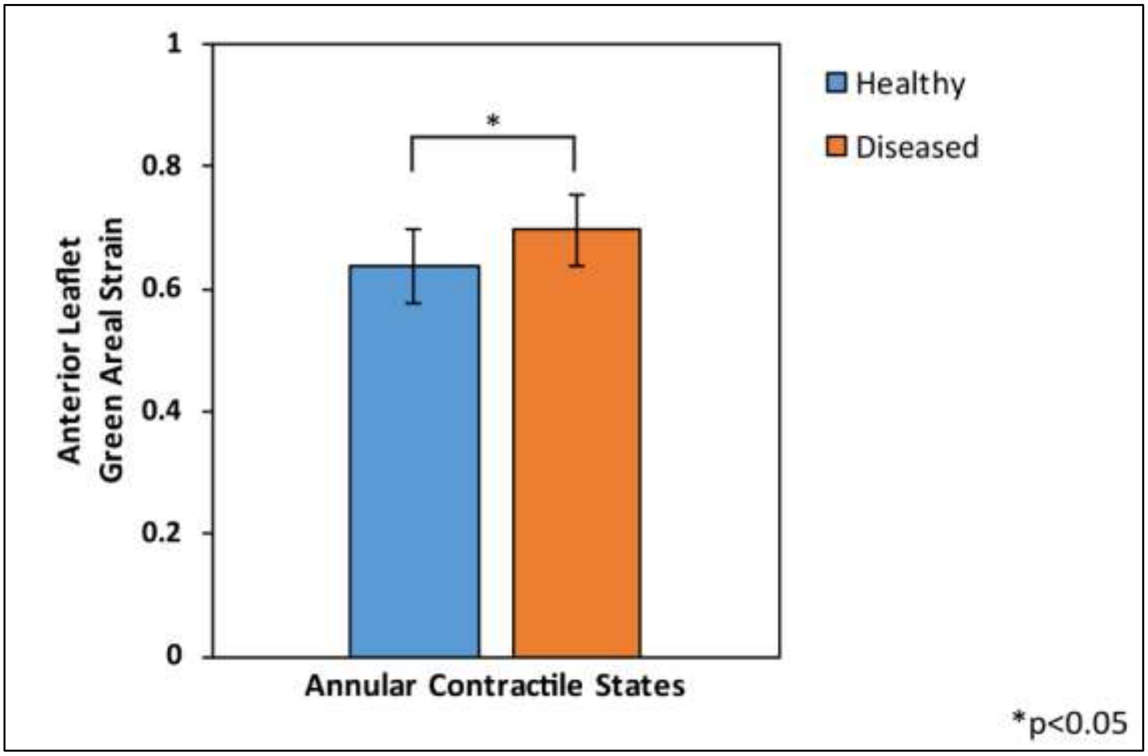

Figure 6-3. (Experiment A) Anterior leaflet resultant mean ± SEM Green areal strain between annular contractile states: healthy and diseased.

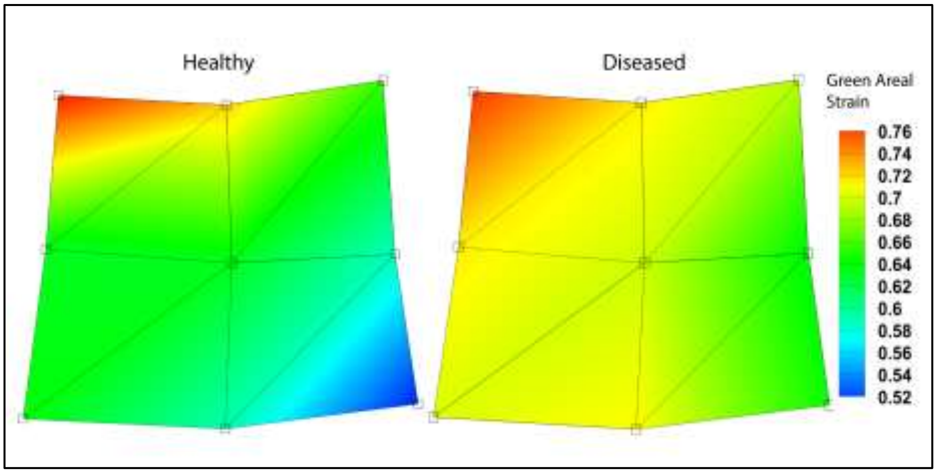

Figure 6-4. **(Experiment A) Anterior leaflet resultant Green areal strain map between annular contractile states: healthy and diseased.**

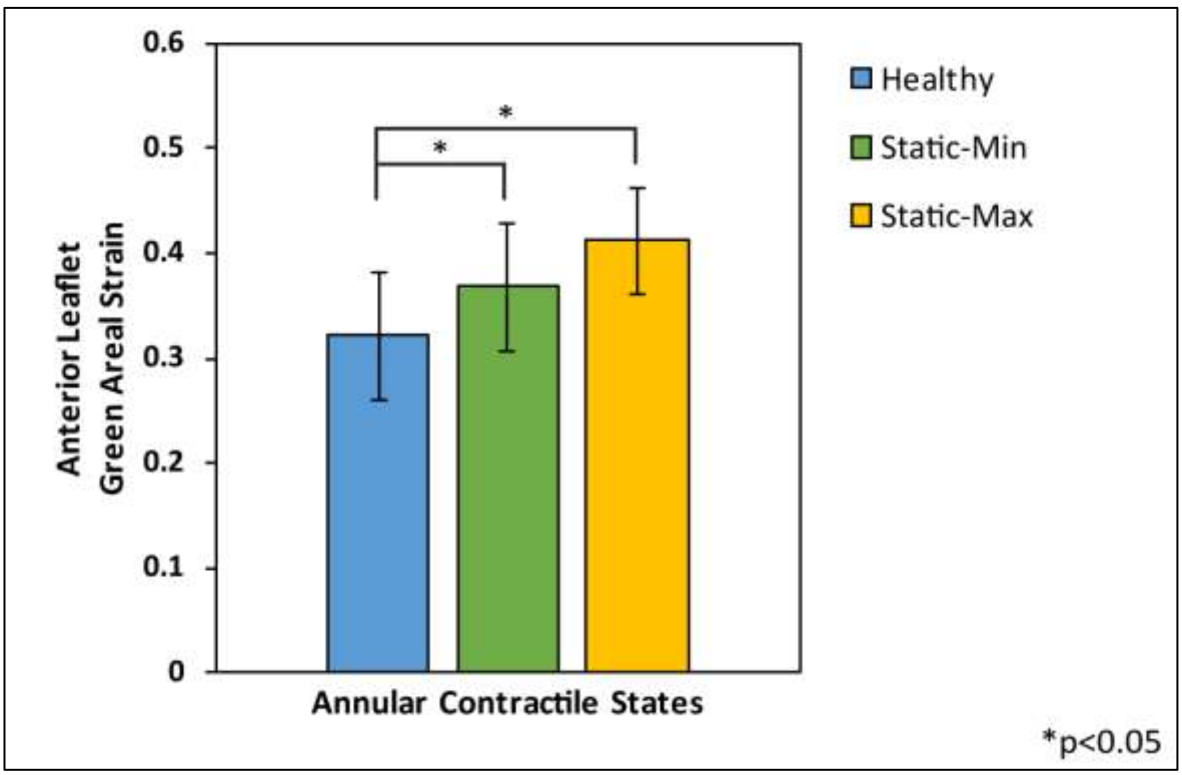

Figure 6-5. **(Experiment B) Anterior leaflet resultant mean ± SEM Green areal strain between annular states: healthy, static-min, and static-max.**

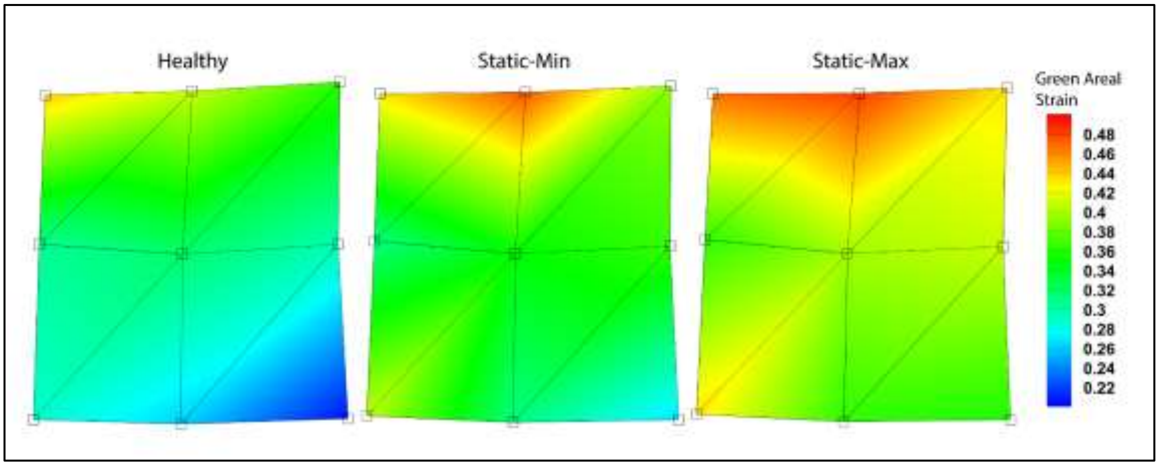

Figure 6-6. (Experiment B) Anterior leaflet resultant Green areal strain map between annular states: healthy, static-min, and static-max.

6.2 Specific Aim 1 Discussion

In pursuit of a mitral valve simulator that more completely represents the dynamic motion of the full valvular apparatus, this study demonstrated the successful operation of a dynamically contracting mitral annulus. Motor accuracy was shown to be in good agreement with the desired waveforms for both the porcine and the ovine annulus plates. It was confirmed that this translated to proper annulus area change during experiments using 4-D echocardiography. With the DCAs shown to reproduce the scaled *in vivo* geometries, it was necessary to show that the MV leaflet mechanics were also reproduced.

When investigating the reproduction of MV leaflet mechanics of the new simulator in Experiment A, it was seen that the diseased contractile state increased anterior leaflet strain compared to the healthy state. In our study, strain in the center of the A2 scallop was evaluated, as that is where the highest strains are seen.[104] Previous porcine *in vitro* studies have seen comparable areal strain magnitudes (70-75% stretch) when only focusing on the central A2 scallop and using stereophotogrammetry.[105] Our results are also in agreement with previous *in vivo* and *in vitro* study trends that IMR increases anterior leaflet strain.[101] It is noted that our results have a greater magnitude of strain compared to the *in vivo* measurements; this is believed to be primarily due to differences seen between *in vivo* and *in vitro* models, using porcine and ovine valves, and the selected area being measured on the leaflet. Previous review articles have highlighted the increased MV leaflet strains seen with porcine compared to ovine as well as *in vivo* compared to *in vitro*.[23] Overall, our results highlight the ability of the simulator to not only reproduce *in vivo* MV annular dynamics, but also MV leaflet mechanics.

In Experiment B, it was also shown *in vitro* that simulated rigid annuloplasty increased mitral anterior leaflet strain compared to a healthy contraction. Previous *in vivo* animal studies have shown similar results where rigid true-sized annuloplasty rings increase anterior mitral leaflet strains.[106] Our work specifically shows that sizing an annuloplasty ring to an MV's diastolic and systolic annular area leads to increased strain in the anterior leaflet. This implies that rigid annuloplasty rings, regardless of size, can lead to increased strain in the anterior leaflet. Additional *in vivo* animal studies have also reported that altering the MV geometry using restrictive annuloplasty rings alters strains in the MV anterior leaflet[107]. Amini, et al.[107] postulates that this annular restriction may affect long-term leaflet durability due to changes in the leaflet's mechanobiological homeostasis. Clinical studies are needed to investigate if anterior leaflet strain is increased in patients with restrictive annuloplasty rings, and, if so, how it impacts repair failure.

Additionally, there was no significant difference seen in coaptation length between states of both experiments. This is believed to be predominantly due to the use of healthy

MVs and the annulus being the only variable changed between experiments. Previous studies have highlighted the effects of isolated annular dilation and papillary muscle (PM) displacement on decreasing leaflet coaptation.[108, 109] Their results show a much larger increase in annular area (greater than 75%), not representative of the 14% increase from the *in vivo* human data used in this study, is needed to have a significant decrease in coaptation. In addition, they also show that PM displacement has an even larger effect on decreasing leaflet coaptation, of which was not changed in this study.

6.2.1 Clinical and Engineering Implications

The work of SA1 provides the first *in vitro* MV simulator with a dynamically contracting annulus. This new left heart simulator will serve as a platform for future studies in MV biomechanics and repair procedures as well as percutaneous replacement device testing. Additionally, this work suggests that striving to maintain the MV annular dynamics during MV repair procedures is beneficial to the loading of the anterior leaflet. It may then beneficial for future annuloplasty devices to have some component of flexibility rather than be completely rigid.

6.2.2 Limitations

The main limitation of this new annular design is that the annulus is flat and its contraction is limited to 2-D, planar motion derived from 2-D projections of 3-D geometry. Physiologically, the MV annulus has a 3-D contractile motion over the cardiac cycle, changing between a saddle-shape and a more flat-shape. It has been previously shown that the saddle-shape of the MV does minimize leaflet strain;[110] it could then be hypothesized that adding this 3-D shape to our study would have presented even greater differences between a saddle-shaped healthy state and the flatter-shaped diseased and annuloplasty states. However, for our study, it was deemed that having a 2-D, planar motion allowed for more use of data as contractile inputs (annular metrics commonly presented as 2-D, planar projections) as well as a simplification that allowed for more control over the experiment.

CHAPTER 7. RESULTS AND DISCUSSION – SPECIFIC AIM 2

7.1 Specific Aim 2 Results

Raw Specific Aim 2 results for plots can be found in APPENDIX G.

7.1.1 Specific Aim 2A: LV Flow with LAMPOON

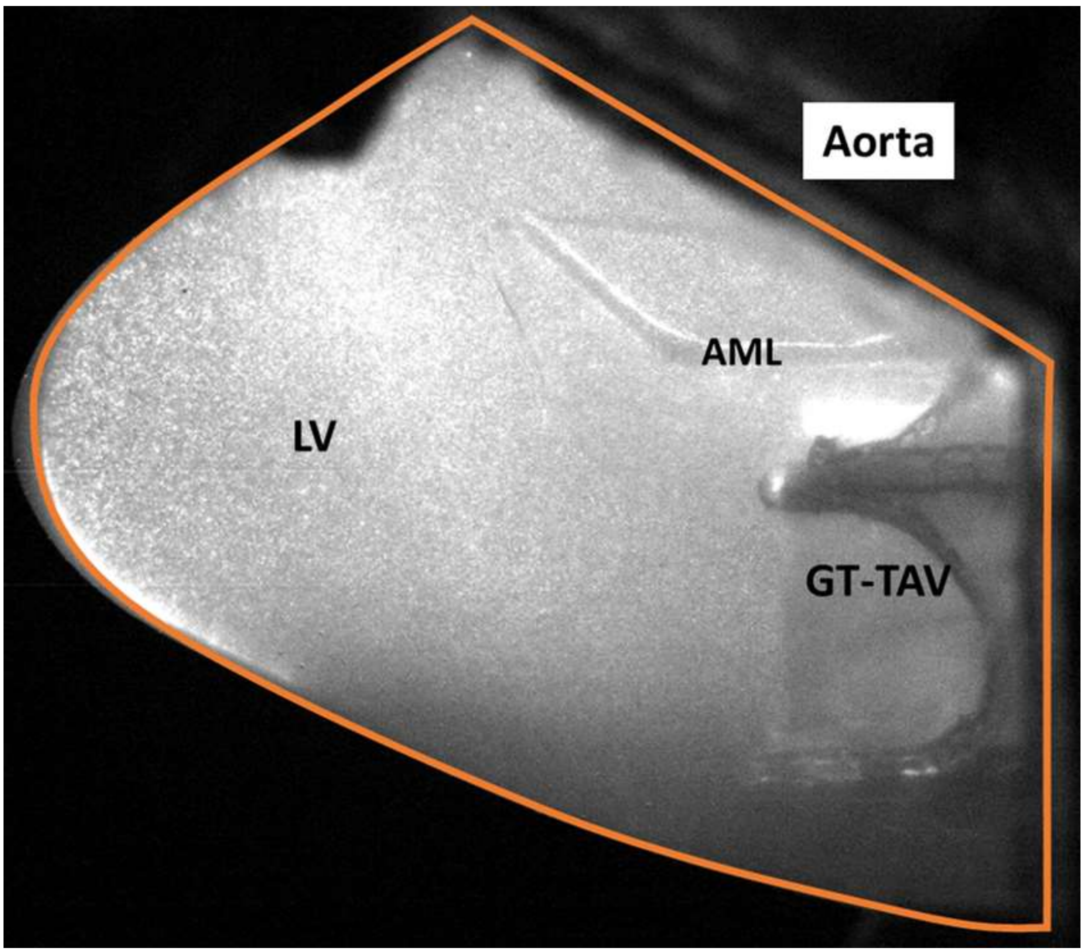

Figure 7-1. Diagram of Long AML raw image for better anatomical reference when looking at Specific Aim 2A PIV results. Orange is the PIV ROI and the AML and GT-TAV are masked out.

During peak systole, the average LVOT velocity measured was 0.46 m/s occurring with 0% LAMPOON at 6.5 L/min. Holding cardiac output constant across conditions, the average LVOT velocity showed a decreasing trend as LAMPOON length increased for 80/20 and 50/50 Long AML conditions, but not for the 50/50 Short (Figure 7-2; Figure 7-3; Figure 7-4; Figure 7-5; Figure 7-6).

Maximum VSS measured over the cardiac cycle peaked at 1.4 N/m^2 occurring with 0% LAMPOON at 6.5 L/min. Holding cardiac output constant across conditions, the maximum VSS showed a decreasing trend as LAMPOON length increased for all deployment and AML lengths (Figure 7-7; Figure 7-8; Figure 7-9; Figure 7-10; Figure 7-11).

Maximum principal RSS measured over the cardiac cycle peaked at 71.2 N/m^2 occurring with 0% LAMPOON at 6.5 L/min. No trend was seen with maximum principal RSS between LAMPOON conditions (Figure 7-12; Figure 7-13; Figure 7-14; Figure 7-15; Figure 7-16).

Maximum TKE measured over the cardiac cycle peaked at 0.084 m^2/s^2 occurring with 0% LAMPOON at 6.5 L/min. No trend was seen with maximum TKE between LAMPOON conditions (Figure 7-17; Figure 7-18; Figure 7-19; Figure 7-20; Figure 7-21).

During mid-diastole, holding cardiac output constant across conditions, vorticity size and magnitude in the LV showed an increasing trend with increasing LAMPOON (Figure 7-22; Figure 7-23; Figure 7-24). The increased vorticity size and magnitude translated to increased flow into the LVOT and anterior side of the GT-TAV during mid-diastole.

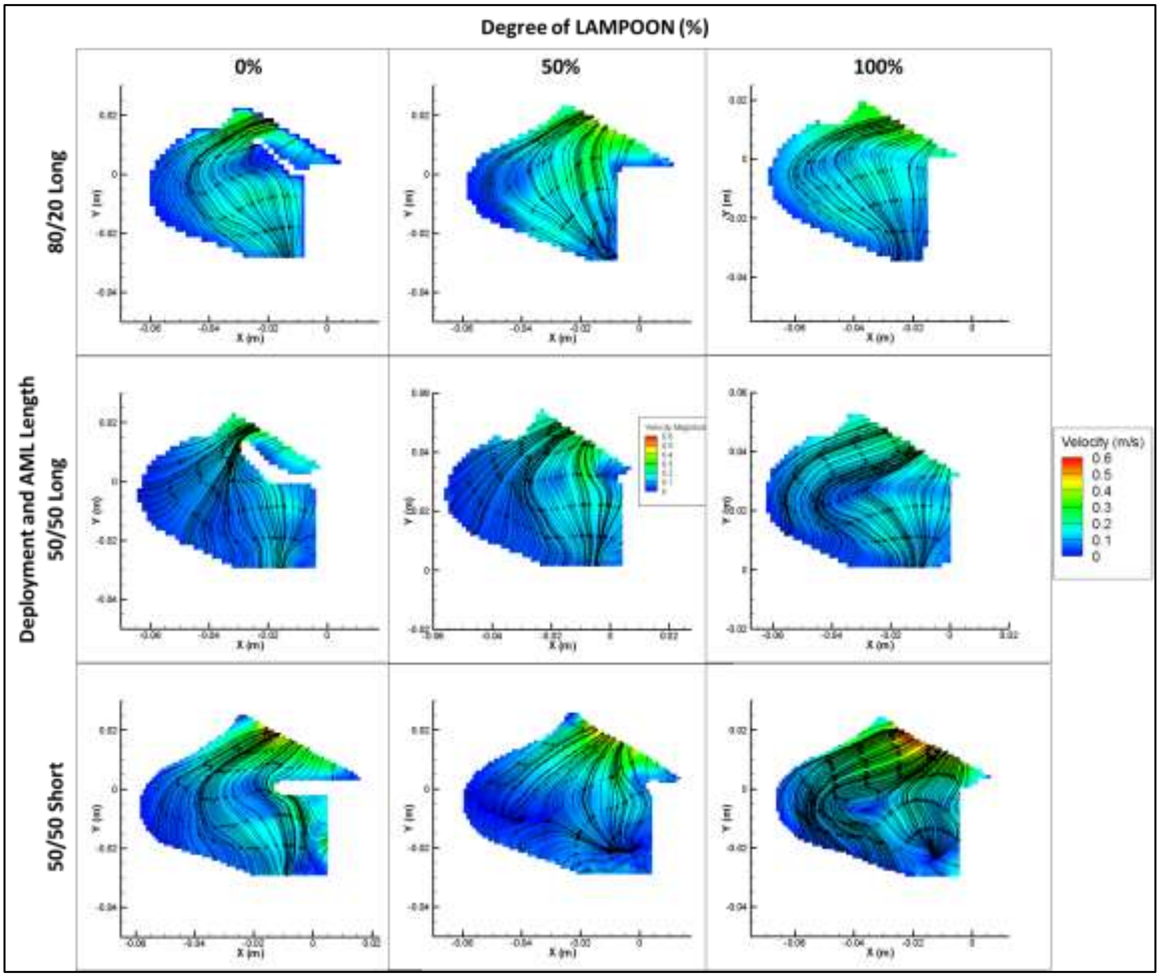

Figure 7-2. Velocity fields with instantaneous streamlines at peak systole at 2.5 L/min at each condition.

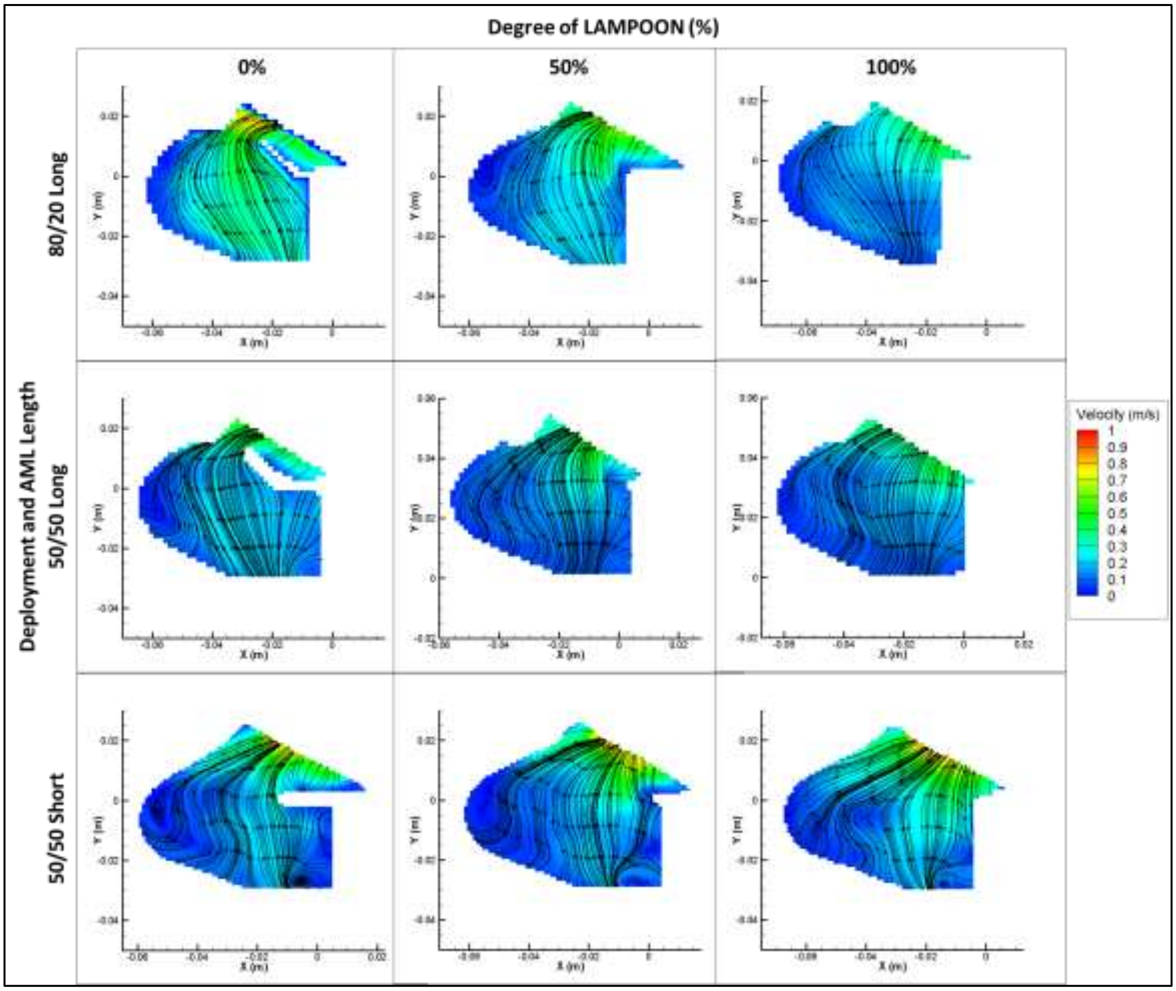

Figure 7-3. Velocity fields with instantaneous streamlines at peak systole at 5.0 L/min at each condition.

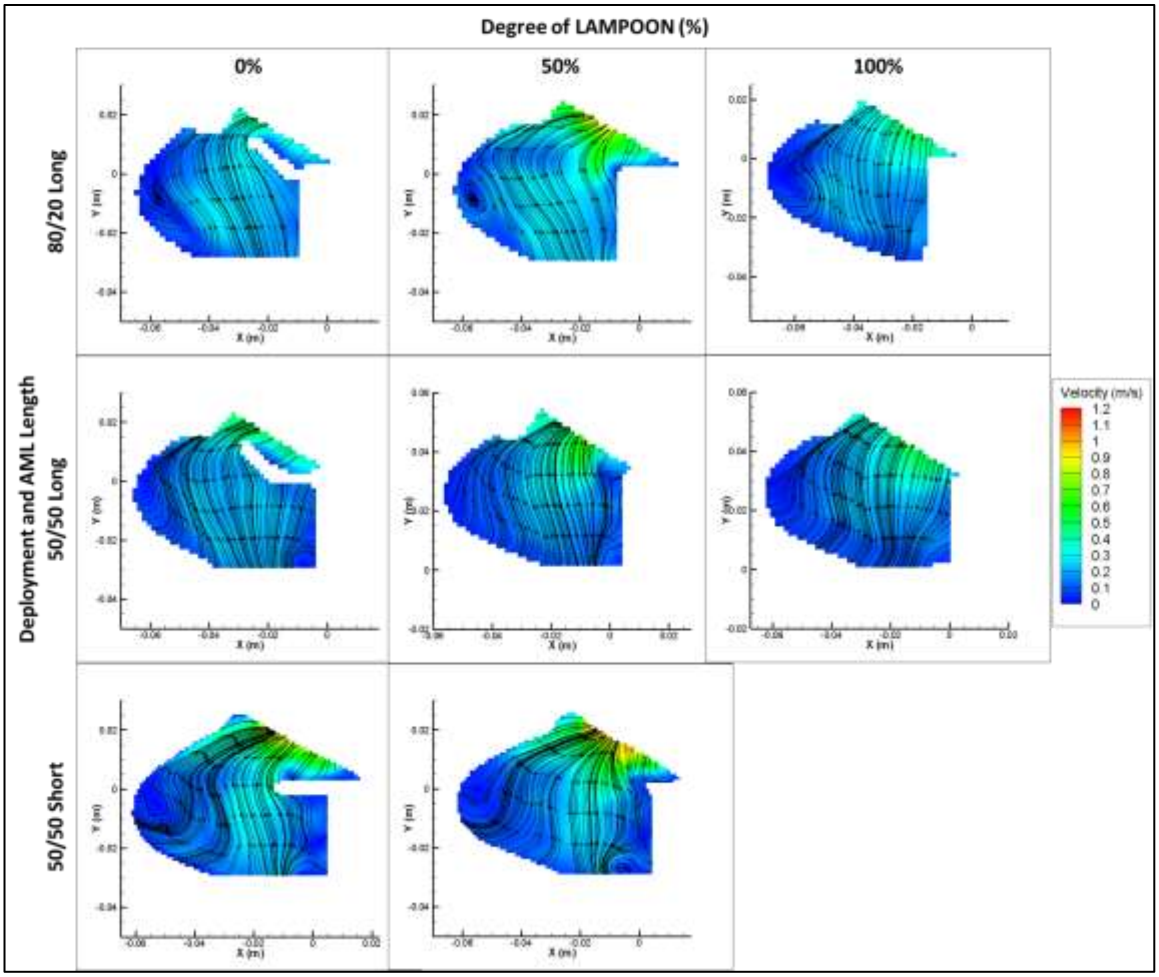

Figure 7-4. Velocity fields with instantaneous streamlines at peak systole at 6.5 L/min at each condition.

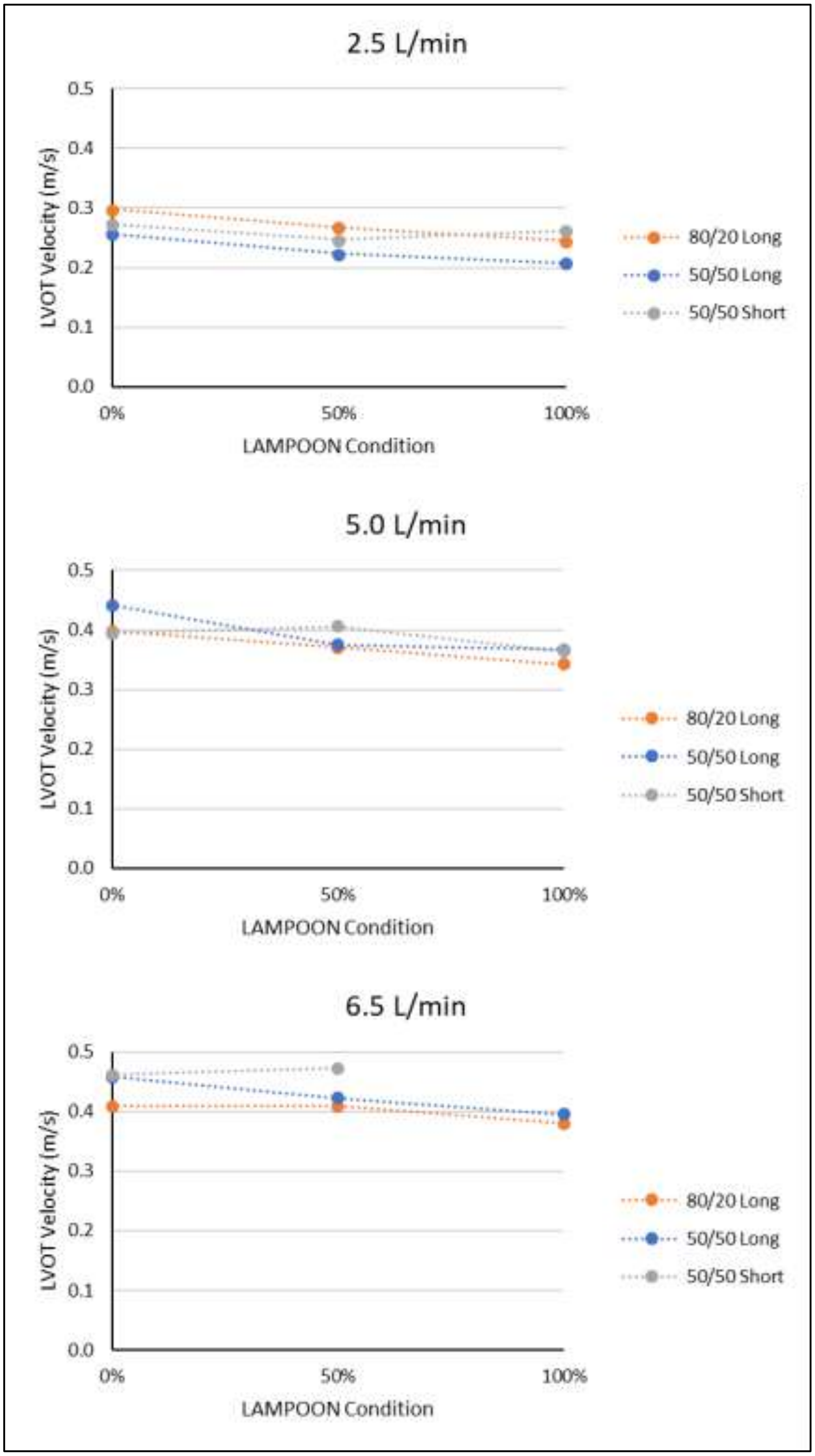

Figure 7-5. **Average LVOT velocities at peak systole at each condition.**

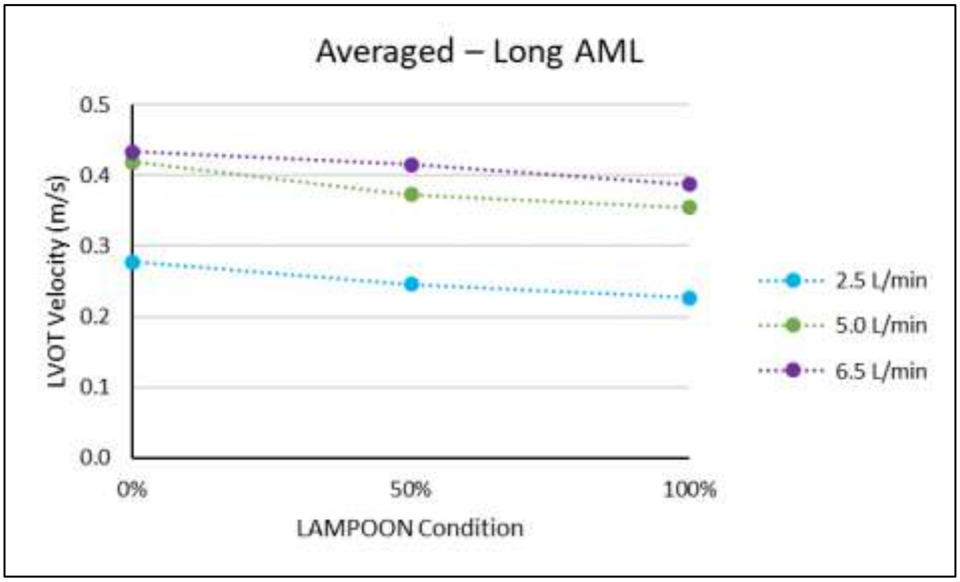

Figure 7-6. Average LVOT velocities at peak systole averaged across both Long AML conditions (80/20 and 50/50 ventricular/atrial).

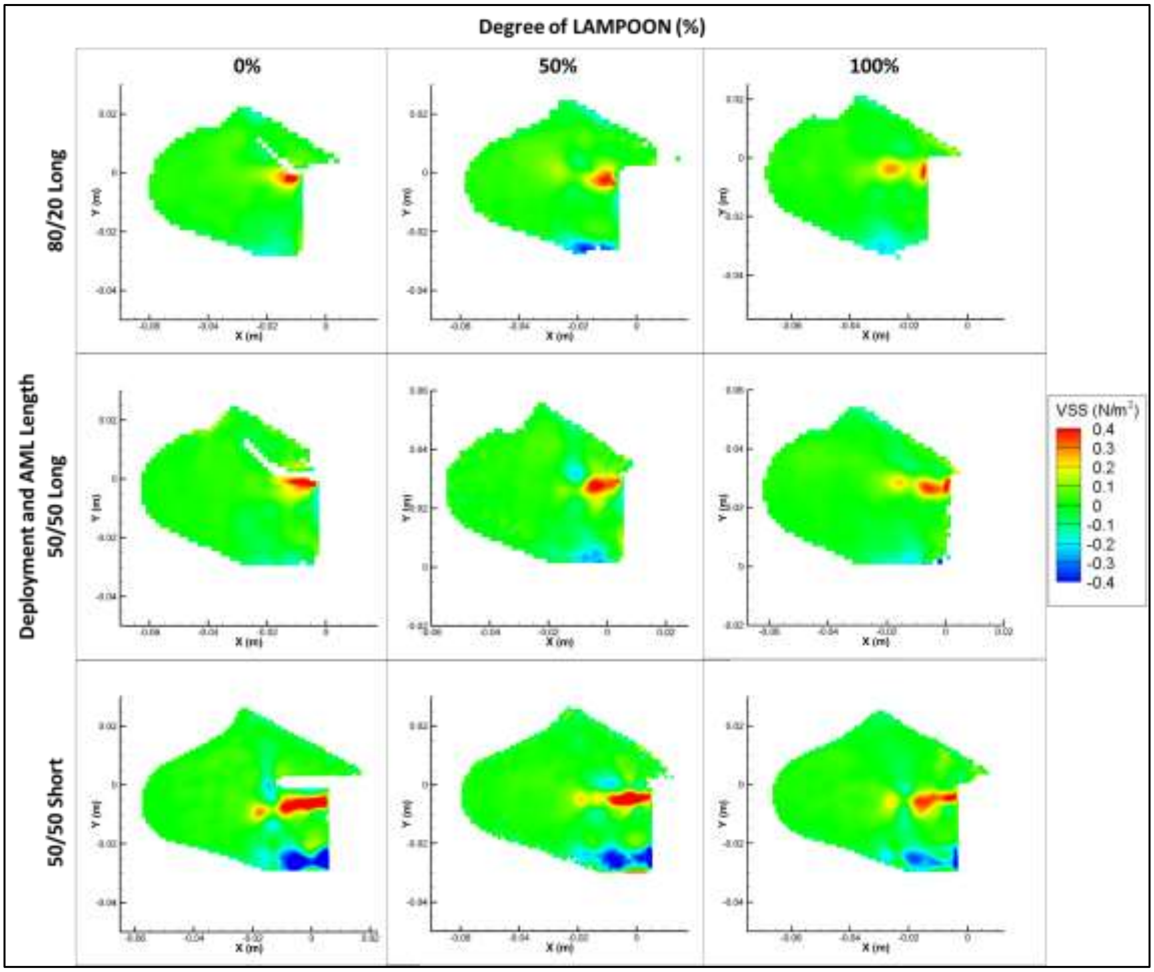

Figure 7-7. Frames containing maximum VSS in the cardiac cycle at 2.5 L/min for each condition.

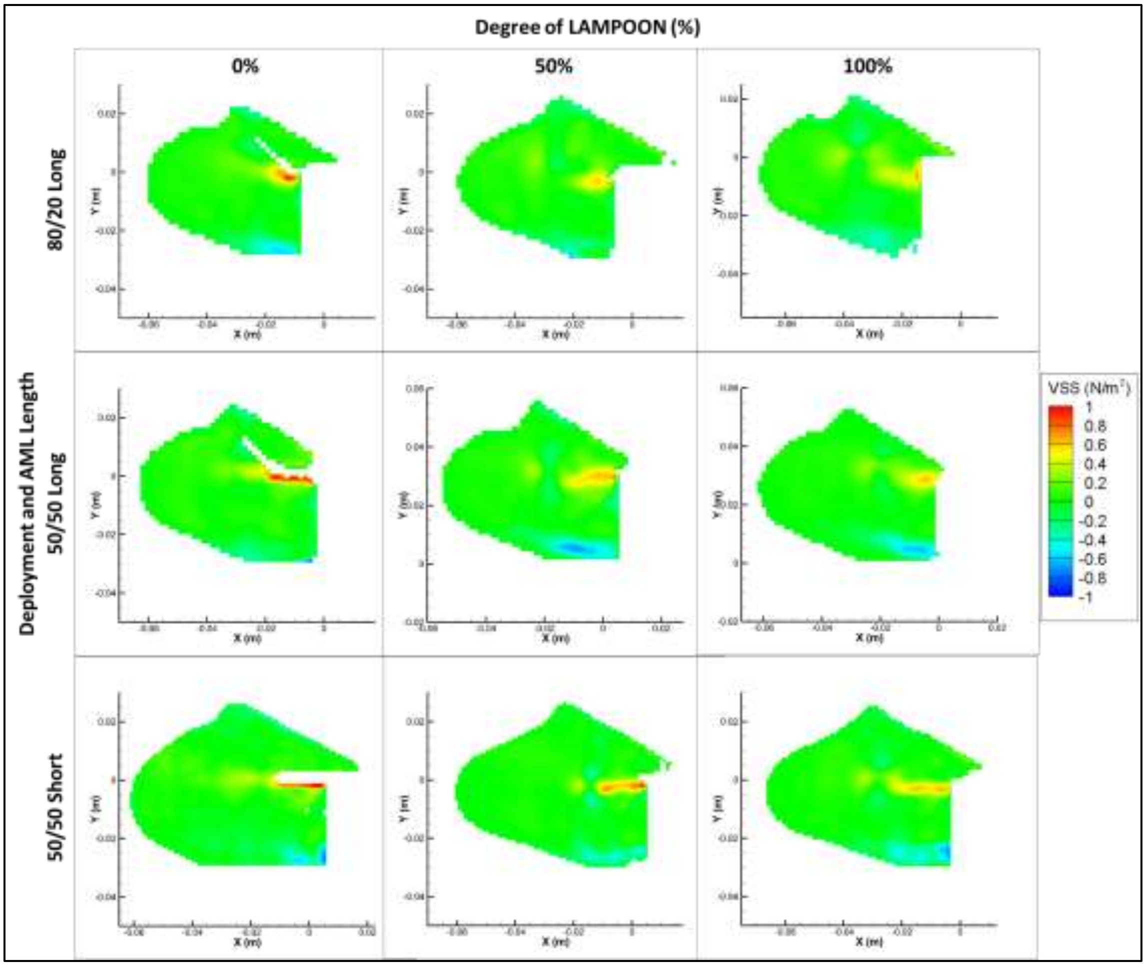

Figure 7-8. Frames containing maximum VSS in the cardiac cycle at 5.0 L/min for each condition.

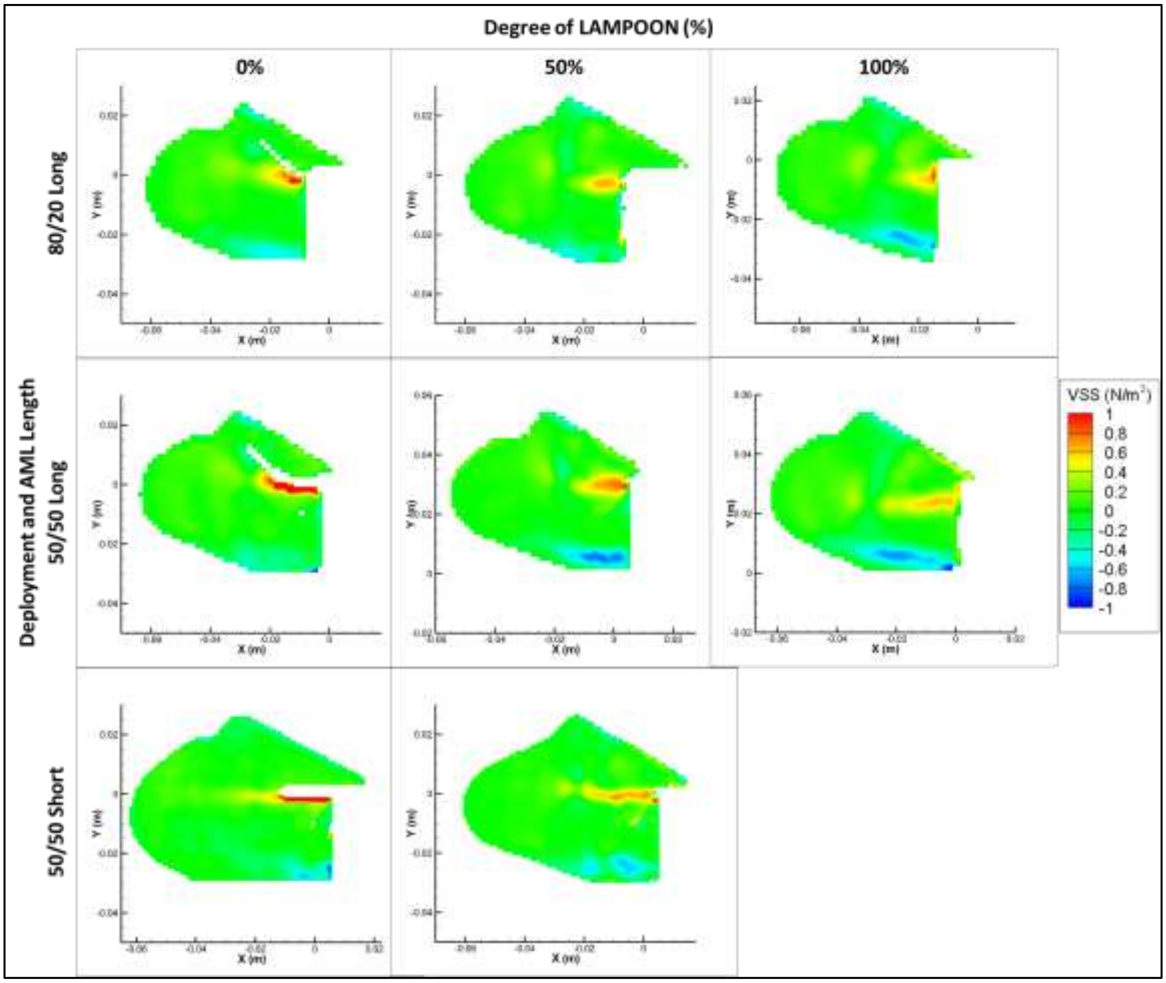

Figure 7-9. Frames containing maximum VSS in the cardiac cycle at 6.5 L/min for each condition.

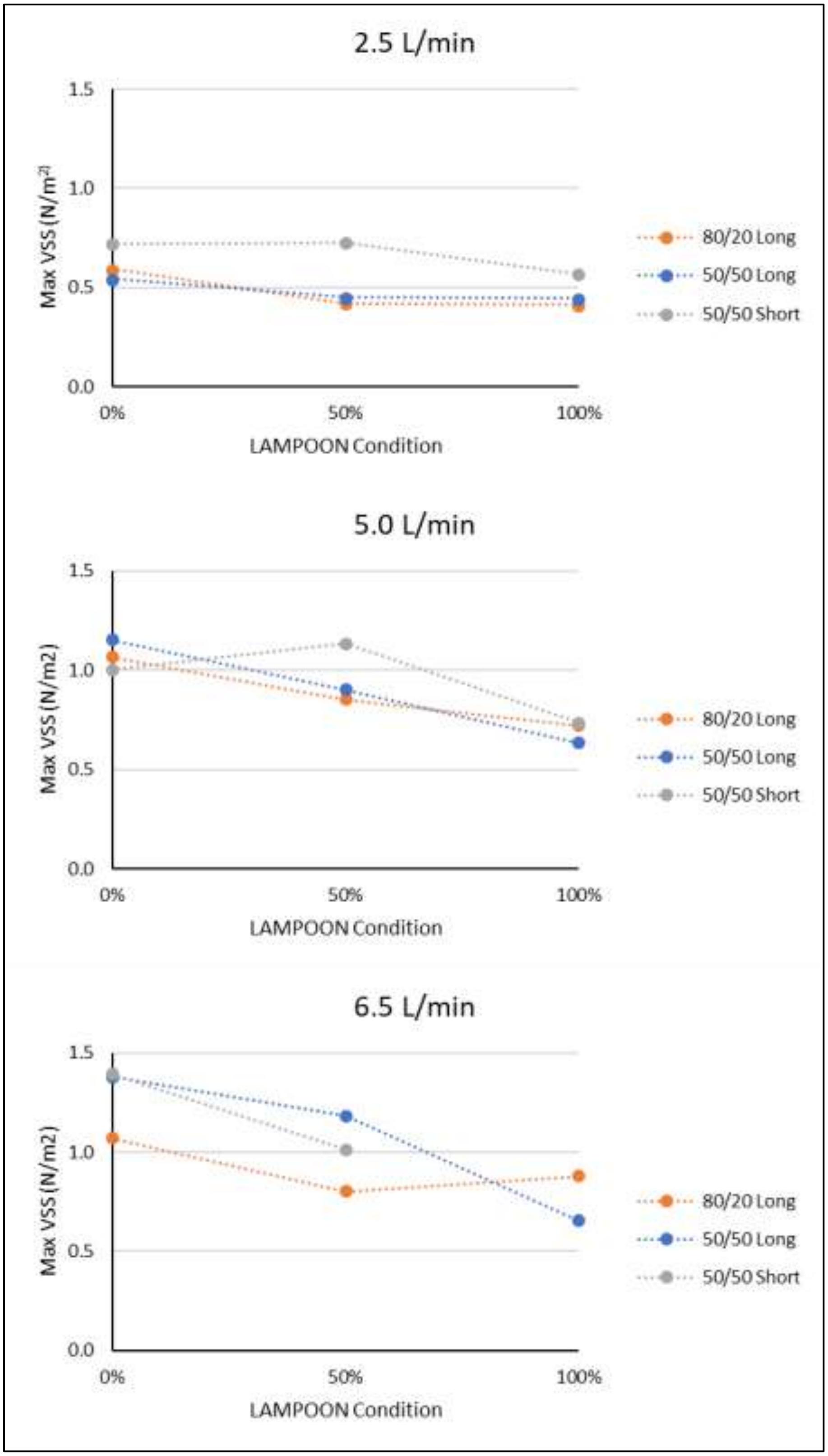

Figure 7-10. Maximum VSS in the LV over the cardiac cycle at each condition.

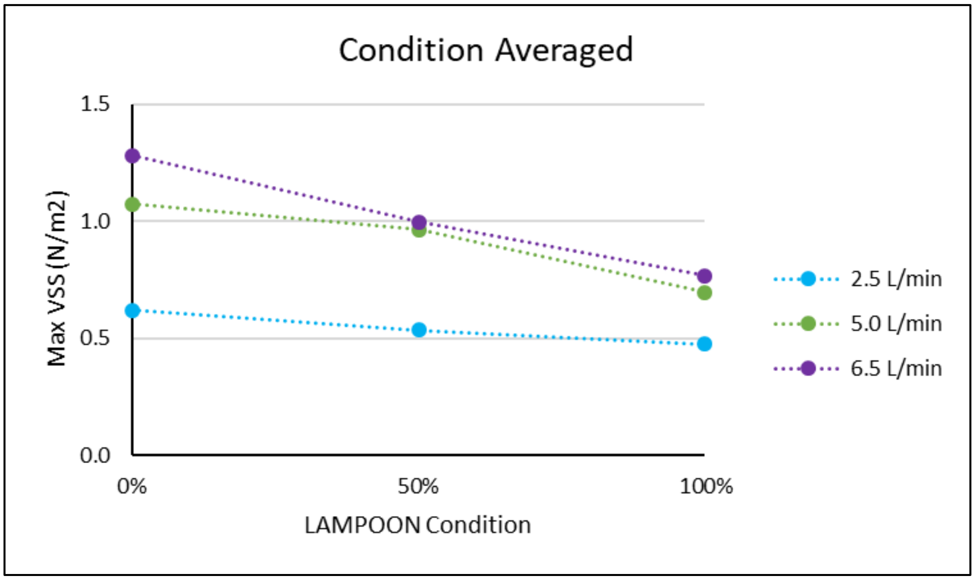

Figure 7-11. Maximum VSS in the LV over the cardiac cycle averaged across all AML and deployment conditions.

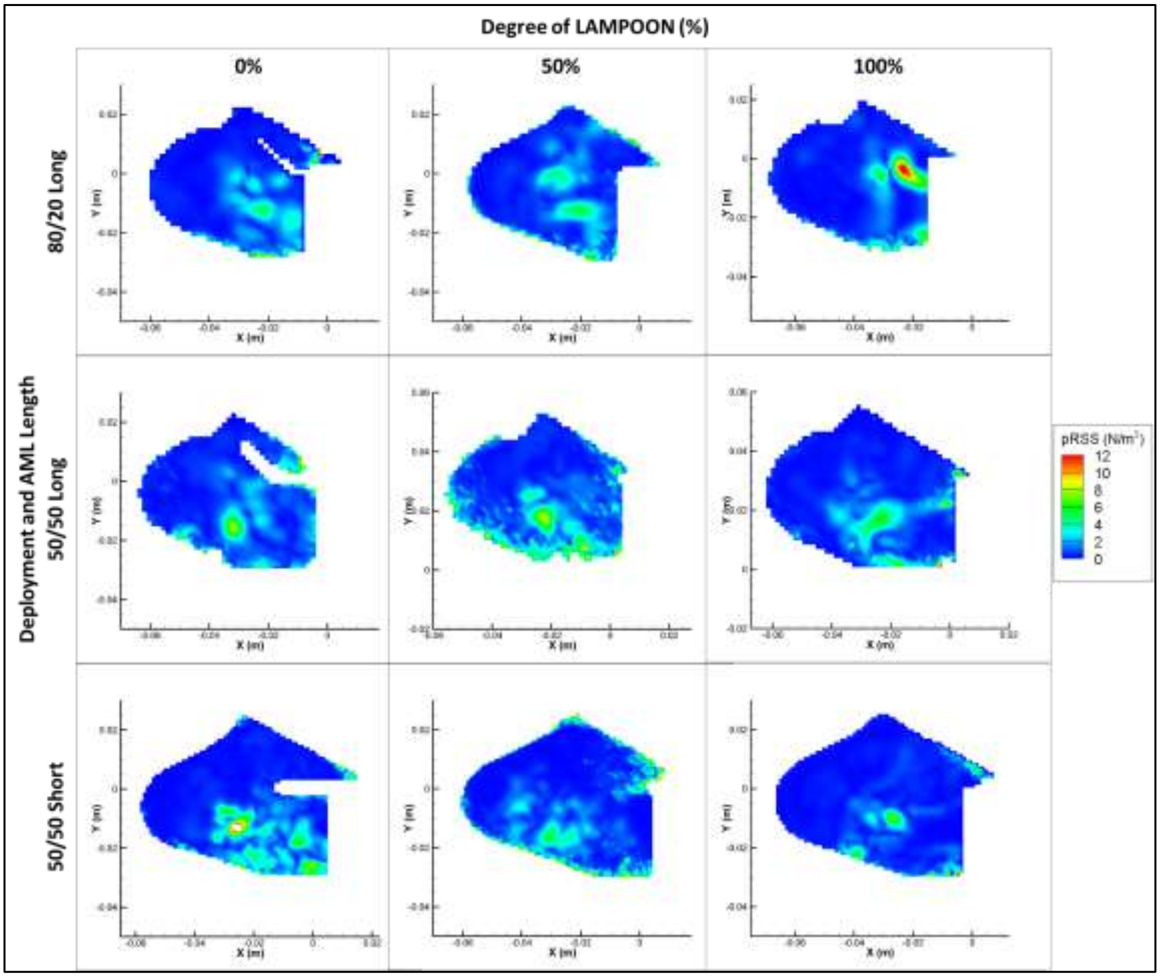

Figure 7-12. Frames containing maximum principal RSS in the cardiac cycle at 2.5 L/min for each condition.

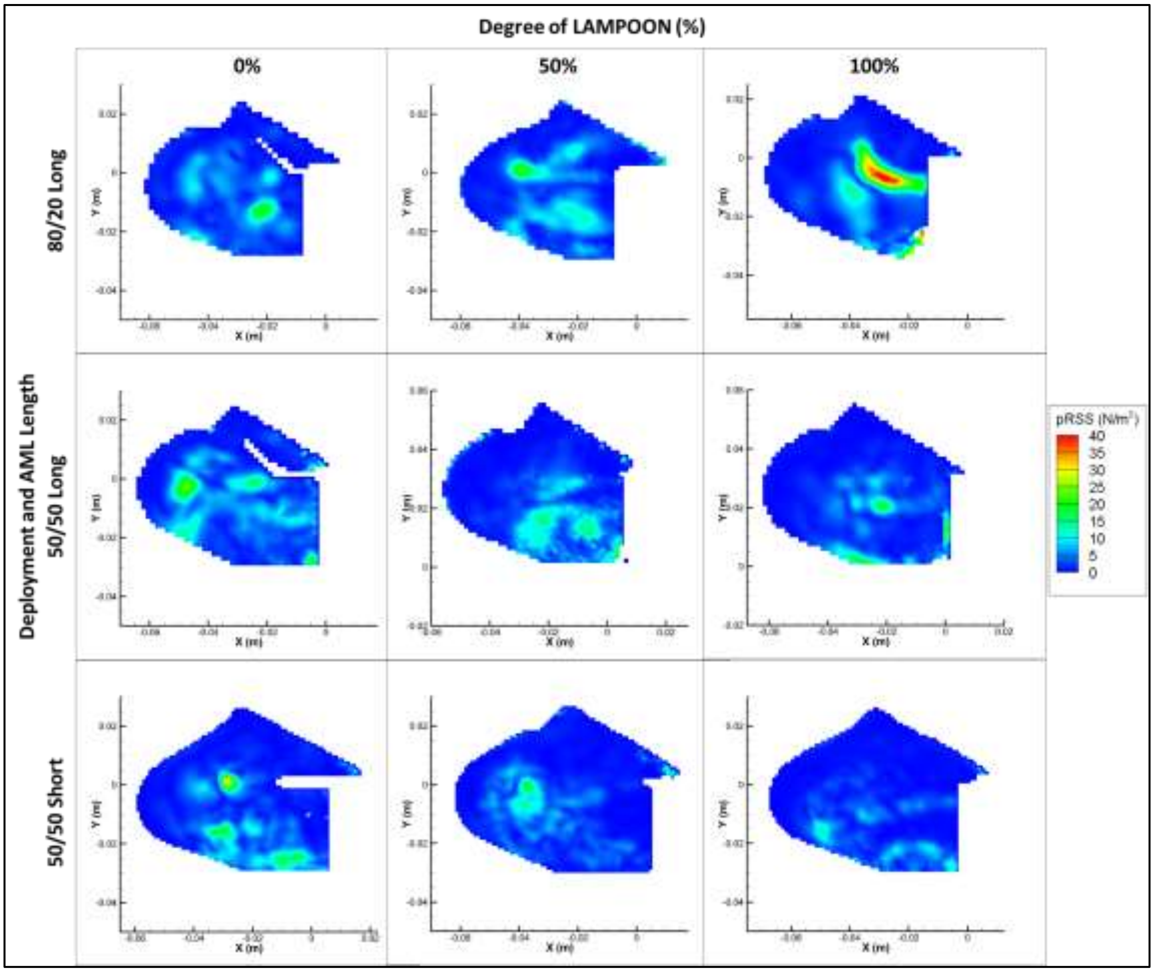

Figure 7-13. Frames containing maximum principal RSS in the cardiac cycle at 5.0 L/min for each condition.

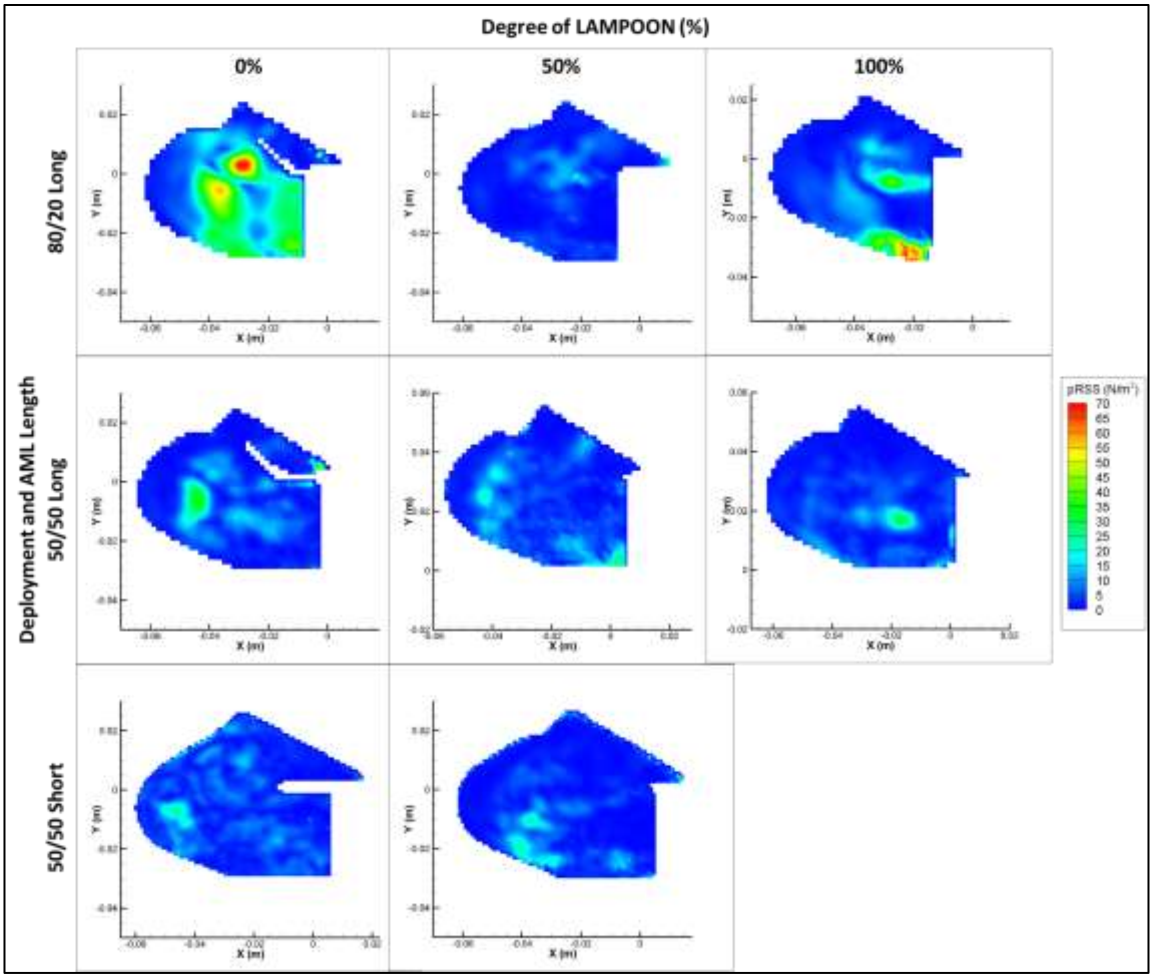

Figure 7-14. Frames containing maximum principal RSS in the cardiac cycle at 6.5 L/min for each condition.

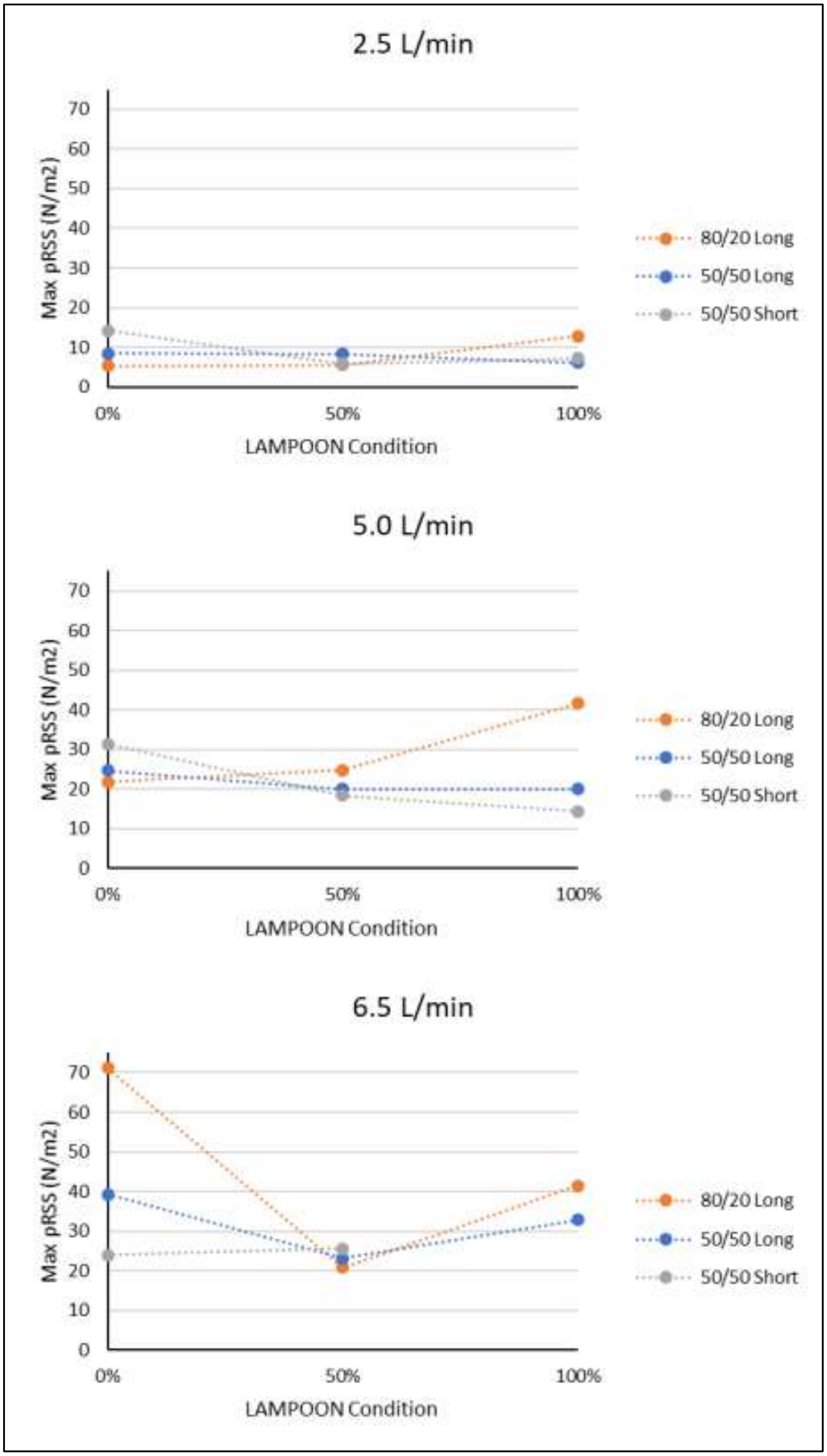

Figure 7-15. Maximum principal RSS over the cardiac cycle at each condition.

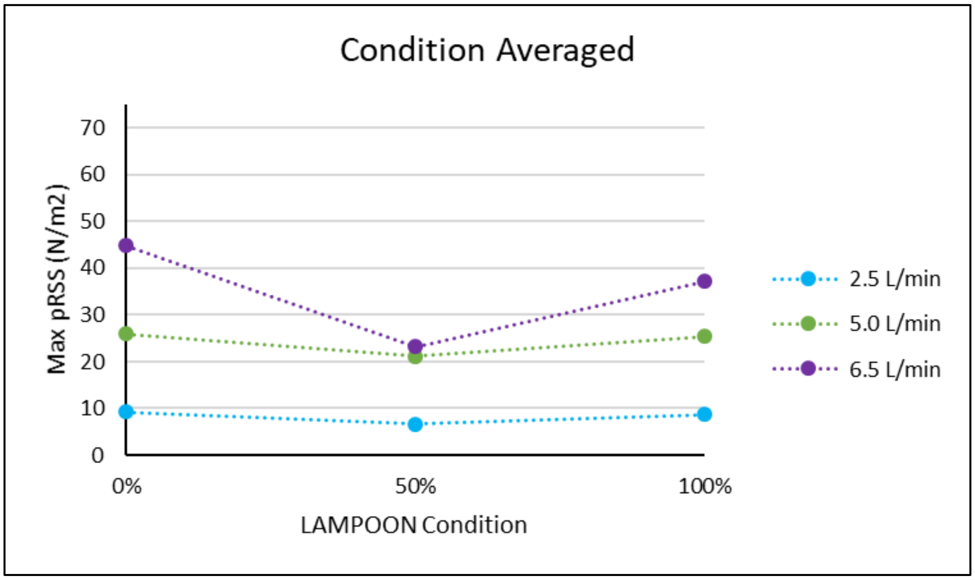

Figure 7-16. Maximum principal RSS over the cardiac cycle averaged across all AML and deployment conditions.

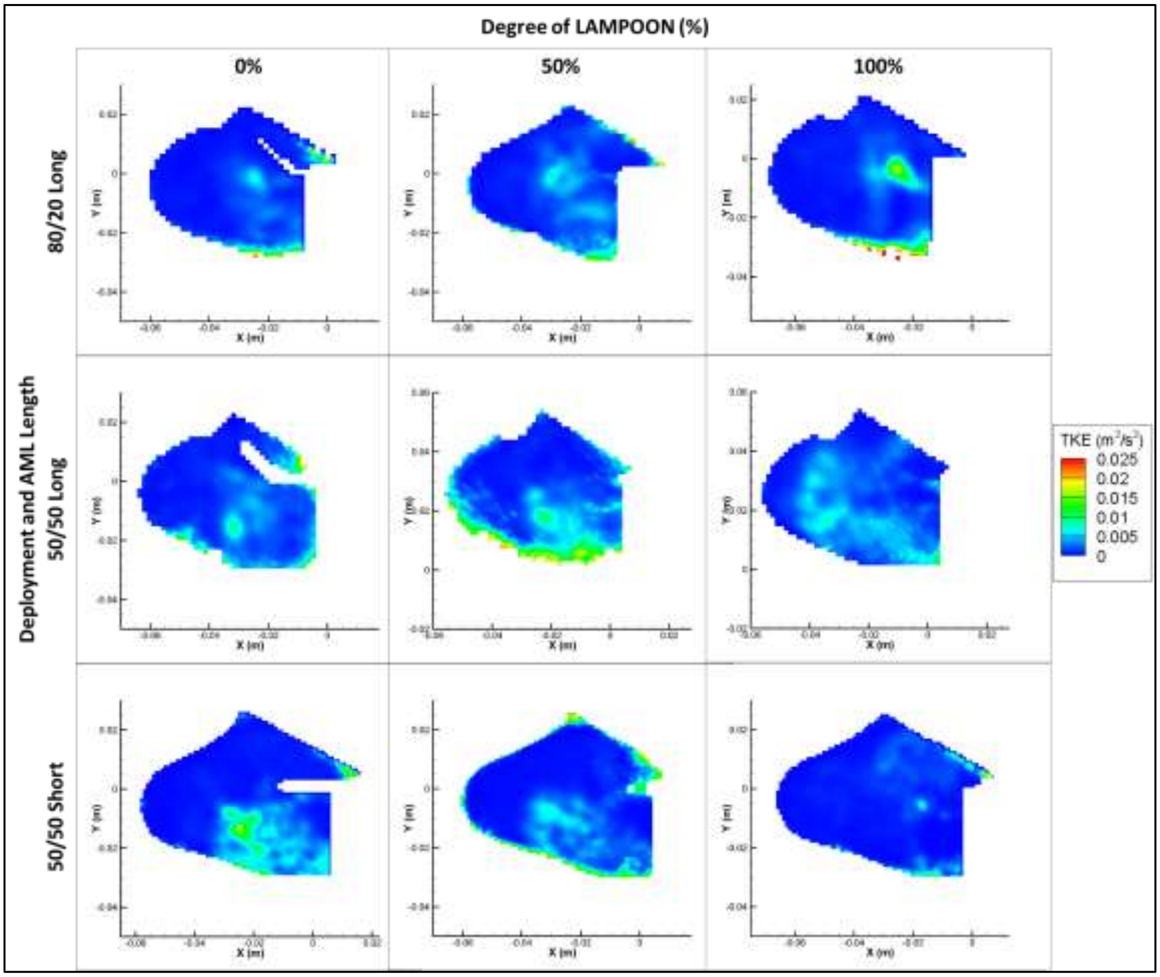

Figure 7-17. Frames containing maximum TKE in the cardiac cycle at 2.5 L/min for each condition.

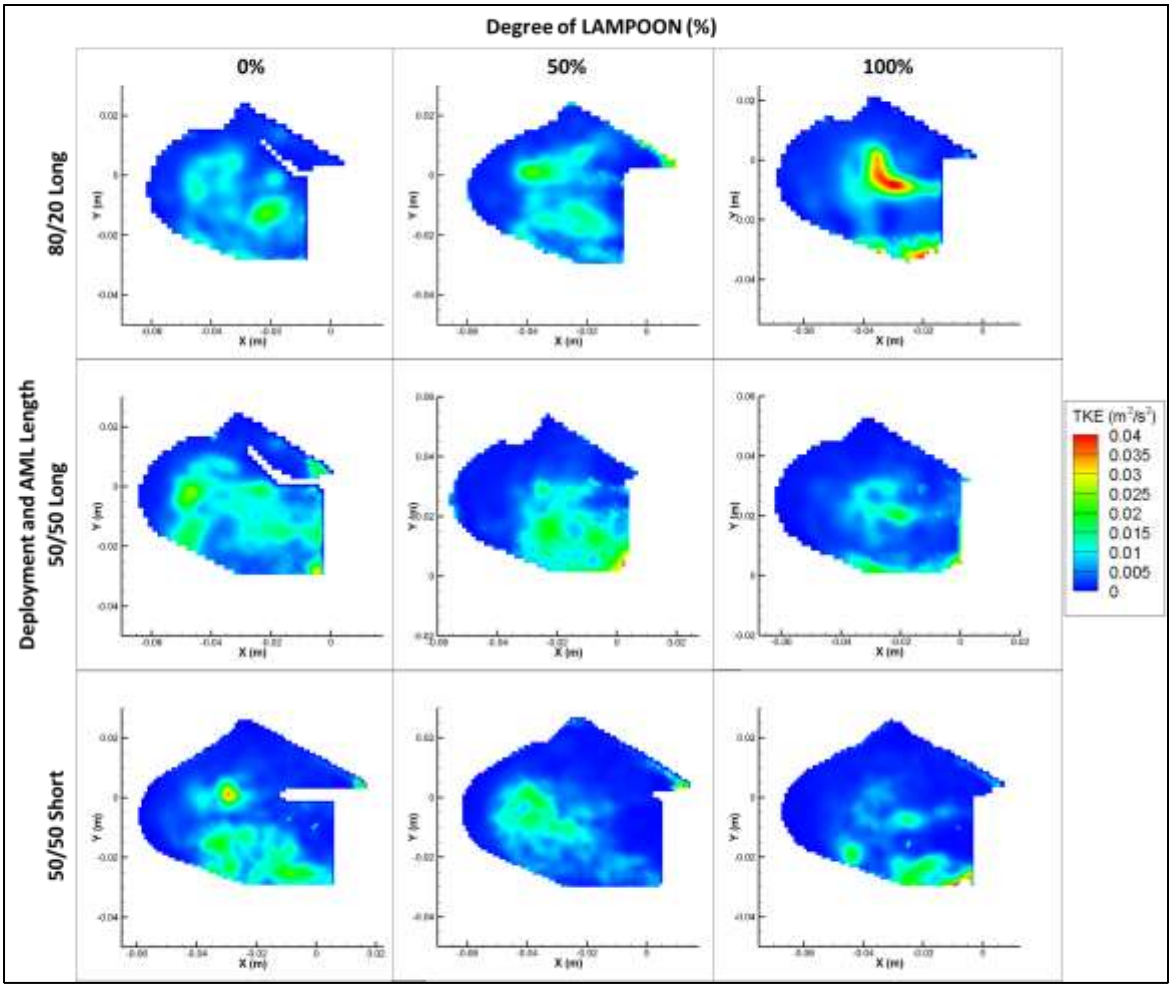

Figure 7-18. Frames containing maximum TKE in the cardiac cycle at 5.0 L/min for each condition.

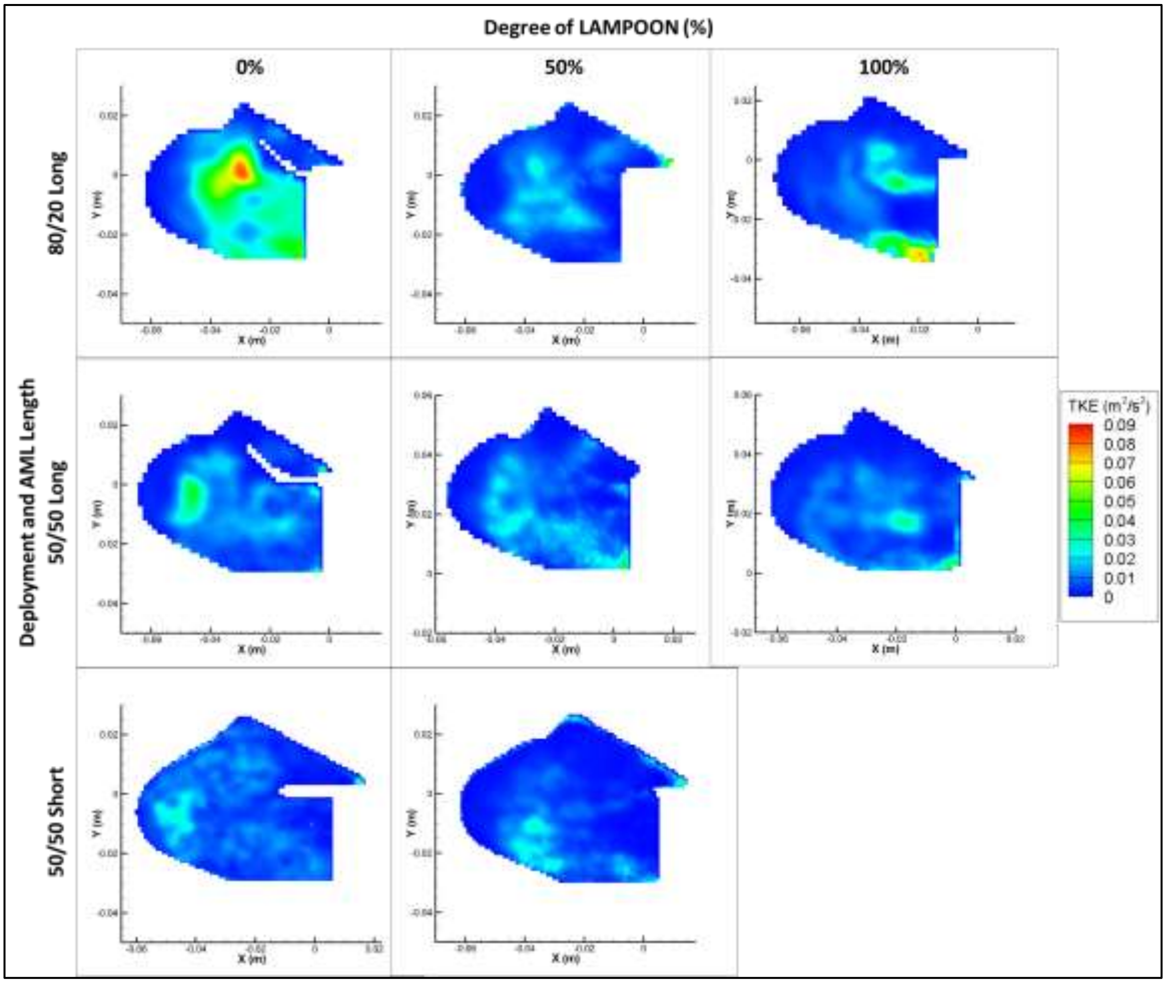

Figure 7-19. Frames containing maximum TKE in the cardiac cycle at 6.5 L/min for each condition.

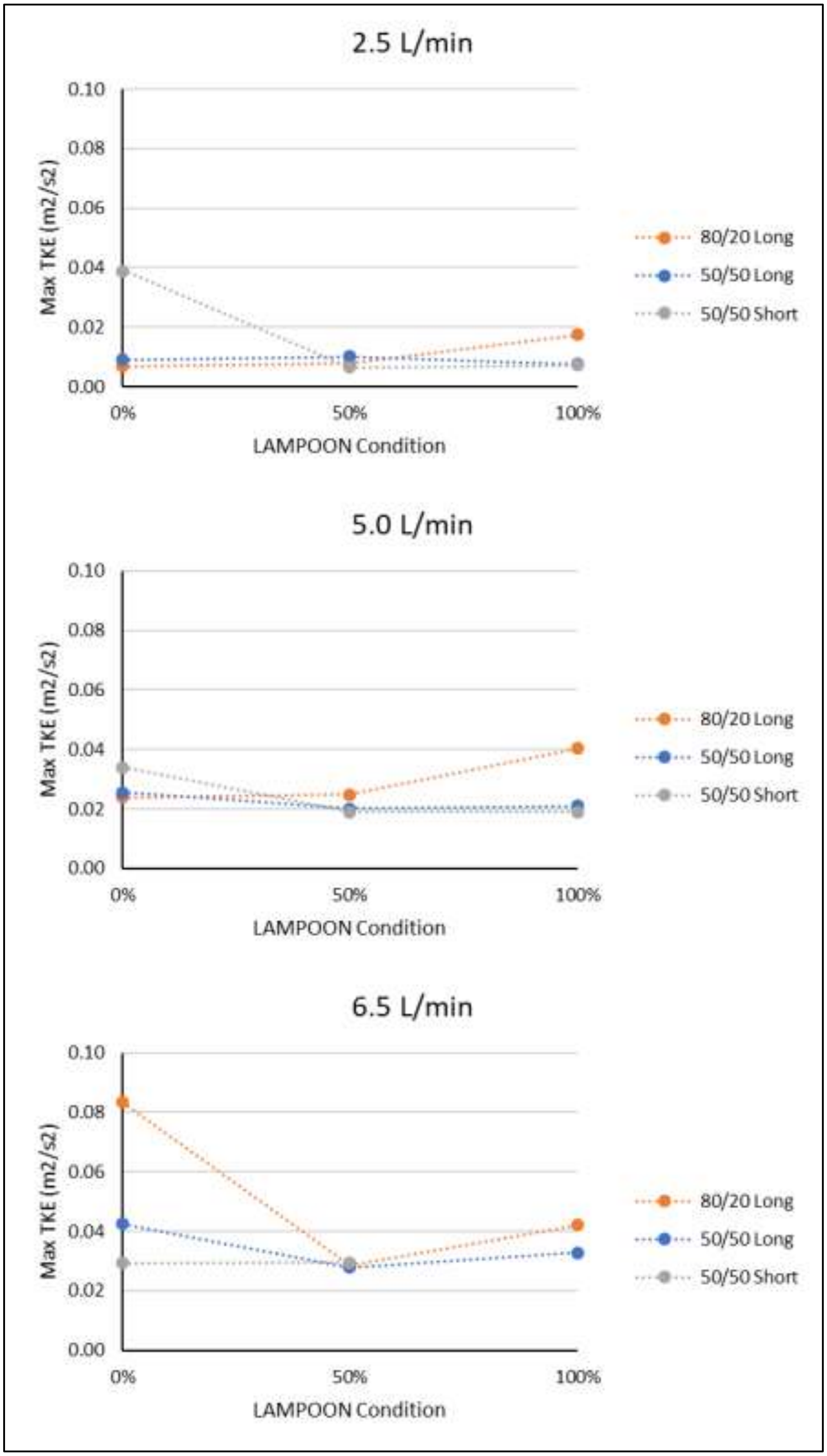

Figure 7-20. Maximum TKE over the cardiac cycle across at each condition.

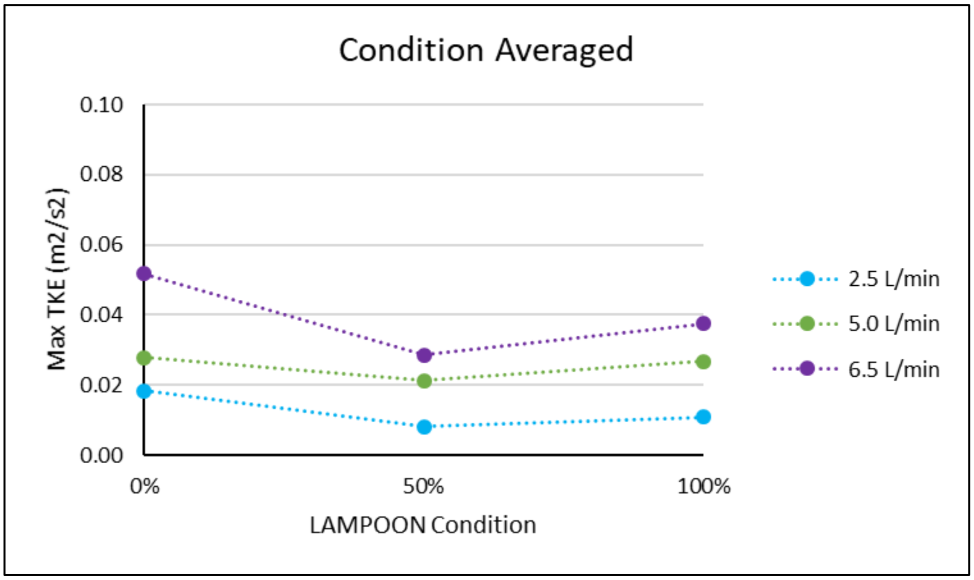

Figure 7-21. Maximum TKE over the cardiac cycle averaged across all AML and deployment conditions.

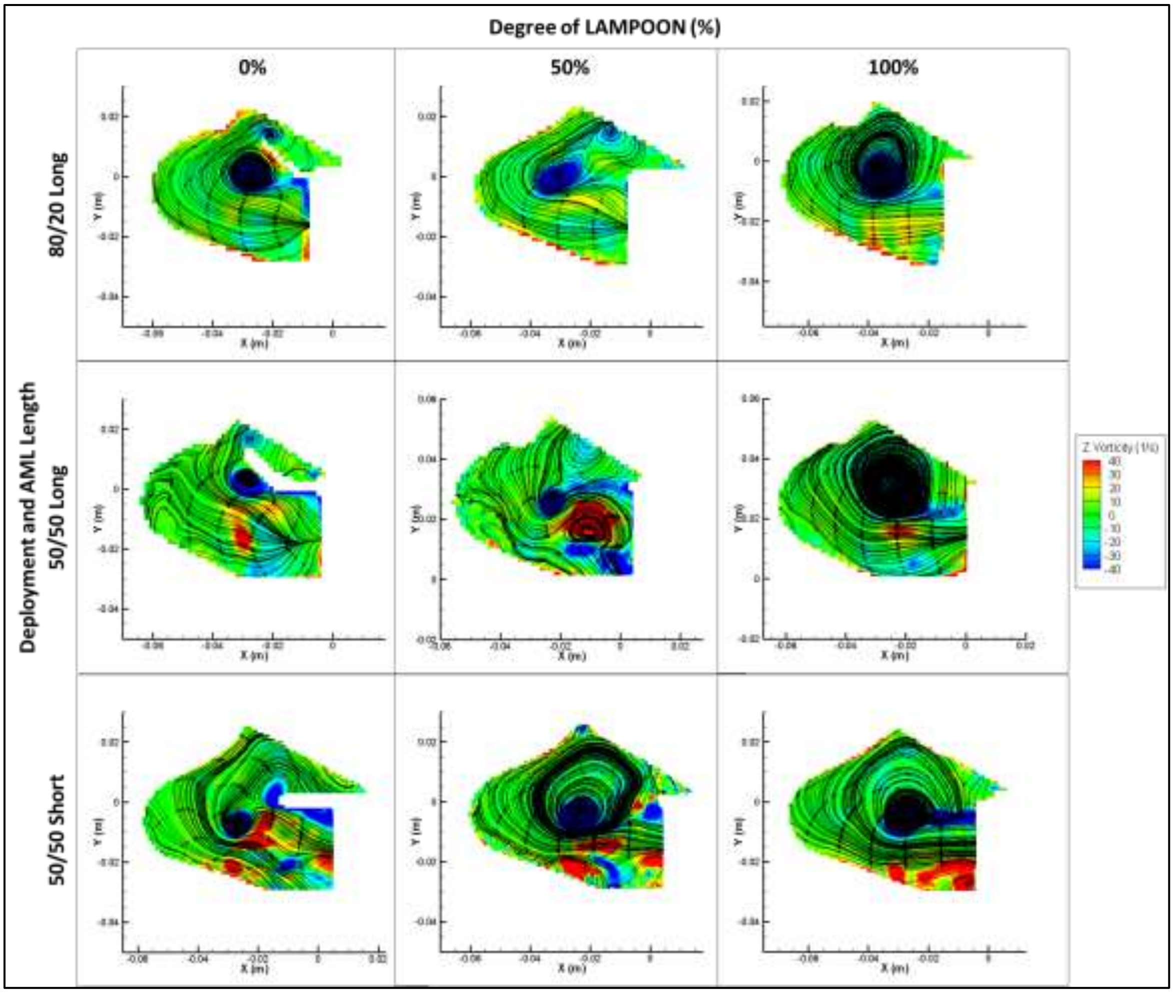

Figure 7-22. Vorticity fields with instantaneous streamlines at mid-diastole at 2.5 L/min at each condition.

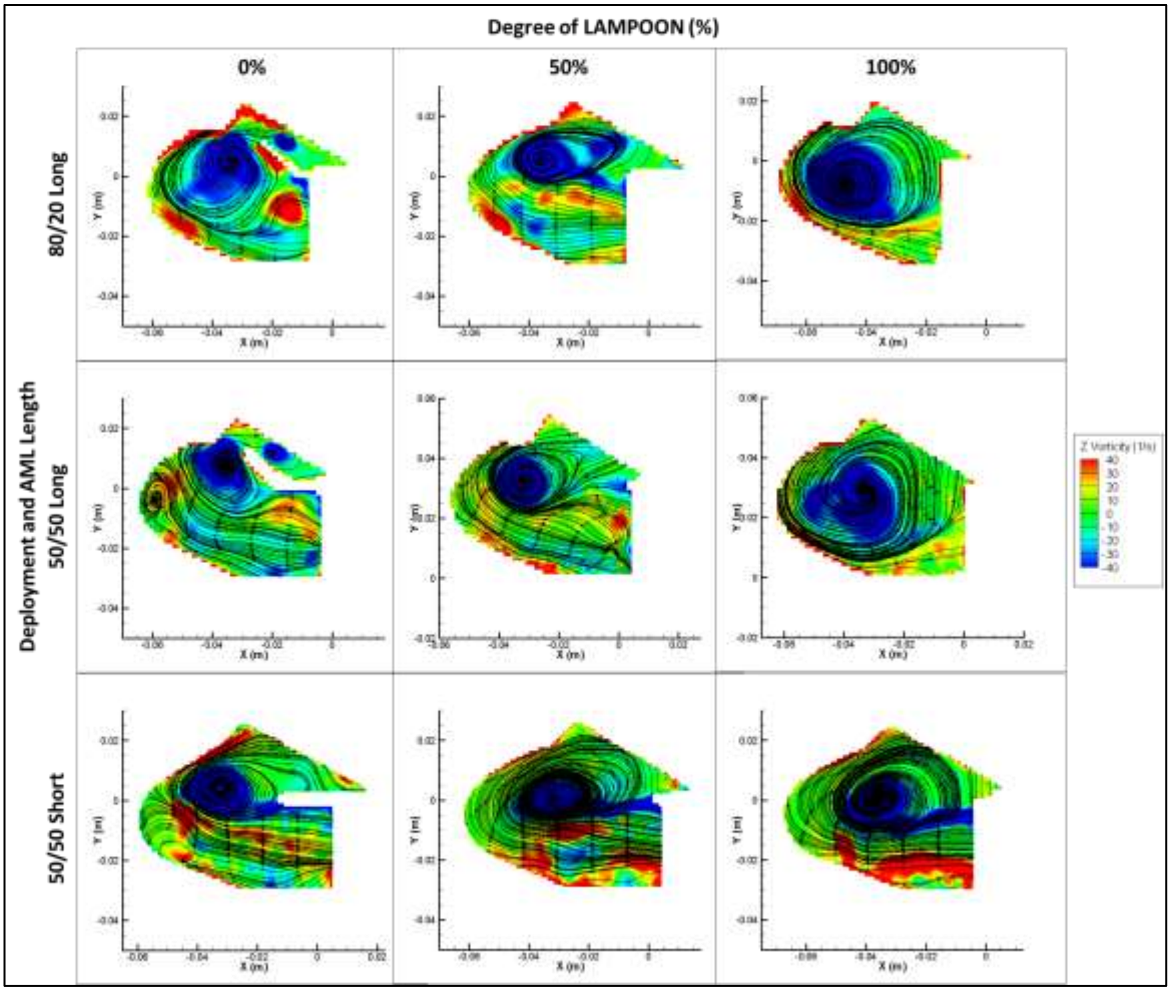

Figure 7-23. Vorticity fields with instantaneous streamlines at mid-diastole at 5.0 L/min at each condition.

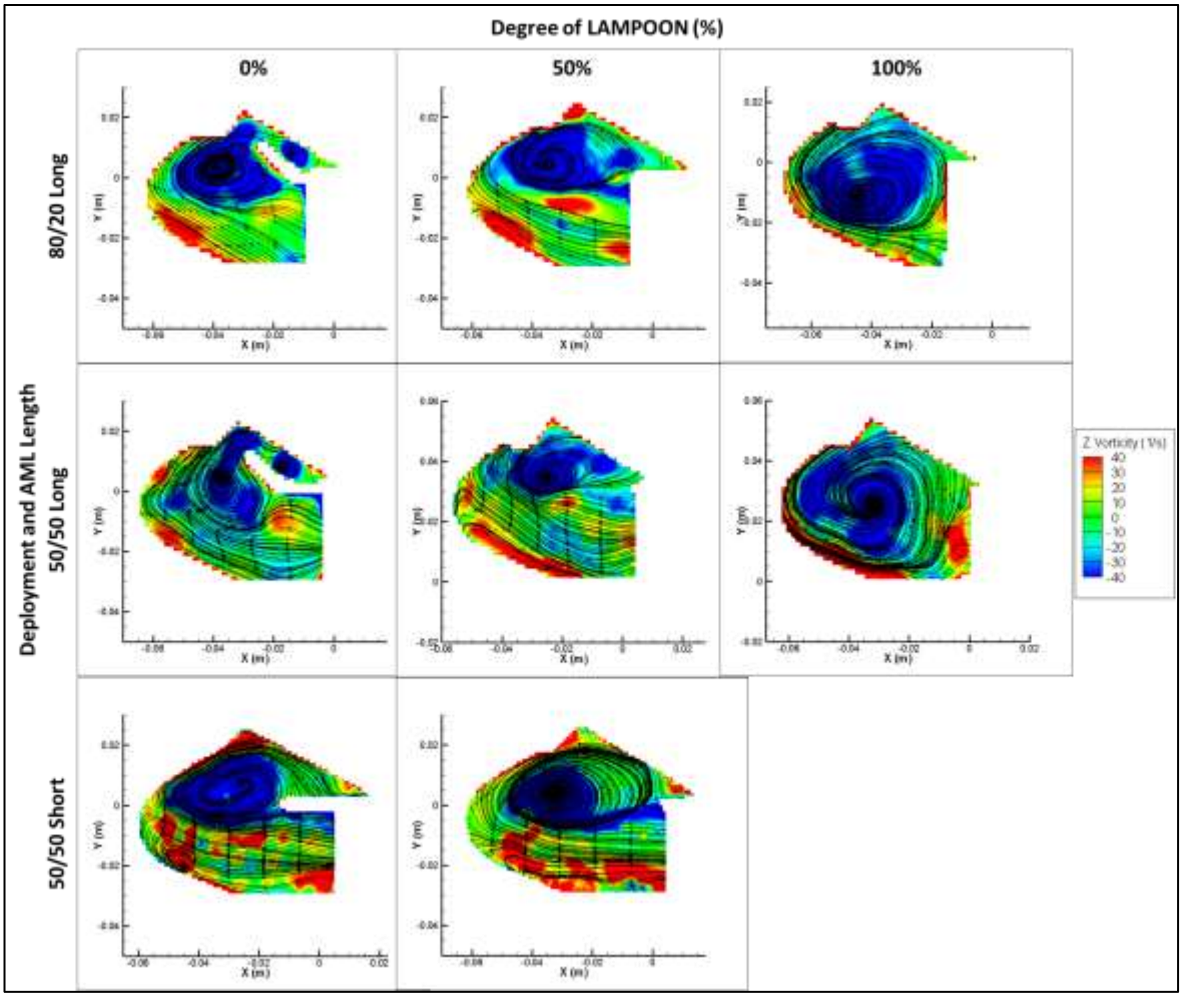

Figure 7-24. Vorticity fields with instantaneous streamlines at mid-diastole at 6.5 L/min at each condition.

7.1.2 Specific Aim 2B: Neo-Sinus Flow with LAMPOON

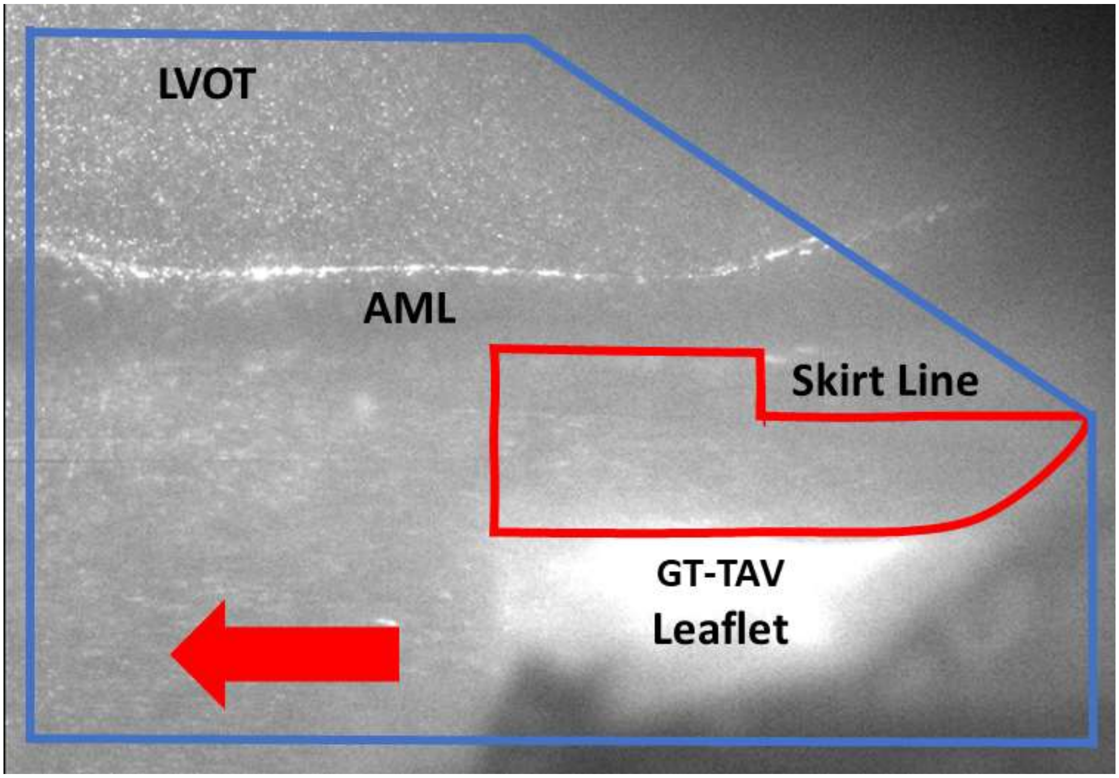

Figure 7-25. Diagram of Long AML raw image for better anatomical reference when looking at Specific Aim 2B PIV results. Blue is the PIV ROI, red is anterior mitral neo-sinus, and the AML and GT-TAV leaflet is masked out.

All LAMPOON conditions at all cardiac outputs showed a maximum velocity magnitude of at least 0.1 m/s in the neo-sinus over the cardiac cycle (Figure 7-26; Figure 7-27; Table 7-1). The majority of the maximum velocities in the neo-sinus were shown to have occurred during systole (Figure 7-28; Figure 7-29; Table 7-2). The 100% LAMPOON condition showed a higher average velocity magnitude in the neo-sinus over the cardiac cycle compare to the 0% and 50% LAMPOON conditions (Figure 7-30; Figure 7-31; Table 7-3). This was shown to be a result of the 100% LAMPOON condition having higher velocity in the neo-sinus during diastole compared to the 0% and 50% LAMPOON conditions (Figure 7-32; Figure 7-33; Table 7-4). The 100% LAMPOON was subsequently shown to have better washout of the neo-sinus during diastole compared to the 0% and 50% LAMPOON conditions from particle tracking (Figure 7-34; Figure 7-35).

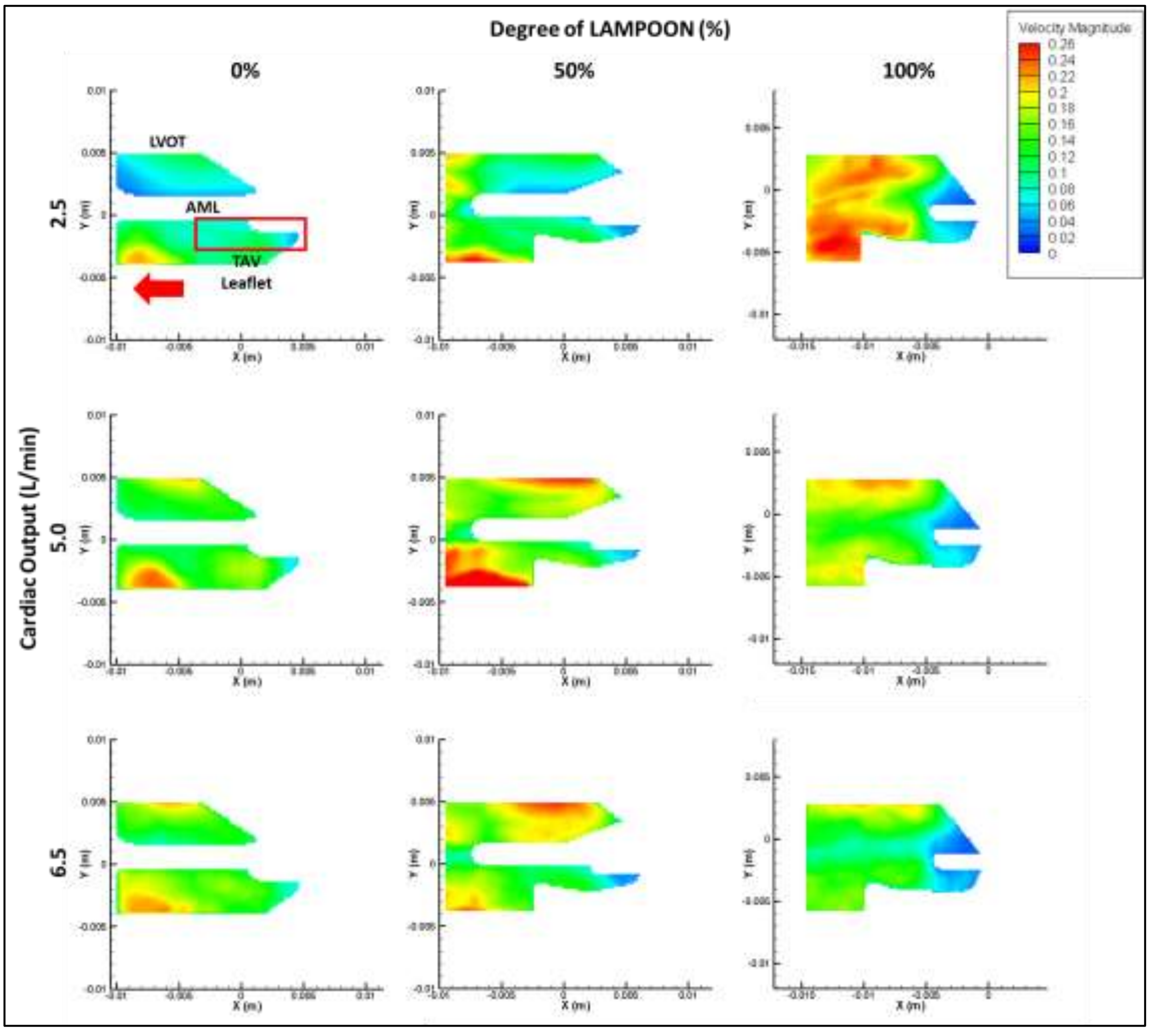

Figure 7-26. Cycle-maximum velocity magnitudes in the neo-sinus (highlighted by red box) of different LAMPOON conditions (0, 50, and 100%) at different cardiac outputs (2.5, 5.0, and 6.5 L/min).

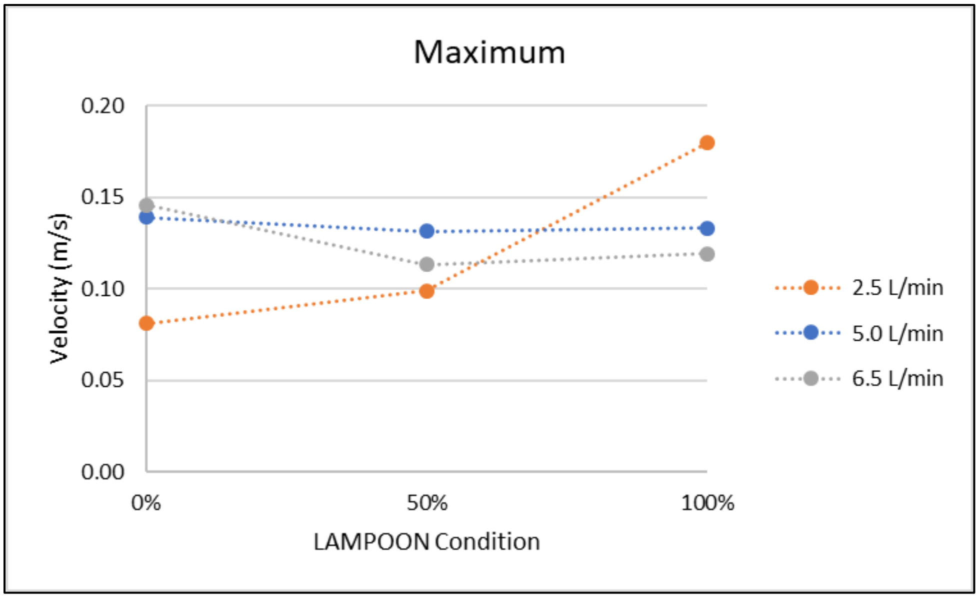

Figure 7-27. Average velocities within the neo-sinus for the cycle-maximum velocity magnitudes. Helps quantify Figure 7-26.

Table 7-1. Average and maximum velocities within the neo-sinus for the cycle-maximum velocity magnitudes. Helps quantify Figure 7-26.

Cardiac Output (L/min)	0% LAMPOON Average (m/s)	0% LAMPOON Maximum (m/s)	50% LAMPOON Average (m/s)	50% LAMPOON Maximum (m/s)	100% LAMPOON Average (m/s)	100% LAMPOON Maximum (m/s)
2.5	0.081	0.108	0.099	0.129	0.180	0.234
5.0	0.139	0.175	0.132	0.169	0.133	0.181
6.5	0.146	0.168	0.113	0.138	0.119	0.151

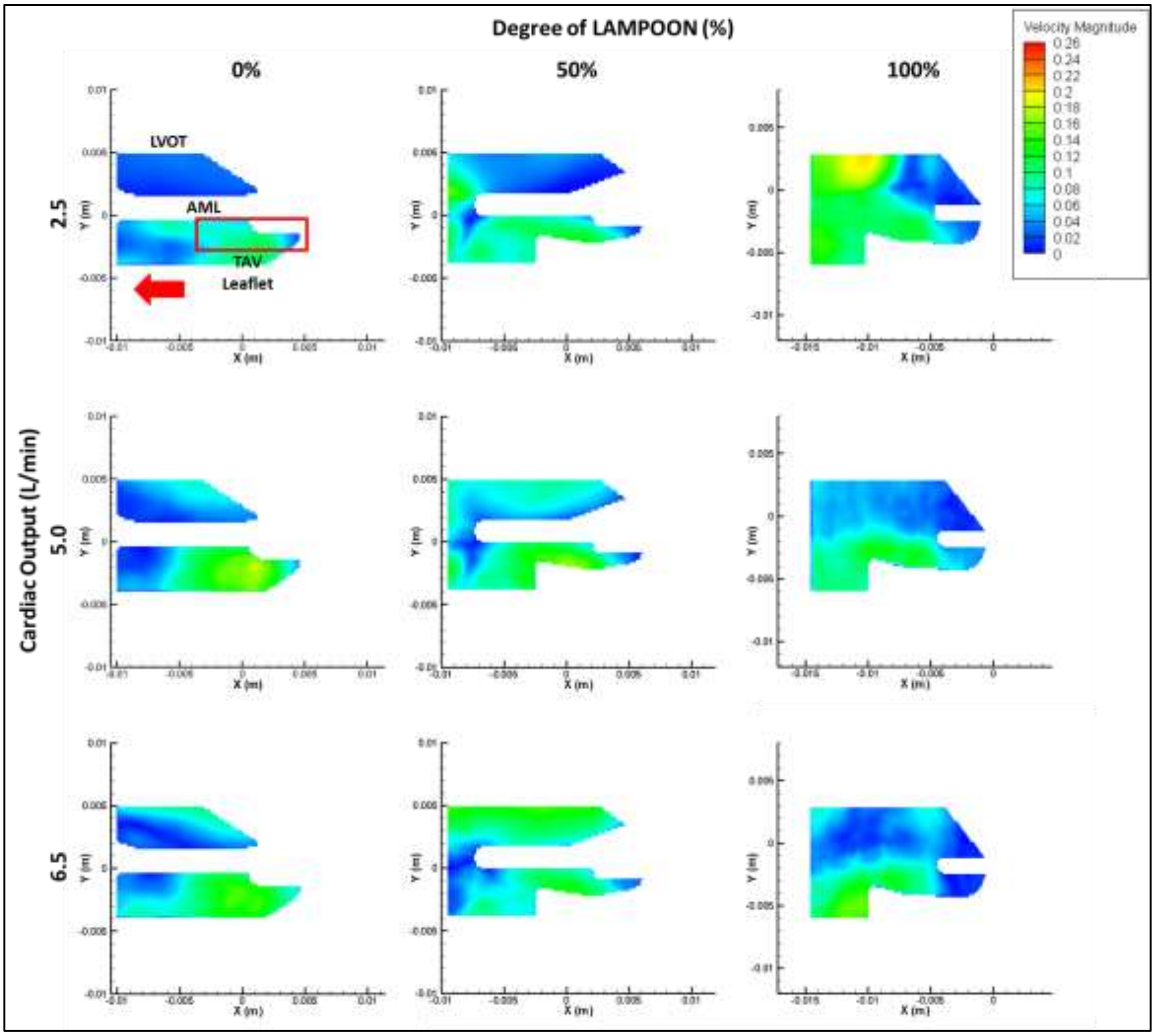

Figure 7-28. Mid-Systolic velocity fields in the neo-sinus (highlighted by red box) of different LAMPOON conditions (0, 50, and 100%) at different cardiac outputs (2.5, 5.0, and 6.5 L/min).

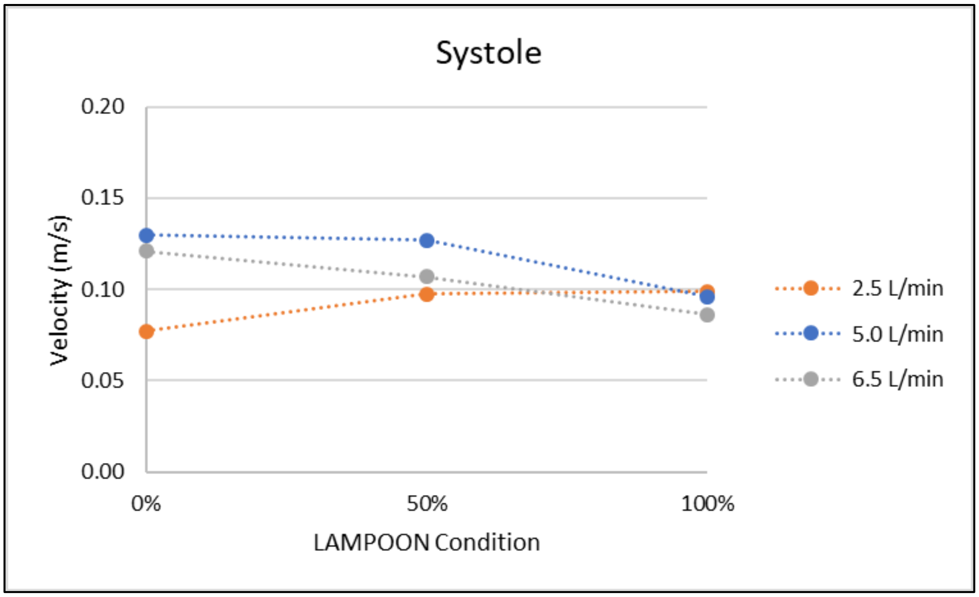

Figure 7-29. Average velocities with the neo-sinus for the mid-systolic velocity fields. Helps quantify Figure 7-28.

Table 7-2. Average and maximum velocities within the neo-sinus for the mid-systolic velocity fields. Helps quantify Figure 7-28.

Cardiac Output (L/min)	0% LAMPOON Average (m/s)	0% LAMPOON Maximum (m/s)	50% LAMPOON Average (m/s)	50% LAMPOON Maximum (m/s)	100% LAMPOON Average (m/s)	100% LAMPOON Maximum (m/s)
2.5	0.077	0.108	0.097	0.129	0.099	0.118
5.0	0.130	0.175	0.127	0.169	0.096	0.130
6.5	0.121	0.146	0.107	0.134	0.086	0.127

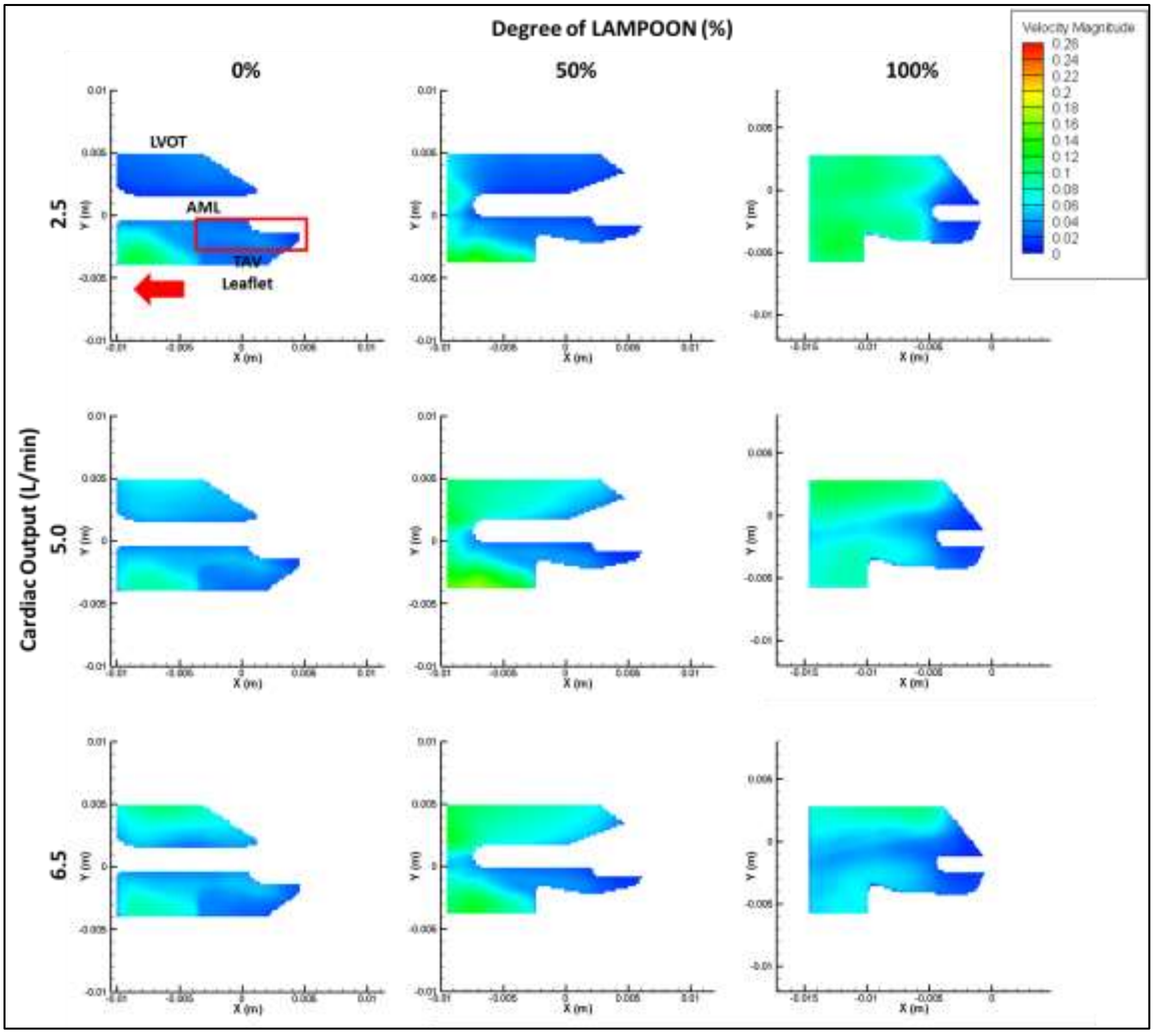

Figure 7-30. Cycle-average velocity magnitudes in the neo-sinus (highlighted by red box) of different LAMPOON conditions (0, 50, and 100%) at different cardiac outputs (2.5, 5.0, and 6.5 L/min).

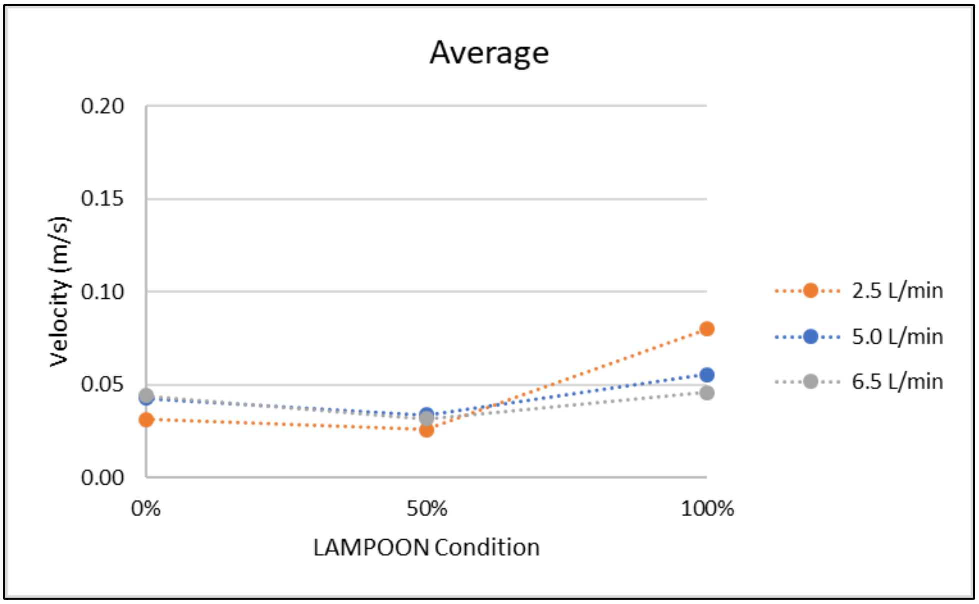

Figure 7-31. Average velocities within the neo-sinus for the cycle-average velocity magnitudes. Helps quantify Figure 7-30.

Table 7-3. Average and maximum velocities within the neo-sinus for the cycle-average velocity magnitudes. Helps quantify Figure 7-30.

Cardiac	0% LAMPOON		50% LAMPOON		100% LAMPOON	
Output (L/min)	Average (m/s)	Maximum (m/s)	Average (m/s)	Maximum (m/s)	Average (m/s)	Maximum (m/s)
2.5	0.031	0.038	0.026	0.031	0.080	0.100
5.0	0.043	0.050	0.034	0.043	0.056	0.075
6.5	0.044	0.051	0.032	0.039	0.046	0.061

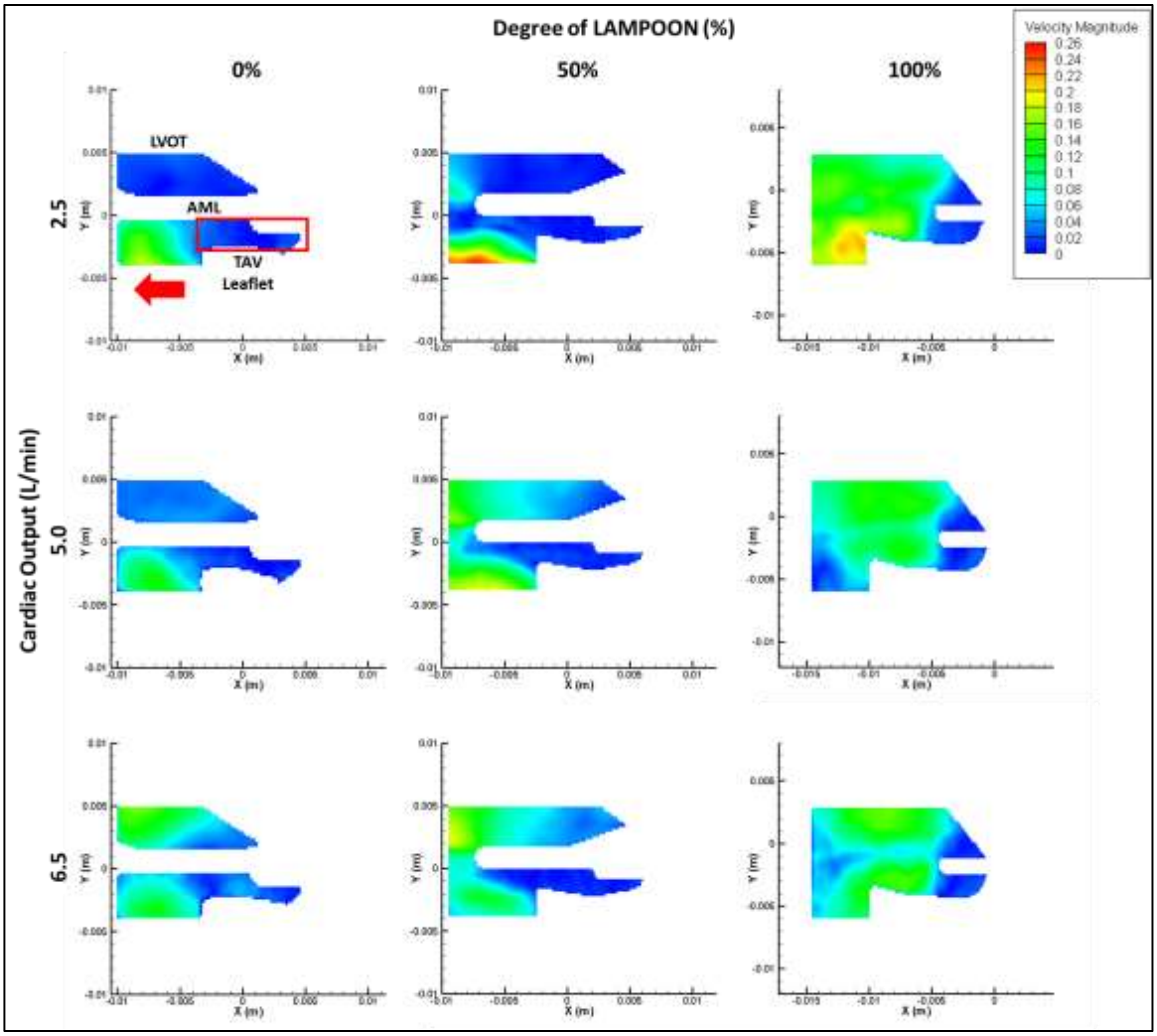

Figure 7-32. Mid-Diastolic velocity fields in the neo-sinus (highlighted by red box) of different LAMPOON conditions (0, 50, and 100%) at different cardiac outputs (2.5, 5.0, and 6.5 L/min).

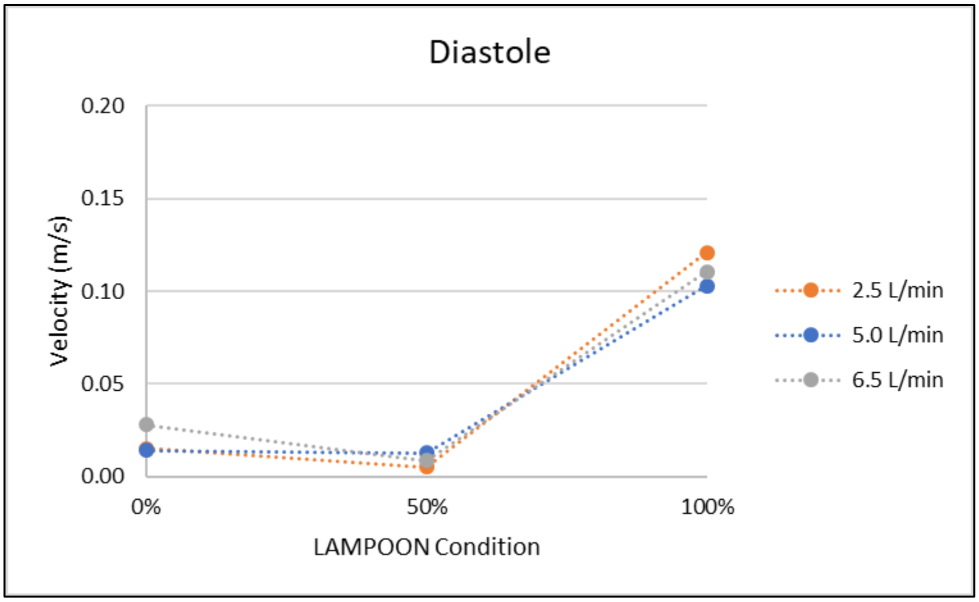

Figure 7-33. Average velocities within the neo-sinus for the mid-systolic velocity fields. Helps quantify Figure 7-32.

Table 7-4. Average and maximum velocities within the neo-sinus for the mid-systolic velocity fields. Helps quantify Figure 7-32.

Cardiac Output (L/min)	0% LAMPOON Average (m/s)	0% LAMPOON Maximum (m/s)	50% LAMPOON Average (m/s)	50% LAMPOON Maximum (m/s)	100% LAMPOON Average (m/s)	100% LAMPOON Maximum (m/s)
2.5	0.015	0.035	0.005	0.019	0.121	0.182
5.0	0.014	0.027	0.013	0.024	0.103	0.141
6.5	0.028	0.048	0.009	0.016	0.111	0.151

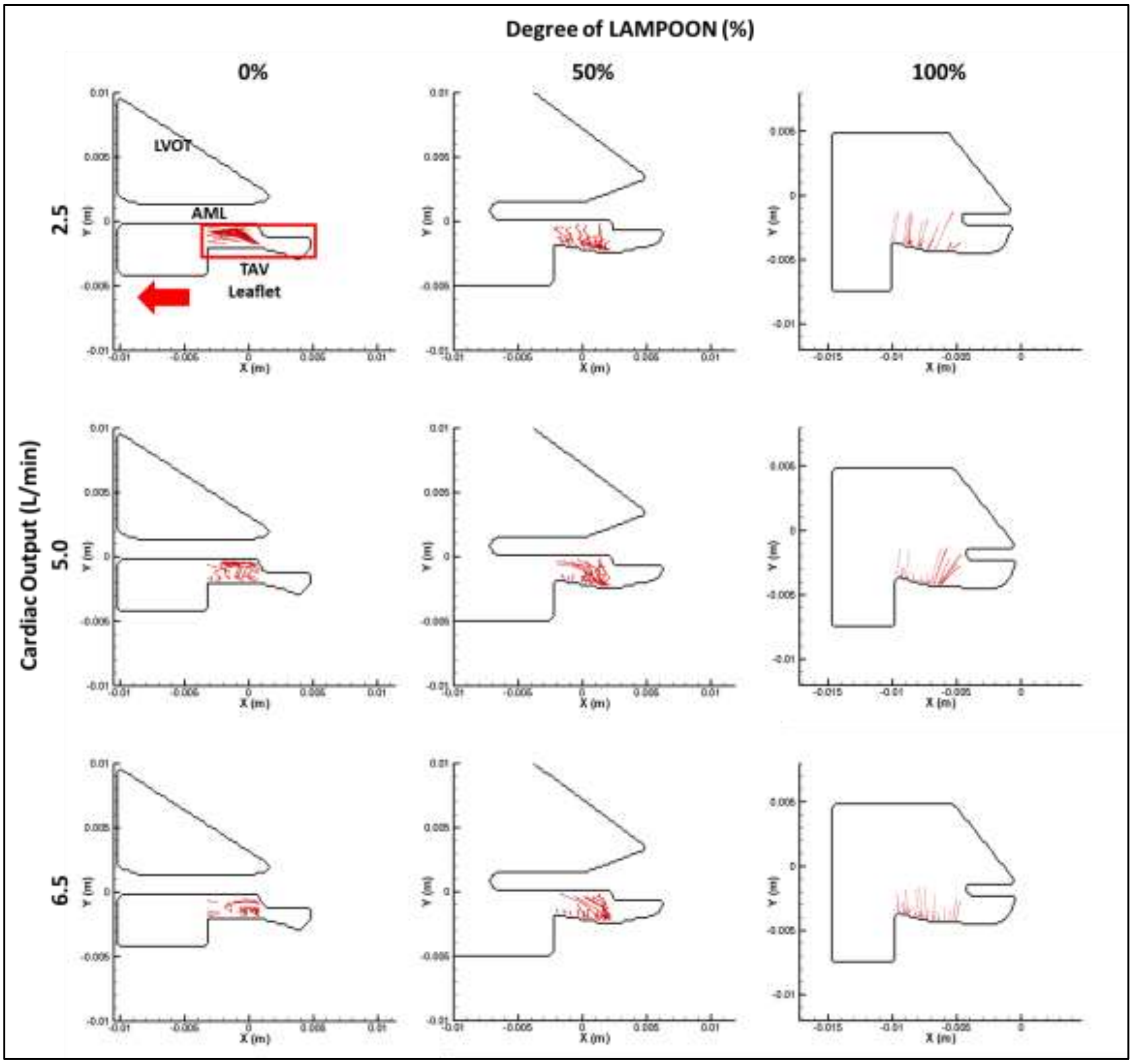

Figure 7-34. 20 particle pathlines in the neo-sinus (highlighted by red box) of different LAMPOON conditions (0, 50, and 100%) at different cardiac outputs (2.5, 5.0, and 6.5 L/min).

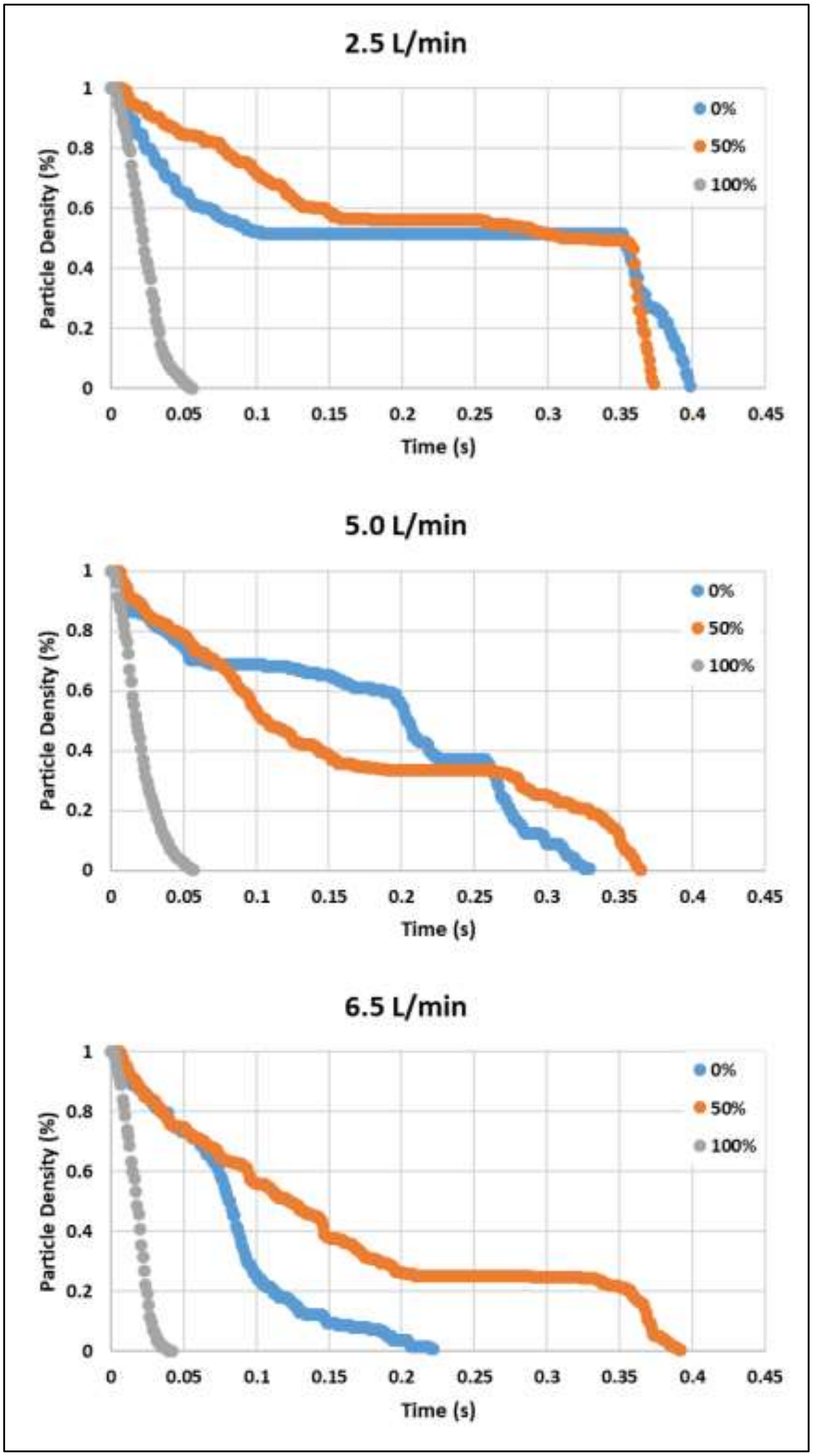

Figure 7-35. Particle washouts between LAMPOON conditions at different flow rates. Particles were seeded 200 ms into diastole.

7.2 Specific Aim 2 Discussion

7.2.1 Specific Aim 2A: LV Flow with LAMPOON

Left ventricular outflow tract (LVOT) obstruction is a risk for patients with transcatheter mitral valve replacements (TMVR).[13, 14, 111] This is primarily caused by current TMVs, off-label TAVs or dedicated TMVs, extending into the LVOT once deployed and consequentially propping the anterior mitral leaflet (AML) into the LVOT. The main goal of the LAMPOON procedure is to proactively prevent this transcatheter valve induced LVOT obstruction by lacerating the AML prior to implantation.[19, 88, 112, 113] This laceration increases the size of the post-TMVR LVOT by allowing the AML to splay around the stent frame as the transcatheter valve expands with help from the chordae pulling the AML apart.

Specific Aim 2A investigated how differing degrees of LAMPOON with different AML lengths and TAV deployment heights would affect flow in the LV. While studying systolic flow, it was found that both deployment heights for the Long AML (80/20 and 50/50 ventricle/atrial) showed decreased systolic velocity magnitude in the LVOT with increased LAMPOON (Figure 7-5; Figure 7-6). This was due to LAMPOON creating a larger LVOT (a larger cross-sectional area) for systolic flow to go through. This decrease in LVOT velocity with LAMPOON could translate to a decrease in LVOT obstruction with an effective lower pressure gradient across the AV. The Short AML (50/50 ventricle/atrial) showed no clear differences in systolic velocity magnitude in the LVOT with increased LAMPOON. This was believed to be due to the already small length of the Short AML condition with no large changes in LVOT cross-sectional area, given the geometry of the

LV and Short AML. Overall the velocity magnitude in the LVOT during peak systole were low, even with the Long AML. This was believed to be due to the size of the LVOT still being large, and the resultant shape of the LVOT in our model resembling a horseshoe shape with 0% LAMPOON, allowing flow to go around the side AML and not just the central, A2 plane (Figure 7-36).

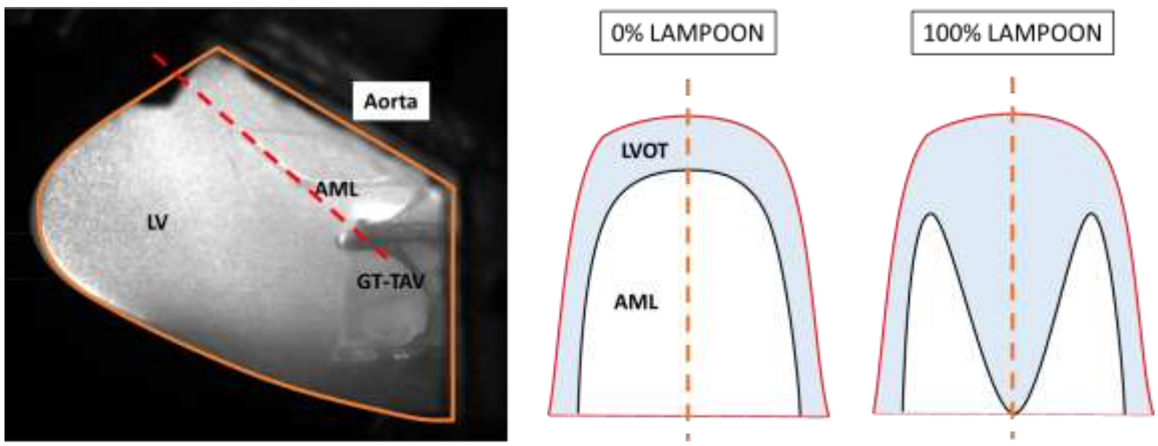

Figure 7-36. Cross-sectional view of the LVOT between 0% and 100% LAMPOON. Red, dashed line is the cross-sectional cut of the LVOT and the orange, dashed line is the central, long-axis plane at which we imaged.

Going forward, this work suggests that when measuring the estimated LVOT size post-TMVR pre-operatively, other planes beside the central long-axis plane should be investigated for measurements and the entire shape of the LVOT be taken into consideration for LVOT obstruction.

Upon investigating the effects on flow in the LV with LAMPOON, it was found that the largest magnitudes of VSS, TKE, and pRSS occurred during diastole. The maximum VSS occurred during the start of the E-wave with the highest velocity inlet jet.

The maximum TKE and pRSS occurred after the E and A-waves and were predominantly found in the same region and time point with the same experiment and showed the same trends. The maximum VSS decreased with increased LAMPOON across all conditions (Figure 7-10; Figure 7-11), however the magnitudes themselves were small (high of 1 N/m^2 with 0% LAMPOON and 6.5 L/min). There were no distinguishable differences between pRSS and TKE at all cardiac output conditions (Figure 7-15; Figure 7-16; Figure 7-20; Figure 7-21). Throughout the LV, pRSS and TKE values were generally small with only intermittent cells of intensity due to the flow fluctuations in the LV after the E and A-waves. It was found that Long AML, 0% LAMPOON at 6.5 L/min reached pRSS of over 70 N/m^2; this was in range of platelet activation levels (32 N/m^2 at 70 ms and 170 N/m^2 at 7 ms exposure),[114-116] but not near blood damage levels (400-800 N/m^2 at 1 ms exposure time-scale).[117, 118] The smaller time scales (1-7 ms) were used as a conservative approach, because we looked at instantaneous shear rates, with our acquisition having 7 ms between frames, without any temporal tracking along pathlines. If we were to track shear stress exposure of platelets throughout the cardiac cycle, not the assumption of a single frame, we could look at lower shear stress thresholds for longer exposure time-scales (Figure 7-37).[116] These lower thresholds could potentially show increased levels of platelet activations, however further studies are needed to confirm this.

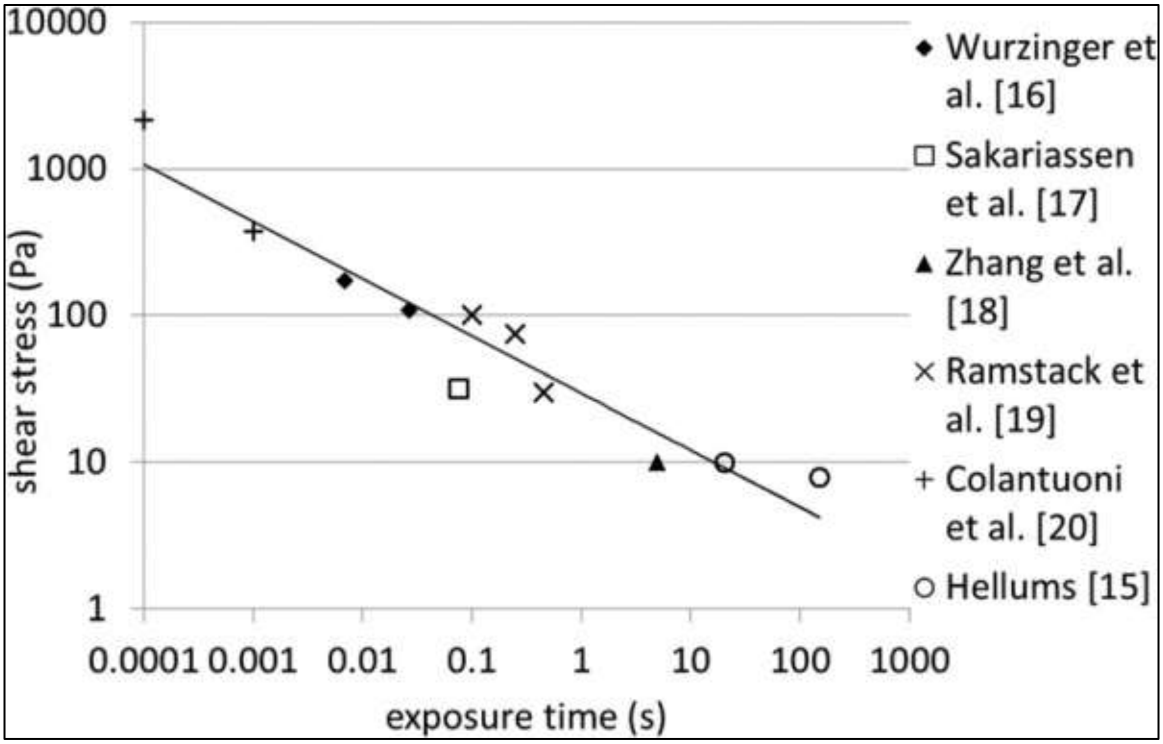

Figure 7-37. "Hellums' shear stress-exposure time threshold required to activate platelets, with some additional data." (Taken from Fraser et al.)[116]

From these results, it is postulated that hemolysis may not be a factor in a valve-in-valve, valve-in-MAC, or valve-in-ring with average LV geometry and normal flow waveforms, but platelet activation may occur. Our experiments used a symmetrically expanded TAV with an aligned deployment, the best case clinical scenario. Future studies should look to quantify how eccentricity and alignment in valve deployment (e.g., deployment into calcium deposits) and irregular flow waveforms (e.g. atrial fibrillation) could affect VSS, pRSS, and TKE in the LV, as no implantation is perfect and valve eccentricity has already been shown to increase these values in bicuspid AVs and TAVs.[119, 120]

Upon investigating the effects on diastolic flow in the LV with LAMPOON, interestingly, it was also found that a larger vortical structure was produced with increasing LAMPOON for all conditions (Figure 7-22; Figure 7-23; Figure 7-24). In addition, the vortical core was able to move more apically into the LV with increased LAMPOON for all conditions. This larger vortical structure increased flow into the LVOT and the anterior side of the GT-TAV during mid-diastole. These mid-diastolic LV flow characteristics helped better explain our Specific Aim 2B findings.

Further clinical studies are needed to confirm these results. Additionally, further *in vitro* and clinical studies are needed to validate the postulations and hypotheses made from these results.

7.2.2 Specific Aim 2B: Neo-Sinus Flow with LAMPOON

Thrombosis has been seen clinically and subclinically with TAVR.[81, 121-124] This has led to recent investigations into the AV neo-sinus where the native AV leaflets wrap around the stent frame creating a cavity of flow stasis between the TAV leaflets and the native AV leaflets.[83, 125-127] With the implantation of TAVs in the MV, thrombosis has now been seen clinically and subclinically with mitral valve-in-ring, valve-in-valve, and valve-in-MAC.[15, 16, 128-132] Previous studies had shown that resecting the AML during SMVR had a lower incidence of thrombosis than those with intact AML.[84] In the same vein as with TAVR, it was hypothesized that an anterior mitral neo-sinus was formed between the TAV leaflets and the AML wrapped around the stent frame with TMVR, thus creating stagnation leading to thrombosis. Furthermore, like the surgical AML resection with SMVR, the use of

LAMPOON with TMVR could offer similar benefits with the potential to lower the risk of thrombosis with TMVR.

Specific Aim 2B studied how differing degrees of LAMPOON would affect the flow in the anterior mitral neo-sinus. All LAMPOON conditions at all cardiac outputs showed a maximum velocity magnitude of at least 0.1 m/s in the neo-sinus over the cardiac cycle which would indicate adequate washout (Figure 7-27). The largest area of high velocities occurred during systole when the GT-TAV closed, and the fluid was pushed into the neo-sinus due to the LV ejection (Figure 7-29). 100% LAMPOON showed higher average velocity in the neo-sinus (from the GT-TAV leaflet edge up to the skirt line) than 0% and 50% LAMPOON at all cardiac outputs (Figure 7-31). This was due to LAMPOON relieving stagnation in the neo-sinus during diastole when the GT-TAV was open (Figure 7-33).

This was further characterized through washout simulation via particle tracking from pathlines (Figure 7-34; Figure 7-35). When the region of the neo-sinus from the leaflet edge to the stent skirt was seeded during diastole (at 200 ms), it was shown that 100% LAMPOON had complete washout within ≈50 ms while the 0% and 50% had to wait until systole for full washout. This systolic washout is most evident in the 0% and 50% LAMPOON conditions at 2.5 L/min due to it being the lowest flow conditions.

Combining the post-TMVR findings of possible stress inducing platelet activation levels (from SA2A) with the AML creating flow stagnation in the neo-sinus during diastole (from SA2B) creates a plausible mechanism for TMVR thrombosis. In addition to its mitigation of LVOT obstruction, the benefit of LAMPOON to relieve anterior neo-sinus stagnation, hindering that pathway of thrombosis, warrants further clinical consideration and discussion.

It was important to note that the laceration in the 50% LAMPOON condition did not reach the TAV leaflet edge, which could explain why there was little difference between 0% and 50% LAMPOON in the neo-sinus. It was postulated from these results that LAMPOON that reaches the TAV leaflet edge could provide increased stagnation relief compared to anything shorter, and that this relief would increase the closer the laceration got to the mitral annulus (100% LAMPOON). However, these results show limited stagnation relief below the skirt line of the TAV, and thus the benefits of LAMPOON for the neo-sinus may be limited to the skirt line (Figure 7-38).

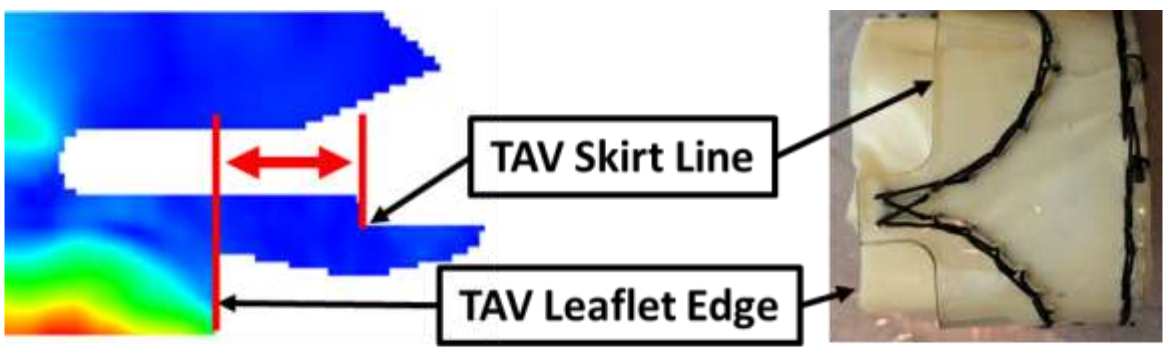

Figure 7-38. Velocity contour of the neo-sinus with 50% LAMPOON with Long AML at 80/20 deployment highlighting the minimum point you may need to lacerate for washout benefits (leaflet edge) and the limiting point for washout (skirt line).

From these results, it was hypothesized that 100% LAMPOON should still be preferred over a shorter length that still reaches the skirt line, because 100% LAMPOON allows for increased splaying of the AML around the stent frame, thus creating a larger opening into the neo-sinus in 3-D space. Additionally, complete chordal sparing AML resection would create an even larger opening into the neo-sinus than 100% LAMPOON and could be the preferred method if percutaneously feasible. It was further hypothesized that LAMPOON will have minimal impact on the flow in the neo-sinus of a closed-cell TMV.

Further clinical studies are needed to confirm these results. Additionally, further *in vitro* and clinical studies are needed to validate the postulations and hypotheses made from these results.

No significant differences were found in the hemodynamics between LAMPOON conditions at the same cardiac outputs. This is believed to be mainly caused by the lack of a large LVOT obstruction from our experimental design (healthy size LV, average aorto-mitral angle, etc.). Additionally, the functioning AV was not directly in the aorto-mitral plane, positioned further upstream. The AML and LVOT were thus believed to be far enough away from the AV that there was plenty of distance for pressure recovery. The lack of a true LVOT obstruction and the AV being placed upstream allowed us to tune each experiment to the same hemodynamic conditions mitigating any changes we would have seen with an induced sub-aortic stenosis from obstruction.

7.2.3 Clinical and Engineering Implications

The work of Specific Aim 2 provides the first *in vitro* simulation of the LAMPOON procedure. This new experimentation platform will serve as a means for future fluid mechanics studies involving the LV, LAMPOON, and TMVRs. Additionally, this work suggests that the LAMPOON procedure can be beneficial by increasing flow in the neo-sinus, increasing diastolic mixing in the LV, and decreasing velocity in the neo-LVOT. These findings could lead to the laceration of the AML with TMVR and the removal of the AML with SMVR becoming a standard of care, provided that it becomes easier to do with regards to TMVR. This also poses a question of whether future TMVR devices should incorporate open-cell or differently shaped stent frames in order to receive the full benefits of the LAMPOON or any leaflet resection procedure, as the relief through LAMPOON may only go as far as the closed enclosure of the transcatheter valve (e.g., sealing skirt, closed-cell stent, etc.).

7.2.4 Limitations

A limitation of Specific Aim 2 was the use of rigid mitral valve leaflets. This was necessary in order to make a transparent anatomically accurate model that could be seamlessly incorporated into the LV phantom. Although when a TAV is deployed into the MV, most of the MV leaflets are wrapped around the TAV stent frame and tethered by the chordae into a static state, the dynamics of the excess leaflet, i.e. the AML edge, is lost in the rigid model.

Another limitation was the use of the LV phantom previously made by Okafor.[103] It was a patient-averaged model of a healthy LV with healthy geometry and stiffness. This was a good starting point for a controlled study looking at the general fluid mechanics of the LAMPOON procedure, however most patients currently receiving LAMPOON have smaller than average LVs with atypical aorto-mitral angulations, hence the risk of LVOT obstruction and use of LAMPOON. It was believed that the use of a smaller LV and irregular aorto-mitral angulation would have helped to induce LVOT obstruction in the 0% LAMPOON condition and shown greater differences in the results.

A limitation with the particle tracking in Tecplot was that the pathlines and seeding were based solely on velocity field data in the ROI with no physical boundary conditions and no velocity data surrounding the ROI. This primarily means that we could not track particles that leave and reenter the ROI due to the small oscillations in the observed neo-sinus flow caused by the small undulations of the TAV leaflets during diastole. A better method would be to enforce a wall boundary condition at the AML and use a velocity field larger than the ROI with the ability to only seed the ROI. For the 0% and 50% LAMPOON cases it was believed that washout would have been even worse if we could have tracked a particle momentarily leaving and reentering the neo-sinus.

A final limitation was the power of the laser used for HSPIV. It's strength and the distance away from the ROI hindered the images' light intensity that limited the quality of the data. This was partially remedied by lowering the acquisition rate for SA2B, because the neo-sinus was furthest away from the laser, but at the cost of a larger time interval between frames. For both SA2A and SA2B, the posterior LV region close to the posterior leaflet had the least light intensity and the worst data.

An overall limitation was that 2-D PIV was used to characterize a 3-D flow field. Neighboring planes within small distances (2-4 mm) of the central plane were studied and showed only small differences in the flow field in that planar direction. However, both the neo-sinus and the neo-LVOT are irregular 3-D shapes and the use of stereographic, plenoptic, or tomographic PIV would provide even better characterization of their flow regions.

CHAPTER 8. CONCLUSIONS AND FUTURE WORK

8.1 Specific Aim 1

8.1.1 Conclusions

This work provides the first *in vitro* MV simulator with a dynamically contracting annulus. The linear actuators in combination with the annular plate designs provided MV annular contraction and reproduced the annulus area change of previous *in vivo* studies and MV leaflet mechanics of previous *in vitro* studies. It was found that ischemic contraction leads to increased AML strain compared to healthy contraction. Additionally, it was seen that a static annulus, mimicking restrictive annuloplasties that are sized to systolic and diastolic sizing increased AML strain. This work suggests that striving to maintain the MV annular dynamics during MV repair procedures is beneficial to the loading of the anterior leaflet.

8.1.2 Future Work

This new left heart simulator will serve as a platform for future studies in MV biomechanics and repair procedures as well as percutaneous replacement device testing. In particular, the addition of annular contraction with TMV deployment in an *in vitro* setting could provide a more robust comprehension of flow characteristics and paravalvular leak.

8.2 Specific Aim 2

8.2.1 Conclusions

In Specific Aim 2A, the results showed that LAMPOON decreased average LVOT velocity magnitude at peak systole, lowered VSS, and increased diastolic flow into the LVOT. SA2A also showed pRSS magnitudes close to platelet activation levels. This suggests that LAMPOON could help mitigate LVOT obstruction and that there could be a risk of platelet activation in the LV with TMVR.

In Specific Aim 2B, the results showed that 100% LAMPOON decreased stagnation in the neo-sinus during diastole and that all conditions had adequate neo-sinus flow during systole. This suggests that LAMPOON could lower the risk of thrombosis in the anterior MV neo-sinus. SA2B also leads to postulation that to have any neo-sinus benefits from LAMPOON the laceration must reach the transcatheter valve's leaflet edge (edge of the neo-sinus) at a minimum.

8.2.2 Future Work

Future work in this area could work on improving the current LV model by making new LV phantoms that are smaller with varying aorto-mitral angulations. Additionally, with advances in silicone 3-D printing or the use of a silicone mold/casting, a flexible and transparent MV leaflet model could replace the current rigid model. Future studies should focus on the effects of eccentricity and irregular flow waveforms on the shear stresses and neo-sinus washout as well as different length and different shaped AML cuts. The length in regard to confirming whether or not the TAV leaflet edge and the skirt line are indeed the boundaries of neo-sinus relief, and the shape to more accurately detail the AML A2-resection from SMVR for valve-in-valve. Lastly, given that we have time-resolved flow fields of the LV over the cardiac cycle, additional work should be made to investigate the shear exposure of platelets and blood cells over the cardiac cycle.

CHAPTER 9. FUNDING AND OTHER SUPPORT

This work was primarily supported by a research grant awarded from the National Heart, Lung, and Blood Institute of the National Institutes of Health (R01HL119297). Specific Aim 2 was additionally supported by an American Heart Association Predoctoral Fellowship (17PRE33661066). Early work and education were supported by a research grant from the Food and Drug Administration (FDA-SOL-1119843).

Special thanks are given to Holifield Farms, Venair, and Proctor & Gamble for their generosity. Holifield Farms donated fresh porcine hearts for use in Specific Aim 1, Venair donated silicone left ventricle phantoms used in Specific Aim 2, and Proctor & Gamble donated glycerin that was used in Specific Aim 2.

APPENDIX A. ASSEMBLY GUIDE – DYNAMICALLY CONTRACTING ANNULUS MOTOR AND CONTROLLER

Summary

This assembly guide outlines how to connect all parts of the dynamically contracting annulus and contains a table of materials used.

A.1 Motor and Controller Wiring

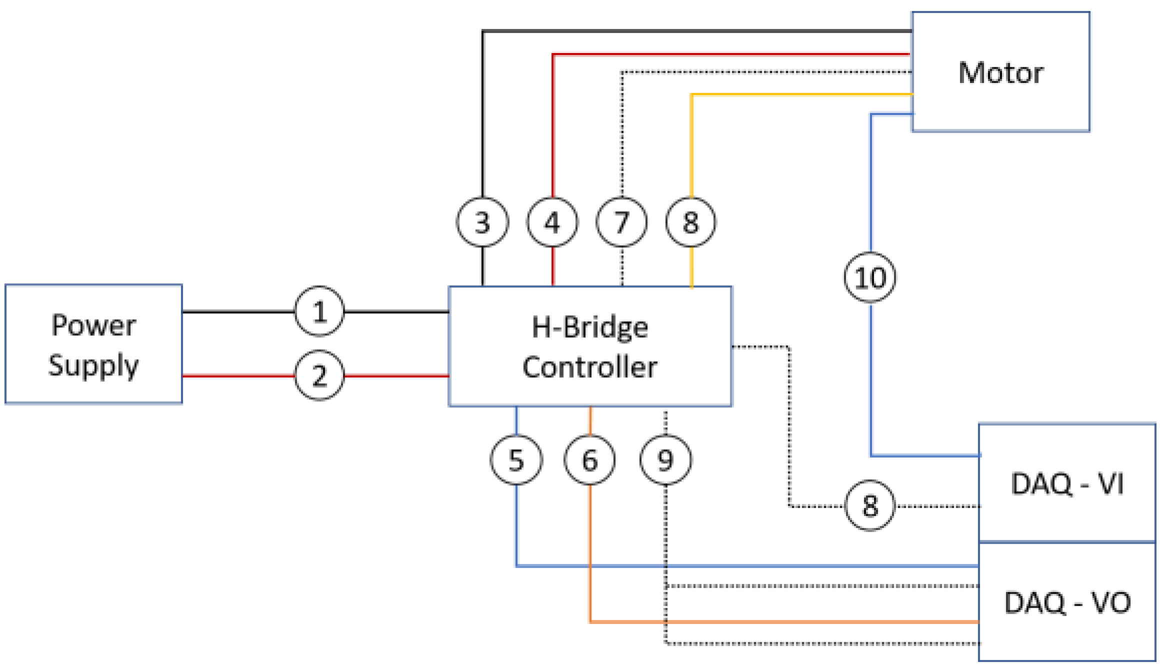

Figure A-1. Wiring diagram for a single motor configuration. See for Table A-1 details.

Table A-1. Wire numbering legend and description.

Item	Figure Legend	Item Legend	Wire Color	Description
Power Supply (Figure A-2)	A	+V ADJ	Turn Screw	Used to adjust the voltage output of the power supply
	0	L/N/Gnd	White/Black /Green	Computer cord taken apart; provides power from wall to power supply
	1	-V	Black	Negative voltage between power supply (-V) and H-Bridge controller (Gnd)
	2	+V	Red	Positive voltage between power supply (+V) and H-Bridge controller (+V)
H-Bridge Controller (Figure A-3)	1	Gnd (9)	Black	Negative voltage between power supply (-V) and H-Bridge controller (Gnd)
	2	+V (8)	Red	Positive voltage between power supply (+V) and H-Bridge controller (+V)
	3	M- (12)	Black	Negative voltage between H-Bridge controller (M-) and motor
	4	M+ (11)	Red	Positive voltage between H-Bridge controller (M+) and motor
	5	Vset or Iset (1)	Blue	Voltage magnitude from DAQ NI-9269 to H-Bridge controller used to control motor speed (voltage magnitude via M)
	6	F/R (2)	Orange	Binary voltage DAQ NI-9269 to H-Bridge controller used to control motor direction (voltage charge via M)
	7	+5v (5)	White	Voltage magnitude from H-Bridge to motor for motor potentiometer to normalize to (0-5 V)

	8	Gnd (6)	Yellow	Ground from H-Bridge to motor for motor potentiometer to normalize to (0-5 V) and DAQ NI-9239
	9	Gnd (9)	White	Ground from H-Bridge to DAQ NI-9269
Motor (Figure A-4)	3	-	Black	Negative voltage between H-Bridge controller (M-) and motor
	4	-	Red	Positive voltage between H-Bridge controller (M+) and motor
	7	-	White	Voltage magnitude from H-Bridge to motor for motor potentiometer to normalize to (5 V max)
	8	-	Yellow	Ground from H-Bridge to motor for motor potentiometer to normalize to (0V min)
	10	-	Blue	Motor potentiometer voltage output to DAQ NI-9239 (0-5 V)
DAQ NI-9269 (Figure A-5)	5	Ch0-0	Blue	Voltage magnitude from DAQ NI-9269 to H-Bridge controller used to control motor speed (voltage magnitude via M)
	6	Ch1-0	Orange	Binary voltage from DAQ NI-9269 to H-Bridge controller used to control motor direction (voltage charge via M)
	9	Ch0-1/ Ch1-1	White	Ground from H-Bridge to DAQ NI-9269
DAQ NI-9239 (Figure A-5)	10	Ch0-0	Blue	Motor potentiometer voltage output to DAQ NI-9239 (0-5 V)
	8	Ch0-1	White	Ground from H-Bridge to DAQ NI-9239

Figure A-2. Single power supply wiring figure. See for Table A-1 details.

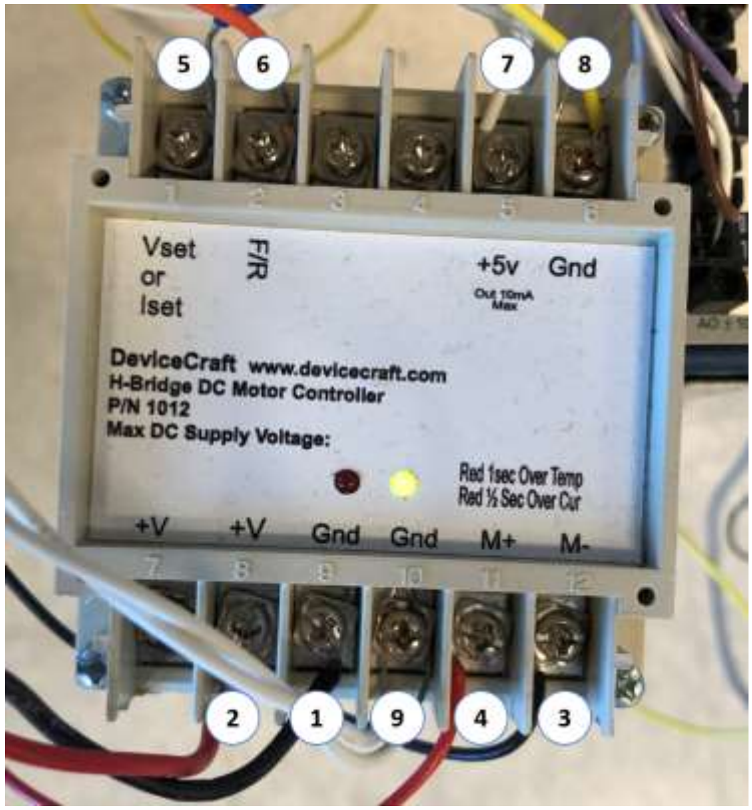

Figure A-3. Single H-Bridge controller wiring figure. See for Table A-1 details.

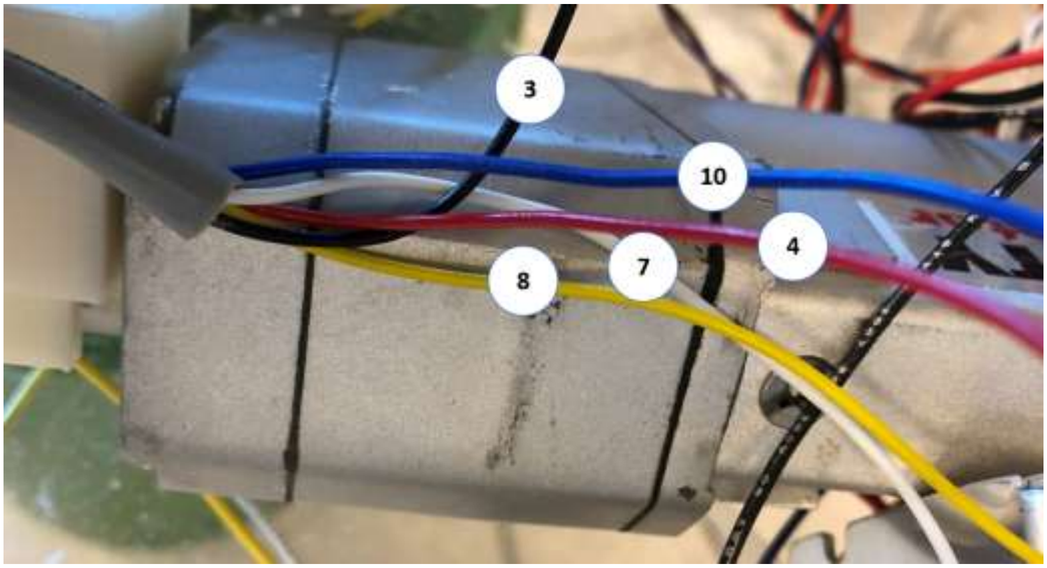

Figure A-4. Single motor wiring figure. See for Table A-1 details.

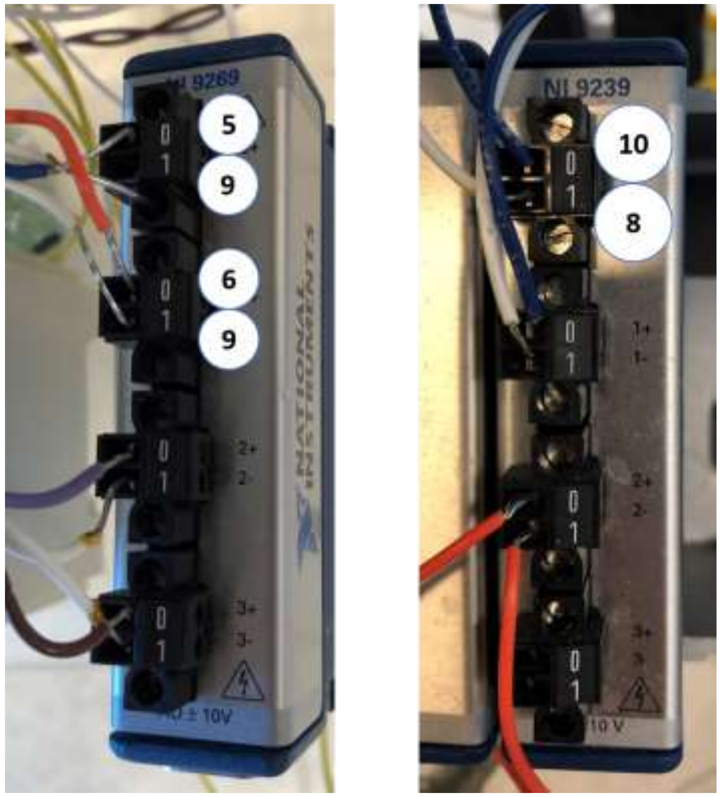

Figure A-5. DAQ wiring figure. NI 6269 – Voltage Output; NI 9239 – Voltage Input. See for Table A-1 details.

A.2 H-Bridge Controller Settings

H-Bridge Controller is the Device Craft 1015B-50V/30A with a Prolific PL2303HX-A serial board. Aside from changing default settings, it is most important to note that Mode 3 was used to operate in a 1-4 V Ain range with the F/R line active (Figure A-6). This is so that any voltage below 1 V is stop and above 4 V is full speed (range 0-5 V), and so you can control directionality.

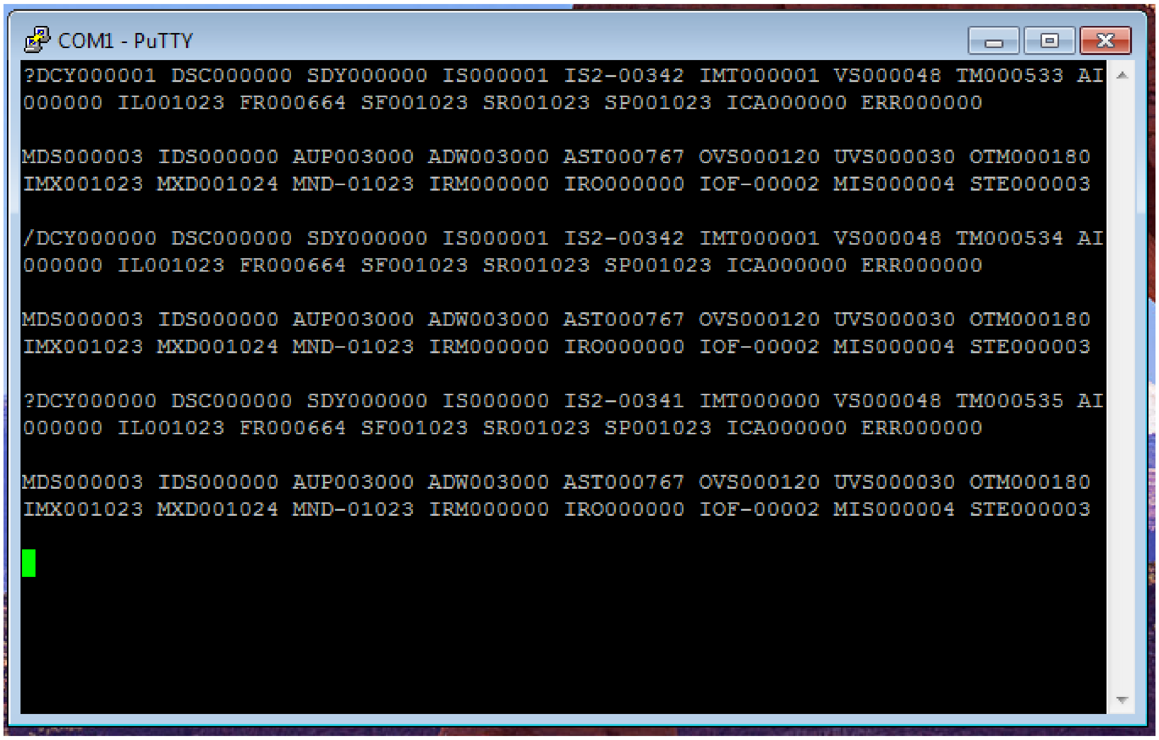

Figure A-6. List of settings for the H-Bridge Controller.

A.3 PID+ Controller Tuning

To help inform, a PID controller is a controller that uses a control loop feedback of the proportional, integral, and derivative terms of the system error (Equation **Error! Reference source not found.**).

$$u(t) = K_p e(t) + K_i \int_0^t e(\tau)d\tau + K_d \frac{d}{dt} e(t) \tag{A-7}$$

The proportional term outputs a value that is proportional to (multiplied by) the current value and is used to correct the current error. However, the integral term outputs a value that is used to correct the offset of the system with the value being relative to the sum of the error over time. Furthermore, the derivative term outputs a value that is used to predict future error of the system by calculating the change of the error over time. Some effects of individually increasing the specified gain values can be seen in Table A-2.

Table A-2. Effects of increasing each respective gain value.

Gain	Rise Time	Overshoot	Settling Time	Steady-State Error
K_p	Decrease	Increase	-	Decrease
K_i	Decrease	Increase	Increase	Decrease
K_d	-	Decrease	Decrease	-

For the motor/H-Bridge controller configuration in this thesis, manually tuning your PID gains by trial-and-error is reasonable given the system, however, that is not always the case and the Ziegler-Nichols tuning method can yield better results. The Ziegler-Nichols tuning method is a tuning method that utilizes the system's determined ultimate gain and the period of oscillation at the ultimate gain to calculate the proportional, integral, and derivative values for the controller using heuristic equations (Table A-3). Using only the proportional controller, the ultimate gain is found by tuning the proportional gain value and manually manipulating the system until its response creates an oscillation with a constant magnitude. The time between those oscillations is the period of oscillation used for calculation.

Table A-3. Ziegler-Nichols tuning method equations to calculate gain constants with ultimate gain and period of oscillation.

Control Type	Gain Values		
	K_p	K_i	K_d
P	$0.5K_u$	-	-
PI	$0.45K_u$	$\frac{1.2K_p}{P_u}$	-
PID	$0.6K_u$	$\frac{2K_p}{P_u}$	$\frac{K_p P_u}{8}$

Next, the resultant velocity versus voltage curve was used to determine the pulse width modulation (PWM) offset voltage. A linear best fit line was made for both directional velocities and the average y-intercept between both directions was used. Note: subtract 1 V from the y-intercept, due to that being the starting point of the PWM output voltage.

Also, a feed-forward controller is a controller that accounts for errors before they occur and affect the system, thus reducing the error without the slowness of a feedback loop. This was tuned last based on the resultant error left in the controller. Given the used motor/H-Bridge controller system, this was also easily tuned manually by trial-and-error.

A.4 Input Waveform Data and Graphs

The input waveforms were derived by Levack et al._ENREF_37[25] human annulus circumferential data (Figure A-7). A matlab code was written to wrip the data from image based on the plot lines and axis scales (K.1).

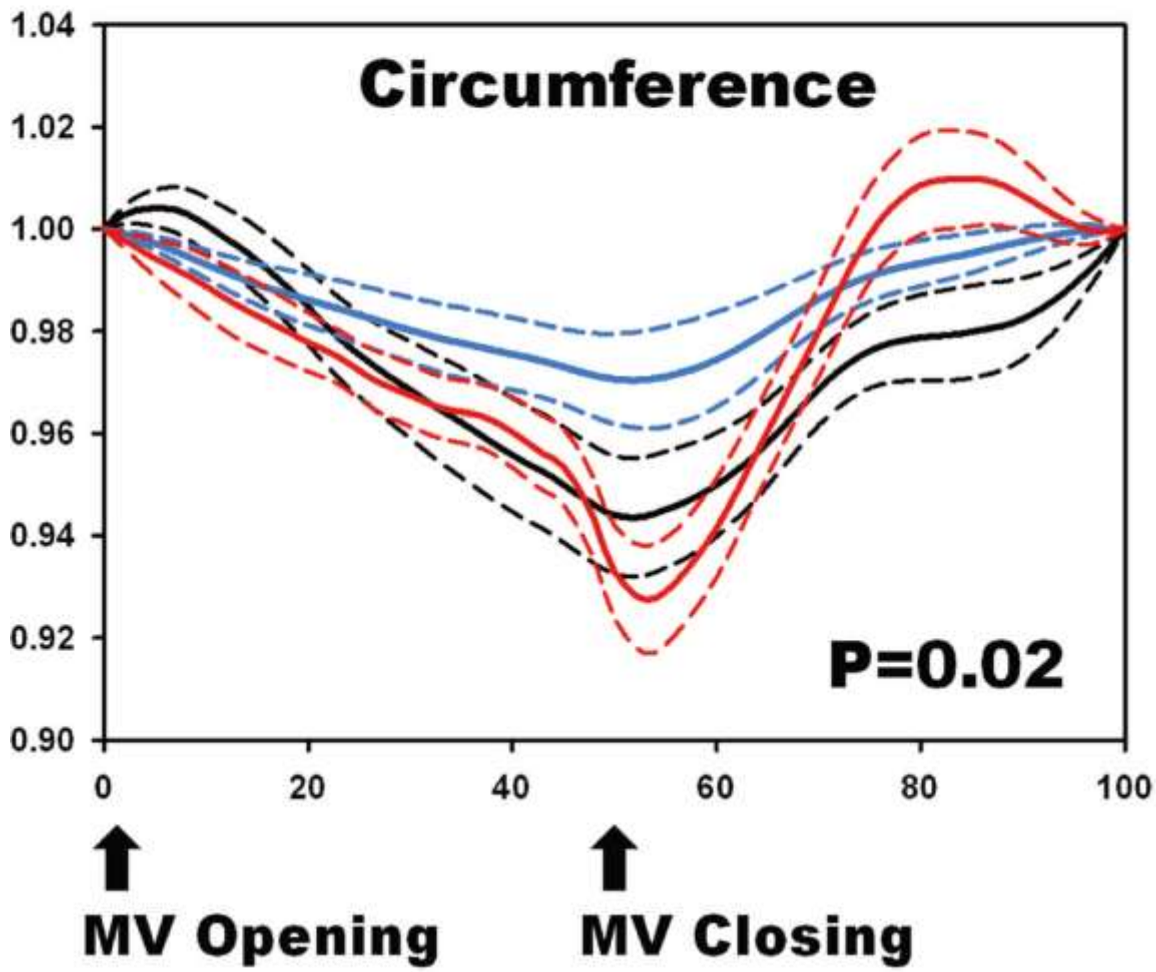

Figure A-7. Average circumferential motion of the annulus over the cardiac cycle normalized to size at the beginning of diastole. Black = Normal, Blue = Ischemic, Red = Myxomatous.[25]

The raw data was then scaled to a 35/65% systole/diastole cardiac cycle, scaled to the size of the annulus plates, and divided by two (using two motors) to be used as the displacement curve of the motors (Table A-4; Table A-5; Table A-6). These can be rescaled to match different sized plates. These displacement curves are used in LabVIEW (J.1) to tune the motors and get a tuned voltage output for each one.

Table A-4. Healthy inputs for DCA code, scaled to max displacement of 0.5 cm. Note: the first column is time (ms), second is displacement (cm), and third through fifth are inputs for a spline fit function in LabVIEW over 856 ms cardiac cycle.

0	-0.23405	0	1	856
9.822951	-0.25676			
23.7388	-0.28153			
43.3847	-0.31757			
58.9377	-0.34459			
72.85355	-0.36712			
91.68087	-0.39865			
107.2339	-0.42342			
126.8798	-0.45721			
140.7956	-0.48423			
157.1672	-0.5			
173.5388	-0.49324			
187.4546	-0.47973			
208.7377	-0.4482			
224.2907	-0.41892			
238.2066	-0.38288			
253.7596	-0.33784			
267.6754	-0.29955			
285.6842	-0.25676			
299.6	-0.23187			
334.565	-0.21396			
371.0503	-0.20721			
401.4546	-0.20045			
427.2984	-0.1982			
462.2634	-0.18018			
491.1475	-0.15766			
520.0317	-0.12613			
542.835	-0.09685			

577.8	-0.03411			
617.3257	-0.00225			
647.7301	0			
675.094	-0.01351			
707.0186	-0.04054			
738.9432	-0.07432			
770.8678	-0.11712			
802.7923	-0.15991			
856	-0.23405			

Table A-5. Ischemic inputs for DCA code, scaled to max displacement of 0.2 cm. Note: the first column is time (ms), second is displacement (cm), and third through fifth are inputs for a spline fit function in LabVIEW over 856 ms cardiac cycle.

0	-0.11574	0	1	856
5.123119	-0.11863			
23.1565	-0.12972			
40.37018	-0.14082			
58.40356	-0.14822			
75.61724	-0.15931			
92.83092	-0.16671			
110.0446	-0.17781			
128.078	-0.1889			
142.0129	-0.1963			
158.4068	-0.2			
177.2599	-0.1963			
191.1948	-0.1889			
209.2282	-0.17226			
226.4419	-0.15376			
242.8358	-0.12972			
258.4101	-0.10753			

275.6238	-0.08719			
299.6	-0.06237			
320.5316	-0.0539			
355.5445	-0.04465			
382.9458	-0.0391			
414.9141	-0.0317			
443.8378	-0.02246			
478.8506	-0.01506			
509.2966	-0.00581			
544.3094	-0.00026			
577.8	0			
608.246	-0.00951			
640.2142	-0.02246			
672.1825	-0.04095			
704.1508	-0.05575			
737.6413	-0.07239			
772.6542	-0.08164			
804.6224	-0.09458			
856	-0.11574			

Table A-6. Myxomatous inputs for DCA code, not scaled to any particular displacement. Note: the first column is time (ms), second is displacement (cm), and third through fifth are inputs for a spline fit function in LabVIEW over 856 ms cardiac cycle.

0	-0.2737	0	1	856
7.5822	-0.2860			
25.6156	-0.3058			
42.8293	-0.3217			
59.2233	-0.3317			
76.4369	-0.3436			

93.6506	-0.3674			
110.0446	-0.3932			
124.7992	-0.4230			
133.8159	-0.4647			
141.1932	-0.5025			
147.7508	-0.5462			
156.7674	-0.5799			
168.2432	-0.5998			
182.1781	-0.5839			
196.9327	-0.5422			
208.4085	-0.5045			
218.2449	-0.4588			
225.6222	-0.4250			
235.4585	-0.3813			
243.6555	-0.3396			
251.8525	-0.2999			
260.8692	-0.2582			
269.8859	-0.2125			
278.9026	-0.1708			
288.7390	-0.1251			
299.6000	-0.0778			
320.5316	-0.0457			
347.9330	-0.0139			
382.9458	-0.0020			
413.3918	0			
448.4047	-0.0119			
480.3729	-0.0338			
509.2966	-0.0576			
538.2202	-0.0715			
577.8000	-0.0726			
617.3798	-0.1033			

650.8703	-0.1251			
682.8386	-0.1490			
713.2845	-0.1748			
743.7305	-0.1946			
777.2211	-0.2185			
807.6670	-0.2383			
856	-0.2737			

APPENDIX B. ASSEMBLY GUIDE – LEFT VENTRICLE BOX CHAMBER

Summary

This assembly guide details the step-by-step instructions for assembling the LV Box Chamber. *Note: each change in LV insert or retrieval of the GT-TAV required complete disassembly and reassembly of the LV box chamber.*

B.1 Assembly LV Box Chamber

This part involves mounting the left ventricle phantom (bag) into the box chamber that will pressurize the surrounding space causing it to contract and relax.

Step 1: Pick which left ventricle (LV) phantom you want to use. They vary in sphericity index and stiffness.

Step 2: Place gaskets on both sides of the LV phantom and place onto the LV box chamber (Figure B-1).

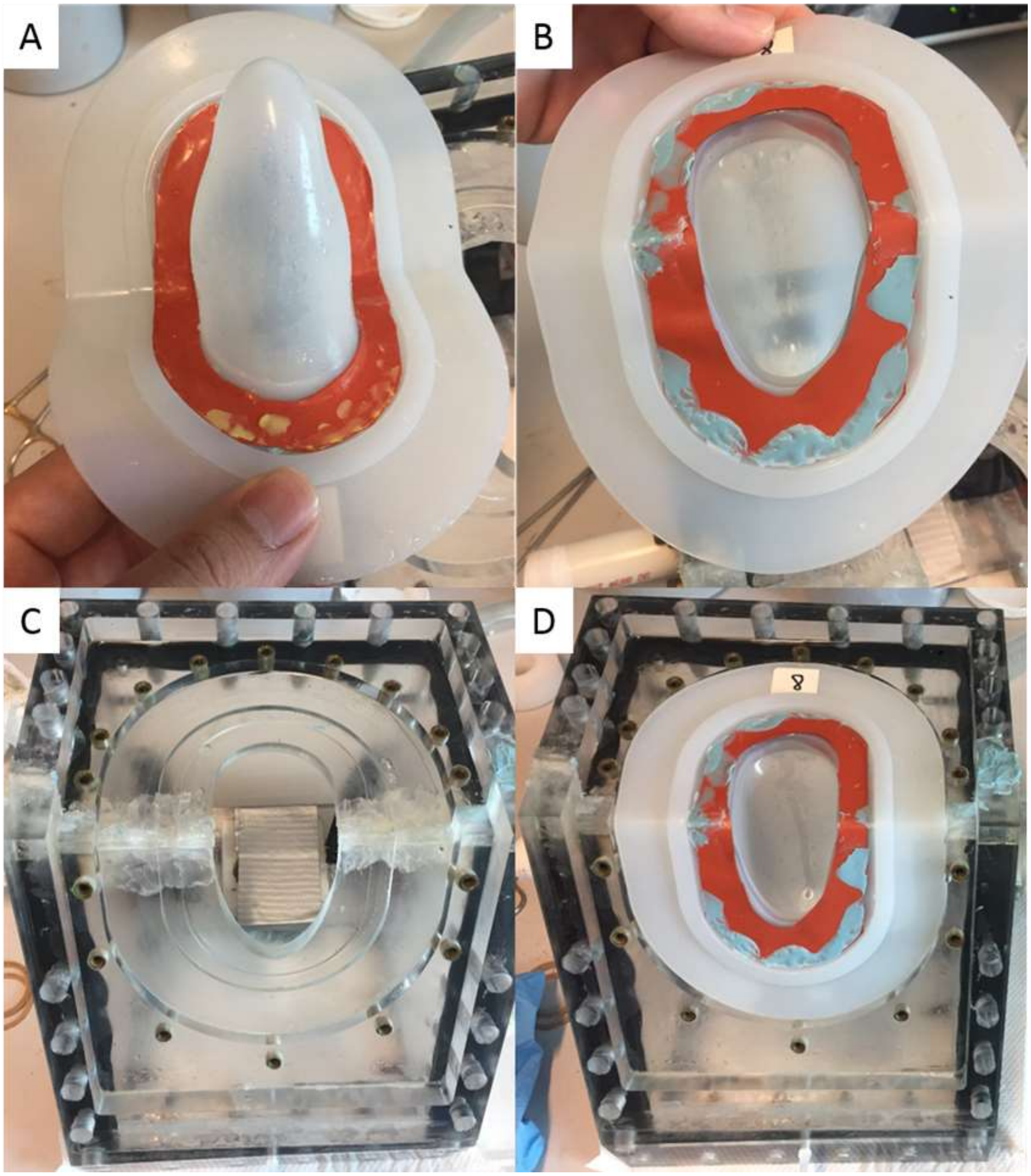

Figure B-1. (A) Gasket on box chamber side; (B) gasket on inside; (C) LV disassembled, (D) LV phantom placed onto LV box.

<u>Step 3:</u> Lay down a line of dental glue around the edges of the aorto-mitral top plate (Figure B-2A). Place the aorto-mitral LV insert into the top plate; smoothen the dental glue at the seam after compression, then trim off any excess for a good seal (Figure B-2B).

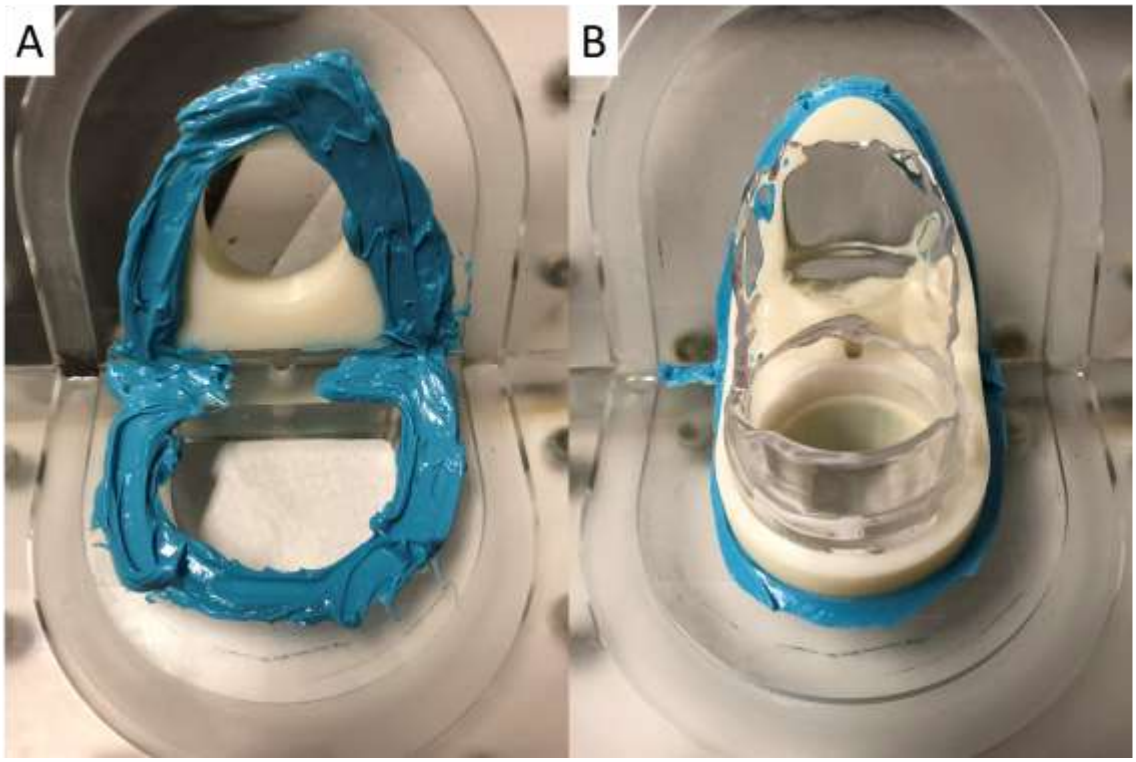

Figure B-2. Placement of LV insert into the aorto-mitral top plate. (A) laying down dental glue and (B) finished placement.

<u>Step 4:</u> Place the aorto-mitral top plate of the LV box over the LV phantom making sure that the ridge of the phantom fits in its groove (Figure B-3A). Be sure not to block the external wall tap for the pressure transducer with the black gasket. Once in place, screw (10-32's) the mitral valve (MV) side into place starting from the center hole and working your way towards the aorto-mitral septum (Figure B-3B). Next, screw the aortic valve (AV) side into place working from the septum down to the center hole (Figure B-3C). For both side, with each order of screws, the plate will compress down and align the next set of holes.

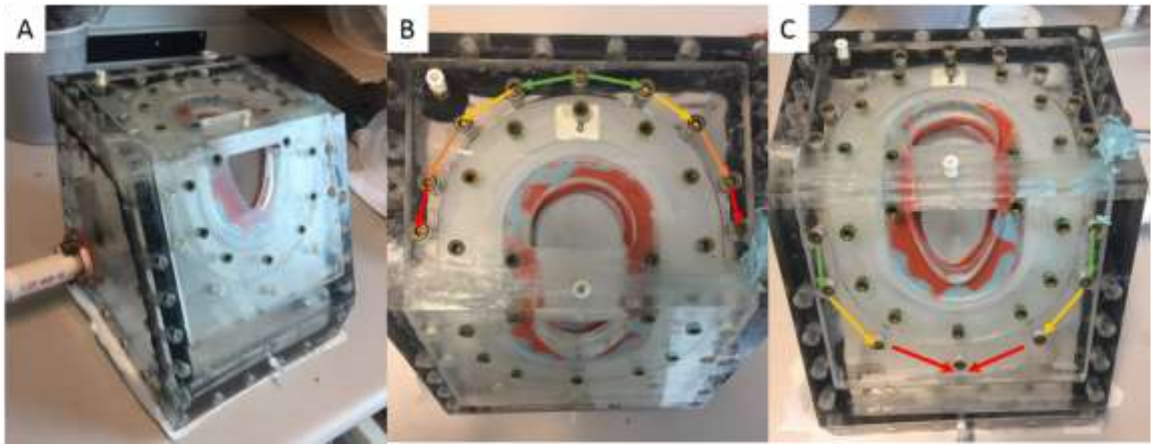

Figure B-3. (A) Top placed over phantom; (B) Order of screwing MV side, from green to red; (C) Order of screwing AV side, from green to red.

<u>Step 5:</u> Perform the leak test by attaching AV/MV leak-plates and gaskets to the box. Screw into place using the 10-32 screws with washers (Figure B-4). One creates a wall while the other is tapped. Add fluid to the LV phantom through the wall tap using a syringe until the LV begins to expand from built up pressure. Check for leaks. If leaking, reassemble, if not, continue to B.2.

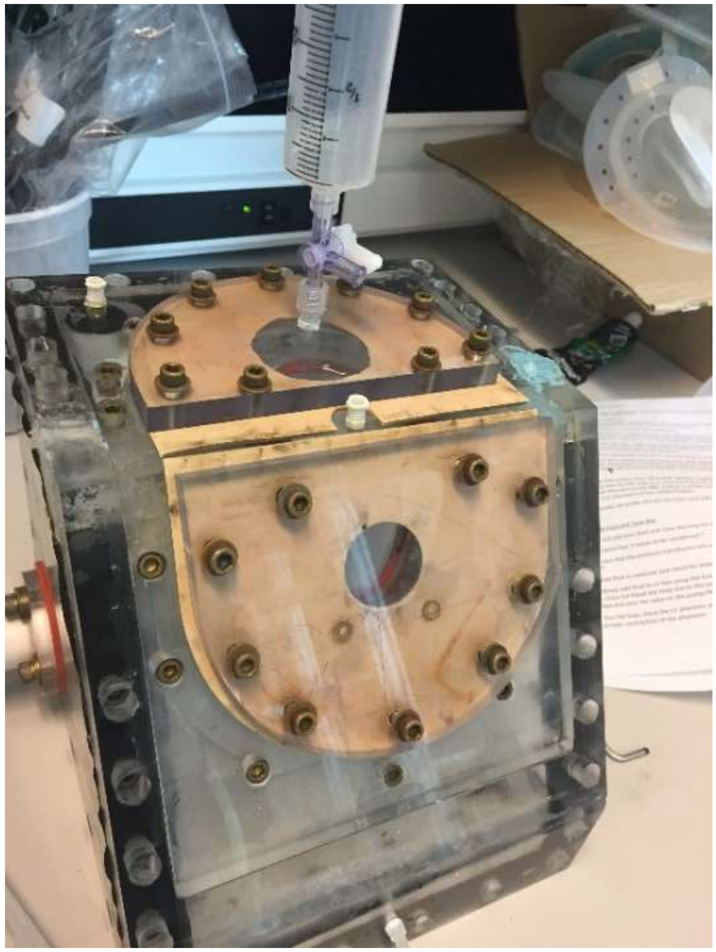

Figure B-4. Set-up for leak test.

B.2 Assemble AV/Aorta and MV/Atrium and Deploy GT-TAV

This part involves mounting the aortic valve and mitral valve into place in their respective aorta and atrium chambers.

Step 1: Place circular spacers into the atrium for uniform internal diameter (Figure B-5A).

Step 2: Lay down a line of dental glue on both sides of the larger block spacer and sandwich between the atrium and the MV/atrium plate. Orientate the block and plate, so that the cut-outs of the plate's flat-edge and the block face the aorto-mitral septum and the pressure tap of the atrium does not face opposite of it (Figure B-5B). Remove excess dental glue from inside and outside. *The cut-outs prevent interference with the LV pressure port on the aorto-mitral top plate. If the atrium pressure tap faces opposite of the cut-out, it will face into the table when finished and thus unusable.*

Step 3: Lastly, screw the MV/atrium plate into place with four 10-32 countersunk screws (Figure B-5C).

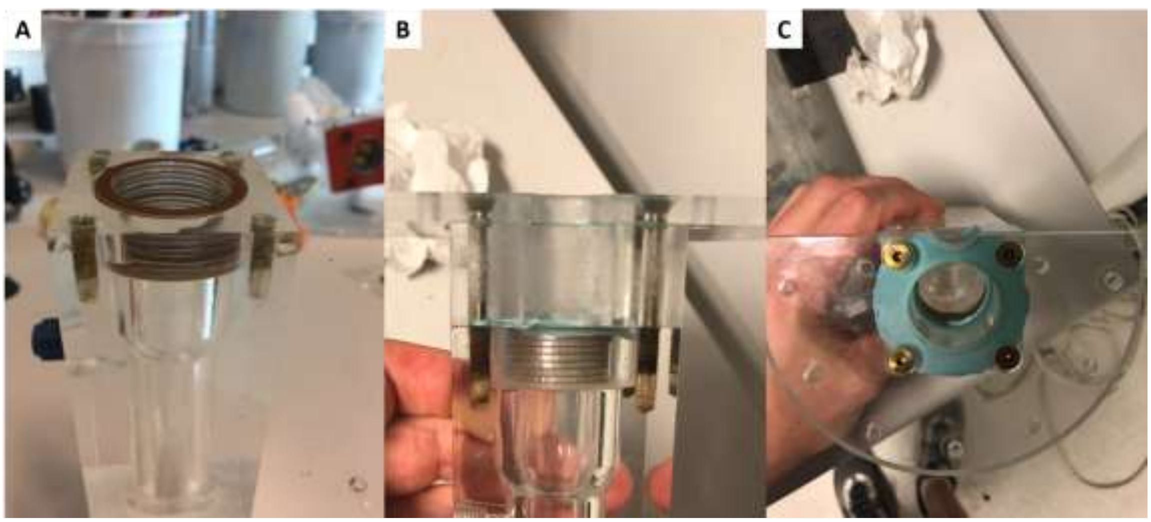

Figure B-5. (A) Circular spacers placed into atrium; (B) Block spacer placed between atrium and MV/atrium plate; (C) MV/atrium plate screwed onto the block spacer and atrium.

Step 4: Unlike the MV where you place the spacers first, first place the AV BHV into the aorta with the leaflets facing into the chamber. Make sure the commissure/stent-post is aligned with the slots in the chamber, so that the leaflets are also aligned with the sinuses.

You may need to loosen screws on the AV end of the chamber to make it easier to put in (Figure B-6A/B).

<u>Step 5:</u> Place spacers on top on the AV BHV to make a flush surface with the edge of the aorta chamber (Figure B-6C).

<u>Step 6:</u> Squeeze out dental glue onto a usable surface and mix together quickly. Spread dental glue over the face of the aorta chamber with the spacers. Be sure to get into the cracks between the spacers and the chamber to provide a proper seal. This needs to be done timely, so that the glue does not dry in the middle of it. Once finished applying dental glue, place the gasket on top of the face followed by the LV/aorta plate (Figure B-6D).

<u>Step 7:</u> Screw four 10-32 countersunk screws into place attaching the AV/aorta plate to the aorta chamber. Be sure to orient the plate with the flat edge facing the aorto/mitral septum and the round edge facing away (Figure B-6E).

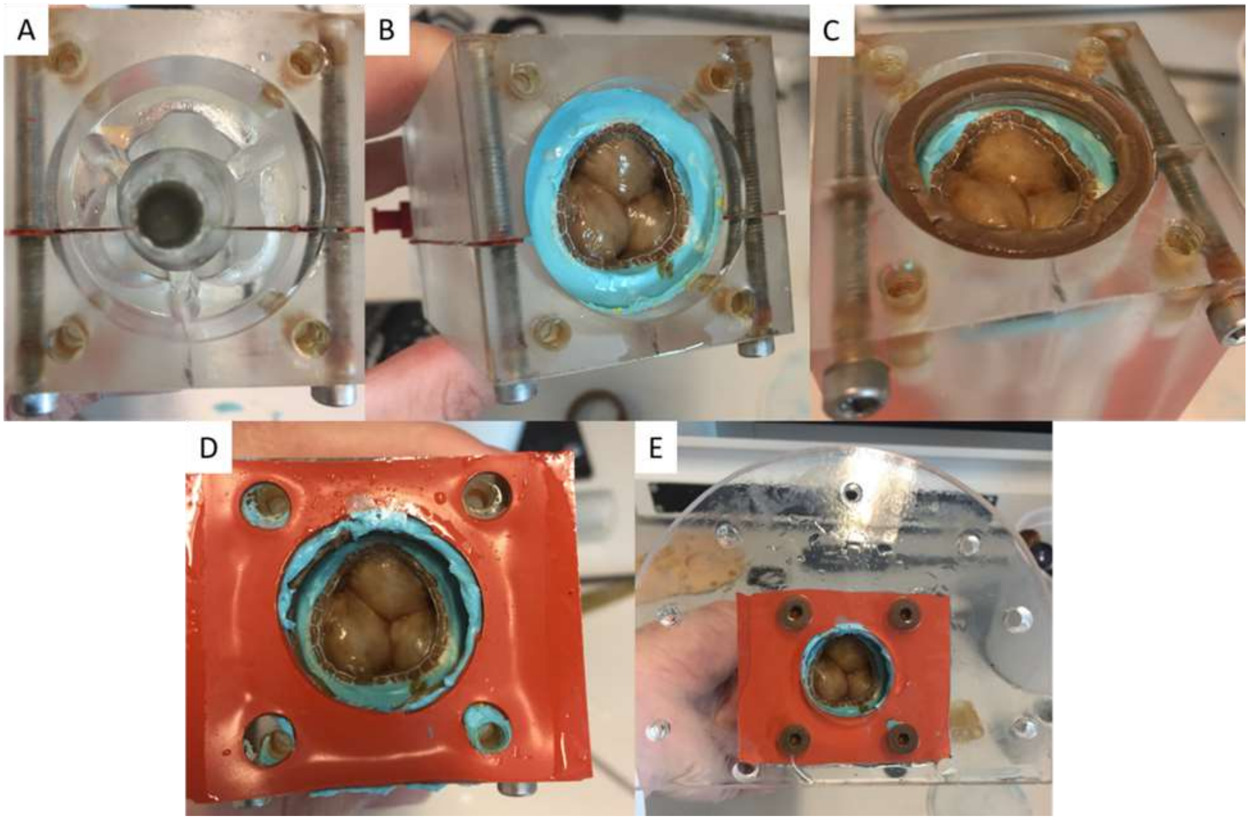

Figure B-6. (A) Showing the stent posts and aortic sinuses of the aorta chamber; (B) AV BHV in position; (C) spacers inserted; (D) dental glue applied and gasket covering it; (E) AV/aorta plate screwed down to aorta chamber.

Step 8: Insert the pressure catheter down the aorta from the lure lock and through the AV, so that it will go directly into the LV when assembled (Figure B-7). It is much easier to do this now instead of while the system is running.

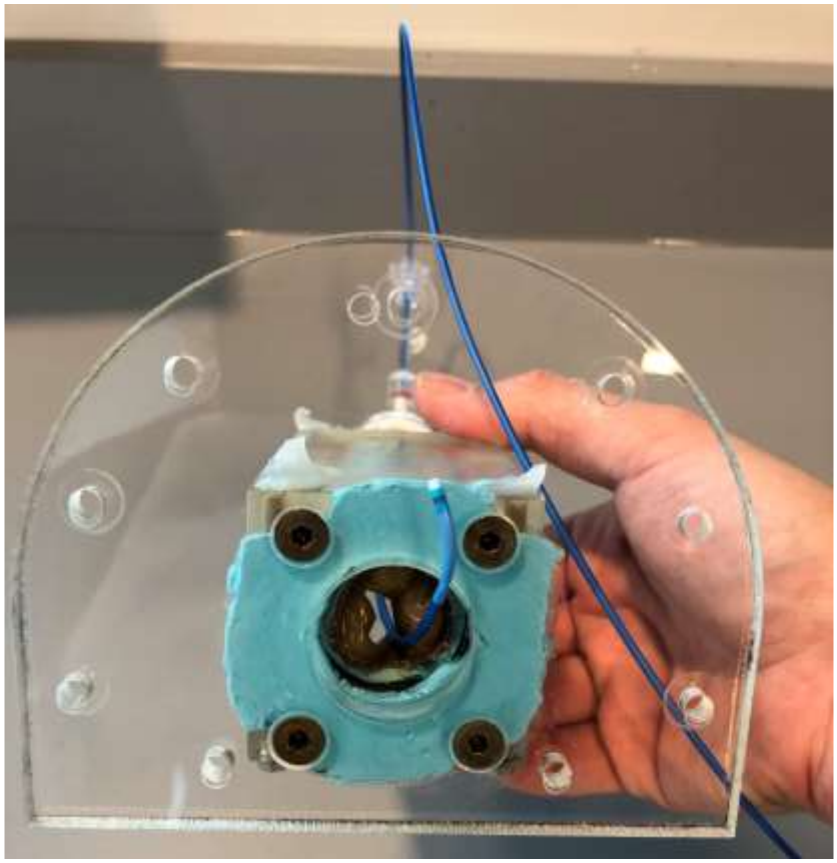

Figure B-7. Insertion of catheter through AV from Aorta before assembly to chamber.

At this point B.1 needs to be completed

<u>Step 9:</u> Take the GT-TAV and place it into the LV insert orientated such that a stent post is aligned with the P2 of the MV, so that a cusp is aligned with the A2 and the AML (Figure B-8A).

Step 10: Take the correct deployment height spacer for the experiment and push it in behind the GT-TAV until the spacer is flush with the LV insert (Figure B-8B). This ensures accurate and precise deployment of the GT-TAV between experiments and also prevents migration.

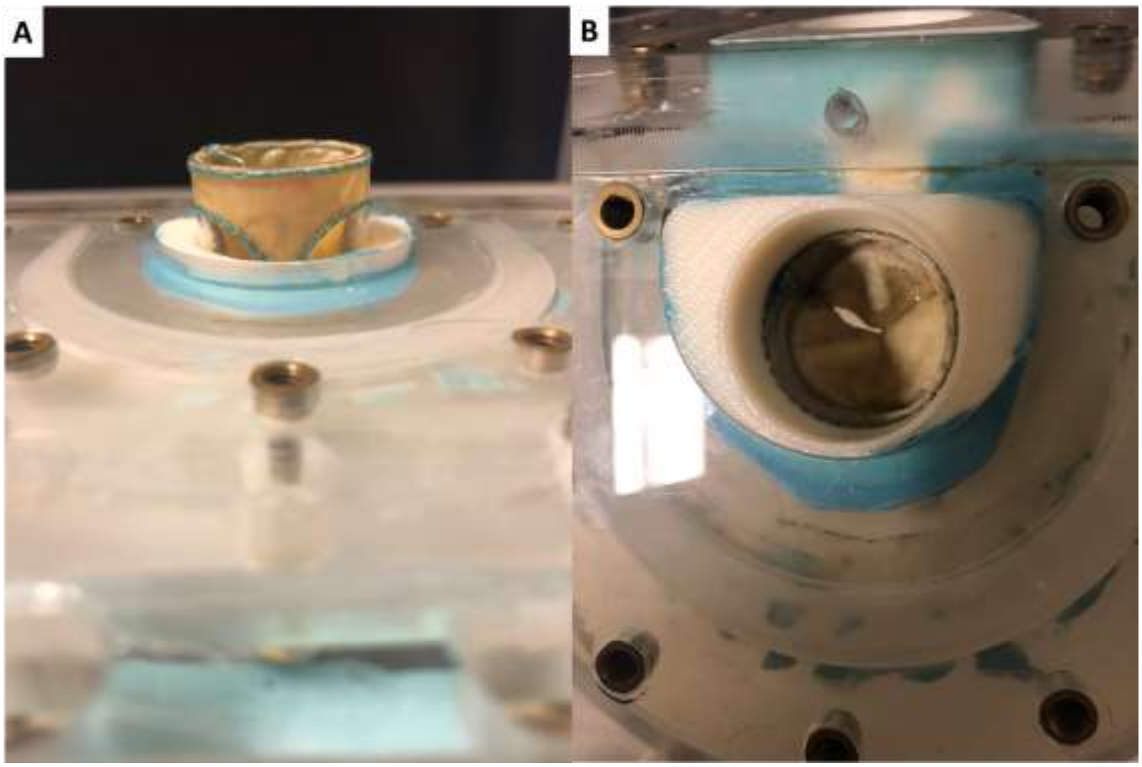

Figure B-8. (A) Showing orientation and direction to insert GT-TAV into the LV insert; (B) Showing resultant deployment of GT-TAV with deployment spacer pushed in behind it.

Step 11: Take remaining 10-32 screws with washers and attach AV/Aorta and MV/Atrium to the LV/Box with gaskets and/or dental glue between each plate and the LV chamber (Figure B-9).

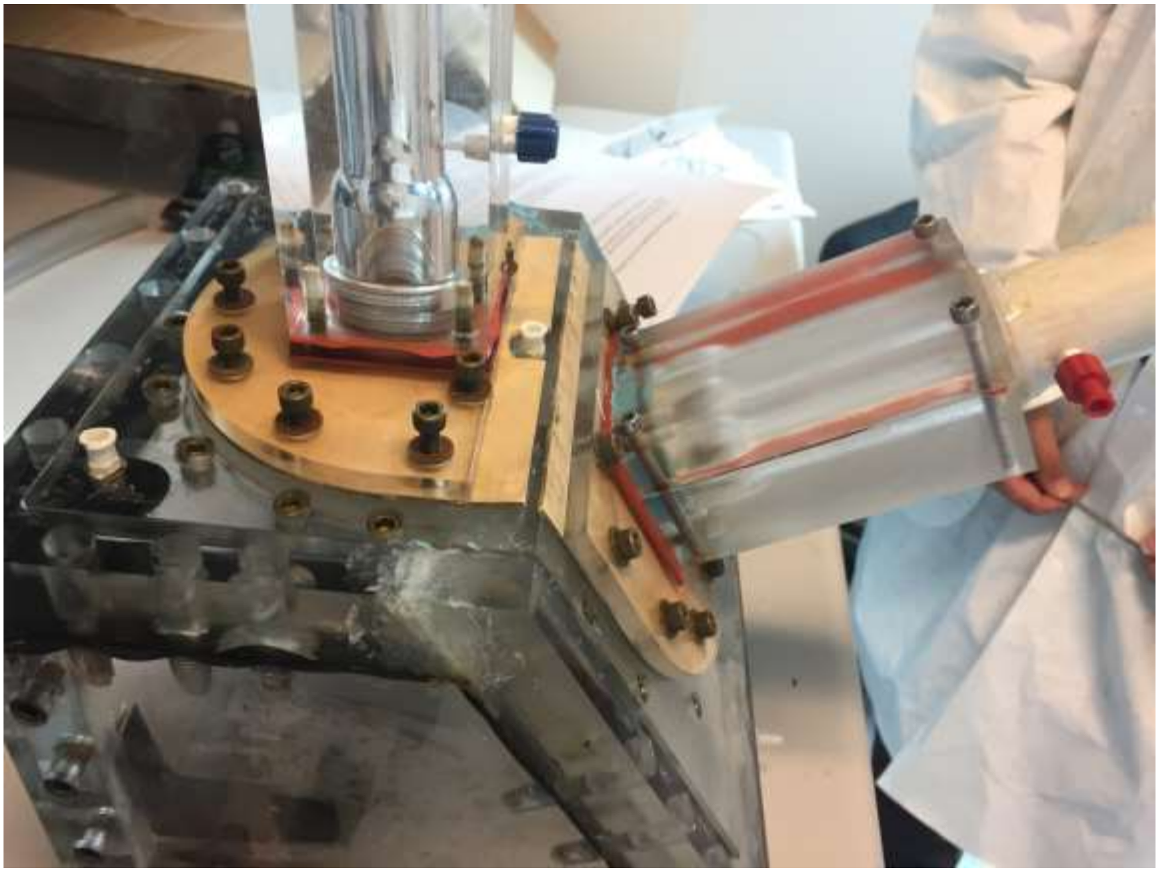

Figure B-9. Assembly of AV/aorta and MV/atrium to the LV box.

B.3 Electrical Wiring

This part involves proper wiring/connections of the motor, pressure and flow probes, their respective power supplies and input boxes, and the cDAQ system.

At this point B.2 needs to be completed

Step 1: Attach pressure probes to wall taps. Take the other ends and plug them in the rear of the pressure probe box's individual conditioner/amplifier boards. For ease of use, configure so that on the pressure probe box, Channel 1 = LV Box; Channel 2 = LV Chamber; Channel 3 = Aorta. (Figure B-10)

Figure B-10. Rear of pressure transducer conditioner/amplifier.

<u>Step 2:</u> Connect the BNC cables from the analog-out BNC splitter to the analog-in BNC cDAQ module (Figure B-11). For ease of use, connect the channels to their respective selves, i.e. 1-to-1, 2-to-2, etc. (BNC splitter has numbers on it corresponding to the probes).

We currently use probes 5, 6, and 7 for channels 1, 2, and 3, respectively

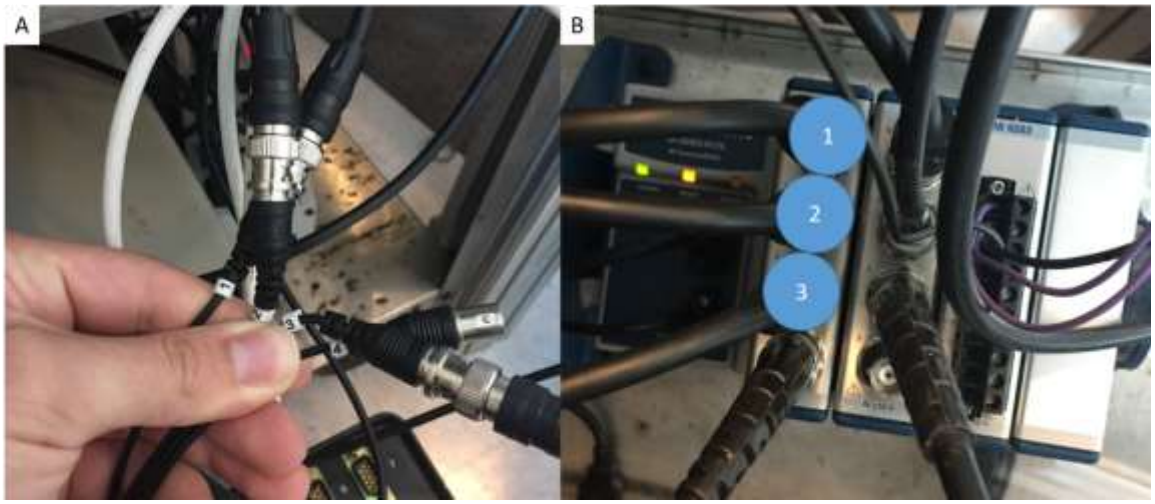

Figure B-11. (A) Notice the respective numbering on the BNC analog-out cords; (B) Analog-in channels on the cDAQ.

<u>**Step 3:**</u> Attach flow probes into the flow loop. One upstream of the MV, just before the atrium chamber, and the other downstream of the AV, just after the aorta chamber. Make sure the positive arrow on the probe is facing in the direction of the flow. If not, you can correct by multiplying by a negative one in LabVIEW.

<u>**Step 4:**</u> Plug flow probes into "flow box" (power supply and conditioner/amplifier). For ease of use, configure so that the MV inlet is in Channel 1 and AV out is in Channel 2. Connect BNC analog out channel from flow box to the BNC analog-in cDAQ module. For ease of use, configure so that the flow BNC input is in Channel 4 of the cDAQ module (Figure B-12).

We currently use probe 207 for MV inlet and 208 for AV outlet

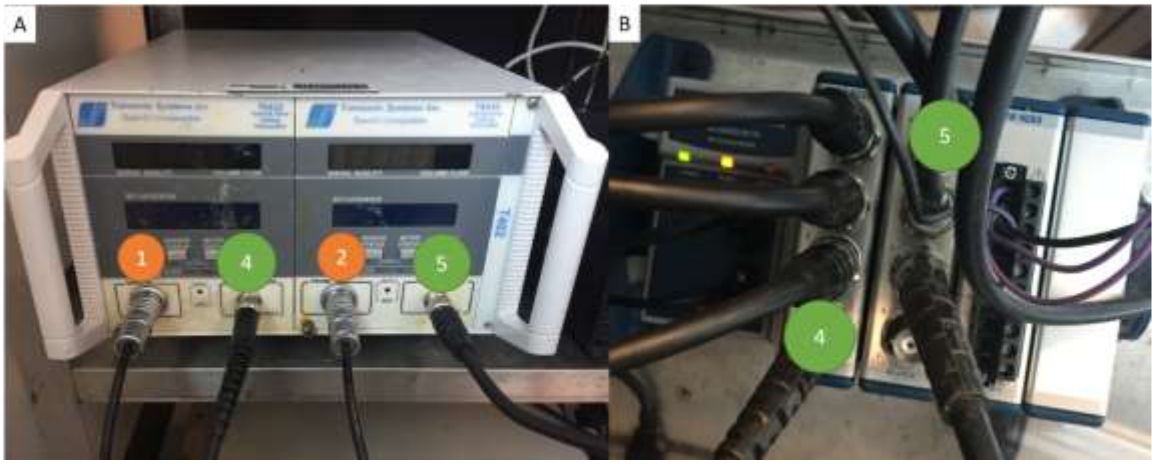

Figure B-12. (A) Flow probe conditioner/amplifier; (B) Analog-in channels on cDAQ. Orange = flow probe inputs, Green = connection between flow box and cDAQ.

B.4 Add Fluid and Tune Phantom

Here you will add your fluid and tune the loop for pressure and flow.

At this point B.3 needs to be completed

Make sure that the pressure transducers are on and that all pipes are closed off, so that there is no leaking

__Step 1:__ Add fluid to flow loop reservoir and check for leaks. If leaks, stop and reassemble, otherwise continue.

__Step 2:__ Slowly add fluid to LV box using the funnel. Make sure the top wall top is open for air to escape the box. Once full blead the hose line to the pump of air using the tap on the pump's piston head. Top off the box and shut the valve on the pump/filling line (Figure B-13).

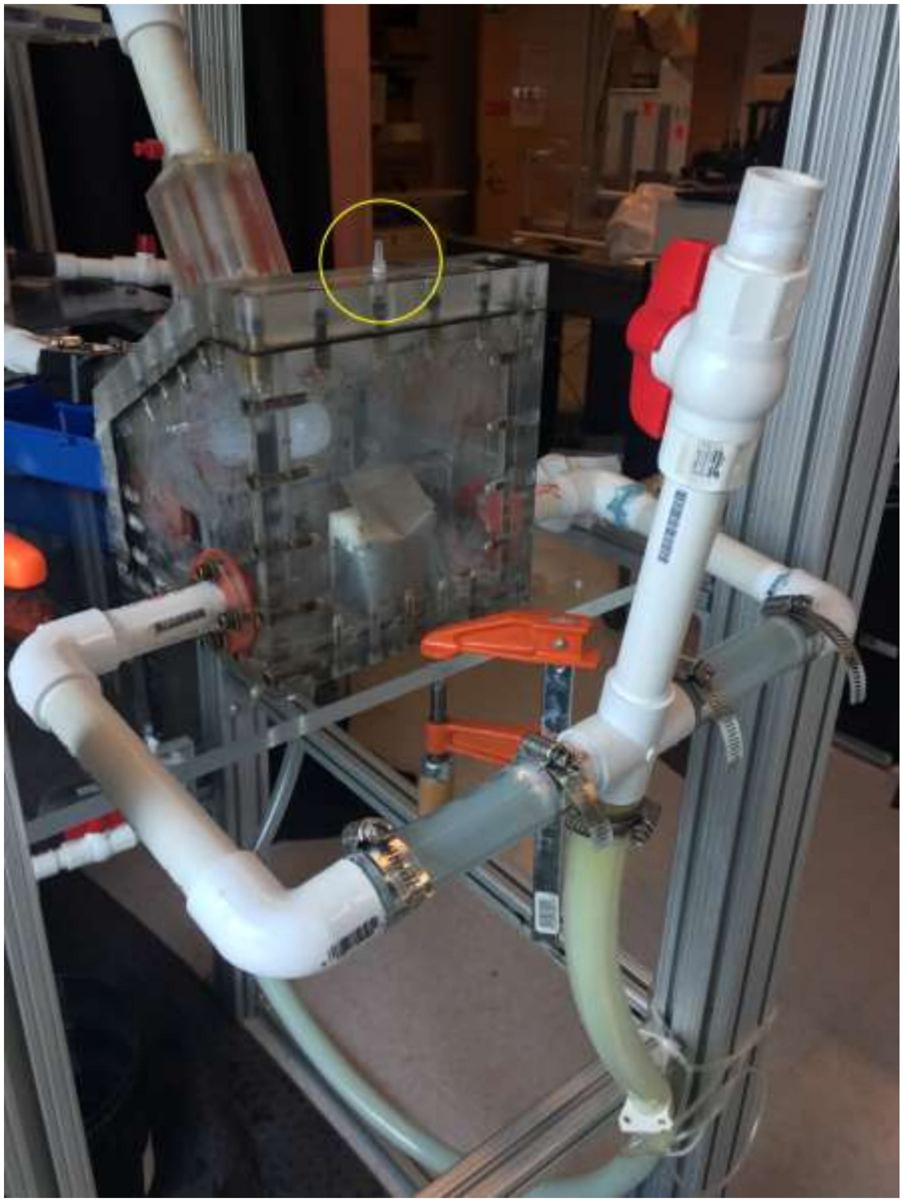

Figure B-13. Funnel goes above vertical tube to fill pump line. Air comes out of the tap (circled in yellow) at the top of the box.

<u>Step 3:</u> Run the flow loop. Once the LV phantom and box are full of liquid you can add/remove liquid to ensure proper contraction of the phantom.

APPENDIX C. MANUFACTURING GUIDE – GEORGIA TECH TRANSCATHETER AORTIC VALVE

Parts of Appendix C were modified from Prem Midha[125]

Summary

This manufacturing guide details the step-by-step instructions for creating a clear GT-TAVR valve. This includes material selection, tissue treatment, and suture technique. The current model is roughly based on the Edwards SAPIEN 3 design; however, this technique can be altered slightly to create models of other transcatheter heart valve designs.

Parts Utilized

- 1/32” Acrylic Sheet: purchased from ZLazr
- Aluminum Rod: purchased from McMaster-Carr
- Bend-and-Stay 316L Stainless Steel Wire: purchased from McMaster-Carr
- Fresh Bovine Pericardium: purchased from Animal Technologies
- Glutaraldehyde Solution: purchased from VWR
- Phosphate Buffered Saline (PBS): purchased from VWR
- Stainless Steel Pins: purchased from McMaster-Carr
- Rubber Sheet: purchased from McMaster-Carr

C.1 Stent Manufacturing

This part involves fabrication of an acrylic stent pattern for the GT-TAVR.

Step 1: Design an appropriate stent pattern. Designing a stent pattern is the most critical step in the manufacturing of a GT-TAVR, as the relevance of your experiment relies on meaningful dimensions. There are many resources that will help guide this process including Mano Thubrikar's textbook "The Aortic Valve",[133] manufacturer drawings of their leaflet patterns, and clinical data on aortic valve dimensions as published by many research groups.[20, 134-138] Ultimately, the design process is not something that can be prescribed in a protocol, but an example design is provided below. Be sure to account for your material thickness in the design.

Step 2: Once you have finalized a design, export the drawing as a *.ai file, with appropriate line coloring (red) and line thickness (0.001 pt or similar) for laser cutting. This drawing stores the vector paths of your design.

Step 3: Cut your designs into the thin acrylic sheet on a laser cutter. The resulting transparent stent should look similar to the Figure C-1 below.

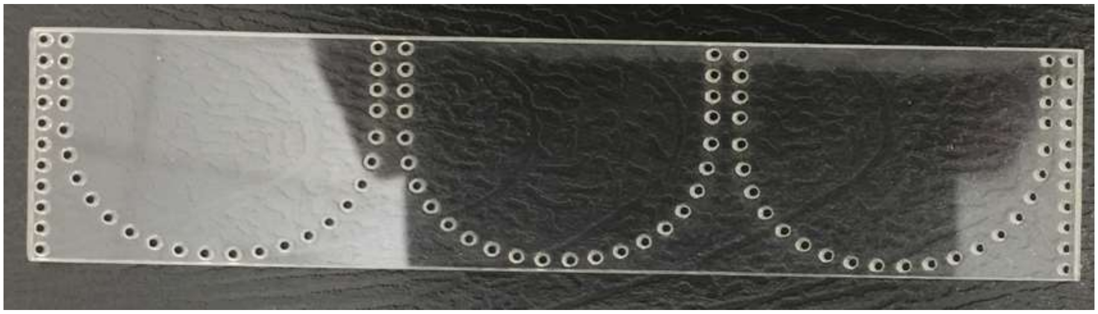

Figure C-1. Example of GT-TAV stent frame post laser cut.

<u>Step 4:</u> The flat pattern will need to be rolled into a cylindrical shape. In order to facilitate this process, machine both an aluminum mandrel for the desired internal stent diameter as well as a clamp for the desired outer stent diameter (Figure C-2). Registration features can also be included to aid with aligning the acrylic material parallel to the curvature in the aluminum tools.

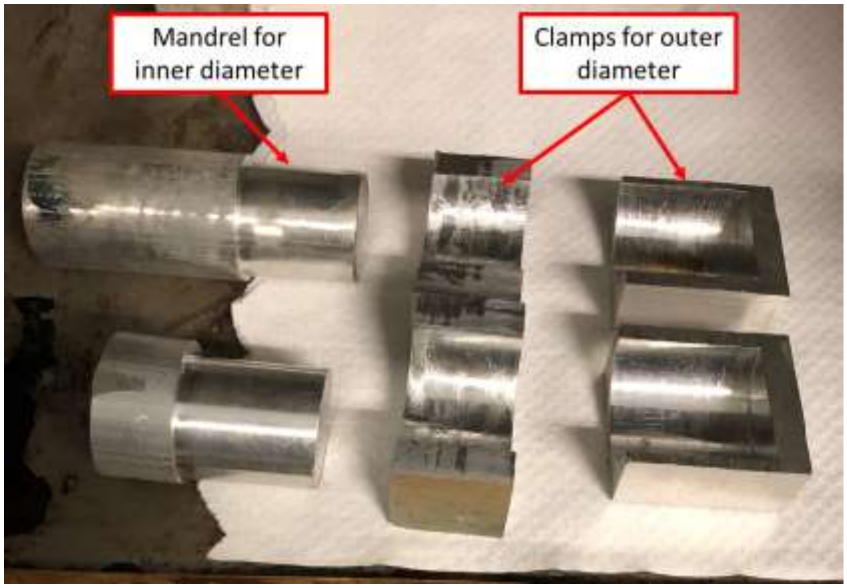

Figure C-2. Machined aluminum mandrels specified to the internal diameter of the GT-TAV and machined clamps specified to the external diameter of the GT-TAV.

<u>Step 5:</u> While heating the oven to 180˚C, place the mandrel, O-clamp, and acrylic stents inside. The melting point of acrylic is 160˚C. Monitor the materials while heating to ensure that the acrylic does not fully melt. Overheating the materials slightly will ensure that the acrylic is very flexible for enough time to allow the aluminum tools to impart a consistent and continuous curve to the rolled acrylic stent. To avoid transference of other materials that may be on the bottom of the oven, place the acrylic stents on a clean metal surface.

<u>Step 6:</u> Once the oven has reached 180˚C, wearing insulated gloves, quickly remove the stent and aluminum tools from the oven. Carefully wrap the stent around the mandrel to achieve a cylindrical shape. Press the stent against the mandrel to ensure that a continuous curve is imparted to the acrylic. The acrylic should be easily malleable at this temperature.

<u>Step 7:</u> Once a general cylindrical shape is imparted to the acrylic (Figure C-3), it may be necessary to refine the shape further. In order to do so, place the acrylic within the O-Clamp and reheat for a short period of time. The acrylic will expand and unfurl within the O-Clamp. Once this is observed, use the insulated gloves and aluminum mandrel to press the acrylic into the O-Clamp to refine the cylindrical shape. It may be necessary to repeat this process. It is also possible to use a heat gun to gently induce flexibility of the acrylic for spot corrections. It is important to ensure that the vertical edges of the acrylic that are joined together when made into a cylinder maintain the appropriate curvature of the cylinder.

Figure C-3. Example of finished GT-TAV stent frame.

C.2 Retaining Ring Manufacturing

This part details the procedure for fabrication of the retaining ring made of stainless steel wire that is used to model the fact that commercial valves are manufactured such that the leaflets are attached perpendicularly to the walls of the stent. In this model, the leaflets are *parallel to the walls of the stent. The retaining ring (Figure C-4) will be inserted into the valve to force the leaflets into the perpendicular configuration.*

Step 1: 3-D print an appropriate mold that outlines the valve leaflet outline (Figure C-4).

Figure C-4. Example of GT-TAV retaining ring and the 3-D printed mold to make it.

Step 2: Cut a section of stainless steel wire longer than you will need.

Step 3: Using a flathead screwdriver and pliers, gently compress the wire into the mold one commissure at a time. Ensure that the retaining ring curvature is continuous and smooth.

Step 4: Trim the excess material and finish forming the retaining ring.

Step 5: Carefully remove the retaining ring from the mold, so as not to distort the shape.

C.3 Pericardium Fixation

This part details the procedure for fixing the pericardium used to make the valve leaflets. Many studies and manufacturer protocols have described pericardial tissue fixation techniques,[139-142] *but most fall within the same general bounds: ~0.625% glutaraldehyde in phosphate buffered saline (PBS) under low pressure (~4mmHg) for approximately 36 hours. For storage, a 0.2% glutaraldehyde in PBS solution is used.*[142]

Step 1: Create a large batch of 0.625% glutaraldehyde solution with PBS.

Step 2: Place a rubber sheet at the bottom of a deep, stainless steel tray. Cut large, flat sections from the fresh pericardial sack and pin the edges to the rubber sheet. Try to minimize any wrinkles or folds in the tissue during this step of the process.

Step 3: Pour approximately 2 inches of 0.625% glutaraldehyde solution on top to generate a 4mmHg pressure head.

Step 4: Let sit in the refrigerator for 36 hours.

Step 5: After 36 hours, rinse the tissue serially in saline and store in 0.2% glutaraldehyde solution.

C.4 Valve Assembly

This part details the procedure for trimming, attaching, and suturing tissue to the acrylic stent to form the valve leaflets.

At this point C.1, C.2, and C.3 need to be completed

Step 1: Trim out a uniform section of fixed pericardium. This section of pericardium should be a rectangle approximately 1 cm taller than the original unrolled acrylic stent height and 1 cm longer than the unrolled acrylic stent width. Trimming the section of pericardium may be easier if the tissue is dried slightly first, however, be cautious not to leave the tissue in this state for more than 5 minutes. Continually rehydrate the valve in saline or storage solution throughout the process of assembly.

Step 2: Insert the pericardium into the rolled stent. The tissue should be aligned such that the making sure to offset the tissue edge 0.25 cm from the bottom edge of the stent. The stent should be aligned like a crown, where the commissure posts point upward and are the top edge of the stent, while the continuous edge of the cylinder is the bottom (Figure C-5). The shorter edge of the pericardium should be aligned 0.25 cm offset from the break in the acrylic, creating a small overlap across the two unconnected edges of the cylindrical acrylic stent.

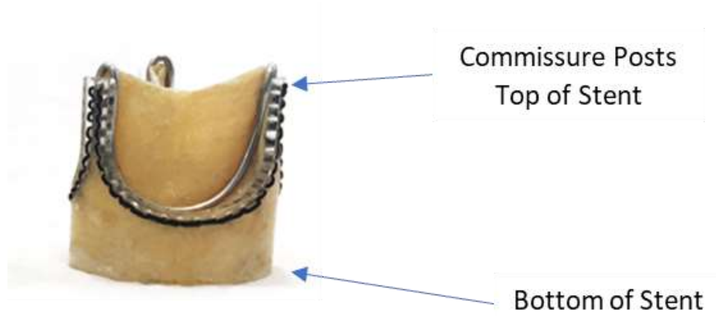

Figure C-5. Diagram of GT-TAV orientation.

<u>Step 3:</u> Suture the pericardium to the stent with a back-stitch (Figure C-6). A back-stitch provides the best seal against leakage. Suturing should first start at the commissure near the seam of the acrylic, then continue across the arches. While suturing, care should be taken to ensure the pericardium tension is evenly distributed across the circumference of the stent. Rehydration of the pericardium consistently is an important factor in achieving an even distribution of tension.

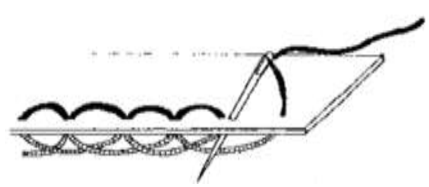

Figure C-6. Diagram of the back-stitch sewing technique.

<u>Step 4:</u> Once the suture comes to the other side of the seam, the suture should continue downwards, binding both edges of the seam together with a running stitch. These stitches should be across two layers of pericardium, due to the original overlap.

Step 5: A back stitch suture should be used across the bottom of the stent to fix the pericardium in place. A knot should then be tied to hold the tension. This knot should be placed away from any delicate structures on the stent design.

Step 6: The tissue should then be trimmed to ensure both minimum overlap across the seam as well as 1 cm of coaptation of the valve leaflets. It may be helpful to first close the leaflets, insert the retention ring, and then trim the valve leaflets to achieve adequate coaptation.

Step 7: In order to test the adequate coaptation of the valves, a valve coaptation test should be conducted. The valve should first be placed in a clear plastic tube with a tight seal around the outside diameter of the plastic stent, then running water should be poured into the plastic tube (Figure C-7). If the valve demonstrates adequate coaptation, the running water will be occluded by the valve. Be sure to examine the center of the stent where the valves meet, as well as the stitches to ensure no leakage.

Figure C-7. Image of GT-TAV leak test with a plastic tube full of water and a 29 mm GT-TAV plugging the bottom. Note: the valve shows good coaptation.

Step 8: Use tissue-grade cyanoacrylate (super glue) to seal the knot of the stent.

Step 9: Insert a retaining ring over the leaflets. The final product should look similar Figure C-8. A very small amount of super glue may be necessary to fix the retaining ring to the top of the stent posts.

Figure C-8. Diagram of different varieties of finished GT-TAVs.

APPENDIX D. EXPERIMENTAL PROTOCOL – HIGH-SPEED PARTICLE IMAGE VELOCIMETRY

Parts of Appendix D were modified from Prem Midha.[125]

Summary

This experimental protocol details the describes the high-speed particle image velocimetry (HSPIV) hardware configuration and data collection procedure.

D.1 Hardware Configuration

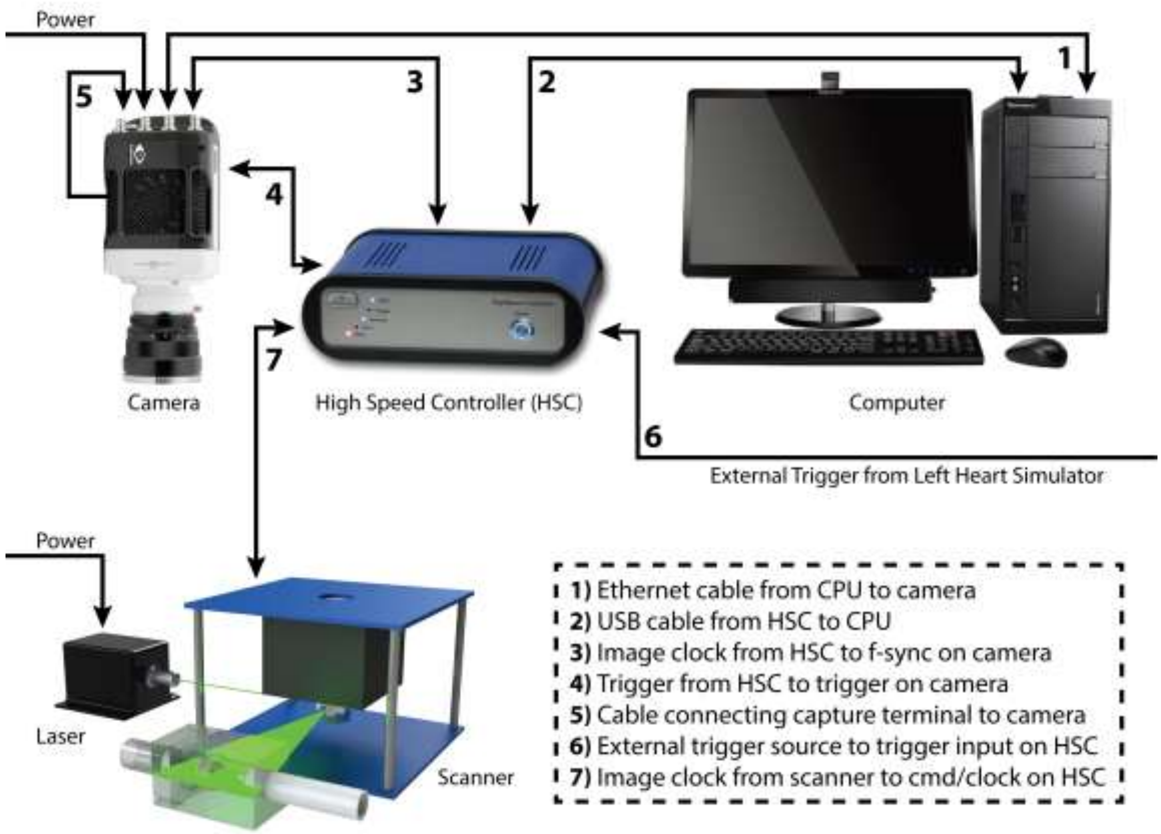

Figure D-1. High-speed PIV hardware configuration.

High-Speed PIV Checklist:

1. DO NOT turn the laser on until scanner is on and the experimental set up is ready.

2. Turn the camera ON before launching the Davis application to ensure camera recognition.

3. The band-pass filter should be installed on the camera lens to filter undesirable frequencies of light.

4. The cap of the camera should be always closed unless acquiring data to minimize risk of sensor damage.

5. Turn the scanner on before turning on the laser. Failure to do so can results in damage to the mirror array and anything the reflected beam hits.

6. Use the vertical traverse to place the pulsed laser sheet at the desired plane within the flow chamber.

7. Focus the camera on the seeding particles within the plane of the laser sheet.

8. Choose a camera aperture setting in the range 2.8 – 4.

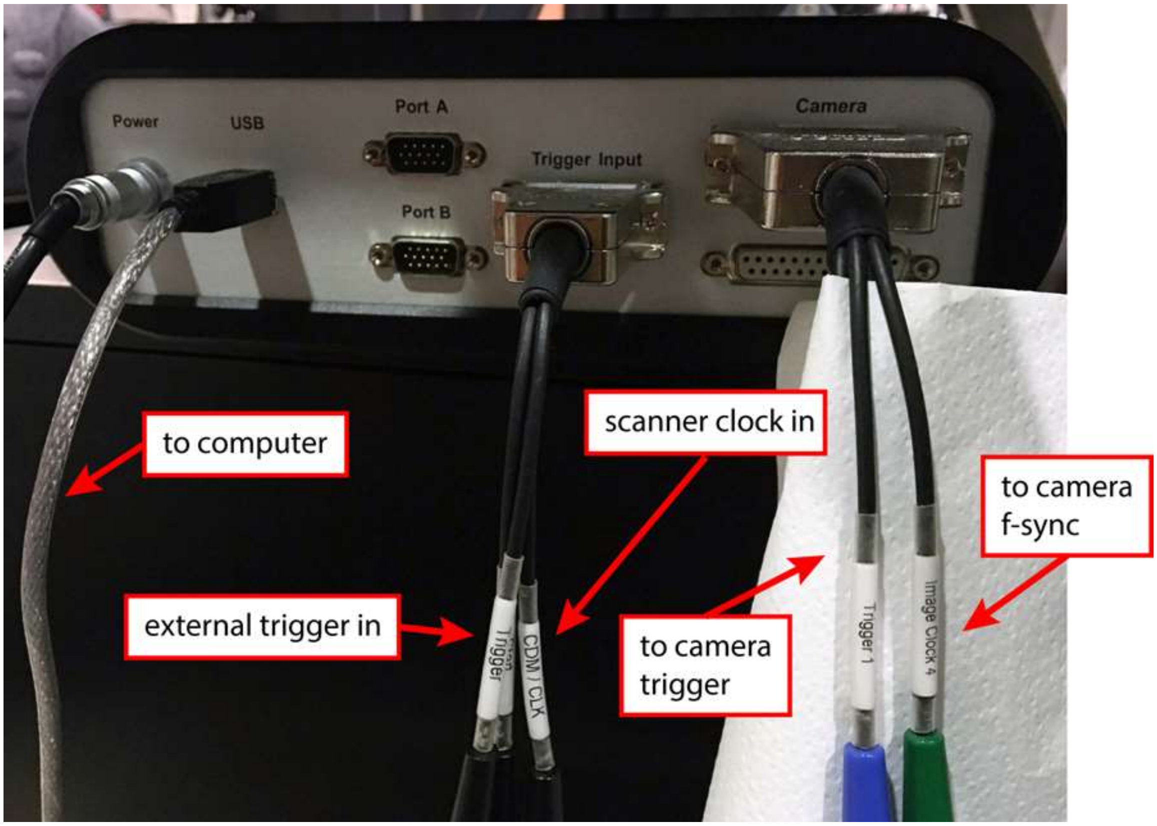

Figure D-2. **Rear of high-speed controller.**

<u>**High-Speed Controller:**</u> The LabView program controlling the realistic left heart simulator sends its trigger (external trigger in) to the high-speed controller (HSC) at the desired time point during a cardiac cycle (e.g. start of diastole) (Figure D-2). The controller augments this trigger and commands the camera to acquire (to camera trigger) at a time (to camera f-sync) that is near the input trigger, but also corresponds to a laser pulse. This link is created through the scanner clock signal (scanner clock in). sends the starting trigger and the frequency of image acquisition to the camera.

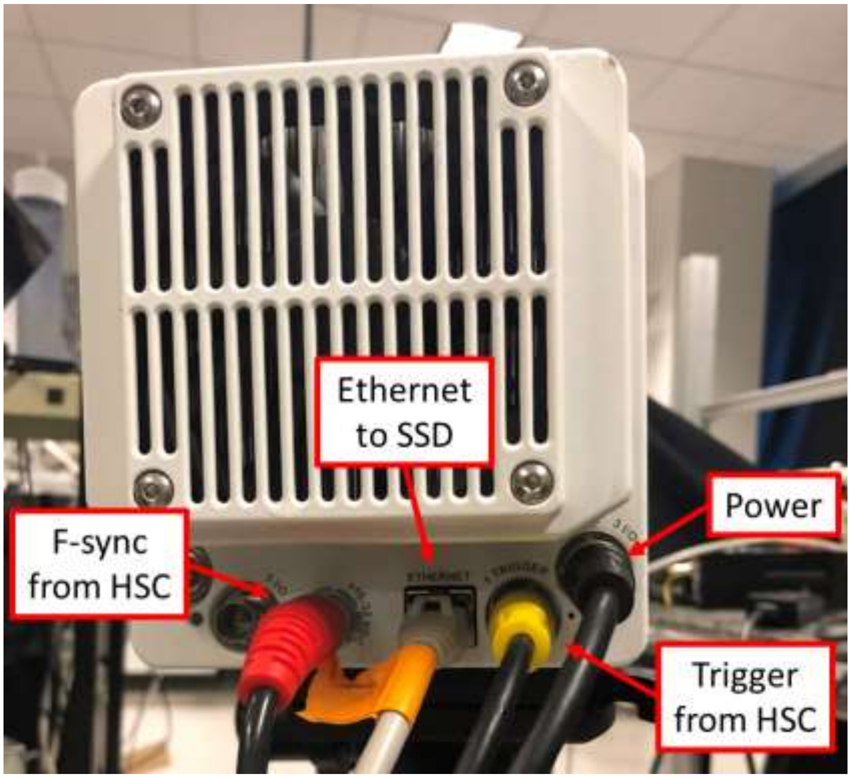

Figure D-3. Rear of Phantom VEO 340L camera.

<u>High-speed camera:</u> The f-sync cable connects to the high-speed controller and provides the camera with the reference times when the laser is pulsing (scanner clock) (Figure D-3). The trigger from the HSC provides a TTL pulse which instructs the camera to begin acquisition. The Ethernet cable transfers data back to the PIV computer.

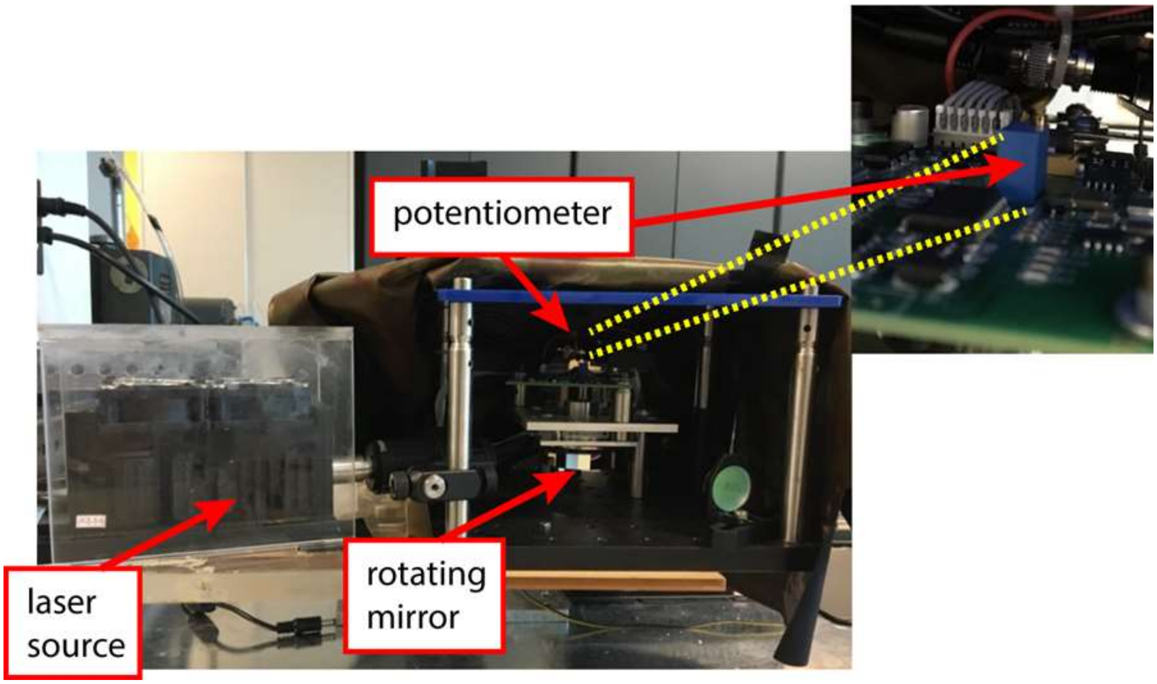

Figure D-4. Primary view of high-speed scanner and laser.

<u>Scanner and Laser Source:</u> The laser source emits a continuous wave laser beam which gets converted into a pulsed laser sheet via rotating mirror array (scanner) (Figure D-4). A portion of the reflected laser sheet hits mirror which again sends a portion of the signal back to an optical sensor which detects the laser pulse frequency. The frequency of laser pulse is adjusted by turning a potentiometer controlling the rotating mirror speed. The potentiometer is accessible from the top of the scanner and fits a small flathead screwdriver. This frequency is provided as the clock input to the high speed controller via the cmd/clock terminal.

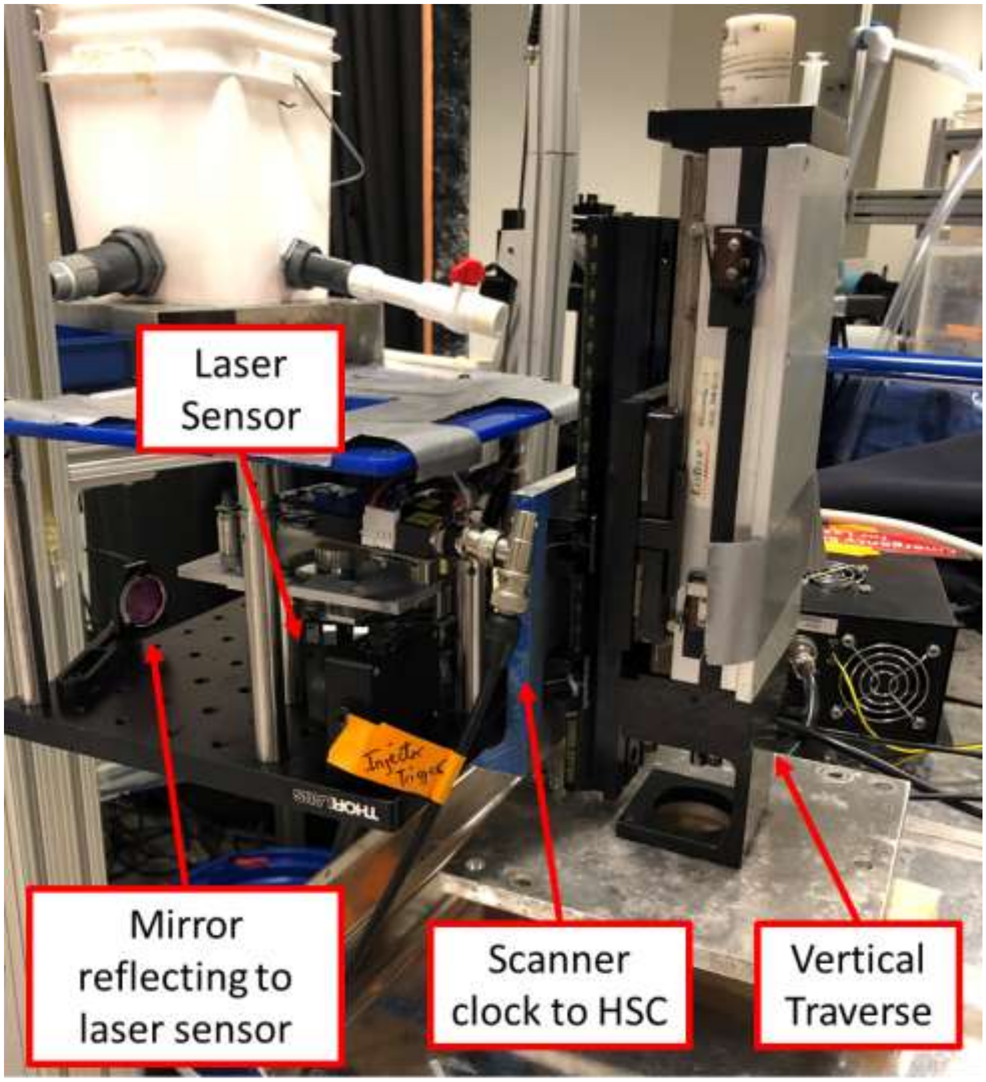

Figure D-5. Secondary view of high-speed scanner and laser system highlighting adjustable traverse system and laser sensor.

<u>Scanner Accessories:</u> The vertical traverse allows for easy adjustment of the z-position of the laser sheet within the flow chamber. The scanner and laser source are mounted to a single plate, which is adjusted by this traverse. The laser power supply has no failsafe and must not be turned on until the scanner is turned on or the laser will damage the mirror array. The high frequency spinning of the array prevents damage.

D.2 Data Collection – DaVis

Make sure the camera is plugged into the high-speed controller on the DaVis computer and turned on

Make sure the trigger is plugged into the high-speed controller on the DaVis computer and a signal is coming from the LabView computer

Step 1: From the starting window, create a new PIV project (Figure D-6). After selecting a MyProjects folder by right-clicking a desired folder from file tree, click the **New+ → Project name: Specify: *"user defined"* → Type of project: PIV → Ok**. After clicking okay, the project should open to the next window.

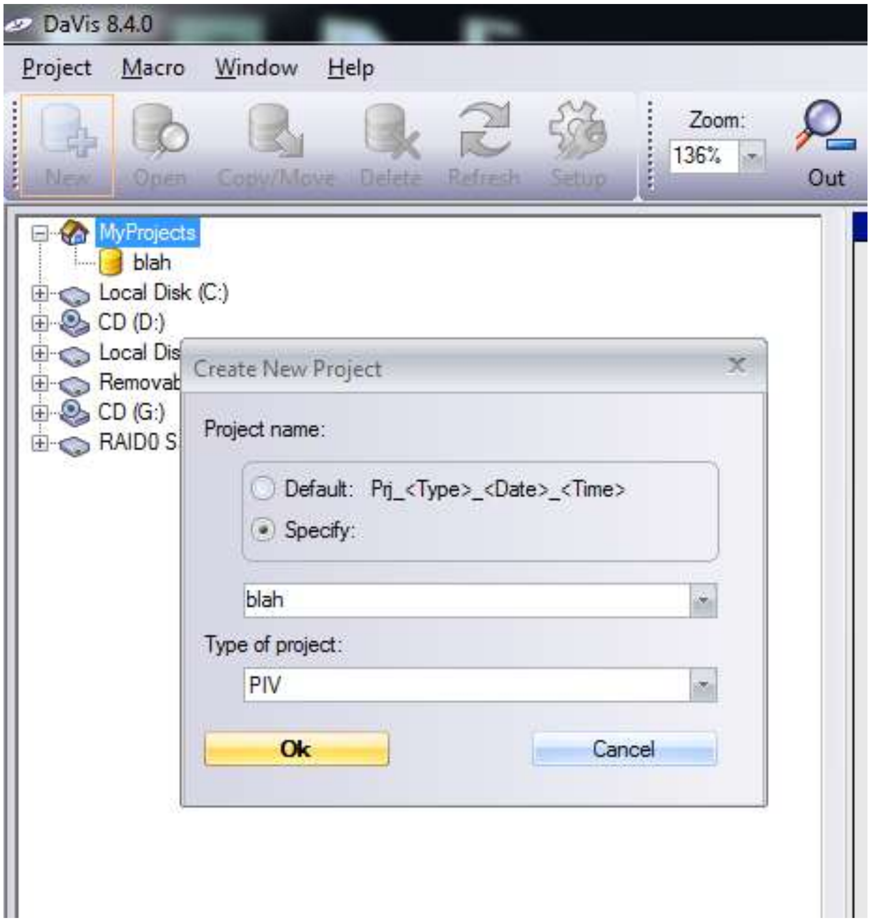

Figure D-6. Starting window where you create a new project.

<u>Step 2:</u> In the new Project window (Figure D-7), click **Recording** to open recording window (Figure D-8).

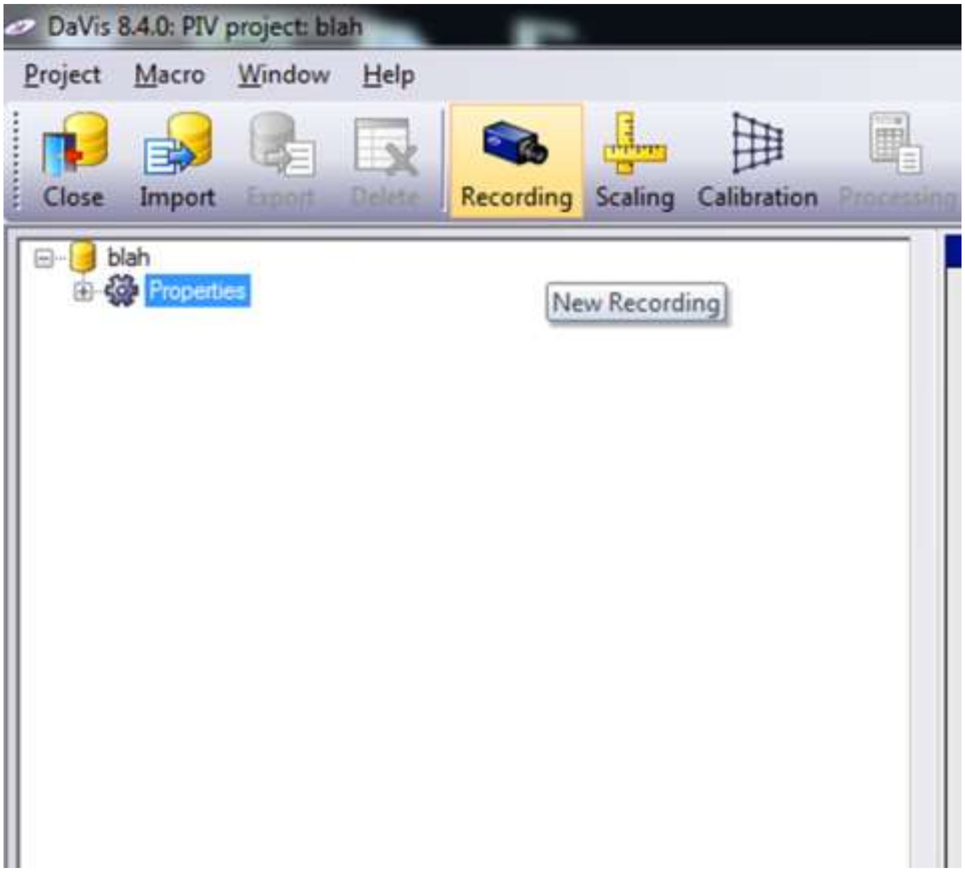

Figure D-7. Project window for PIV where you access tasks such as recording, scaling/ calibration, and processing.

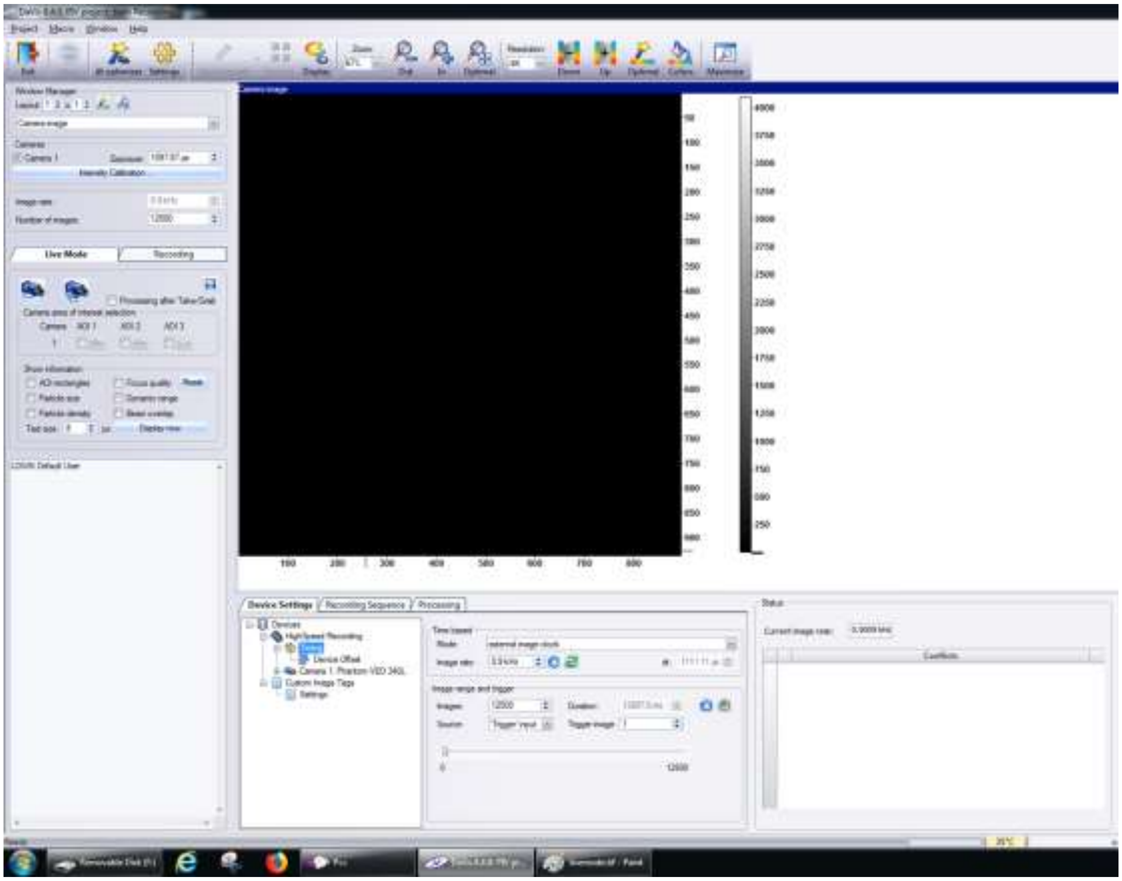

Figure D-8. Recording window for PIV acquisition.

Make sure the laser sensor is plugged into the high-speed controller on the DaVis computer with the laser and scanner turned on

<u>Step 3:</u> From recording window, configure Device Settings tab under the **Devices → HighSpeed Recording → Timing** (Figure D-9). You should see a current image rate signal to the right if the laser if correctly hitting the laser sensor. If it is not, adjust the laser. Set **Time based>>Mode:** to **external image clock** and click the refresh button next to **Time**

based>>Image rate: to sync with **current image rate**. Next set **Image range and trigger>>Images:** to ***"user defined"*** and **Image range and trigger>>Source:** to **'Trigger' input**.

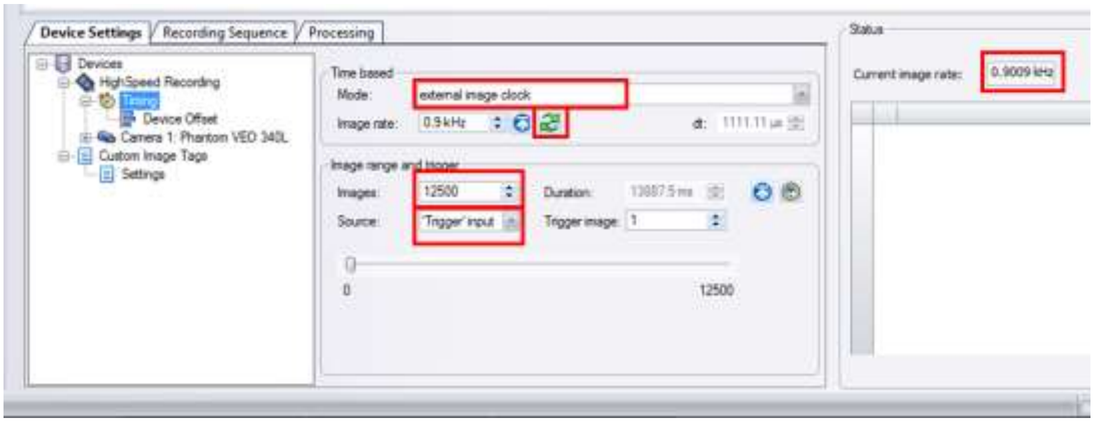

Figure D-9. Record window zoomed in on Device Settings.

<u>Step 4:</u> In the **Window Manager → Live Mode** section, click on the continuous grab icon to get the live camera view and adjust the image exposure and focus (Figure D-10).

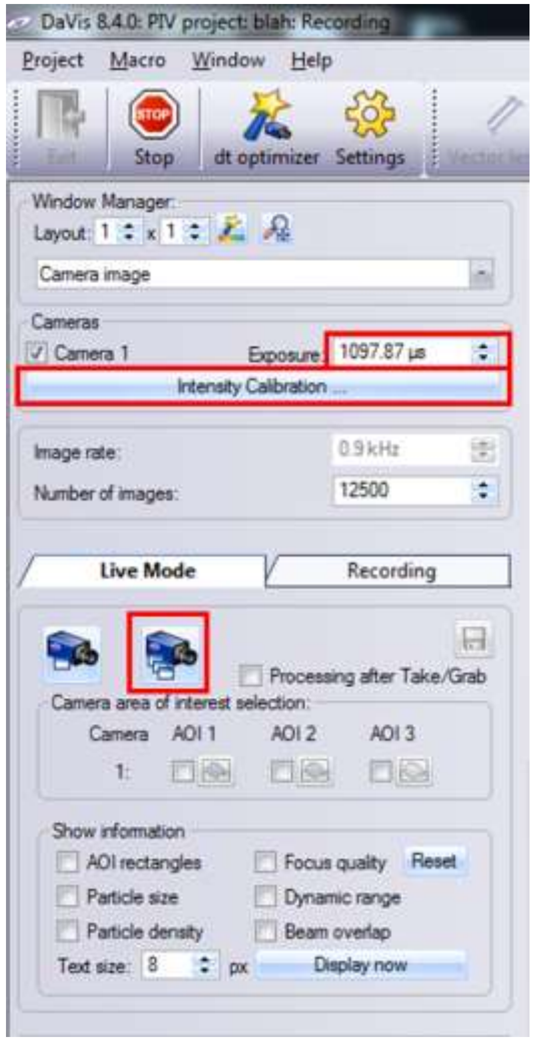

Figure D-10. Recording window zoomed in on Intensity Calibration and Live Mode.

<u>Step 5:</u> To fix any noise patterns in the image you must do an intensity calibration. This step must be performed each time you start the system or any time you change the area of interest.

While leaving DaVis open, go to PSS 2.8 to restore camera to factor defaults by selecting **Manager Tab** *(top right corner)* → **Phantom Nucleus** *(bottom right corner)* →

Restore Settings → Reload factory Settings → Ok (Figure D-11). Note: make sure to select the correct camera ID.

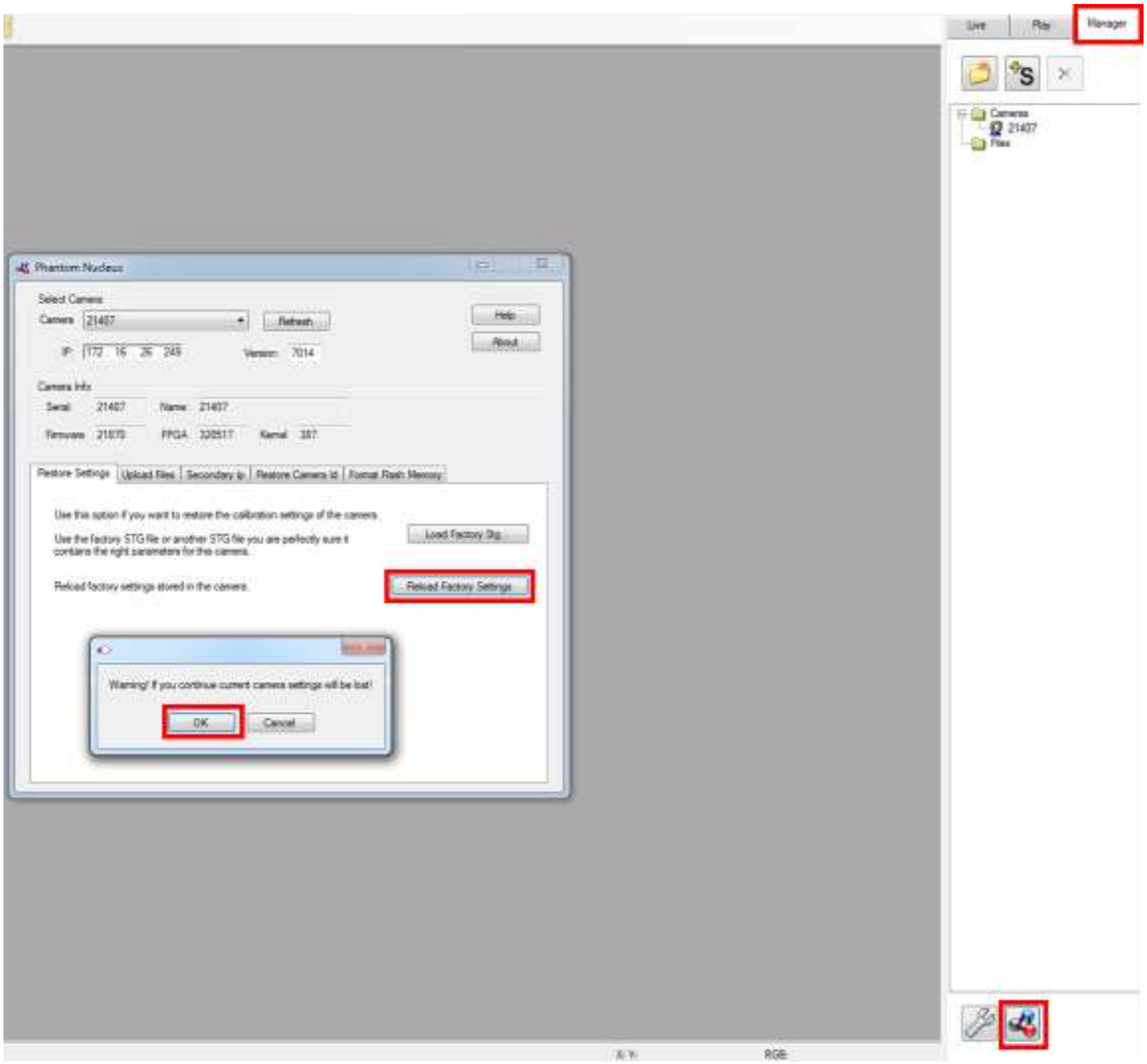

Figure D-11. Manager tab in PCC 2.8 for resetting camera to factory defaults.

Next, close the camera shutter to provide a black image for intensity calibration. Do this by selecting **Live tab** *(top right corner)* **→ Cine Settings → Close Shutter** (Figure

D-12). Note: make sure to select the correct camera ID. An icon will appear saying the shutter is closed with a new button to open it (don't click this yet).

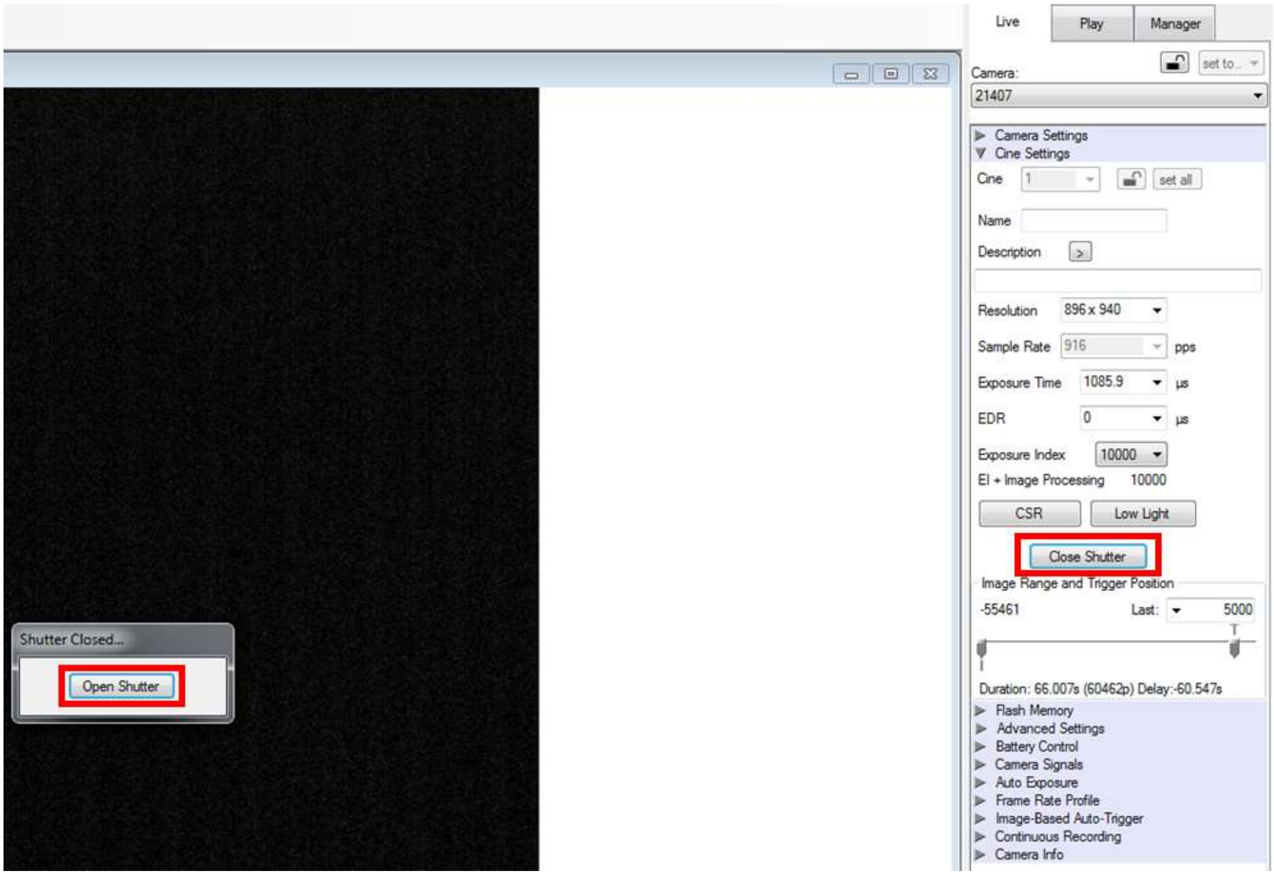

Figure D-12. Live tab in PCC 2.8 for opening and closing the camera shutter.

Lastly, go back to DaVis and click the **Intensity Calibration** button and then max out the **Exposure** (Figure D-10). Once the intensity calibration is done you can click the **Open Shutter** button in PCC to proceed with image acquisition (Figure D-12).

<u>Step 6:</u> Acquire HSPIV images. To acquire the images, go to **Window Manager → Recording** tab and click the **Record Icon** (Figure D-13). The file name can be left default to capture the information displayed below and modified later if needed.

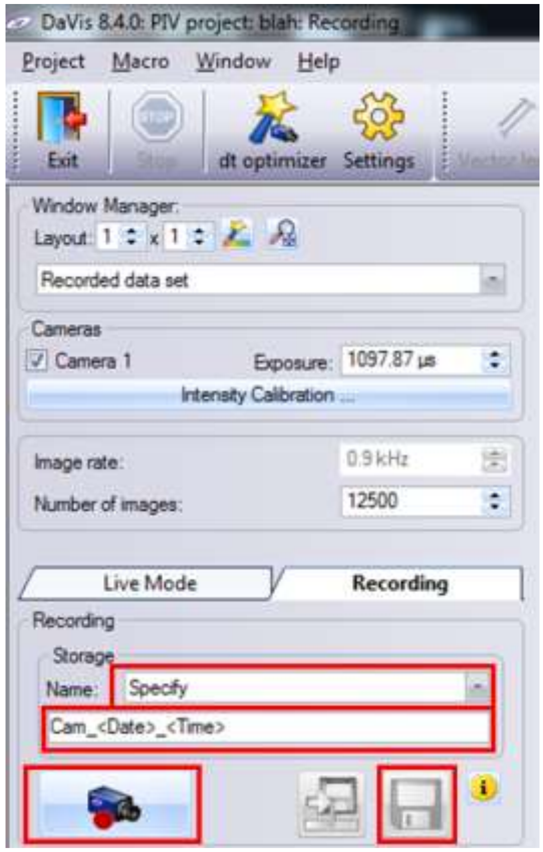

Figure D-13. Recording window zoomed in on Intensity Calibration and Recording.

Upon completion of the recording, check the images by scrolling through the acquired sequence. If satisfied save the images to the computer; specify the acquisition name via **Recording → Storage → Name: → Specify → "user defined"** and then click the **Save Icon** in the Window Manager (Figure D-13).

APPENDIX E. PROCESSING PROTOCOL – SPECIFIC AIM 2

E.1 High-Speed Particle Image Velocimetry – DaVis

E.1.1 HSPIV – DaVis 8.4 – Specific Aim 2A

Step 1: Mask Out Image (Figure E-1). This operation was used to mask out areas outside the ROI and solid objects inside the ROI (e.g. the AML or GT-TAV) from the raw image. The geometric mask was used for the AML, GT-TAV, aorto-mitral plane, and give a boundary for the maximum LV size in the 6.5 L/min condition. The algorithmic mask was used to account for the moving LV wall throughout the cardiac cycle. Variables for the algorithmic mask were slightly changed between experiments (mainly the final "below threshold" parameter).

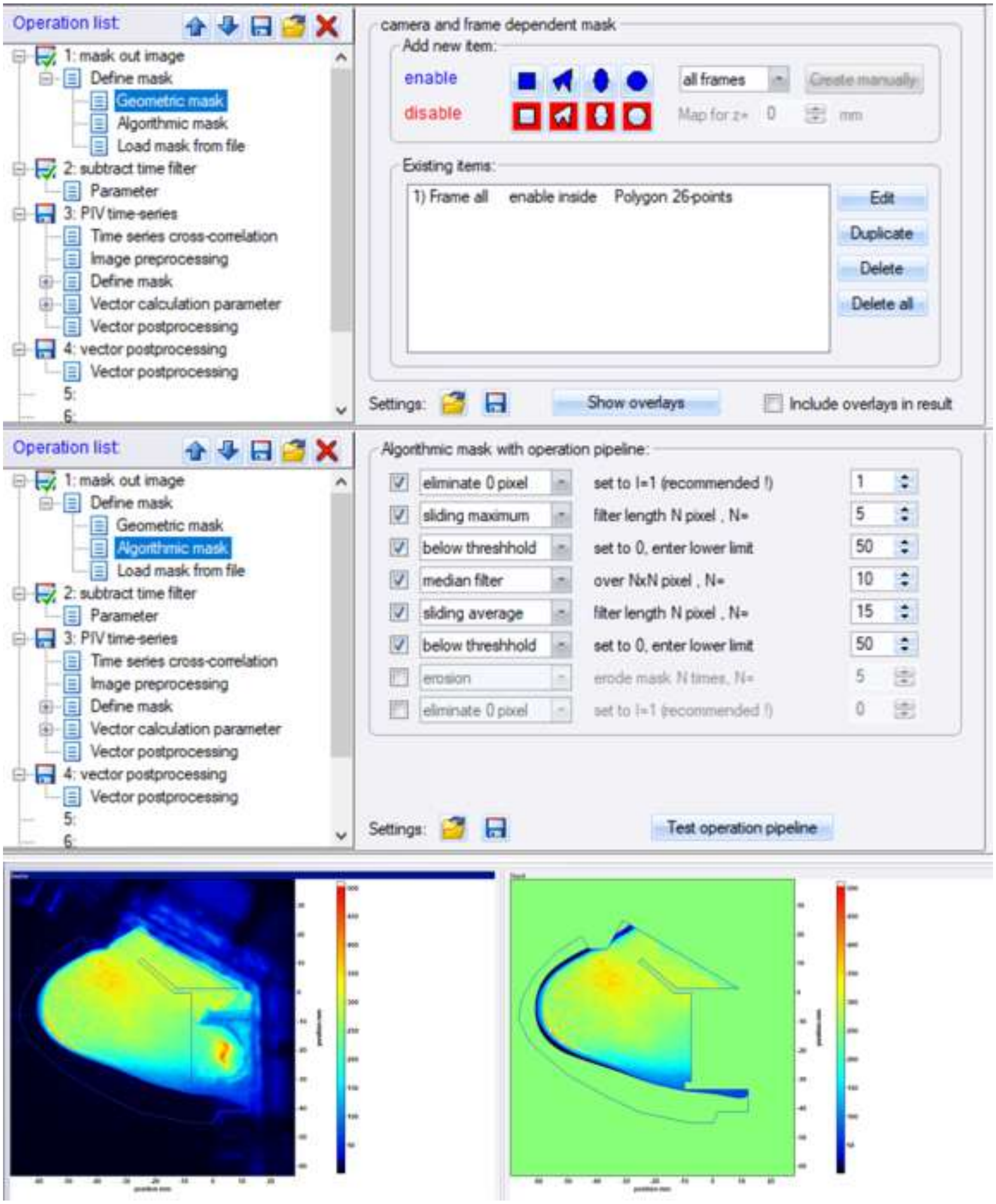

Figure E-1. Example of a Mask Out Image operation for Specific Aim 2A. Geometric and algorithmic masks were used.

Step 2: Subtract Time Filter (Figure E-2). This operation was used to subtract background noise from the masked images. For SA2A, a minimum intensity subtraction with a symmetric filter length of 5 images was used.

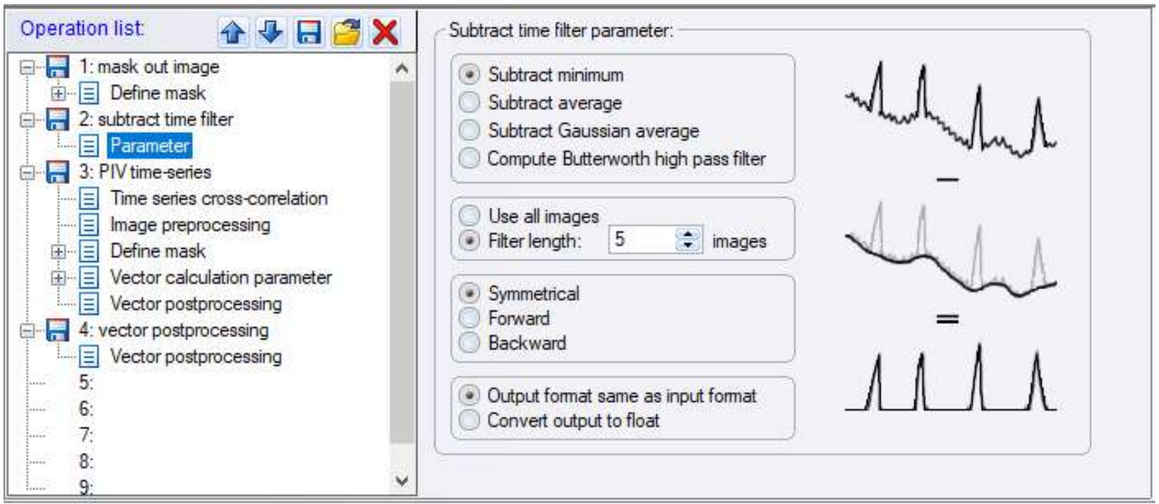

Figure E-2. Example of Subtract Time Filter operation for Specific Aim 2A.

Step 3: PIV Time-Series (Figure E-3). This operation encompasses the calculation of velocity fields via cross-correlation from the masked and filtered images. Details include:

- The previous result as a reference shift for the *Time series cross-correlation*
- Sequential cross-correlation with a data source of 0+1, 1+2, 2+3… as a *vector calculation parameter* with a multi-pass interrogation window of decreasing size and variable shape (64x64/square to 32x32/circle) with 50% overlap and 2 passes for each size. A high accuracy mode was also used for the final pass
- Default values were used for *Multi-pass options* and *Multi-pass postprocessing*.
- *Image preprocessing*, *Define mask*, and *Vector postprocessing* were not used.

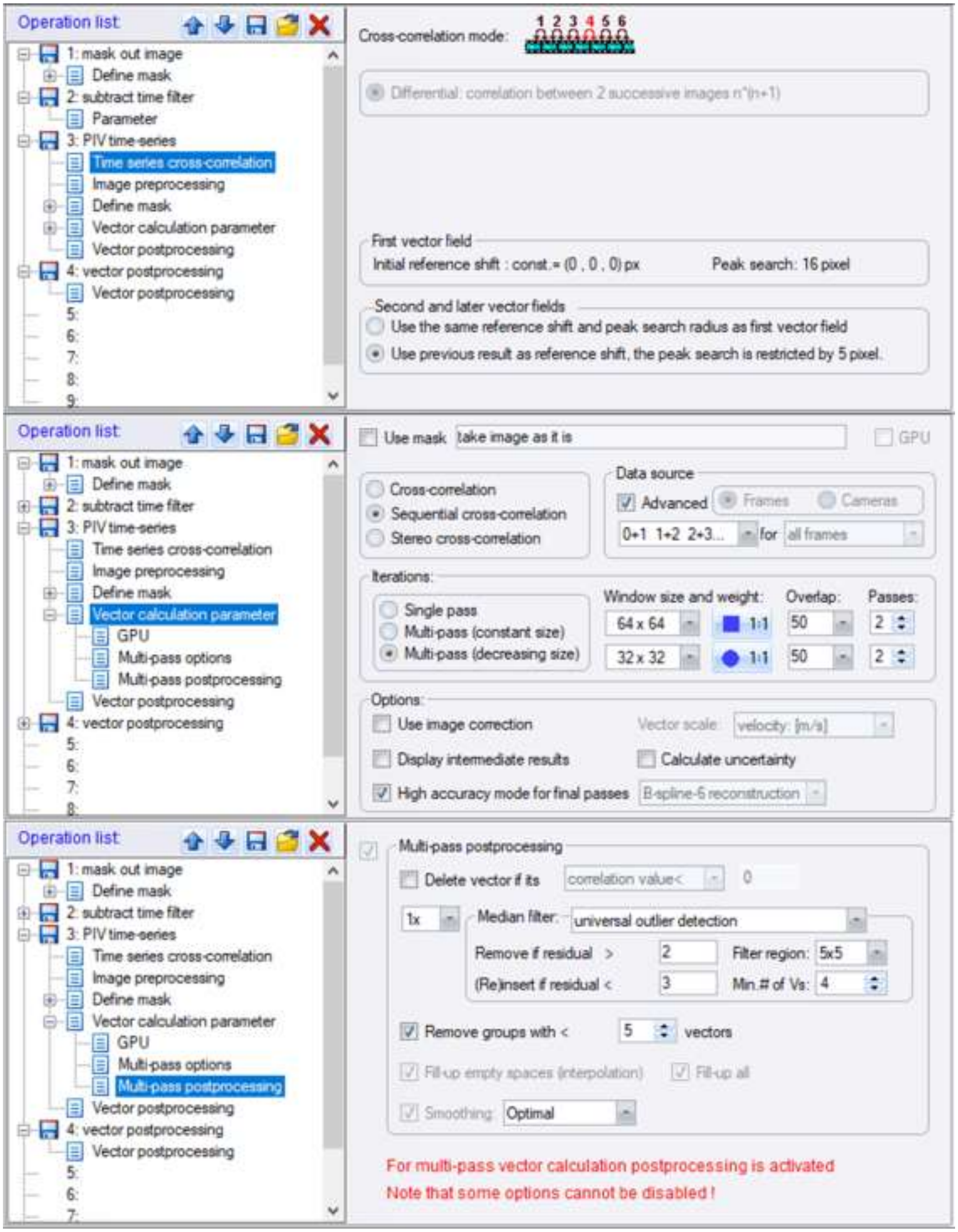

Figure E-3. Example of PIV Time-Series operation for Specific Aim 2A.

__Step 4:__ Vector Post-processing (Figure E-4). This operation was used to remove erroneous vectors and smooth the field. Details include:

- Deleting a vector if its peak ration Q< 1.3
- 2x Median filter: strongly remove & iteratively replace (if average differs by 2 and but less than 3 standard deviations from neighboring group, respectively)
- Removing groups with <5 vectors
- 1x Smoothing by a 3x3 grid
- Note: no interpolation or extrapolation was done.

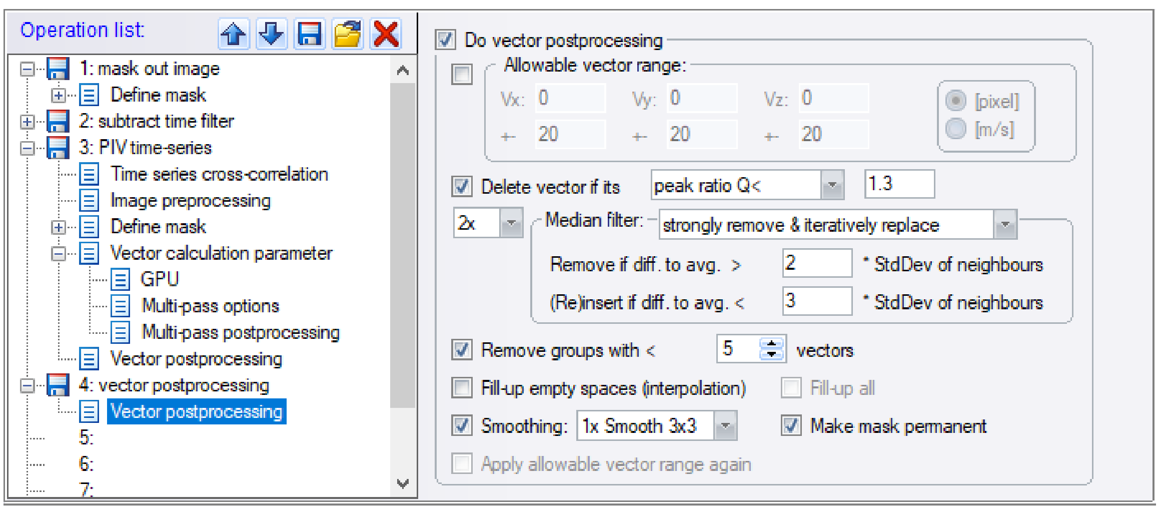

Figure E-4. Example of Vector Postprocessing for Specific Aim 2A.

E.1.2 HSPIV – DaVis 10 – Specific Aim 2B

__Step 1:__ Mask Out Image (). This operation was used to mask out areas outside the ROI and solid objects inside the ROI (e.g. the AML or GT-TAV) from the raw image. The geometric mask was used for the AML, GT-TAV, aorto-mitral plane, and give a boundary for the maximum opening of the GT-TAV leaflet size in the 6.5 L/min condition. For the 0% LAMPOON condition, the algorithmic mask was used to account for the moving GT-TAV leaflet throughout the cardiac cycle instead of the static geometric mask at the maximum opening.

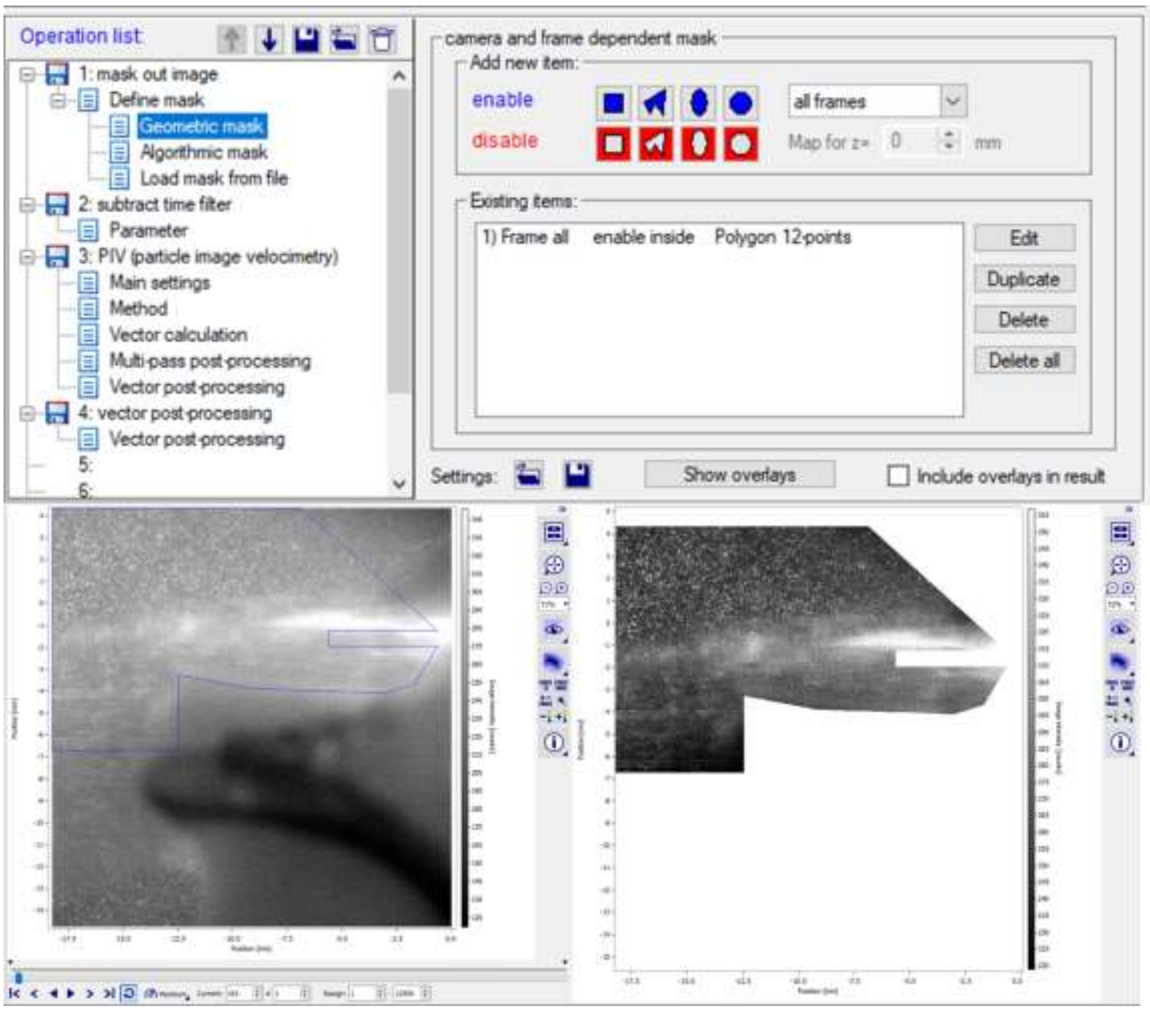

Figure E-5. Example of Mask Out Image operation with only geometric mask for Specific Aim 2B.

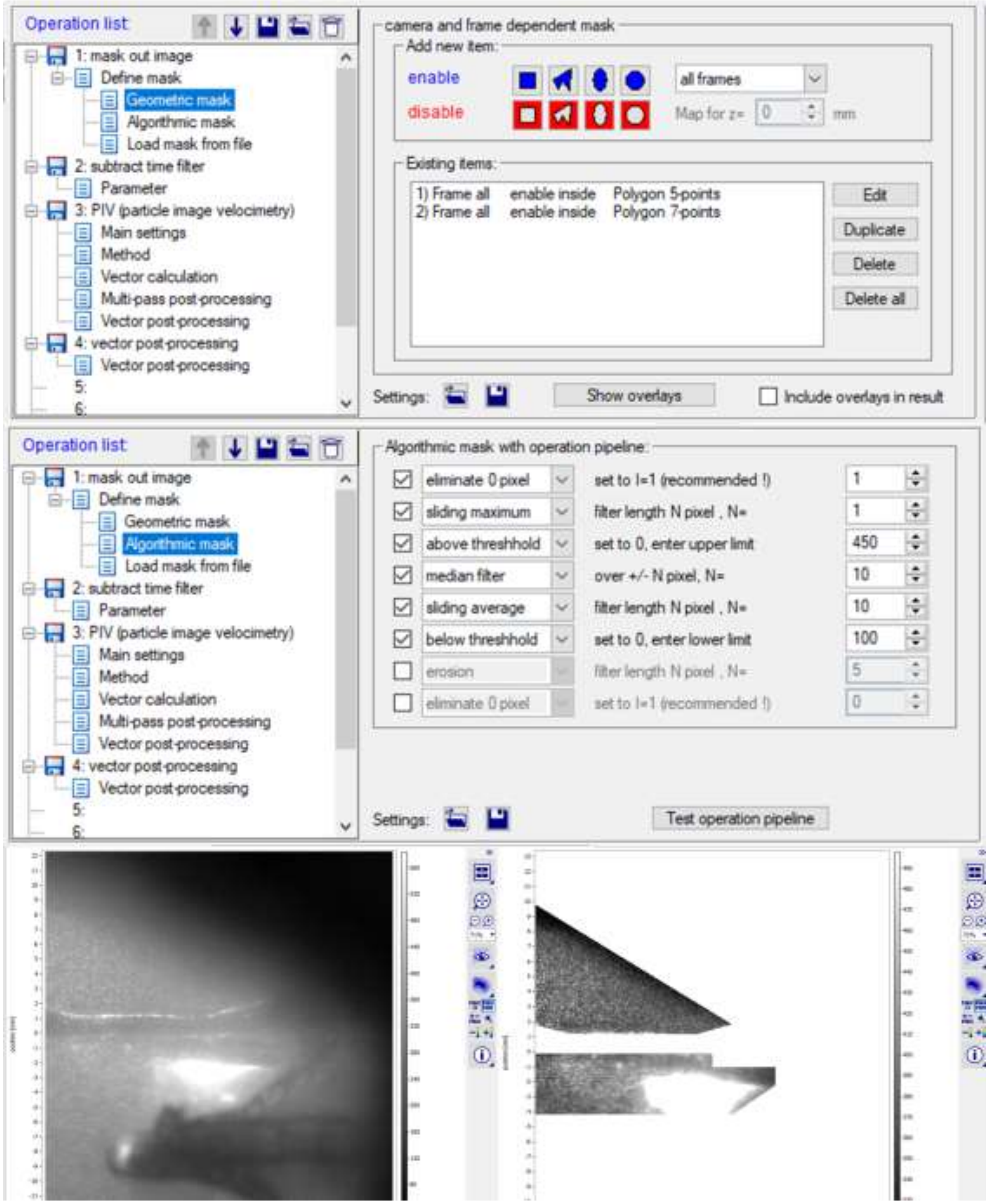

Figure E-6. **Example of Mask Out Image operation with geometric and algorithmic masks for Specific Aim 2B.**

Step 2: Subtract Time Filter (Figure E-7). This operation was used to subtract background noise from the masked images. For SA2B, a minimum intensity subtraction with a symmetric filter length of 5 images was used for 0% and 100% LAMPOON, and a filter length of 7 images was used for 50% LAMPOON.

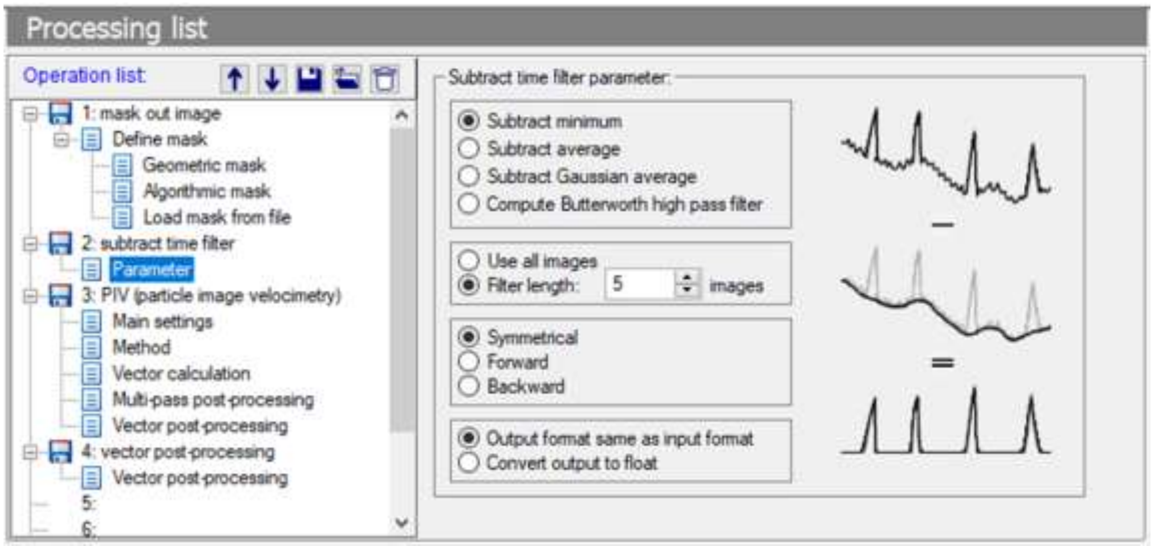

Figure E-7. Example of Subtract Time Filter operation for Specific Aim 2B.

Step 3: PIV (Particle Image Velocimetry) (Figure E-8). This operation encompasses the calculation of velocity fields via cross-correlation from the masked and filtered images. Details include:

- Use of GPU for the *Method*: cross-correlation for time resolved 2D-PIV (2D2C).
- *Vector calculation* was used with a multi-pass interrogation window of decreasing size and variable shape (64x64/square to 32x32/square to 16x16/circle) with 50% overlap for each, and 3 passes for 64x64 and 32x32 and 5 passes for 16x16.
- Default values were used for *Multi-pass postprocessing*.

- Image pre-processing and define mask in *Main Settings* as well as *Vector post-processing* were not used.

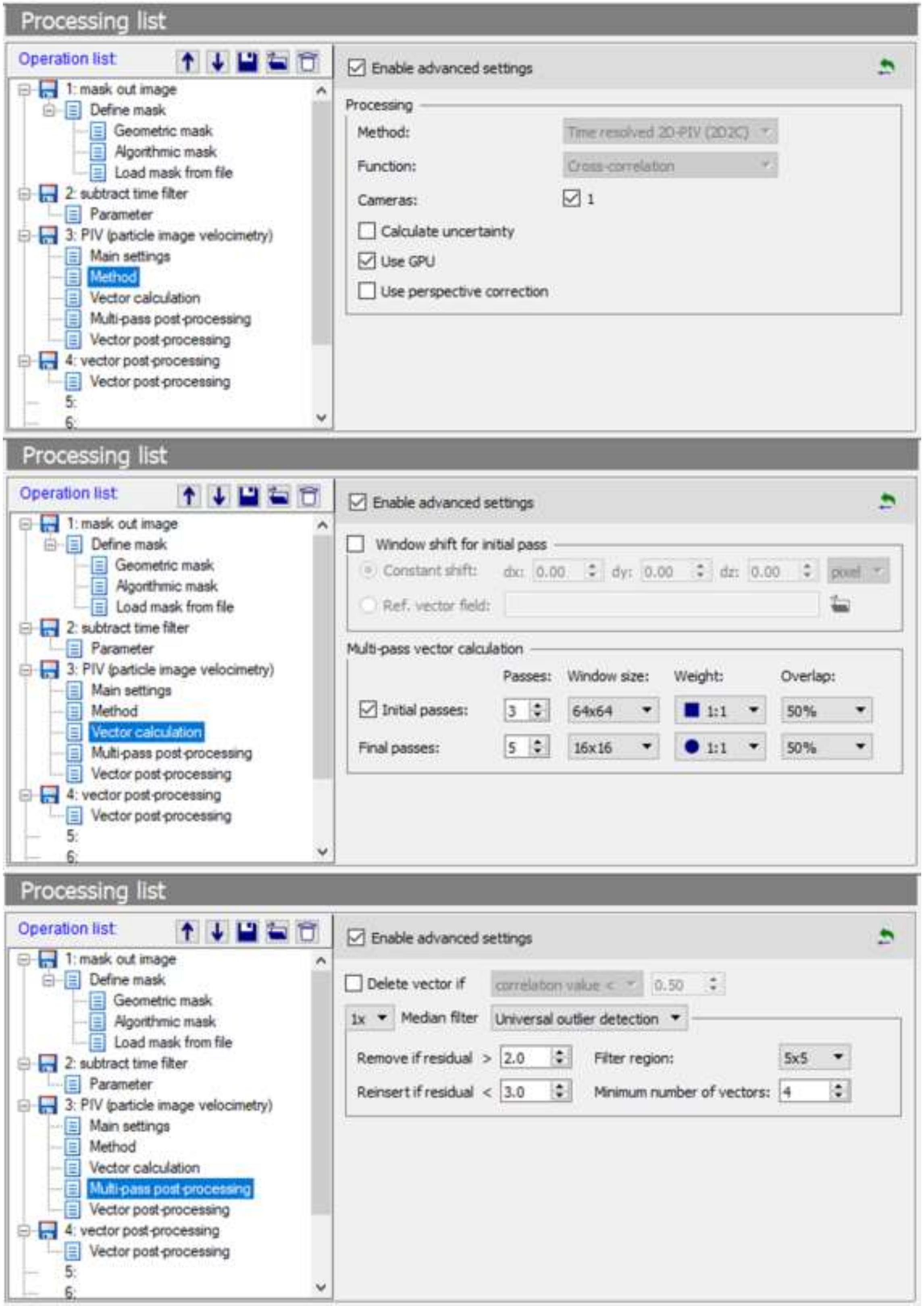

Figure E-8. **Example of PIV operation for Specific Aim 2B.**

__Step 4:__ Vector Post-processing (Figure E-9). This operation was used to remove low sample groups (<5 vectors) and smooth the field (1x smooth 3x3). Less is done here than in SA2A, because the use of the GPU produces already corrected results for cross-correlation.

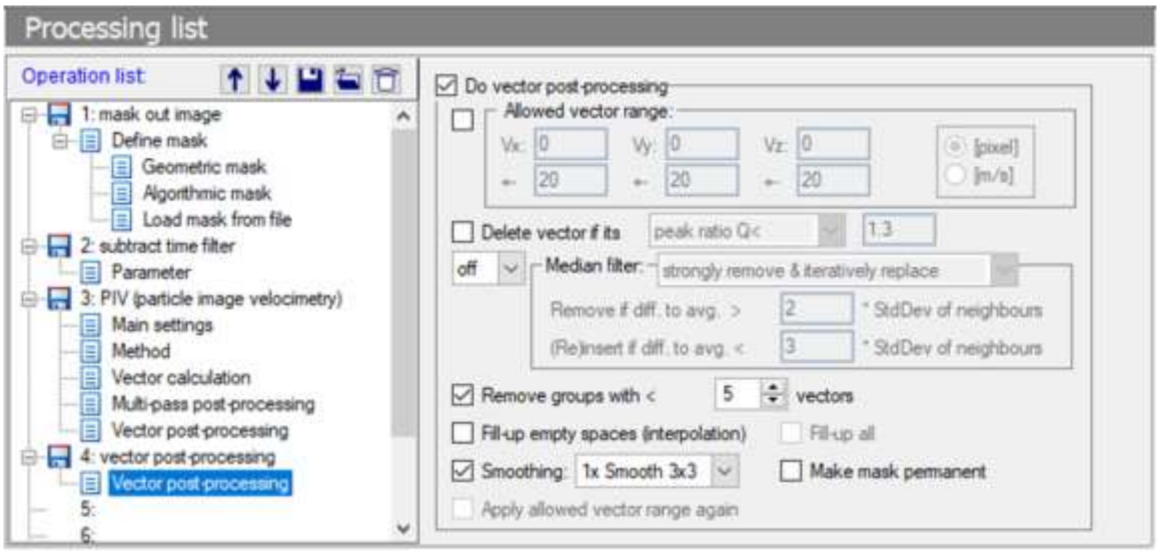

Figure E-9. Example of Vector Post-processing operation for Specific Aim 2B.

E.2 High-Speed Particle Image Velocimetry – MATLAB and Tecplot 360

__Step 1:__ Bin-Average (BinAVG.m). This MATLAB code averaged neighboring frames into one, knowing to start at the beginning of each cycle. For the purposes of this study, the bin-size was between 3-5 frames depending on the acquisition frame rate. This resulted in a time of 7-8 ms between bin-averaged frames. *Note: it is important to use the correct number of frames per cycle for the acquisition rate used for each condition (399 Hz ≈ 342 frames and 401Hz ≈ 343 frames at 856 ms a cycle); if you do not, the beginning of each* *subsequent cycle used for calculations will be displaced by the error, thus affecting the results.* This code exported x (m), y (m), u (m/s), v (m/s).

<u>Step 2:</u> Scale (ScalingData.m). The Scaling operator in DaVis assumed the camera is perpendicular to the flow and scaled both the x and y direction equally. This MATLAB code scaled the resultant data by an x and y component to calibrate for a non-perpendicular single camera. These calibration constants needed to be calculated by measuring pixel distances and the x/y distances in DaVis used for calculations with the known x/y distances. This code exported x (m), y (m), u (m/s), v (m/s).

<u>Step 3:</u> Reorganize Bin-Averaged or Scaled data (PIV_Organizing_final_v1.m). In order for the following fluid mechanics calculations code to work, the frames of each time point in all cycles had to be filed together. This MATLAB code copies and reorganizes the sequentially acquired data into folders with all cycle frames at each time point, i.e. there were the same number of folders as bin-averaged time points in a cycle and each folder contained the same number of files as cycles. This code exported x (m), y (m), u (m/s), v (m/s).

<u>Step 4:</u> Calculating Velocity Magnitude, VSS, pRSS, and TKE (Master_PIV2_TFE_new.m). This MATLAB code calculates the velocity magnitude, viscous shear stress, Reynolds shear stress, and turbulent kinetic energy from the reorganized file structure of the bin-averaged or scaled data. This code exported x (m), y (m), z (m), u (m/s), v (m/s), vel_mag (m/s), du/dx (s^{-1}), du/dy (s^{-1}), dv/dx (s^{-1}), dv/dy (s^{-1}), ω_z (s^{-1}), VSS (N/m^2), ρu'u' (N/m^2), ρv'v' (N/m^2), ρu'v' (N/m^2), TKE (m^2/s^2), pRSS (N/m^2).

Step 5: Phase-Averaging (PhaseAvgBinnedData.m). The images were acquired sequentially over multiple cardiac cycles. This MATLAB code averaged each time point in the bin-averaged or scaled data over all cycles. Although this was already done in Step 4, the file sizes are much smaller (only velocity) and formatted for Step 6. This code exported x (m), y (m), u (m/s), v (m/s).

Step 6: Calculate Minimum, Maximum, and Average Velocity (Extract_min_max_avg_vel_TFE.m). This MATLAB code calculated the minimum, maximum, and average velocity magnitude and time at which they occured of each spatial location over the cardiac cycle. This code exported min_vel (m/s), min_time (ms), max_vel (m/s), max_time (ms), avg_vel (m/s).

Step 7: Reorganizing Phase-Average (PIV_Renaming_v1.m). This MATLAB code copied and renamed the phase-averaged data files to start at whatever time-point in the cycle desired. For this study the data was made to start at 200 ms. This was done in order to start the particle seeding and pathline calculation in Tecplot at the time of interest.

Step 8: Export Pathlines. In Tecplot, ask to make 350 streamlines, calculate pathlines at a minimum of 0.001 s time steps with no particle mass, and export the resultant data as a space delimited .txt file with X and Y positions for only the particles.

Step 9: Calculate Particle Tracking (ParticleTrackingTecplotToExcelAndEPS_TFE.m). This MATLAB code took the resultant pathlines from Tecplot and made a particle tracking video as an *.avi and exported an *.xls spreadsheet of the particles for residency time calculations.

Step 10: Calculate Residency Time (ParticleTrackingWashout.m). This MATLAB code took the *.xls of the particle pathlines and calculated the residency time over the cardiac cycle.

APPENDIX F. RAW DATA – SPECIFIC AIM 1

F.1 Motor Tracking Raw Results

Table F-1. Specific Aim 1 raw motor tracking results pertaining to Figure 4-1.

Porcine - Healthy			Porcine - Diseased			Ovine - Healthy		
Time	Desired	Measured	Time	Desired	Measured	Time	Desired	Measured
0	-0.23241	-0.241776	0	-0.11519	-0.111481	0	-0.21232	-0.206626
2.002	-0.23524	-0.243172	2.001	-0.11598	-0.111494	2.001	-0.21885	-0.207307
5.004	-0.24251	-0.247498	4.003	-0.11678	-0.112685	4.003	-0.22517	-0.210612
7.005	-0.24725	-0.250247	6.005	-0.1179	-0.113388	6.004	-0.23108	-0.212353
9.007	-0.25184	-0.255375	8.018	-0.11903	-0.114497	9.005	-0.23871	-0.213803
11.008	-0.25622	-0.25739	10.019	-0.12017	-0.116762	11.008	-0.24269	-0.216868
13.01	-0.26033	-0.261027	12.02	-0.12132	-0.116892	14.01	-0.24705	-0.220158
15.011	-0.26418	-0.264505	14.022	-0.12248	-0.118128	16.011	-0.24908	-0.226213
17.012	-0.26783	-0.268008	16.022	-0.12367	-0.12023	18.012	-0.25055	-0.226932
19.014	-0.27132	-0.273078	18.013	-0.12488	-0.121929	20.014	-0.25161	-0.230622
21.015	-0.27472	-0.277618	20.014	-0.12611	-0.121995	23.006	-0.2527	-0.232177
23.017	-0.27808	-0.279403	22.027	-0.12737	-0.123218	25.008	-0.25329	-0.235245
25.018	-0.28146	-0.282442	24.017	-0.12866	-0.124497	27.009	-0.25393	-0.240112
27.02	-0.28491	-0.286493	26.019	-0.12998	-0.126954	29.01	-0.25475	-0.241476
29.021	-0.28844	-0.28969	28.02	-0.13134	-0.127492	31.024	-0.25588	-0.246445
31.022	-0.29205	-0.29441	30.021	-0.13273	-0.129847	33.026	-0.25746	-0.250114
33.024	-0.29571	-0.29769	32.023	-0.13413	-0.130281	36.028	-0.26087	-0.253105
35.025	-0.29942	-0.303919	34.024	-0.13552	-0.129982	39.03	-0.26535	-0.256478
37.027	-0.30315	-0.305959	36.025	-0.13688	-0.131059	42.032	-0.27049	-0.260543
39.028	-0.30689	-0.309264	38.027	-0.1382	-0.132626	44.033	-0.27409	-0.264487
41.03	-0.31064	-0.312876	40.04	-0.13945	-0.134197	46.035	-0.2777	-0.267993
43.031	-0.31436	-0.316273	42.042	-0.14061	-0.13395	48.036	-0.28121	-0.272037
45.032	-0.31805	-0.321787	44.044	-0.14167	-0.136229	50.038	-0.28449	-0.274865
47.034	-0.3217	-0.325896	46.044	-0.14262	-0.137851	52.039	-0.28754	-0.275988
49.035	-0.3253	-0.327342	48.034	-0.14346	-0.138322	54.04	-0.29035	-0.278247
51.037	-0.32885	-0.330972	51.046	-0.1446	-0.139248	56.042	-0.29294	-0.280704
53.038	-0.33235	-0.335185	53.047	-0.14532	-0.14011	58.043	-0.2953	-0.282595
55.039	-0.3358	-0.339146	55.049	-0.14604	-0.142697	60.045	-0.29746	-0.288553
57.041	-0.33921	-0.344553	57.05	-0.1468	-0.143558	62.046	-0.29942	-0.289562
59.042	-0.34257	-0.348395	59.051	-0.14762	-0.145731	64.045	-0.30119	-0.292867
61.044	-0.34589	-0.350506	61.053	-0.14854	-0.149594	66.046	-0.30277	-0.295147

63.045	-0.34916	-0.353957	63.054	-0.14958	-0.150287	68.047	-0.30419	-0.298198
65.047	-0.3524	-0.356882	66.057	-0.15139	-0.150361	70.049	-0.30549	-0.302402
67.049	-0.35562	-0.36047	68.058	-0.15271	-0.152705	72.05	-0.30671	-0.304907
69.063	-0.35883	-0.364952	70.059	-0.15408	-0.153177	74.052	-0.3079	-0.308631
71.063	-0.36205	-0.368109	72.061	-0.15547	-0.153833	76.053	-0.30912	-0.315772
73.052	-0.36528	-0.37407	74.062	-0.15685	-0.154563	78.055	-0.3104	-0.315287
75.053	-0.36855	-0.381448	76.064	-0.15818	-0.154745	80.056	-0.31179	-0.317569
77.055	-0.37185	-0.385153	78.065	-0.15942	-0.158601	82.057	-0.31334	-0.320673
79.056	-0.37519	-0.389089	80.066	-0.16056	-0.158214	85.06	-0.31607	-0.323056
81.058	-0.37856	-0.390647	82.068	-0.16156	-0.158582	87.061	-0.31821	-0.325904
83.059	-0.38193	-0.394696	84.07	-0.16246	-0.161042	89.063	-0.3206	-0.331089
85.06	-0.38532	-0.398079	86.061	-0.16329	-0.161763	92.065	-0.32459	-0.333653
87.062	-0.3887	-0.402027	88.062	-0.16407	-0.163839	94.066	-0.32747	-0.337338
89.063	-0.39206	-0.407488	90.076	-0.16483	-0.164533	96.068	-0.33048	-0.338646
91.065	-0.39541	-0.410366	92.077	-0.16561	-0.166371	99.07	-0.3352	-0.341556
93.066	-0.39872	-0.414967	94.079	-0.16644	-0.168371	102.072	-0.34006	-0.34531
95.068	-0.40199	-0.416464	96.078	-0.16734	-0.169781	104.073	-0.34332	-0.345722
97.069	-0.40523	-0.419921	98.079	-0.16836	-0.170515	106.078	-0.34655	-0.347172
99.084	-0.40843	-0.423058	101.081	-0.17007	-0.171835	108.079	-0.34965	-0.348762
101.071	-0.41161	-0.429221	103.083	-0.17132	-0.173326	110.077	-0.35255	-0.351618
103.073	-0.41478	-0.432961	106.085	-0.1733	-0.175525	112.079	-0.35515	-0.351442
105.075	-0.41793	-0.435756	108.086	-0.17468	-0.176342	114.08	-0.35737	-0.35399
107.076	-0.42109	-0.438223	110.087	-0.17606	-0.178927	116.084	-0.35912	-0.357615
109.077	-0.42424	-0.442948	112.089	-0.17745	-0.180116	118.086	-0.36031	-0.359946
111.079	-0.42742	-0.445964	114.094	-0.17882	-0.181868	120.084	-0.36099	-0.359334
113.08	-0.43061	-0.451104	116.092	-0.18015	-0.183457	122.086	-0.36125	-0.360275
115.082	-0.43385	-0.456578	118.093	-0.18144	-0.183599	124.087	-0.36119	-0.361084
117.083	-0.43713	-0.459515	120.085	-0.18271	-0.185278	126.091	-0.3609	-0.363879
119.085	-0.44048	-0.461427	122.086	-0.18395	-0.185592	129.093	-0.36028	-0.363525
121.086	-0.44391	-0.464466	124.088	-0.18517	-0.188505	131.095	-0.35988	-0.364276
124.088	-0.44922	-0.468751	127.089	-0.18696	-0.19023	133.097	-0.35961	-0.36575
127.102	-0.45477	-0.471342	129.091	-0.18814	-0.190736	135.097	-0.35957	-0.365687
129.092	-0.45863	-0.477297	131.092	-0.18931	-0.192131	137.1	-0.35982	-0.365082
131.093	-0.46262	-0.477821	133.094	-0.19048	-0.195234	139.1	-0.36031	-0.365523
133.095	-0.46667	-0.483439	135.095	-0.19165	-0.195053	141.102	-0.36094	-0.366236
135.096	-0.47074	-0.484875	137.097	-0.19279	-0.194295	143.103	-0.36161	-0.365886
137.097	-0.47474	-0.489148	139.098	-0.1939	-0.195974	145.105	-0.36225	-0.364888
139.098	-0.47863	-0.491948	141.099	-0.19496	-0.196773	148.107	-0.36293	-0.365452
141.1	-0.48232	-0.494779	143.113	-0.19597	-0.196844	150.096	-0.36306	-0.365237
143.101	-0.48576	-0.497317	145.117	-0.1969	-0.197734	152.107	-0.36283	-0.365819
145.103	-0.4889	-0.498696	148.117	-0.19814	-0.197528	155.099	-0.36178	-0.364749

147.104	-0.49172	-0.499003	150.117	-0.19884	-0.19913	157.102	-0.3607	-0.363265
149.106	-0.4942	-0.501814	152.119	-0.19946	-0.196829	159.102	-0.35936	-0.367663
151.107	-0.49633	-0.502955	155.119	-0.20019	-0.198974	161.103	-0.35784	-0.365266
153.108	-0.4981	-0.502847	157.122	-0.20056	-0.198432	163.105	-0.35617	-0.362497
155.11	-0.49951	-0.50631	159.124	-0.20082	-0.198798	165.106	-0.35443	-0.362053
157.111	-0.50053	-0.504871	161.126	-0.20099	-0.198948	167.108	-0.35265	-0.359267
159.113	-0.50116	-0.506037	163.127	-0.20105	-0.199525	170.11	-0.35006	-0.356911
161.114	-0.50138	-0.506	166.117	-0.20094	-0.198615	172.111	-0.34839	-0.356223
163.115	-0.50124	-0.505409	168.13	-0.20075	-0.198304	174.112	-0.34674	-0.354252
165.117	-0.50077	-0.507661	170.132	-0.20046	-0.198699	177.116	-0.34426	-0.352547
167.118	-0.5	-0.506722	172.133	-0.20009	-0.198164	179.116	-0.34258	-0.350678
169.12	-0.49899	-0.50659	174.134	-0.19963	-0.198824	181.117	-0.34085	-0.347565
171.121	-0.49777	-0.506189	177.125	-0.1988	-0.1981	183.12	-0.33905	-0.344273
173.123	-0.49638	-0.507638	179.126	-0.19815	-0.197457	185.12	-0.33715	-0.34205
175.124	-0.49486	-0.507328	181.128	-0.19744	-0.199224	187.122	-0.33515	-0.338357
177.126	-0.49325	-0.506451	183.129	-0.19666	-0.198048	189.124	-0.33302	-0.333852
179.139	-0.49156	-0.506006	185.131	-0.19581	-0.195674	191.124	-0.33076	-0.334361
181.131	-0.48977	-0.501911	187.132	-0.19487	-0.195269	193.126	-0.32836	-0.330549
183.13	-0.48787	-0.502778	189.133	-0.19385	-0.19352	195.127	-0.32581	-0.327176
185.143	-0.48586	-0.500992	191.135	-0.19271	-0.191209	197.13	-0.3231	-0.327292
187.145	-0.48373	-0.499452	193.136	-0.19146	-0.189625	199.13	-0.32023	-0.320504
190.144	-0.48027	-0.496464	195.137	-0.19008	-0.189448	201.132	-0.31718	-0.319185
192.146	-0.47778	-0.495579	197.139	-0.18857	-0.186701	203.133	-0.31395	-0.314956
194.147	-0.47516	-0.488048	199.14	-0.18694	-0.18564	205.135	-0.31057	-0.308833
196.148	-0.47241	-0.493279	201.142	-0.18519	-0.18204	207.148	-0.30706	-0.306503
198.15	-0.46955	-0.487975	203.143	-0.18336	-0.180777	210.151	-0.30162	-0.303098
200.152	-0.46658	-0.48499	205.145	-0.18146	-0.180554	212.152	-0.29792	-0.299089
202.153	-0.46353	-0.48081	207.146	-0.17951	-0.177867	214.153	-0.2942	-0.292527
204.154	-0.4604	-0.477441	209.147	-0.17753	-0.174648	216.155	-0.29047	-0.288622
206.156	-0.45719	-0.476168	211.149	-0.17553	-0.175632	218.156	-0.28678	-0.284666
208.157	-0.45393	-0.468612	213.15	-0.17353	-0.170871	220.157	-0.28312	-0.277593
210.159	-0.45062	-0.466439	215.152	-0.17154	-0.168969	222.156	-0.27949	-0.274944
212.16	-0.44727	-0.459676	217.153	-0.16956	-0.167954	225.159	-0.27401	-0.267681
214.161	-0.44387	-0.45645	219.155	-0.16756	-0.165514	228.164	-0.26843	-0.265775
216.162	-0.44039	-0.454421	221.156	-0.16553	-0.162897	230.164	-0.26461	-0.26039
218.165	-0.4368	-0.450137	223.157	-0.16344	-0.160728	232.166	-0.26067	-0.253269
220.165	-0.43307	-0.446916	225.159	-0.16127	-0.156898	234.168	-0.25659	-0.250257
222.167	-0.42918	-0.441246	228.161	-0.15782	-0.153737	236.169	-0.25234	-0.247925
224.169	-0.42508	-0.431828	230.162	-0.15537	-0.150937	239.171	-0.24561	-0.243052
226.169	-0.42076	-0.426536	232.164	-0.15277	-0.147073	241.172	-0.24091	-0.238307
228.171	-0.41619	-0.426153	234.165	-0.15003	-0.144537	243.173	-0.23612	-0.233894

230.172	-0.41137	-0.421324	236.167	-0.14718	-0.141004	245.175	-0.23132	-0.229089
232.175	-0.40635	-0.415724	238.168	-0.14424	-0.138577	247.177	-0.22658	-0.219842
234.175	-0.40114	-0.410355	240.169	-0.14124	-0.135543	249.179	-0.22198	-0.215934
236.177	-0.39577	-0.400624	242.171	-0.13818	-0.133161	251.177	-0.2176	-0.216576
238.178	-0.39027	-0.398005	244.172	-0.13511	-0.128274	253.178	-0.2135	-0.213854
240.18	-0.38466	-0.390468	246.174	-0.13204	-0.127056	255.182	-0.20966	-0.209121
242.181	-0.37896	-0.387012	248.175	-0.12899	-0.124348	257.184	-0.20605	-0.201731
244.182	-0.37321	-0.381559	250.176	-0.12598	-0.121393	259.186	-0.20262	-0.19988
246.184	-0.36741	-0.37571	252.178	-0.12301	-0.118754	261.187	-0.19934	-0.190574
248.185	-0.36158	-0.364714	254.179	-0.1201	-0.114582	264.189	-0.19461	-0.191812
250.186	-0.35574	-0.361308	256.181	-0.11724	-0.113174	266.19	-0.19153	-0.188278
253.179	-0.347	-0.357794	258.182	-0.11445	-0.110598	268.192	-0.18844	-0.185429
255.191	-0.34121	-0.352795	260.183	-0.11174	-0.107727	270.19	-0.18532	-0.182107
257.191	-0.33548	-0.347003	262.185	-0.1091	-0.104872	272.192	-0.18214	-0.176397
259.193	-0.3298	-0.337144	264.186	-0.10655	-0.102558	274.195	-0.17893	-0.173529
262.185	-0.32141	-0.33126	267.188	-0.10286	-0.100226	276.194	-0.17577	-0.172439
264.187	-0.31591	-0.326187	269.19	-0.10048	-0.096866	279.197	-0.17126	-0.170135
266.188	-0.31049	-0.327048	271.191	-0.09814	-0.092131	281.199	-0.16851	-0.166835
268.19	-0.30515	-0.319841	273.193	-0.09583	-0.092937	283.202	-0.16604	-0.160793
270.192	-0.29989	-0.314421	275.194	-0.09353	-0.089831	285.201	-0.16391	-0.158111
272.192	-0.29473	-0.308989	277.195	-0.09124	-0.088101	287.202	-0.16219	-0.158153
274.194	-0.28967	-0.300458	279.197	-0.08895	-0.085012	289.203	-0.16087	-0.156052
276.195	-0.28471	-0.294966	281.198	-0.08663	-0.083672	291.205	-0.15987	-0.15423
278.197	-0.27985	-0.291143	283.2	-0.08429	-0.076535	293.207	-0.15912	-0.153156
280.198	-0.2751	-0.286252	285.201	-0.08196	-0.075952	295.208	-0.15855	-0.150189
282.2	-0.27046	-0.28157	287.203	-0.07964	-0.07735	297.21	-0.15809	-0.147718
284.201	-0.26595	-0.273925	289.204	-0.07736	-0.074353	299.21	-0.15766	-0.146258
286.203	-0.26155	-0.270658	291.205	-0.07514	-0.070698	301.212	-0.1572	-0.143842
288.216	-0.25728	-0.264096	293.206	-0.07298	-0.06864	303.213	-0.15669	-0.143411
290.205	-0.25315	-0.259253	295.208	-0.07091	-0.067308	305.215	-0.15613	-0.142096
292.207	-0.24917	-0.252746	297.21	-0.06895	-0.065972	307.216	-0.15555	-0.140042
294.208	-0.24538	-0.251941	299.211	-0.0671	-0.063373	309.218	-0.15493	-0.140566
296.209	-0.24179	-0.248529	301.213	-0.0654	-0.061593	311.219	-0.15431	-0.138993
298.211	-0.23844	-0.246498	303.214	-0.06385	-0.061255	313.22	-0.15367	-0.138647
300.225	-0.23534	-0.242253	305.228	-0.06246	-0.060146	316.223	-0.15273	-0.137055
302.213	-0.23252	-0.238103	307.217	-0.06125	-0.058684	318.224	-0.15213	-0.13634
304.215	-0.22999	-0.232848	309.218	-0.06018	-0.056556	320.226	-0.15154	-0.135887
306.229	-0.22775	-0.230662	311.219	-0.05924	-0.055794	322.227	-0.151	-0.134315
308.23	-0.22576	-0.228562	313.221	-0.05841	-0.055078	324.228	-0.15049	-0.133841
310.231	-0.22402	-0.226478	315.223	-0.05768	-0.053546	326.23	-0.15004	-0.133479
312.233	-0.2225	-0.224615	317.224	-0.05702	-0.051979	328.231	-0.14963	-0.132638

314.234	-0.22118	-0.219799	319.225	-0.05643	-0.050906	330.235	-0.14926	-0.132122
316.235	-0.22006	-0.218474	321.228	-0.05587	-0.049633	332.237	-0.14894	-0.132698
318.242	-0.21911	-0.217692	323.228	-0.05534	-0.049445	334.236	-0.14865	-0.131338
320.244	-0.2183	-0.215118	325.229	-0.05481	-0.04909	337.239	-0.14829	-0.13076
322.243	-0.21764	-0.21318	327.231	-0.05428	-0.047777	340.241	-0.14799	-0.130753
324.244	-0.21709	-0.212319	329.232	-0.05374	-0.047173	342.241	-0.14783	-0.130606
326.246	-0.21664	-0.210351	331.234	-0.0532	-0.045643	344.243	-0.14769	-0.130035
328.247	-0.21626	-0.208186	333.235	-0.05265	-0.045521	346.244	-0.14757	-0.129951
330.244	-0.21595	-0.205038	335.249	-0.05211	-0.043865	348.245	-0.14747	-0.129857
333.245	-0.21557	-0.204401	337.25	-0.05156	-0.043982	350.247	-0.14739	-0.130472
335.247	-0.21534	-0.203114	340.253	-0.05074	-0.043484	353.249	-0.14728	-0.12965
337.249	-0.2151	-0.203193	342.253	-0.05019	-0.042415	355.25	-0.14723	-0.130216
339.249	-0.21486	-0.200745	344.255	-0.04965	-0.041677	357.252	-0.14718	-0.130076
342.242	-0.21446	-0.199863	346.254	-0.04911	-0.040433	359.253	-0.14713	-0.129721
344.253	-0.21418	-0.198237	348.255	-0.04858	-0.040353	361.255	-0.14708	-0.130426
346.254	-0.21388	-0.197241	350.247	-0.04805	-0.039799	363.256	-0.14701	-0.129933
348.256	-0.21357	-0.196406	352.258	-0.04754	-0.039396	365.257	-0.14694	-0.130397
350.257	-0.21324	-0.195521	354.259	-0.04703	-0.038733	367.258	-0.14684	-0.129569
352.258	-0.2129	-0.194457	356.252	-0.04654	-0.038676	369.26	-0.14673	-0.130201
354.26	-0.21254	-0.193774	358.253	-0.04605	-0.038491	371.262	-0.14658	-0.129883
356.261	-0.21217	-0.192251	360.254	-0.04558	-0.037634	373.263	-0.14641	-0.129866
358.263	-0.21178	-0.191768	362.255	-0.04513	-0.037659	375.255	-0.14619	-0.129916
360.265	-0.21138	-0.190681	364.257	-0.04469	-0.037553	377.266	-0.14594	-0.129849
362.265	-0.21097	-0.19034	366.258	-0.04426	-0.036068	379.268	-0.14563	-0.129371
364.267	-0.21054	-0.189311	368.26	-0.04383	-0.036594	381.268	-0.14528	-0.128797
366.268	-0.21009	-0.188902	370.261	-0.04342	-0.035337	383.27	-0.14487	-0.129883
368.27	-0.20963	-0.188414	372.263	-0.04302	-0.035825	385.274	-0.1444	-0.12872
370.271	-0.20915	-0.187983	374.264	-0.04262	-0.034913	387.275	-0.14386	-0.127763
372.273	-0.20866	-0.187126	376.265	-0.04223	-0.035055	389.277	-0.14326	-0.127905
374.264	-0.20816	-0.187174	378.267	-0.04185	-0.034495	391.278	-0.14259	-0.128454
376.276	-0.20764	-0.186061	380.268	-0.04147	-0.034408	393.28	-0.14186	-0.127473
378.277	-0.20711	-0.18504	382.27	-0.04108	-0.033605	395.281	-0.14108	-0.127612
380.278	-0.20658	-0.185591	384.271	-0.0407	-0.033472	397.28	-0.14026	-0.126486
382.28	-0.20605	-0.184927	386.273	-0.04032	-0.033678	399.282	-0.1394	-0.126265
384.281	-0.20553	-0.184889	388.274	-0.03994	-0.03347	401.283	-0.13851	-0.125413
386.283	-0.20501	-0.18447	390.275	-0.03955	-0.033504	403.284	-0.1376	-0.128402
388.284	-0.20451	-0.184539	392.277	-0.03916	-0.032985	405.276	-0.13666	-0.122584
390.285	-0.20403	-0.184151	394.278	-0.03877	-0.032429	407.277	-0.13572	-0.12377
392.287	-0.20358	-0.18436	396.279	-0.03836	-0.032772	409.278	-0.13478	-0.12365
394.289	-0.20315	-0.183725	398.281	-0.03795	-0.032875	411.28	-0.13384	-0.124021
396.28	-0.20275	-0.184065	400.282	-0.03752	-0.031221	413.281	-0.1329	-0.123334

398.281	-0.20239	-0.183514	402.283	-0.03709	-0.032048	415.295	-0.13198	-0.121873
400.283	-0.20208	-0.183781	404.285	-0.03664	-0.031371	417.297	-0.13105	-0.12164
403.285	-0.20169	-0.183771	406.287	-0.03618	-0.031554	419.298	-0.13013	-0.120448
405.286	-0.2015	-0.183513	408.288	-0.0357	-0.030791	421.287	-0.1292	-0.119981
407.288	-0.20135	-0.183468	410.29	-0.0352	-0.02912	423.288	-0.12826	-0.119497
409.289	-0.20123	-0.182529	412.29	-0.03469	-0.031138	425.29	-0.12731	-0.11874
411.29	-0.20114	-0.182989	414.292	-0.03415	-0.029918	427.291	-0.12633	-0.115269
413.292	-0.20106	-0.182258	416.294	-0.0336	-0.029534	429.293	-0.12533	-0.116051
415.293	-0.20098	-0.182792	418.295	-0.03302	-0.028953	432.307	-0.12377	-0.115449
417.295	-0.20089	-0.182392	420.296	-0.03241	-0.028582	434.308	-0.12269	-0.114021
419.296	-0.20078	-0.182483	422.298	-0.03179	-0.028979	436.312	-0.12156	-0.11241
421.298	-0.20063	-0.181506	424.3	-0.03114	-0.027504	438.313	-0.12039	-0.110859
423.299	-0.20043	-0.181973	426.301	-0.03048	-0.027462	441.316	-0.11853	-0.108927
425.3	-0.20018	-0.181099	428.302	-0.02981	-0.027795	444.315	-0.11654	-0.106348
427.302	-0.19986	-0.180714	430.303	-0.02913	-0.027278	446.32	-0.11514	-0.105331
429.303	-0.19946	-0.180363	432.305	-0.02845	-0.026936	448.318	-0.11368	-0.104788
431.305	-0.19896	-0.180882	434.306	-0.02778	-0.026979	450.322	-0.11218	-0.102318
433.306	-0.19838	-0.17994	436.308	-0.02711	-0.027054	452.321	-0.11062	-0.101183
435.307	-0.19772	-0.179982	438.309	-0.02645	-0.026165	454.323	-0.10902	-0.0998
437.309	-0.19697	-0.179407	440.31	-0.0258	-0.025753	457.327	-0.10655	-0.098769
439.323	-0.19615	-0.179227	442.312	-0.02517	-0.025728	460.328	-0.10401	-0.097498
441.325	-0.19526	-0.17772	444.313	-0.02457	-0.025773	462.331	-0.10228	-0.096903
443.325	-0.19431	-0.17793	446.315	-0.024	-0.024926	464.333	-0.10052	-0.095127
445.325	-0.19329	-0.177352	448.316	-0.02345	-0.02493	466.328	-0.09874	-0.093508
447.326	-0.19222	-0.177281	450.318	-0.02294	-0.024938	468.334	-0.09695	-0.091997
450.328	-0.19052	-0.173178	452.319	-0.02247	-0.024598	470.332	-0.09514	-0.090019
452.329	-0.18933	-0.17454	454.332	-0.02201	-0.024911	473.324	-0.09242	-0.087424
454.331	-0.18811	-0.174021	456.334	-0.02159	-0.024132	475.337	-0.0906	-0.086103
457.332	-0.1862	-0.173366	459.337	-0.02098	-0.024143	477.34	-0.08878	-0.084364
459.324	-0.1849	-0.173272	462.326	-0.0204	-0.023532	479.328	-0.08697	-0.083866
461.326	-0.18357	-0.171639	464.337	-0.02003	-0.023145	481.344	-0.08515	-0.08141
463.327	-0.18223	-0.170068	466.339	-0.01965	-0.023195	483.342	-0.08332	-0.079983
465.328	-0.18087	-0.169045	468.34	-0.01928	-0.022989	485.346	-0.08148	-0.077178
467.33	-0.1795	-0.165721	471.342	-0.01871	-0.023191	487.345	-0.07964	-0.07595
469.348	-0.17812	-0.167671	473.344	-0.01832	-0.022333	490.346	-0.07683	-0.074182
471.349	-0.17672	-0.166898	475.346	-0.01791	-0.022433	492.349	-0.07494	-0.072557
473.347	-0.1753	-0.165509	478.347	-0.01727	-0.02148	494.349	-0.07302	-0.070257
475.348	-0.17385	-0.163835	480.349	-0.01681	-0.022042	497.352	-0.0701	-0.067241
477.349	-0.17237	-0.162628	482.351	-0.01632	-0.020263	500.353	-0.06711	-0.065418
479.35	-0.17085	-0.164156	485.343	-0.01552	-0.020411	503.354	-0.06403	-0.064066
481.351	-0.1693	-0.159975	487.354	-0.01495	-0.019554	506.347	-0.06087	-0.059947

483.351	-0.16771	-0.158763	489.355	-0.01436	-0.019754	508.348	-0.0587	-0.058591
485.353	-0.16607	-0.157641	491.357	-0.01375	-0.018314	510.349	-0.0565	-0.057059
487.354	-0.16438	-0.156597	493.358	-0.01312	-0.018968	513.352	-0.05312	-0.054393
489.355	-0.16264	-0.153583	495.359	-0.01248	-0.018523	514.365	-0.05199	-0.055075
491.357	-0.16085	-0.152787	497.36	-0.01183	-0.017864	517.354	-0.04857	-0.051384
493.359	-0.15899	-0.151213	499.353	-0.01118	-0.016443	518.369	-0.04743	-0.047652
495.36	-0.15707	-0.150042	501.355	-0.01053	-0.016187	520.369	-0.04515	-0.046547
497.361	-0.15509	-0.148389	503.367	-0.00989	-0.015923	522.371	-0.04289	-0.042585
500.363	-0.15201	-0.145767	505.357	-0.00926	-0.015433	524.372	-0.04066	-0.042765
502.365	-0.1499	-0.142451	507.359	-0.00864	-0.015225	526.371	-0.03847	-0.04093
505.357	-0.14666	-0.14234	509.369	-0.00805	-0.014496	528.373	-0.03632	-0.038607
507.368	-0.14446	-0.141129	511.37	-0.00747	-0.014804	530.373	-0.03423	-0.036429
509.37	-0.14223	-0.137913	513.362	-0.00693	-0.013799	533.366	-0.03122	-0.034261
512.372	-0.13883	-0.136799	515.363	-0.00642	-0.013635	535.367	-0.02932	-0.033731
514.373	-0.13655	-0.134514	517.365	-0.00594	-0.013598	537.379	-0.02751	-0.031861
516.374	-0.13425	-0.129948	519.367	-0.00549	-0.0128	539.38	-0.0258	-0.030035
518.376	-0.13195	-0.130433	521.367	-0.00507	-0.012998	541.381	-0.0242	-0.028216
520.367	-0.12965	-0.129289	523.369	-0.00468	-0.01225	543.383	-0.02268	-0.025381
522.369	-0.12735	-0.126684	525.371	-0.00431	-0.012065	545.385	-0.02125	-0.023868
524.37	-0.12506	-0.1225	527.372	-0.00397	-0.011659	547.388	-0.0199	-0.022965
526.372	-0.12276	-0.119652	529.373	-0.00365	-0.011297	549.39	-0.01863	-0.021227
528.373	-0.12045	-0.116961	531.374	-0.00335	-0.010602	551.389	-0.01742	-0.019564
530.374	-0.11809	-0.116448	533.376	-0.00306	-0.010874	553.393	-0.01628	-0.018623
532.376	-0.11569	-0.11339	535.378	-0.0028	-0.010262	556.395	-0.01468	-0.016126
534.377	-0.11322	-0.111076	537.379	-0.00254	-0.010479	558.396	-0.01367	-0.012574
536.379	-0.11067	-0.107856	539.38	-0.0023	-0.009842	560.397	-0.01271	-0.013655
538.38	-0.10802	-0.103383	541.382	-0.00208	-0.01026	562.399	-0.01178	-0.012763
540.382	-0.10526	-0.101043	543.383	-0.00185	-0.00929	564.4	-0.01089	-0.011099
542.383	-0.10238	-0.099186	545.386	-0.00164	-0.009072	566.399	-0.01002	-0.010257
544.384	-0.09935	-0.095833	547.386	-0.00144	-0.009174	568.403	-0.00916	-0.007699
546.386	-0.09616	-0.093187	549.388	-0.00123	-0.006039	570.392	-0.00833	-0.006936
548.387	-0.09283	-0.087337	551.389	-0.00103	-0.008668	572.393	-0.00751	-0.006163
550.389	-0.08936	-0.082843	553.39	-0.00084	-0.009176	574.395	-0.00672	-0.004385
552.39	-0.08578	-0.08356	555.392	-0.00066	-0.009488	576.396	-0.00595	-0.004223
554.391	-0.08211	-0.078157	557.393	-0.0005	-0.009572	578.398	-0.0052	-0.00279
556.393	-0.07836	-0.072929	559.407	-0.00035	-0.008082	580.412	-0.00449	-0.002796
558.394	-0.07457	-0.069918	562.409	-0.00017	-0.009177	582.413	-0.00382	-0.000339
560.395	-0.07074	-0.068816	564.41	-8.1E-05	-0.009086	584.402	-0.00319	-0.000433
562.397	-0.06689	-0.066089	566.399	-2.3E-05	-0.008966	586.403	-0.0026	0.001425
564.399	-0.06306	-0.062628	568.411	0	-0.009188	588.405	-0.00207	-0.000387
566.4	-0.05925	-0.05804	570.402	-1.3E-05	-0.00907	590.406	-0.00158	0.000277

568.401	-0.05549	-0.055779	572.404	-6.7E-05	-0.008824	592.408	-0.00116	0.001965
570.402	-0.05179	-0.050352	574.405	-0.00017	-0.009327	594.409	-0.00079	0.001974
572.404	-0.04818	-0.048331	576.407	-0.00031	-0.008887	596.41	-0.00049	0.002704
574.405	-0.04467	-0.044352	578.408	-0.00051	-0.009236	598.412	-0.00025	0.002573
576.407	-0.0413	-0.041118	580.409	-0.00076	-0.008685	600.413	-9.1E-05	0.002556
578.408	-0.03806	-0.040029	582.411	-0.00107	-0.008784	602.427	-6E-06	0.003072
580.41	-0.035	-0.03827	584.412	-0.00144	-0.009223	604.429	0	0.002905
582.411	-0.03211	-0.035063	587.414	-0.0021	-0.009149	606.43	-6.9E-05	0.003046
584.412	-0.0294	-0.032917	589.416	-0.00261	-0.008554	608.431	-0.00021	0.002938
586.414	-0.02686	-0.028637	591.417	-0.00316	-0.008148	610.43	-0.00041	0.003037
588.415	-0.02448	-0.027432	593.418	-0.00374	-0.009248	612.421	-0.00068	0.002864
590.417	-0.02225	-0.025664	595.42	-0.00437	-0.008842	614.423	-0.001	0.00324
592.418	-0.02018	-0.023467	597.421	-0.00502	-0.009352	616.424	-0.00136	0.002604
594.42	-0.01825	-0.021296	599.423	-0.0057	-0.00884	618.426	-0.00178	0.002704
596.421	-0.01646	-0.019493	601.424	-0.00641	-0.008825	620.427	-0.00223	0.003199
599.423	-0.01401	-0.018382	603.426	-0.00713	-0.009563	622.429	-0.00271	0.002677
601.425	-0.01253	-0.013985	605.428	-0.00786	-0.008919	624.431	-0.00322	0.002626
603.426	-0.01117	-0.014621	607.428	-0.0086	-0.009563	626.432	-0.00375	0.002893
605.427	-0.00991	-0.013066	609.43	-0.00935	-0.010414	629.446	-0.00458	0.003235
607.429	-0.00875	-0.010631	611.431	-0.01009	-0.010419	631.447	-0.00514	0.003015
609.43	-0.00769	-0.009077	613.433	-0.01083	-0.010801	633.449	-0.00571	0.0033
611.432	-0.00671	-0.00826	615.434	-0.01156	-0.012252	635.45	-0.00628	0.001805
613.433	-0.00582	-0.006811	617.436	-0.01228	-0.0124	637.452	-0.00685	0.001888
615.434	-0.005	-0.006121	619.437	-0.01301	-0.012841	639.453	-0.00743	0.001708
617.437	-0.00424	-0.005305	621.438	-0.01374	-0.012989	641.455	-0.00803	7.3E-05
619.45	-0.00355	-0.003625	623.441	-0.01447	-0.014148	643.456	-0.00865	-0.00066
622.452	-0.00262	-0.002871	625.442	-0.01522	-0.014571	645.457	-0.0093	-0.001839
624.453	-0.00206	-0.001396	627.454	-0.01597	-0.015219	647.459	-0.00998	-0.003073
627.443	-0.00135	-0.000771	630.457	-0.01714	-0.016001	649.458	-0.01071	-0.003627
629.444	-0.00095	-0.00039	633.447	-0.01835	-0.016461	651.459	-0.01148	-0.00444
631.446	-0.00062	9.6E-05	635.448	-0.01919	-0.017855	653.461	-0.01231	-0.006065
633.447	-0.00035	0.001686	637.45	-0.02006	-0.018704	655.462	-0.0132	-0.007305
635.449	-0.00016	0.002602	639.451	-0.02096	-0.020292	657.464	-0.01465	-0.010115
637.45	-4.2E-05	0.001337	641.452	-0.0219	-0.02103	659.465	-0.01571	-0.010424
639.451	0	0.001897	643.454	-0.02288	-0.021716	661.466	-0.01685	-0.011644
641.453	-3.7E-05	0.002292	645.456	-0.0239	-0.022478	663.467	-0.01808	-0.012607
643.454	-0.00016	0.002585	647.457	-0.02497	-0.023556	665.469	-0.01941	-0.014006
645.456	-0.00036	0.002642	649.458	-0.02607	-0.024094	667.47	-0.02082	-0.016697
647.457	-0.00065	0.002282	651.459	-0.0272	-0.024958	669.472	-0.02233	-0.017551
649.459	-0.00103	0.002668	653.461	-0.02836	-0.027149	671.473	-0.02392	-0.019062
651.46	-0.0015	0.002639	655.463	-0.02954	-0.027953	673.475	-0.02558	-0.020048

653.461	-0.00206	0.002516	657.464	-0.03074	-0.028433	675.476	-0.0273	-0.022212
655.462	-0.00271	0.002711	659.465	-0.03195	-0.02989	677.478	-0.02907	-0.024684
657.464	-0.00344	0.002911	661.466	-0.03316	-0.030373	679.479	-0.03088	-0.026696
659.466	-0.00426	0.002162	663.468	-0.03438	-0.03128	681.481	-0.03272	-0.028187
661.467	-0.00515	0.002713	665.471	-0.03559	-0.033081	683.472	-0.03458	-0.031158
663.468	-0.00611	0.002446	667.471	-0.03678	-0.033653	685.483	-0.03645	-0.031843
665.47	-0.00715	0.002357	669.472	-0.03796	-0.0345	687.475	-0.03832	-0.032906
667.471	-0.00825	0.00229	671.474	-0.03912	-0.03504	689.476	-0.04019	-0.034702
669.472	-0.00941	0.001087	673.475	-0.04026	-0.036601	691.477	-0.04204	-0.036568
671.474	-0.01064	-4.1E-05	675.476	-0.04136	-0.03688	693.479	-0.04385	-0.037867
673.475	-0.01192	-0.000972	677.478	-0.04242	-0.038761	695.48	-0.04563	-0.039231
675.477	-0.01325	-0.002291	679.479	-0.04344	-0.039642	697.482	-0.04737	-0.042341
677.478	-0.01464	-0.003766	681.48	-0.04443	-0.039732	699.483	-0.04908	-0.042227
679.48	-0.01607	-0.005653	683.482	-0.04539	-0.040342	701.497	-0.05075	-0.045243
681.481	-0.01754	-0.006085	685.485	-0.04633	-0.04157	703.498	-0.05238	-0.046176
683.482	-0.01906	-0.007077	687.485	-0.04724	-0.04183	705.5	-0.05399	-0.048796
685.484	-0.02061	-0.008931	689.486	-0.04814	-0.042682	707.501	-0.05557	-0.050457
687.485	-0.02221	-0.009858	691.488	-0.04903	-0.044468	709.503	-0.05713	-0.052185
689.487	-0.02384	-0.011022	693.489	-0.0499	-0.045079	711.504	-0.05867	-0.054822
691.488	-0.0255	-0.013263	695.491	-0.05078	-0.045624	713.505	-0.06019	-0.05657
693.489	-0.0272	-0.014135	697.491	-0.05166	-0.046636	715.507	-0.06169	-0.056414
695.491	-0.02893	-0.015653	699.493	-0.05254	-0.048198	717.506	-0.06318	-0.058715
697.492	-0.03068	-0.017674	701.494	-0.05343	-0.04857	719.507	-0.06466	-0.060901
699.494	-0.03247	-0.019152	703.496	-0.05434	-0.048873	721.508	-0.06613	-0.065282
701.495	-0.03427	-0.020464	705.498	-0.05527	-0.049681	723.51	-0.0676	-0.065025
703.497	-0.03611	-0.023771	707.499	-0.05622	-0.051886	725.511	-0.06907	-0.066799
705.498	-0.03796	-0.02499	709.501	-0.05721	-0.052451	727.512	-0.07054	-0.068535
707.499	-0.03983	-0.027269	711.502	-0.05822	-0.053842	729.514	-0.07201	-0.070301
709.501	-0.04171	-0.028171	713.503	-0.05925	-0.055786	732.516	-0.07423	-0.073967
711.503	-0.04362	-0.030443	715.504	-0.0603	-0.055281	734.518	-0.07573	-0.074568
713.505	-0.04554	-0.03269	717.506	-0.06137	-0.056038	736.522	-0.07725	-0.076209
715.506	-0.04748	-0.034938	719.507	-0.06244	-0.056943	738.52	-0.07878	-0.078266
718.52	-0.05043	-0.037427	721.509	-0.06352	-0.058395	740.523	-0.08035	-0.079677
721.51	-0.05344	-0.038599	723.51	-0.06459	-0.060564	742.524	-0.08194	-0.083108
723.51	-0.05548	-0.040364	725.512	-0.06565	-0.061722	744.525	-0.08358	-0.085137
725.512	-0.05755	-0.042417	727.513	-0.0667	-0.061439	746.526	-0.08525	-0.088589
727.514	-0.05966	-0.044432	729.514	-0.06773	-0.062012	748.528	-0.08696	-0.090725
729.515	-0.06181	-0.047227	731.516	-0.06873	-0.063327	750.529	-0.08873	-0.091397
731.516	-0.06399	-0.04847	733.517	-0.06971	-0.064032	752.53	-0.09055	-0.093457
733.518	-0.06622	-0.051542	735.519	-0.07064	-0.06514	754.532	-0.09243	-0.095041
735.519	-0.06849	-0.053038	737.52	-0.07154	-0.066065	756.538	-0.09437	-0.097699

737.52	-0.07081	-0.055801	739.522	-0.07239	-0.066565	758.534	-0.09637	-0.10093
739.522	-0.07317	-0.060049	741.523	-0.07319	-0.067115	761.536	-0.09952	-0.102941
741.523	-0.07558	-0.061887	743.524	-0.07393	-0.068825	763.538	-0.10171	-0.106877
743.525	-0.07805	-0.065566	745.526	-0.07461	-0.068715	765.54	-0.10397	-0.108219
745.526	-0.08057	-0.066543	747.527	-0.07525	-0.069725	767.541	-0.10629	-0.11197
747.527	-0.08313	-0.068935	749.529	-0.07584	-0.070419	769.542	-0.10866	-0.112247
749.529	-0.08573	-0.071883	751.529	-0.07639	-0.07151	771.544	-0.11106	-0.115014
751.53	-0.08836	-0.076334	753.532	-0.07691	-0.071866	773.546	-0.1135	-0.117759
753.532	-0.09103	-0.078315	755.533	-0.07741	-0.072172	776.538	-0.11718	-0.1219
755.533	-0.09373	-0.080935	757.534	-0.07788	-0.072649	779.549	-0.12088	-0.124083
757.535	-0.09644	-0.085226	759.536	-0.07834	-0.074058	781.551	-0.12333	-0.125762
759.536	-0.09918	-0.088262	761.537	-0.07879	-0.074018	783.542	-0.12577	-0.127871
761.537	-0.10193	-0.089852	763.539	-0.07924	-0.074357	785.544	-0.12818	-0.131645
763.539	-0.10469	-0.092944	765.54	-0.07969	-0.075513	787.545	-0.13055	-0.133697
765.54	-0.10746	-0.096235	767.541	-0.08015	-0.076299	789.546	-0.13287	-0.13557
767.542	-0.11022	-0.100132	769.543	-0.08063	-0.076579	791.548	-0.13513	-0.138102
769.543	-0.11299	-0.101475	771.544	-0.08112	-0.077305	793.562	-0.13734	-0.141827
771.545	-0.11574	-0.104325	773.545	-0.08164	-0.078173	795.563	-0.13948	-0.143167
773.546	-0.11849	-0.10734	775.547	-0.08219	-0.077736	797.564	-0.14156	-0.145424
775.547	-0.12122	-0.110585	777.549	-0.08278	-0.079641	800.567	-0.14459	-0.146875
777.549	-0.12393	-0.112601	779.55	-0.08341	-0.079754	802.569	-0.14655	-0.148594
779.55	-0.12664	-0.116218	781.551	-0.08408	-0.081413	804.57	-0.14846	-0.1508
781.552	-0.12933	-0.120645	783.552	-0.08479	-0.080627	806.571	-0.15033	-0.154118
783.553	-0.13201	-0.121891	785.555	-0.08553	-0.082419	808.573	-0.15216	-0.154911
785.554	-0.13468	-0.125461	787.555	-0.08629	-0.083139	810.575	-0.15396	-0.157001
787.556	-0.13735	-0.128376	789.557	-0.08709	-0.083426	812.576	-0.15572	-0.158236
789.557	-0.14002	-0.131777	791.558	-0.0879	-0.083995	814.576	-0.15746	-0.160226
791.558	-0.14268	-0.136308	793.559	-0.08874	-0.085149	817.579	-0.16002	-0.163129
793.56	-0.14534	-0.139442	795.561	-0.08959	-0.086704	819.578	-0.1617	-0.165207
795.566	-0.148	-0.142963	797.562	-0.09046	-0.086864	821.579	-0.16336	-0.165063
797.563	-0.15067	-0.148191	799.564	-0.09134	-0.08875	823.583	-0.16502	-0.168382
799.564	-0.15333	-0.151356	801.565	-0.09223	-0.089373	825.582	-0.16666	-0.169783
802.566	-0.15735	-0.154118	803.567	-0.09312	-0.089277	827.584	-0.16829	-0.170556
804.568	-0.16003	-0.158483	805.569	-0.09401	-0.090464	829.584	-0.16992	-0.175786
806.569	-0.16273	-0.159986	807.569	-0.0949	-0.091431	832.587	-0.17235	-0.177221
808.571	-0.16543	-0.163205	809.571	-0.09579	-0.092282	835.589	-0.17476	-0.179767
810.572	-0.16815	-0.166559	811.572	-0.09667	-0.092955	837.593	-0.17636	-0.182689
812.573	-0.17087	-0.169078	813.574	-0.09754	-0.092866	839.595	-0.17796	-0.183899
814.592	-0.17361	-0.174804	815.575	-0.09841	-0.094354	841.596	-0.17955	-0.186209
816.593	-0.17635	-0.177681	817.576	-0.09927	-0.095384	843.597	-0.18114	-0.187579
818.595	-0.1791	-0.179262	819.578	-0.10012	-0.096159	845.599	-0.18273	-0.191317

820.592	-0.18186	-0.182727	821.579	-0.10097	-0.097277	848.598	-0.1851	-0.194912
822.593	-0.18463	-0.188477	823.581	-0.10182	-0.097535	850.6	-0.18668	-0.197266
824.591	-0.1874	-0.190559	825.583	-0.10265	-0.098393	853.601	-0.18905	-0.200139
826.594	-0.19018	-0.193977	827.584	-0.10349	-0.098732			
828.594	-0.19297	-0.195232	829.585	-0.10432	-0.099842			
830.596	-0.19576	-0.199223	831.587	-0.10514	-0.101028			
832.597	-0.19855	-0.202033	833.588	-0.10596	-0.102002			
834.599	-0.20136	-0.206473	835.589	-0.10678	-0.101785			
836.6	-0.20416	-0.208587	837.602	-0.10759	-0.103478			
838.601	-0.20698	-0.213308	840.593	-0.1088	-0.103396			
840.604	-0.20979	-0.215972	842.594	-0.10961	-0.105428			
843.605	-0.21402	-0.221286	844.596	-0.11041	-0.105343			
845.607	-0.21685	-0.223783	845.597	-0.11081	-0.107642			
847.608	-0.21967	-0.226645	847.598	-0.11161	-0.107751			
850.6	-0.22392	-0.230057	849.599	-0.11241	-0.1072			
852.602	-0.22675	-0.23266	851.665	-0.1132	-0.109305			
854.603	-0.22958	-0.237216	854.681	-0.1144	-0.110488			
856.604	-0.23241	-0.243077	856.682	-0.11519	-0.110584			

F.2 Echocardiography Tracking Raw Results

Table F-2. Specific Aim 1 echocardiography tracking raw results pertaining to Figure 6-2.

Porcine	**Healthy**		
	Diastole (cm^2)	**Systole (cm^2)**	**Percent Change**
DCAS001	11.56	9.92	-14.19
DCAS002	11.50	10.11	-12.09
DCAS003	11.67	10.15	-13.02
DCAS004	11.75	9.93	-15.49
DCAS005	11.39	10.00	-12.20
DCAS006	11.40	9.87	-13.42
DCAS007	11.40	9.85	-13.60
DCAS008	11.53	9.91	-14.05

Diseased			Ovine	Healthy		
Diastole (cm^2)	**Systole (cm^2)**	**Percent Change**		**Diastole (cm^2)**	**Systole (cm^2)**	**Percent Change**
13.46	12.62	-6.24	DCA009B	5.54	4.55	-17.87
12.97	12.29	-5.24	DCA010	5.46	4.45	-18.50
13.17	12.26	-6.91	DCA011	4.94	3.97	-19.64
13.20	12.45	-5.68	DCA012	5.72	4.67	-18.36
12.97	12.23	-5.71	DCA013	5.54	4.57	-17.51
12.92	12.30	-4.80	DCA014	5.36	4.44	-17.16
12.94	12.30	-4.95	DCA015	5.31	4.28	-19.40
13.06	12.33	-5.59	DCA016	5.94	4.60	-22.56

F.3 Bar Graph Raw Results

Table F-3. Specific Aim 1 Experiment A raw results pertaining to Figure 6-3.

Strain	Mean
MV	Healthy
1	0.5783
2	0.5754
3	0.7972
4	0.2857
5	0.6824
6	0.6469
7	0.8595
8	0.6781

	Standard Deviation		Minimum		Maximum		Coaptation Length	
Ischemic	Healthy	Ischemic	Healthy	Ischemic	Healthy	Ischemic	Healthy	Ischemic
0.5721	0.2054	0.1533	0.2740	0.3415	0.8519	0.7726	11.5	12.0
0.6217	0.1272	0.0894	0.3536	0.4728	0.7450	0.7476	14.2	14.5
0.8417	0.0684	0.0599	0.7121	0.7857	0.9220	0.9744	9.5	9.0
0.3839	0.1897	0.1840	0.0595	0.1389	0.6644	0.6538	11.9	11.5
0.7603	0.0903	0.0537	0.5697	0.6963	0.8237	0.8555	13.4	13.6
0.7470	0.3124	0.2284	0.2892	0.3529	1.1151	1.0249	11.7	11.5
0.9003	0.0831	0.0792	0.7709	0.8153	1.0061	1.0361	12.8	11.5
0.7441	0.1053	0.1222	0.4888	0.5805	0.8697	0.9313	13.3	12.2

Table F-4. Specific Aim 1 Experiment B raw results pertaining to Figure 6-5.

Strain
MV
1
2
3
4
5
6
7
8

Mean			Standard Deviation			Minimum			Maximu
Healthy	Static-Min	Static-Max	Healthy	Static-Min	Static-Max	Healthy	Static-Min	Static-Max	Healthy
0.5794	0.5506	0.6504	0.1313	0.1399	0.1986	0.3932	0.3462	0.4044	0.8054
0.5558	0.6373	0.5756	0.1017	0.0937	0.1381	0.4544	0.5062	0.3396	0.7889
0.1247	0.2835	0.1844	0.1623	0.1671	0.1344	-0.0600	0.0649	-0.0255	0.4659
0.1865	0.2685	0.2700	0.1079	0.0515	0.1073	-0.0531	0.1780	0.1563	0.3085
0.3655	0.4569	0.4053	0.1137	0.0852	0.0724	0.2002	0.3106	0.2927	0.5176
0.2463	0.4618	0.2946	0.1553	0.1028	0.1371	-0.0116	0.3411	0.0759	0.5338
0.1708	0.2540	0.1762	0.0629	0.0388	0.0529	0.0574	0.1936	0.1050	0.2599
0.3404	0.3810	0.3847	0.1030	0.0875	0.1059	0.1735	0.2000	0.1998	0.5337

		Coaptation Length		
Static-Min	Static-Max	Healthy	Static-Min	Static-Max
0.8020	1.0254	4.5	4.4	4.7
0.8212	0.8019	4.9	4.6	4.7
0.6494	0.4564	3.7	3.8	3.5
0.3404	0.4850	4.9	4.8	4.5
0.6105	0.5331	4.4	4.3	4.5
0.6423	0.5994	4.9	4.7	4.6
0.3112	0.2607	5.5	5.1	5.2
0.5062	0.5914	5.3	4.8	4.4

F.4 Strain Maps

Table F-5. Specific Aim 1 Experiment A raw data pertaining to Figure 6-4 Healthy state.

Node	X0	Y0
1	5.128041	13.38475
2	3.225573	13.62131
3	1.424509	14.28975
4	5.323275	11.29459
5	3.153105	11.51484
6	0.8563	11.9915
7	5.350225	8.974963
8	3.007876	9.281488
9	0.607463	10.03624

Z0	X1	Y1	Z1	Green Areal	Green Circ	Green Radial	Green Max Princ	Green Min Princ	Almansi Areal	Almansi Circ
-3.76008	11.57093	15.7595	5.110199	0.772839	0.156528	0.67671	0.760424	0.134324	0.431037	0.105417
-2.52454	9.254025	16.12475	6.388225	0.723623	0.131752	0.652435	0.720652	0.114628	0.398995	0.080089
-1.54002	6.8872	16.92675	6.997335	0.654911	0.14125	0.560047	0.593654	0.13537	0.369412	0.088562
-3.17728	11.57026	12.53088	5.388075	0.631891	0.129247	0.568454	0.629041	0.099998	0.377724	0.091591
-1.89058	9.153713	12.73521	6.7777	0.631911	0.131736	0.555021	0.639551	0.094304	0.370449	0.082487
-1.42389	6.5881	13.57695	7.203771	0.587724	0.10569	0.523671	0.597269	0.082077	0.340761	0.058472
-3.02499	11.31211	9.056663	5.234275	0.637926	0.12634	0.585802	0.613464	0.10814	0.376252	0.094061
-1.61387	8.728875	9.556025	6.854588	0.591818	0.142627	0.517181	0.577255	0.098153	0.361334	0.097098
-0.6558	5.843624	10.80031	7.493089	0.508881	0.137506	0.406655	0.497672	0.082728	0.319099	0.081253

Almansi radial	Almansi Max Princ	Almansi Min Princ	Connectivity		
0.273589	0.295553	0.099898	1	2	4
0.263065	0.284909	0.074903	2	5	4
0.239797	0.259155	0.085335	2	3	5
0.243976	0.268484	0.077213	3	6	5
0.237324	0.268844	0.06378	4	5	7
0.228632	0.257542	0.043682	5	8	7
0.249936	0.264311	0.083708	5	6	8
0.226867	0.257599	0.073626	6	9	8
0.196275	0.238176	0.047687			

Table F-6. Specific Aim 1 Experiment A raw data pertaining to Figure 6-4 Diseased state.

Node	X0	Y0	Z0	X1
1	5.128041	13.38475	-3.76008	11.84719
2	3.225573	13.62131	-2.52454	9.5567
3	1.424509	14.28975	-1.54002	7.23575
4	5.323275	11.29459	-3.17728	11.95625
5	3.153105	11.51484	-1.89058	9.621175
6	0.8563	11.9915	-1.42389	7.003388
7	5.350225	8.974963	-3.02499	11.79495
8	3.007876	9.281488	-1.61387	9.177413
9	0.607463	10.03624	-0.6558	6.258186

Y1	Z1	Green Areal	Green Circ	Green Radial	Green Max Princ	Green Min Princ	Almansi Areal	Almansi Circ	Almansi radial	Almansi Max Princ
15.8343	5.699413	0.764725	0.158783	0.658268	0.742798	0.131156	0.427674	0.110189	0.267763	0.294277
16.17599	7.019338	0.713695	0.13665	0.634107	0.710609	0.111077	0.400254	0.087651	0.256214	0.285374
17.03138	7.754285	0.689388	0.140997	0.595504	0.648728	0.1234	0.386375	0.092984	0.248397	0.273152
12.53181	6.083225	0.713746	0.150911	0.633994	0.700211	0.116203	0.41245	0.103106	0.264918	0.288076
12.78194	7.740138	0.696206	0.148283	0.605549	0.699358	0.105971	0.399189	0.088455	0.256288	0.285706
13.62545	8.099284	0.635955	0.128619	0.545046	0.645089	0.089931	0.368069	0.069171	0.242611	0.272964
9.001713	6.11225	0.701044	0.157772	0.612829	0.647966	0.133474	0.404968	0.112764	0.261679	0.276497
9.427088	7.736025	0.710117	0.161682	0.629985	0.690659	0.120198	0.408973	0.102862	0.261482	0.28548
10.69155	8.291976	0.642672	0.162894	0.518663	0.63019	0.105429	0.374182	0.082103	0.242206	0.271768

Almansi Min Princ	Connectivity		
0.09855	1	2	4
0.077314	2	5	4
0.083563	2	3	5
0.089673	3	6	5
0.074245	4	5	7
0.055774	5	8	7
0.101897	5	6	8
0.088836	6	9	8
0.064985			

Table F-7. Specific Aim 1 Experiment B raw data pertaining to Figure 6-6 Healthy state.

Node	X0	Y0	Z0	X1	Y1	Z1
1	3.216149	5.848109	-9.63405	7.005663	7.279375	-0.22412
2	1.759408	6.515723	-9.10546	5.581775	8.02205	0.724696
3	0.334006	7.26995	-8.51654	3.998824	8.7206	1.276281
4	2.741245	4.119115	-9.46684	6.62995	5.057831	0.213619
5	1.314519	4.663863	-8.80594	5.25325	5.58595	1.340111
6	-0.26737	5.362251	-8.42881	3.52819	6.248338	1.917946
7	2.350374	2.323336	-8.70935	6.261638	2.842813	0.588675
8	0.829962	2.866224	-8.2453	4.886925	3.406038	1.774034
9	-0.85968	3.586839	-7.76091	2.93105	4.16374	2.303859

Green Areal	Green Circ	Green Radial	Green Max Princ	Green Min Princ	Almansi Areal	Almansi Circ	Almansi radial	Almansi Max Princ	Almansi Min Princ	Connectivity	
0.439622	0.117469	0.334049	0.419094	0.072312	0.295421	0.084877	0.173606	0.220461	0.049165	1	2
0.40909	0.080827	0.35605	0.430602	0.040856	0.271959	0.044451	0.184323	0.223924	0.013193	2	5
0.364015	0.042698	0.370673	0.457172	-0.01224	0.244137	0.01373	0.174327	0.23057	-0.03179	2	3
0.306972	0.116953	0.211242	0.334569	0.018346	0.214861	0.086645	0.093272	0.188881	-0.00158	3	6
0.317621	0.097252	0.250678	0.350797	0.018798	0.217207	0.063564	0.113205	0.194969	-0.01122	4	5
0.297068	0.049782	0.289627	0.371452	-0.01023	0.198566	0.020808	0.130982	0.200439	-0.04349	5	8
0.28847	0.159587	0.14163	0.301563	0.020638	0.194568	0.105839	0.057666	0.177549	-0.00588	5	6
0.262589	0.133838	0.159798	0.303657	0.002419	0.185136	0.089592	0.057023	0.178564	-0.02428	6	9
0.205015	0.096229	0.157249	0.284001	-0.02821	0.140744	0.053833	0.039221	0.169758	-0.0699		

4
4
5
5
7
7
8
8

Table F-8. Specific Aim 1 Experiment B raw data pertaining to Figure 6-6 Static-Min state.

Node	X0	Y0	Z0	X1	Y1	Z1	Green Areal	Green Circ
1	3.216149	5.848109	-9.63405	6.703088	7.060784	-0.56047	0.431799	0.131446
2	1.759408	6.515723	-9.10546	5.274649	7.81645	0.389478	0.474442	0.114931
3	0.334006	7.26995	-8.51654	3.779216	8.565975	1.100106	0.391072	0.046748
4	2.741245	4.119115	-9.46684	6.410975	4.916838	0.083524	0.31237	0.110534
5	1.314519	4.663863	-8.80594	5.011459	5.365313	1.110073	0.3494	0.119293
6	-0.26737	5.362251	-8.42881	3.190566	6.024576	1.611071	0.364736	0.089997
7	2.350374	2.323336	-8.70935	5.962713	2.610989	0.48522	0.406402	0.17597
8	0.829962	2.866224	-8.2453	4.63565	3.206863	1.712808	0.312022	0.135197
9	-0.85968	3.586839	-7.76091	2.625398	3.9464	2.176839	0.266719	0.13104

Green Radial	Green Max Princ	Green Min Princ	Almansi Areal	Almansi Circ	Almansi radial	Almansi Max Princ	Almansi Min Princ	Connectivity		
0.33272	0.442716	0.057744	0.278189	0.077876	0.150052	0.221607	0.018821	1	2	4
0.383737	0.466902	0.071212	0.293219	0.063732	0.183903	0.226908	0.036051	2	5	4
0.388129	0.465108	0.003366	0.254366	0.018876	0.182428	0.229111	-0.01497	2	3	5
0.234507	0.341023	0.024308	0.224986	0.071353	0.113012	0.190399	0.002672	3	6	5
0.263982	0.377646	0.028972	0.235604	0.072547	0.121587	0.201237	0.001485	4	5	7
0.313612	0.414715	0.0153	0.2365	0.050001	0.142186	0.211726	-0.01088	5	8	7
0.236115	0.338661	0.092688	0.274268	0.110734	0.136483	0.191356	0.071058	5	6	8
0.20062	0.313356	0.036167	0.22546	0.086379	0.107257	0.183166	0.020001	6	9	8
0.176701	0.322935	-0.00834	0.19382	0.079818	0.078845	0.187984	-0.02559			

Table F-9. Specific Aim 1 Experiment B raw data pertaining to Figure 6-6 Static-Max state.

Node	X0	Y0	Z0	X1	Y1	Z1	Green Areal	Green Circ	Green Radial
1	3.216149	5.848109	-9.63405	6.750288	7.205888	-0.0817	0.467894	0.111032	0.381762
2	1.759408	6.515723	-9.10546	5.263579	7.953513	0.788588	0.48206	0.110027	0.393987
3	0.334006	7.26995	-8.51654	3.799122	8.796638	1.568131	0.431889	0.068084	0.398209
4	2.741245	4.119115	-9.46684	6.354863	4.996409	0.597606	0.362853	0.096331	0.295735
5	1.314519	4.663863	-8.80594	4.931345	5.508079	1.550221	0.397721	0.105898	0.320594
6	-0.26737	5.362251	-8.42881	3.242738	6.279	2.268849	0.408812	0.085473	0.353005
7	2.350374	2.323336	-8.70935	5.8107	2.600834	1.030431	0.432893	0.172356	0.265262
8	0.829962	2.866224	-8.2453	4.42879	3.183854	2.139663	0.362961	0.132447	0.254833
9	-0.85968	3.586839	-7.76091	2.490848	4.026959	2.821463	0.358184	0.128375	0.258935

Green Max Princ	Green Min Princ	Almansi Areal	Almansi Circ	Almansi radial	Almansi Max Princ	Almansi Min Princ	Connectivity		
0.475512	0.062484	0.30762	0.069664	0.187024	0.237108	0.035233	1	2	4
0.479031	0.066859	0.312589	0.071966	0.197594	0.238577	0.043259	2	5	4
0.489022	0.019448	0.290246	0.050761	0.196157	0.241466	0.011798	2	3	5
0.381256	0.036473	0.25435	0.063861	0.148688	0.207452	0.01636	3	6	5
0.406445	0.047696	0.271486	0.069179	0.159656	0.215193	0.026122	4	5	7
0.427794	0.041079	0.276331	0.059331	0.176239	0.22181	0.023684	5	8	7
0.340839	0.112946	0.283131	0.109667	0.146896	0.194693	0.077083	5	6	8
0.344708	0.056788	0.252687	0.08606	0.132741	0.195891	0.034699	6	9	8
0.343834	0.054287	0.250738	0.08401	0.131071	0.194616	0.033379			

APPENDIX G. RAW DATA – SPECIFIC AIM 2

G.1 Specific Aim 2A – Peak Systolic LVOT Average Velocity

Table G-1. 50/50 Short AML peak systolic LVOT average velocity at all LAMPOON and CO conditions.

	50/50 Short AML		
Cardiac Output (L/min)	0% LAMPOON Velocity (m/s)	50% LAMPOON Velocity (m/s)	100% LAMPOON Velocity (m/s)
2.5	0.273	0.247	0.262
5.0	0.394	0.406	0.364
6.5	0.462	0.473	
Average	0.334	0.327	0.313

Table G-2. 50/50 Long AML peak systolic LVOT average velocity at all LAMPOON and CO conditions.

	50/50 Long AML		
Cardiac Output (L/min)	0% LAMPOON Velocity (m/s)	50% LAMPOON Velocity (m/s)	100% LAMPOON Velocity (m/s)
2.5	0.257	0.223	0.208
5.0	0.441	0.375	0.367
6.5	0.458	0.423	0.395
Average	0.385	0.340	0.323

Table G-3. 80/20 Long AML peak systolic LVOT average velocity at all LAMPOON and CO conditions.

	80/20 Long AML

Cardiac Output (L/min)	0% LAMPOON	50% LAMPOON	100% LAMPOON
	Velocity (m/s)	Velocity (m/s)	Velocity (m/s)
2.5	0.298	0.268	0.245
5.0	0.398	0.371	0.342
6.5	0.409	0.409	0.380
Average	0.368	0.349	0.322

Table G-4. Combined average of Long AML peak systolic LVOT average velocity at all LAMPOON and CO conditions.

	Combined Averaged – Long AML		
Cardiac Output (L/min)	0% LAMPOON	50% LAMPOON	100% LAMPOON
	Velocity (m/s)	Velocity (m/s)	Velocity (m/s)
2.5	0.278	0.246	0.227
5.0	0.420	0.373	0.355
6.5	0.434	0.416	0.388
Average	0.362	0.339	0.320

G.2 Specific Aim 2A – Maximum VSS

Table G-5. 50/50 Short AML maximum VSS and time it occurred at all LAMPOON and CO conditions.

	50/50 Short AML					
Cardiac Output (L/min)	0% LAMPOON		50% LAMPOON		100% LAMPOON	
	VSS (N/m^2)	Time (ms)	VSS (N/m^2)	Time (ms)	VSS (N/m^2)	Time (ms)
2.5	0.723	139	0.728	149	0.568	193
5.0	1.002	439	1.135	99	0.734	149
6.5	1.393	445	1.014	122		
Average	0.862	289	0.931	124	0.651	171

Table G-6. 50/50 Long AML maximum VSS and time it occurred at all LAMPOON and CO conditions.

	50/50 Long AML					
Cardiac Output (L/min)	0% LAMPOON		50% LAMPOON		100% LAMPOON	
	VSS (N/m^2)	Time (ms)	VSS (N/m^2)	Time (ms)	VSS (N/m^2)	Time (ms)
2.5	0.544	121	0.452	144	0.446	173
5.0	1.154	107	0.903	115	0.633	115
6.5	1.381	107	1.182	94	0.655	129
Average	1.026	112	0.845	117	0.578	139

Table G-7. 80/20 Long AML maximum VSS and time it occurred at all LAMPOON and CO conditions.

	80/20 Long AML					
Cardiac Output (L/min)	0% LAMPOON		50% LAMPOON		100% LAMPOON	
	VSS (N/m^2)	Time (ms)	VSS (N/m^2)	Time (ms)	VSS (N/m^2)	Time (ms)
2.5	0.593	143	0.422	121	0.414	165
5.0	1.065	107	0.853	121	0.720	137
6.5	1.071	128	0.801	128	0.880	108
Average	0.910	126	0.692	123	0.671	137

Table G-8. Combined average of all deployment and AML lengths maximum VSS and time it occurred at all LAMPOON and CO conditions.

	Combined Average – ALL					
Cardiac Output (L/min)	0% LAMPOON		50% LAMPOON		100% LAMPOON	
	VSS (N/m^2)	Time (ms)	VSS (N/m^2)	Time (ms)	VSS (N/m^2)	Time (ms)
2.5	0.620	134	0.534	138	0.476	177
5.0	1.074	218	0.963	112	0.696	134
6.5	1.281	227	0.999	114	0.768	119
Average	0.933	176	0.823	122	0.633	149

G.3 Specific Aim 2A – Maximum Principal RSS

Table G-9. 50/50 Short AML maximum principal RSS and time it occurred at all LAMPOON and CO conditions.

	50/50 Short AML					
Cardiac Output (L/min)	0% LAMPOON		50% LAMPOON		100% LAMPOON	
	pRSS (N/m^2)	Time (ms)	pRSS (N/m^2)	Time (ms)	pRSS (N/m^2)	Time (ms)
2.5	14.15	250	5.87	342	7.25	298
5.0	31.36	183	18.42	282	14.41	254
6.5	23.96	233	25.62	226		
Average	22.757	217	12.147	312	10.829	276

Table G-10. 50/50 Long AML maximum principal RSS and time it occurred at all LAMPOON and CO conditions.

	50/50 Long AML					
Cardiac Output (L/min)	0% LAMPOON		50% LAMPOON		100% LAMPOON	
	pRSS (N/m^2)	Time (ms)	pRSS (N/m^2)	Time (ms)	pRSS (N/m^2)	Time (ms)
2.5	8.39	250	8.32	266	6.10	288
5.0	24.73	200	20.05	173	20.02	180
6.5	39.33	171	23.13	180	32.89	180
Average	24.151	207	17.166	206	19.671	216

Table G-11. 50/50 Short AML maximum principal RSS and time it occurred at all LAMPOON and CO conditions.

	80/20 Long AML					
Cardiac Output (L/min)	0% LAMPOON		50% LAMPOON		100% LAMPOON	
	pRSS (N/m^2)	Time (ms)	pRSS (N/m^2)	Time (ms)	pRSS (N/m^2)	Time (ms)

2.5	5.27	228	5.62	221	12.85	180
5.0	21.80	200	24.83	193	41.69	144
6.5	71.20	157	20.85	178	41.46	122
Average	32.757	195	17.100	197	32.000	149

Table G-12. Combined average of all deployment heights and AML lengths maximum principal RSS and time it occurred at all LAMPOON and CO conditions.

	Combined Average – ALL					
Cardiac Output (L/min)	**0% LAMPOON**		**50% LAMPOON**		**100% LAMPOON**	
	pRSS (N/m^2)	**Time (ms)**	**pRSS (N/m^2)**	**Time (ms)**	**pRSS (N/m^2)**	**Time (ms)**
2.5	9.270	243	6.603	276	8.733	255
5.0	25.964	194	21.102	216	25.373	193
6.5	44.832	187	23.200	195	37.176	151
Average	26.555	206	15.471	238	20.833	214

G.4 Specific Aim 2A – Maximum TKE

Table G-13. 50/50 Long AML maximum TKE and time it occurred at all LAMPOON and CO conditions.

	50/50 Short AML					
Cardiac Output (L/min)	**0% LAMPOON**		**50% LAMPOON**		**100% LAMPOON**	
	Value (m^2/s^2)	**Time (ms)**	**Value (m^2/s^2)**	**Time (ms)**	**Value (m^2/s^2)**	**Time (ms)**
2.5	0.0391	245	0.0065	282	0.0073	160
5.0	0.0340	189	0.0190	276	0.0191	226
6.5	0.0296	233	0.0296	226		
Average	0.037	217	0.013	279	0.013	193

Table G-14. 50/50 Long AML maximum TKE and time it occurred at all LAMPOON and CO conditions.

Cardiac Output (L/min)	50/50 Long AML					
	0% LAMPOON		50% LAMPOON		100% LAMPOON	
	Value (m^2/s^2)	Time (ms)	Value (m^2/s^2)	Time (ms)	Value (m^2/s^2)	Time (ms)
2.5	0.0091	250	0.0102	259	0.0076	288
5.0	0.0257	200	0.0201	173	0.0210	180
6.5	0.0425	178	0.0279	173	0.0328	180
Average	0.026	209	0.019	201	0.020	216

Table G-15. 80/20 Long AML maximum TKE and time it occurred at all LAMPOON and CO conditions.

Cardiac Output (L/min)	80/20 Long AML					
	0% LAMPOON		50% LAMPOON		100% LAMPOON	
	Value (m^2/s^2)	Time (ms)	Value (m^2/s^2)	Time (ms)	Value (m^2/s^2)	Time (ms)
2.5	0.0068	214	0.0078	207	0.0175	187
5.0	0.0239	200	0.0248	193	0.0404	151
6.5	0.0834	164	0.0284	207	0.0421	122
Average	0.038	193	0.020	202	0.033	153

Table G-16. Combined average of all deployment heights and AML lengths maximum TKE and time it occurred at all LAMPOON and CO conditions.

Cardiac Output (L/min)	Combined Average – ALL					
	0% LAMPOON		50% LAMPOON		100% LAMPOON	
	Value (m^2/s^2)	Time (ms)	Value (m^2/s^2)	Time (ms)	Value (m^2/s^2)	Time (ms)
2.5	0.018	236	0.008	249	0.011	212
5.0	0.028	196	0.021	214	0.027	186
6.5	0.052	192	0.029	202	0.037	151
Average	0.033	206	0.017	228	0.022	187

G.5 Specific Aim 2B – Neo-Sinus Particle Tracking

Table G-17. 80/20 Long AML neo-sinus particle tracking results for 2.5 L/min.

0% LAMPOON			50% LAMPOON			100% LAMPOON		
Time (s)	Cycle (#)	Particle Density (%)	Time (s)	Cycle (#)	Particle Density (%)	Time (s)	Cycle (#)	Particle Density (%)
0	0	1	0	0	1	0	0	1
0.001	0.00117	1	0.001	0.00117	1	0.001	0.00117	1
0.002	0.00234	1	0.002	0.00234	1	0.002	0.00234	1
0.003	0.00350	1	0.003	0.00350	1	0.003	0.00350	0.99143
0.004	0.00467	0.98551	0.004	0.00467	1	0.004	0.00467	0.98000
0.005	0.00584	0.94928	0.005	0.00584	1	0.005	0.00584	0.94857
0.006	0.00701	0.94928	0.006	0.00701	1	0.006	0.00701	0.93714
0.007	0.00818	0.94928	0.007	0.00818	1	0.007	0.00818	0.91714
0.008	0.00935	0.94928	0.008	0.00935	0.99578	0.008	0.00935	0.89143
0.009	0.01051	0.94928	0.009	0.01051	0.99578	0.009	0.01051	0.87714
0.01	0.01168	0.93478	0.01	0.01168	0.99156	0.01	0.01168	0.85429
0.011	0.01285	0.91304	0.011	0.01285	0.98312	0.011	0.01285	0.82857
0.012	0.01402	0.89855	0.012	0.01402	0.97468	0.012	0.01402	0.80286
0.013	0.01519	0.89855	0.013	0.01519	0.95781	0.013	0.01519	0.78857
0.014	0.01636	0.89855	0.014	0.01636	0.94937	0.014	0.01636	0.74286
0.015	0.01752	0.89855	0.015	0.01752	0.94937	0.015	0.01752	0.71143
0.016	0.01869	0.89130	0.016	0.01869	0.94515	0.016	0.01869	0.68286
0.017	0.01986	0.86232	0.017	0.01986	0.94515	0.017	0.01986	0.64857
0.018	0.02103	0.84783	0.018	0.02103	0.94093	0.018	0.02103	0.61714
0.019	0.02220	0.84783	0.019	0.02220	0.93671	0.019	0.02220	0.59143
0.02	0.02336	0.84783	0.02	0.02336	0.93671	0.02	0.02336	0.56286
0.021	0.02453	0.84783	0.021	0.02453	0.93671	0.021	0.02453	0.52571
0.022	0.02570	0.83333	0.022	0.02570	0.93671	0.022	0.02570	0.49714
0.023	0.02687	0.81159	0.023	0.02687	0.93671	0.023	0.02687	0.45714
0.024	0.02804	0.79710	0.024	0.02804	0.92827	0.024	0.02804	0.42571
0.025	0.02921	0.79710	0.025	0.02921	0.91561	0.025	0.02921	0.41429
0.026	0.03037	0.79710	0.026	0.03037	0.91561	0.026	0.03037	0.38857
0.027	0.03154	0.79710	0.027	0.03154	0.91139	0.027	0.03154	0.36571
0.028	0.03271	0.78986	0.028	0.03271	0.90717	0.028	0.03271	0.32000
0.029	0.03388	0.77536	0.029	0.03388	0.90295	0.029	0.03388	0.29429
0.03	0.03505	0.76087	0.03	0.03505	0.90295	0.03	0.03505	0.26286
0.031	0.03621	0.75362	0.031	0.03621	0.90295	0.031	0.03621	0.22571
0.032	0.03738	0.74638	0.032	0.03738	0.90295	0.032	0.03738	0.20571

0.033	0.03855	0.74638	0.033	0.03855	0.90295	0.033	0.03855	0.18571
0.034	0.03972	0.74638	0.034	0.03972	0.89873	0.034	0.03972	0.14857
0.035	0.04089	0.74638	0.035	0.04089	0.88608	0.035	0.04089	0.13143
0.036	0.04206	0.72464	0.036	0.04206	0.88186	0.036	0.04206	0.11429
0.037	0.04322	0.71014	0.037	0.04322	0.87764	0.037	0.04322	0.10571
0.038	0.04439	0.70290	0.038	0.04439	0.87764	0.038	0.04439	0.10000
0.039	0.04556	0.70290	0.039	0.04556	0.87764	0.039	0.04556	0.08857
0.04	0.04673	0.70290	0.04	0.04673	0.87342	0.04	0.04673	0.07714
0.041	0.04790	0.69565	0.041	0.04790	0.87342	0.041	0.04790	0.07143
0.042	0.04907	0.69565	0.042	0.04907	0.87342	0.042	0.04907	0.06286
0.043	0.05023	0.69565	0.043	0.05023	0.86920	0.043	0.05023	0.05714
0.044	0.05140	0.68116	0.044	0.05140	0.86498	0.044	0.05140	0.05429
0.045	0.05257	0.66667	0.045	0.05257	0.86076	0.045	0.05257	0.04857
0.046	0.05374	0.65942	0.046	0.05374	0.85232	0.046	0.05374	0.04571
0.047	0.05491	0.65942	0.047	0.05491	0.85232	0.047	0.05491	0.04286
0.048	0.05607	0.65942	0.048	0.05607	0.84810	0.048	0.05607	0.03143
0.049	0.05724	0.65217	0.049	0.05724	0.84810	0.049	0.05724	0.02857
0.05	0.05841	0.65217	0.05	0.05841	0.84810	0.05	0.05841	0.02000
0.051	0.05958	0.65217	0.051	0.05958	0.84810	0.051	0.05958	0.01429
0.052	0.06075	0.65217	0.052	0.06075	0.84388	0.052	0.06075	0.01429
0.053	0.06192	0.64493	0.053	0.06192	0.84388	0.053	0.06192	0.00857
0.054	0.06308	0.63768	0.054	0.06308	0.84388	0.054	0.06308	0.00571
0.055	0.06425	0.62319	0.055	0.06425	0.84388	0.055	0.06425	0.00286
0.056	0.06542	0.61594	0.056	0.06542	0.84388	0.056	0.06542	0.00286
0.057	0.06659	0.61594	0.057	0.06659	0.84388			
0.058	0.06776	0.60870	0.058	0.06776	0.83966			
0.059	0.06893	0.60870	0.059	0.06893	0.83966			
0.06	0.07009	0.60870	0.06	0.07009	0.83966			
0.061	0.07126	0.60870	0.061	0.07126	0.83966			
0.062	0.07243	0.60870	0.062	0.07243	0.83544			
0.063	0.07360	0.60145	0.063	0.07360	0.83122			
0.064	0.07477	0.60145	0.064	0.07477	0.82278			
0.065	0.07593	0.60145	0.065	0.07593	0.82278			
0.066	0.07710	0.60145	0.066	0.07710	0.82278			
0.067	0.07827	0.60145	0.067	0.07827	0.82278			
0.068	0.07944	0.60145	0.068	0.07944	0.82278			
0.069	0.08061	0.59420	0.069	0.08061	0.82278			
0.07	0.08178	0.59420	0.07	0.08178	0.82278			
0.071	0.08294	0.59420	0.071	0.08294	0.81857			
0.072	0.08411	0.57971	0.072	0.08411	0.81857			
0.073	0.08528	0.57971	0.073	0.08528	0.81857			

0.074	0.08645	0.57246	0.074	0.08645	0.81857			
0.075	0.08762	0.57246	0.075	0.08762	0.81435			
0.076	0.08879	0.57246	0.076	0.08879	0.80169			
0.077	0.08995	0.56522	0.077	0.08995	0.79747			
0.078	0.09112	0.56522	0.078	0.09112	0.79747			
0.079	0.09229	0.56522	0.079	0.09229	0.78903			
0.08	0.09346	0.55797	0.08	0.09346	0.78059			
0.081	0.09463	0.55797	0.081	0.09463	0.78059			
0.082	0.09579	0.55797	0.082	0.09579	0.77637			
0.083	0.09696	0.55797	0.083	0.09696	0.77215			
0.084	0.09813	0.55797	0.084	0.09813	0.77215			
0.085	0.09930	0.55797	0.085	0.09930	0.76371			
0.086	0.10047	0.55072	0.086	0.10047	0.75949			
0.087	0.10164	0.55072	0.087	0.10164	0.75949			
0.088	0.10280	0.54348	0.088	0.10280	0.75527			
0.089	0.10397	0.54348	0.089	0.10397	0.75527			
0.09	0.10514	0.54348	0.09	0.10514	0.75527			
0.091	0.10631	0.54348	0.091	0.10631	0.75527			
0.092	0.10748	0.54348	0.092	0.10748	0.75527			
0.093	0.10864	0.52899	0.093	0.10864	0.75527			
0.094	0.10981	0.52899	0.094	0.10981	0.75105			
0.095	0.11098	0.52899	0.095	0.11098	0.74262			
0.096	0.11215	0.52899	0.096	0.11215	0.74262			
0.097	0.11332	0.52174	0.097	0.11332	0.73418			
0.098	0.11449	0.52174	0.098	0.11449	0.72574			
0.099	0.11565	0.52174	0.099	0.11565	0.72152			
0.1	0.11682	0.52174	0.1	0.11682	0.71730			
0.101	0.11799	0.52174	0.101	0.11799	0.71308			
0.102	0.11916	0.52174	0.102	0.11916	0.71308			
0.103	0.12033	0.52174	0.103	0.12033	0.70886			
0.104	0.12150	0.51449	0.104	0.12150	0.70042			
0.105	0.12266	0.51449	0.105	0.12266	0.70042			
0.106	0.12383	0.51449	0.106	0.12383	0.69620			
0.107	0.12500	0.51449	0.107	0.12500	0.69198			
0.108	0.12617	0.51449	0.108	0.12617	0.69198			
0.109	0.12734	0.51449	0.109	0.12734	0.68776			
0.11	0.12850	0.51449	0.11	0.12850	0.68354			
0.111	0.12967	0.51449	0.111	0.12967	0.68354			
0.112	0.13084	0.51449	0.112	0.13084	0.67932			
0.113	0.13201	0.51449	0.113	0.13201	0.67932			
0.114	0.13318	0.51449	0.114	0.13318	0.67932			

0.115	0.13435	0.51449	0.115	0.13435	0.67932			
0.116	0.13551	0.51449	0.116	0.13551	0.67932			
0.117	0.13668	0.51449	0.117	0.13668	0.67511			
0.118	0.13785	0.51449	0.118	0.13785	0.67089			
0.119	0.13902	0.51449	0.119	0.13902	0.66245			
0.12	0.14019	0.51449	0.12	0.14019	0.65823			
0.121	0.14136	0.51449	0.121	0.14136	0.64557			
0.122	0.14252	0.51449	0.122	0.14252	0.64557			
0.123	0.14369	0.51449	0.123	0.14369	0.64557			
0.124	0.14486	0.51449	0.124	0.14486	0.63713			
0.125	0.14603	0.51449	0.125	0.14603	0.63291			
0.126	0.14720	0.51449	0.126	0.14720	0.62869			
0.127	0.14836	0.51449	0.127	0.14836	0.62447			
0.128	0.14953	0.51449	0.128	0.14953	0.62025			
0.129	0.15070	0.51449	0.129	0.15070	0.61603			
0.13	0.15187	0.51449	0.13	0.15187	0.61603			
0.131	0.15304	0.51449	0.131	0.15304	0.60759			
0.132	0.15421	0.51449	0.132	0.15421	0.60338			
0.133	0.15537	0.51449	0.133	0.15537	0.60338			
0.134	0.15654	0.51449	0.134	0.15654	0.60338			
0.135	0.15771	0.51449	0.135	0.15771	0.60338			
0.136	0.15888	0.51449	0.136	0.15888	0.60338			
0.137	0.16005	0.51449	0.137	0.16005	0.60338			
0.138	0.16121	0.51449	0.138	0.16121	0.60338			
0.139	0.16238	0.51449	0.139	0.16238	0.59916			
0.14	0.16355	0.51449	0.14	0.16355	0.59916			
0.141	0.16472	0.51449	0.141	0.16472	0.59916			
0.142	0.16589	0.51449	0.142	0.16589	0.59916			
0.143	0.16706	0.51449	0.143	0.16706	0.59916			
0.144	0.16822	0.51449	0.144	0.16822	0.59916			
0.145	0.16939	0.51449	0.145	0.16939	0.59916			
0.146	0.17056	0.51449	0.146	0.17056	0.59916			
0.147	0.17173	0.51449	0.147	0.17173	0.59916			
0.148	0.17290	0.51449	0.148	0.17290	0.59494			
0.149	0.17407	0.51449	0.149	0.17407	0.59072			
0.15	0.17523	0.51449	0.15	0.17523	0.58228			
0.151	0.17640	0.51449	0.151	0.17640	0.58228			
0.152	0.17757	0.51449	0.152	0.17757	0.58228			
0.153	0.17874	0.51449	0.153	0.17874	0.57384			
0.154	0.17991	0.51449	0.154	0.17991	0.57384			
0.155	0.18107	0.51449	0.155	0.18107	0.57384			

0.156	0.18224	0.51449	0.156	0.18224	0.57384			
0.157	0.18341	0.51449	0.157	0.18341	0.56962			
0.158	0.18458	0.51449	0.158	0.18458	0.56540			
0.159	0.18575	0.51449	0.159	0.18575	0.56540			
0.16	0.18692	0.51449	0.16	0.18692	0.56540			
0.161	0.18808	0.51449	0.161	0.18808	0.56540			
0.162	0.18925	0.51449	0.162	0.18925	0.56540			
0.163	0.19042	0.51449	0.163	0.19042	0.56540			
0.164	0.19159	0.51449	0.164	0.19159	0.56540			
0.165	0.19276	0.51449	0.165	0.19276	0.56540			
0.166	0.19393	0.51449	0.166	0.19393	0.56540			
0.167	0.19509	0.51449	0.167	0.19509	0.56540			
0.168	0.19626	0.51449	0.168	0.19626	0.56540			
0.169	0.19743	0.51449	0.169	0.19743	0.56540			
0.17	0.19860	0.51449	0.17	0.19860	0.56540			
0.171	0.19977	0.51449	0.171	0.19977	0.56540			
0.172	0.20093	0.51449	0.172	0.20093	0.56540			
0.173	0.20210	0.51449	0.173	0.20210	0.56540			
0.174	0.20327	0.51449	0.174	0.20327	0.56540			
0.175	0.20444	0.51449	0.175	0.20444	0.56540			
0.176	0.20561	0.51449	0.176	0.20561	0.56540			
0.177	0.20678	0.51449	0.177	0.20678	0.56540			
0.178	0.20794	0.51449	0.178	0.20794	0.56540			
0.179	0.20911	0.51449	0.179	0.20911	0.56118			
0.18	0.21028	0.51449	0.18	0.21028	0.56118			
0.181	0.21145	0.51449	0.181	0.21145	0.56118			
0.182	0.21262	0.51449	0.182	0.21262	0.56118			
0.183	0.21379	0.51449	0.183	0.21379	0.56118			
0.184	0.21495	0.51449	0.184	0.21495	0.56118			
0.185	0.21612	0.51449	0.185	0.21612	0.56118			
0.186	0.21729	0.51449	0.186	0.21729	0.56118			
0.187	0.21846	0.51449	0.187	0.21846	0.56118			
0.188	0.21963	0.51449	0.188	0.21963	0.56118			
0.189	0.22079	0.51449	0.189	0.22079	0.56118			
0.19	0.22196	0.51449	0.19	0.22196	0.56118			
0.191	0.22313	0.51449	0.191	0.22313	0.56118			
0.192	0.22430	0.51449	0.192	0.22430	0.56118			
0.193	0.22547	0.51449	0.193	0.22547	0.56118			
0.194	0.22664	0.51449	0.194	0.22664	0.56118			
0.195	0.22780	0.51449	0.195	0.22780	0.56118			
0.196	0.22897	0.51449	0.196	0.22897	0.56118			

0.197	0.23014	0.51449	0.197	0.23014	0.56118			
0.198	0.23131	0.51449	0.198	0.23131	0.56118			
0.199	0.23248	0.51449	0.199	0.23248	0.56118			
0.2	0.23364	0.51449	0.2	0.23364	0.56118			
0.201	0.23481	0.51449	0.201	0.23481	0.56118			
0.202	0.23598	0.51449	0.202	0.23598	0.56118			
0.203	0.23715	0.51449	0.203	0.23715	0.56118			
0.204	0.23832	0.51449	0.204	0.23832	0.56118			
0.205	0.23949	0.51449	0.205	0.23949	0.56118			
0.206	0.24065	0.51449	0.206	0.24065	0.56118			
0.207	0.24182	0.51449	0.207	0.24182	0.56118			
0.208	0.24299	0.51449	0.208	0.24299	0.56118			
0.209	0.24416	0.51449	0.209	0.24416	0.56118			
0.21	0.24533	0.51449	0.21	0.24533	0.56118			
0.211	0.24650	0.51449	0.211	0.24650	0.56118			
0.212	0.24766	0.51449	0.212	0.24766	0.56118			
0.213	0.24883	0.51449	0.213	0.24883	0.56118			
0.214	0.25000	0.51449	0.214	0.25000	0.56118			
0.215	0.25117	0.51449	0.215	0.25117	0.56118			
0.216	0.25234	0.51449	0.216	0.25234	0.56118			
0.217	0.25350	0.51449	0.217	0.25350	0.56118			
0.218	0.25467	0.51449	0.218	0.25467	0.56118			
0.219	0.25584	0.51449	0.219	0.25584	0.56118			
0.22	0.25701	0.51449	0.22	0.25701	0.56118			
0.221	0.25818	0.51449	0.221	0.25818	0.56118			
0.222	0.25935	0.51449	0.222	0.25935	0.56118			
0.223	0.26051	0.51449	0.223	0.26051	0.56118			
0.224	0.26168	0.51449	0.224	0.26168	0.56118			
0.225	0.26285	0.51449	0.225	0.26285	0.56118			
0.226	0.26402	0.51449	0.226	0.26402	0.56118			
0.227	0.26519	0.51449	0.227	0.26519	0.56118			
0.228	0.26636	0.51449	0.228	0.26636	0.56118			
0.229	0.26752	0.51449	0.229	0.26752	0.56118			
0.23	0.26869	0.51449	0.23	0.26869	0.56118			
0.231	0.26986	0.51449	0.231	0.26986	0.56118			
0.232	0.27103	0.51449	0.232	0.27103	0.56118			
0.233	0.27220	0.51449	0.233	0.27220	0.56118			
0.234	0.27336	0.51449	0.234	0.27336	0.56118			
0.235	0.27453	0.51449	0.235	0.27453	0.56118			
0.236	0.27570	0.51449	0.236	0.27570	0.56118			
0.237	0.27687	0.51449	0.237	0.27687	0.56118			

0.238	0.27804	0.51449	0.238	0.27804	0.56118			
0.239	0.27921	0.51449	0.239	0.27921	0.56118			
0.24	0.28037	0.51449	0.24	0.28037	0.56118			
0.241	0.28154	0.51449	0.241	0.28154	0.56118			
0.242	0.28271	0.51449	0.242	0.28271	0.56118			
0.243	0.28388	0.51449	0.243	0.28388	0.56118			
0.244	0.28505	0.51449	0.244	0.28505	0.56118			
0.245	0.28621	0.51449	0.245	0.28621	0.56118			
0.246	0.28738	0.51449	0.246	0.28738	0.56118			
0.247	0.28855	0.51449	0.247	0.28855	0.56118			
0.248	0.28972	0.51449	0.248	0.28972	0.56118			
0.249	0.29089	0.51449	0.249	0.29089	0.56118			
0.25	0.29206	0.51449	0.25	0.29206	0.56118			
0.251	0.29322	0.51449	0.251	0.29322	0.56118			
0.252	0.29439	0.51449	0.252	0.29439	0.56118			
0.253	0.29556	0.51449	0.253	0.29556	0.56118			
0.254	0.29673	0.51449	0.254	0.29673	0.56118			
0.255	0.29790	0.51449	0.255	0.29790	0.56118			
0.256	0.29907	0.51449	0.256	0.29907	0.55696			
0.257	0.30023	0.51449	0.257	0.30023	0.55696			
0.258	0.30140	0.51449	0.258	0.30140	0.55696			
0.259	0.30257	0.51449	0.259	0.30257	0.55274			
0.26	0.30374	0.51449	0.26	0.30374	0.54852			
0.261	0.30491	0.51449	0.261	0.30491	0.54852			
0.262	0.30607	0.51449	0.262	0.30607	0.54852			
0.263	0.30724	0.51449	0.263	0.30724	0.54852			
0.264	0.30841	0.51449	0.264	0.30841	0.54852			
0.265	0.30958	0.51449	0.265	0.30958	0.54852			
0.266	0.31075	0.51449	0.266	0.31075	0.54852			
0.267	0.31192	0.51449	0.267	0.31192	0.54852			
0.268	0.31308	0.51449	0.268	0.31308	0.54852			
0.269	0.31425	0.51449	0.269	0.31425	0.54852			
0.27	0.31542	0.51449	0.27	0.31542	0.54852			
0.271	0.31659	0.51449	0.271	0.31659	0.54852			
0.272	0.31776	0.51449	0.272	0.31776	0.54852			
0.273	0.31893	0.51449	0.273	0.31893	0.54430			
0.274	0.32009	0.51449	0.274	0.32009	0.54430			
0.275	0.32126	0.51449	0.275	0.32126	0.54430			
0.276	0.32243	0.51449	0.276	0.32243	0.54008			
0.277	0.32360	0.51449	0.277	0.32360	0.54008			
0.278	0.32477	0.51449	0.278	0.32477	0.54008			

0.279	0.32593	0.51449	0.279	0.32593	0.54008			
0.28	0.32710	0.51449	0.28	0.32710	0.54008			
0.281	0.32827	0.51449	0.281	0.32827	0.54008			
0.282	0.32944	0.51449	0.282	0.32944	0.53586			
0.283	0.33061	0.51449	0.283	0.33061	0.53586			
0.284	0.33178	0.51449	0.284	0.33178	0.53586			
0.285	0.33294	0.51449	0.285	0.33294	0.53586			
0.286	0.33411	0.51449	0.286	0.33411	0.53586			
0.287	0.33528	0.51449	0.287	0.33528	0.53586			
0.288	0.33645	0.51449	0.288	0.33645	0.53165			
0.289	0.33762	0.51449	0.289	0.33762	0.53165			
0.29	0.33879	0.51449	0.29	0.33879	0.52743			
0.291	0.33995	0.51449	0.291	0.33995	0.52321			
0.292	0.34112	0.51449	0.292	0.34112	0.52321			
0.293	0.34229	0.51449	0.293	0.34229	0.52321			
0.294	0.34346	0.51449	0.294	0.34346	0.52321			
0.295	0.34463	0.51449	0.295	0.34463	0.52321			
0.296	0.34579	0.51449	0.296	0.34579	0.51899			
0.297	0.34696	0.51449	0.297	0.34696	0.51899			
0.298	0.34813	0.51449	0.298	0.34813	0.51899			
0.299	0.34930	0.51449	0.299	0.34930	0.51477			
0.3	0.35047	0.51449	0.3	0.35047	0.51055			
0.301	0.35164	0.51449	0.301	0.35164	0.51055			
0.302	0.35280	0.51449	0.302	0.35280	0.51055			
0.303	0.35397	0.51449	0.303	0.35397	0.51055			
0.304	0.35514	0.51449	0.304	0.35514	0.51055			
0.305	0.35631	0.51449	0.305	0.35631	0.51055			
0.306	0.35748	0.51449	0.306	0.35748	0.50633			
0.307	0.35864	0.51449	0.307	0.35864	0.50633			
0.308	0.35981	0.51449	0.308	0.35981	0.50633			
0.309	0.36098	0.51449	0.309	0.36098	0.50633			
0.31	0.36215	0.51449	0.31	0.36215	0.50211			
0.311	0.36332	0.51449	0.311	0.36332	0.50211			
0.312	0.36449	0.51449	0.312	0.36449	0.50211			
0.313	0.36565	0.51449	0.313	0.36565	0.50211			
0.314	0.36682	0.51449	0.314	0.36682	0.50211			
0.315	0.36799	0.51449	0.315	0.36799	0.50211			
0.316	0.36916	0.51449	0.316	0.36916	0.50211			
0.317	0.37033	0.51449	0.317	0.37033	0.50211			
0.318	0.37150	0.51449	0.318	0.37150	0.50211			
0.319	0.37266	0.51449	0.319	0.37266	0.50211			

0.32	0.37383	0.51449	0.32	0.37383	0.50211			
0.321	0.37500	0.51449	0.321	0.37500	0.50211			
0.322	0.37617	0.51449	0.322	0.37617	0.50211			
0.323	0.37734	0.51449	0.323	0.37734	0.50211			
0.324	0.37850	0.51449	0.324	0.37850	0.50211			
0.325	0.37967	0.51449	0.325	0.37967	0.50211			
0.326	0.38084	0.51449	0.326	0.38084	0.50211			
0.327	0.38201	0.51449	0.327	0.38201	0.50211			
0.328	0.38318	0.51449	0.328	0.38318	0.50211			
0.329	0.38435	0.51449	0.329	0.38435	0.49789			
0.33	0.38551	0.51449	0.33	0.38551	0.49789			
0.331	0.38668	0.51449	0.331	0.38668	0.49789			
0.332	0.38785	0.51449	0.332	0.38785	0.49789			
0.333	0.38902	0.51449	0.333	0.38902	0.49789			
0.334	0.39019	0.51449	0.334	0.39019	0.49789			
0.335	0.39136	0.51449	0.335	0.39136	0.49789			
0.336	0.39252	0.51449	0.336	0.39252	0.49789			
0.337	0.39369	0.51449	0.337	0.39369	0.49789			
0.338	0.39486	0.51449	0.338	0.39486	0.49367			
0.339	0.39603	0.51449	0.339	0.39603	0.49367			
0.34	0.39720	0.51449	0.34	0.39720	0.49367			
0.341	0.39836	0.51449	0.341	0.39836	0.49367			
0.342	0.39953	0.51449	0.342	0.39953	0.49367			
0.343	0.40070	0.51449	0.343	0.40070	0.49367			
0.344	0.40187	0.51449	0.344	0.40187	0.49367			
0.345	0.40304	0.51449	0.345	0.40304	0.49367			
0.346	0.40421	0.51449	0.346	0.40421	0.49367			
0.347	0.40537	0.51449	0.347	0.40537	0.49367			
0.348	0.40654	0.51449	0.348	0.40654	0.49367			
0.349	0.40771	0.51449	0.349	0.40771	0.49367			
0.35	0.40888	0.51449	0.35	0.40888	0.49367			
0.351	0.41005	0.51449	0.351	0.41005	0.49367			
0.352	0.41121	0.51449	0.352	0.41121	0.49367			
0.353	0.41238	0.49275	0.353	0.41238	0.48945			
0.354	0.41355	0.47826	0.354	0.41355	0.48523			
0.355	0.41472	0.47101	0.355	0.41472	0.48523			
0.356	0.41589	0.45652	0.356	0.41589	0.48523			
0.357	0.41706	0.44203	0.357	0.41706	0.48101			
0.358	0.41822	0.42754	0.358	0.41822	0.47257			
0.359	0.41939	0.42029	0.359	0.41939	0.46414			
0.36	0.42056	0.39130	0.36	0.42056	0.41350			

0.361	0.42173	0.37681	0.361	0.42173	0.35021			
0.362	0.42290	0.36957	0.362	0.42290	0.30380			
0.363	0.42407	0.33333	0.363	0.42407	0.26160			
0.364	0.42523	0.31884	0.364	0.42523	0.25316			
0.365	0.42640	0.31884	0.365	0.42640	0.22363			
0.366	0.42757	0.31884	0.366	0.42757	0.19409			
0.367	0.42874	0.31159	0.367	0.42874	0.18143			
0.368	0.42991	0.28261	0.368	0.42991	0.14346			
0.369	0.43107	0.27536	0.369	0.43107	0.12658			
0.37	0.43224	0.27536	0.37	0.43224	0.09283			
0.371	0.43341	0.26812	0.371	0.43341	0.06329			
0.372	0.43458	0.26812	0.372	0.43458	0.03376			
0.373	0.43575	0.26812	0.373	0.43575	0.01688			
0.374	0.43692	0.26812						
0.375	0.43808	0.26087						
0.376	0.43925	0.26087						
0.377	0.44042	0.25362						
0.378	0.44159	0.24638						
0.379	0.44276	0.24638						
0.38	0.44393	0.21739						
0.381	0.44509	0.21739						
0.382	0.44626	0.21739						
0.383	0.44743	0.21739						
0.384	0.44860	0.19565						
0.385	0.44977	0.18841						
0.386	0.45093	0.17391						
0.387	0.45210	0.16667						
0.388	0.45327	0.14493						
0.389	0.45444	0.14493						
0.39	0.45561	0.13768						
0.391	0.45678	0.13043						
0.392	0.45794	0.10145						
0.393	0.45911	0.09420						
0.394	0.46028	0.08696						
0.395	0.46145	0.05072						
0.396	0.46262	0.05072						
0.397	0.46379	0.03623						
0.398	0.46495	0.00725						

Table G-18. 80/20 Long AML neo-sinus particle tracking results for 5.0 L/min.

0% LAMPOON			50% LAMPOON			100% LAMPOON		
Time (s)	Cycle (#)	Particle Density (%)	Time (s)	Cycle (#)	Particle Density (%)	Time (s)	Cycle (#)	Particle Density (%)
0	0	1	0	0	1	0	0	1
0.001	0.00117	1	0.001	0.00117	1	0.001	0.00117	0.99714
0.002	0.00234	1	0.002	0.00234	1	0.002	0.00234	0.99714
0.003	0.00350	1	0.003	0.00350	1	0.003	0.00350	0.98000
0.004	0.00467	1	0.004	0.00467	1	0.004	0.00467	0.96000
0.005	0.00584	1	0.005	0.00584	1	0.005	0.00584	0.91429
0.006	0.00701	0.99275	0.006	0.00701	1	0.006	0.00701	0.88286
0.007	0.00818	0.97101	0.007	0.00818	0.99578	0.007	0.00818	0.86857
0.008	0.00935	0.96377	0.008	0.00935	0.96624	0.008	0.00935	0.83714
0.009	0.01051	0.96377	0.009	0.01051	0.95359	0.009	0.01051	0.81714
0.01	0.01168	0.95652	0.01	0.01168	0.95359	0.01	0.01168	0.78571
0.011	0.01285	0.93478	0.011	0.01285	0.94515	0.011	0.01285	0.76286
0.012	0.01402	0.91304	0.012	0.01402	0.91983	0.012	0.01402	0.72286
0.013	0.01519	0.91304	0.013	0.01519	0.91561	0.013	0.01519	0.66857
0.014	0.01636	0.87681	0.014	0.01636	0.91139	0.014	0.01636	0.63143
0.015	0.01752	0.86232	0.015	0.01752	0.90717	0.015	0.01752	0.58000
0.016	0.01869	0.86232	0.016	0.01869	0.90295	0.016	0.01869	0.55143
0.017	0.01986	0.86232	0.017	0.01986	0.90295	0.017	0.01986	0.51714
0.018	0.02103	0.86232	0.018	0.02103	0.90295	0.018	0.02103	0.48857
0.019	0.02220	0.86232	0.019	0.02220	0.89030	0.019	0.02220	0.46571
0.02	0.02336	0.86232	0.02	0.02336	0.89030	0.02	0.02336	0.44000
0.021	0.02453	0.85507	0.021	0.02453	0.89030	0.021	0.02453	0.40571
0.022	0.02570	0.85507	0.022	0.02570	0.88186	0.022	0.02570	0.37143
0.023	0.02687	0.85507	0.023	0.02687	0.86920	0.023	0.02687	0.34286
0.024	0.02804	0.85507	0.024	0.02804	0.86498	0.024	0.02804	0.31429
0.025	0.02921	0.84783	0.025	0.02921	0.85654	0.025	0.02921	0.29429
0.026	0.03037	0.84058	0.026	0.03037	0.85232	0.026	0.03037	0.27429
0.027	0.03154	0.84058	0.027	0.03154	0.84810	0.027	0.03154	0.26000
0.028	0.03271	0.82609	0.028	0.03271	0.84388	0.028	0.03271	0.24286
0.029	0.03388	0.82609	0.029	0.03388	0.83966	0.029	0.03388	0.22571
0.03	0.03505	0.82609	0.03	0.03505	0.83544	0.03	0.03505	0.21714
0.031	0.03621	0.81159	0.031	0.03621	0.83544	0.031	0.03621	0.19714
0.032	0.03738	0.81159	0.032	0.03738	0.83544	0.032	0.03738	0.17714

0.033	0.03855	0.81159	0.033	0.03855	0.83122	0.033	0.03855	0.16286
0.034	0.03972	0.81159	0.034	0.03972	0.83122	0.034	0.03972	0.15143
0.035	0.04089	0.80435	0.035	0.04089	0.82700	0.035	0.04089	0.13429
0.036	0.04206	0.80435	0.036	0.04206	0.82278	0.036	0.04206	0.12000
0.037	0.04322	0.80435	0.037	0.04322	0.82278	0.037	0.04322	0.11429
0.038	0.04439	0.79710	0.038	0.04439	0.82278	0.038	0.04439	0.10286
0.039	0.04556	0.78986	0.039	0.04556	0.81857	0.039	0.04556	0.09714
0.04	0.04673	0.78986	0.04	0.04673	0.81013	0.04	0.04673	0.08571
0.041	0.04790	0.78986	0.041	0.04790	0.80591	0.041	0.04790	0.07143
0.042	0.04907	0.78261	0.042	0.04907	0.80169	0.042	0.04907	0.06571
0.043	0.05023	0.77536	0.043	0.05023	0.80169	0.043	0.05023	0.06286
0.044	0.05140	0.77536	0.044	0.05140	0.79747	0.044	0.05140	0.05429
0.045	0.05257	0.76812	0.045	0.05257	0.79747	0.045	0.05257	0.04571
0.046	0.05374	0.76812	0.046	0.05374	0.79747	0.046	0.05374	0.04286
0.047	0.05491	0.76087	0.047	0.05491	0.78903	0.047	0.05491	0.04000
0.048	0.05607	0.76087	0.048	0.05607	0.78903	0.048	0.05607	0.03429
0.049	0.05724	0.75362	0.049	0.05724	0.78903	0.049	0.05724	0.03143
0.05	0.05841	0.74638	0.05	0.05841	0.78903	0.05	0.05841	0.02857
0.051	0.05958	0.74638	0.051	0.05958	0.78481	0.051	0.05958	0.02000
0.052	0.06075	0.73913	0.052	0.06075	0.78059	0.052	0.06075	0.01714
0.053	0.06192	0.72464	0.053	0.06192	0.77215	0.053	0.06192	0.01429
0.054	0.06308	0.71014	0.054	0.06308	0.76371	0.054	0.06308	0.00857
0.055	0.06425	0.70290	0.055	0.06425	0.75527	0.055	0.06425	0.00571
0.056	0.06542	0.70290	0.056	0.06542	0.75105	0.056	0.06542	0.00286
0.057	0.06659	0.70290	0.057	0.06659	0.74684	0.057	0.06659	0.00286
0.058	0.06776	0.70290	0.058	0.06776	0.73418			
0.059	0.06893	0.70290	0.059	0.06893	0.73418			
0.06	0.07009	0.70290	0.06	0.07009	0.73418			
0.061	0.07126	0.70290	0.061	0.07126	0.72574			
0.062	0.07243	0.70290	0.062	0.07243	0.72574			
0.063	0.07360	0.70290	0.063	0.07360	0.72574			
0.064	0.07477	0.70290	0.064	0.07477	0.72574			
0.065	0.07593	0.69565	0.065	0.07593	0.71308			
0.066	0.07710	0.69565	0.066	0.07710	0.71308			
0.067	0.07827	0.69565	0.067	0.07827	0.71308			
0.068	0.07944	0.69565	0.068	0.07944	0.70886			
0.069	0.08061	0.68841	0.069	0.08061	0.70464			
0.07	0.08178	0.68841	0.07	0.08178	0.70464			
0.071	0.08294	0.68841	0.071	0.08294	0.70464			
0.072	0.08411	0.68841	0.072	0.08411	0.70042			
0.073	0.08528	0.68841	0.073	0.08528	0.69198			

0.074	0.08645	0.68841	0.074	0.08645	0.69198			
0.075	0.08762	0.68841	0.075	0.08762	0.68354			
0.076	0.08879	0.68841	0.076	0.08879	0.67932			
0.077	0.08995	0.68841	0.077	0.08995	0.67932			
0.078	0.09112	0.68841	0.078	0.09112	0.67511			
0.079	0.09229	0.68841	0.079	0.09229	0.67511			
0.08	0.09346	0.68841	0.08	0.09346	0.66667			
0.081	0.09463	0.68841	0.081	0.09463	0.66245			
0.082	0.09579	0.68841	0.082	0.09579	0.65823			
0.083	0.09696	0.68841	0.083	0.09696	0.64979			
0.084	0.09813	0.68841	0.084	0.09813	0.63713			
0.085	0.09930	0.68841	0.085	0.09930	0.63713			
0.086	0.10047	0.68841	0.086	0.10047	0.63291			
0.087	0.10164	0.68841	0.087	0.10164	0.61603			
0.088	0.10280	0.68841	0.088	0.10280	0.61181			
0.089	0.10397	0.68841	0.089	0.10397	0.60338			
0.09	0.10514	0.68841	0.09	0.10514	0.60338			
0.091	0.10631	0.68841	0.091	0.10631	0.59916			
0.092	0.10748	0.68841	0.092	0.10748	0.59072			
0.093	0.10864	0.68841	0.093	0.10864	0.59072			
0.094	0.10981	0.68841	0.094	0.10981	0.58650			
0.095	0.11098	0.68841	0.095	0.11098	0.57806			
0.096	0.11215	0.68841	0.096	0.11215	0.56540			
0.097	0.11332	0.68841	0.097	0.11332	0.55274			
0.098	0.11449	0.68841	0.098	0.11449	0.54852			
0.099	0.11565	0.68841	0.099	0.11565	0.54008			
0.1	0.11682	0.68841	0.1	0.11682	0.53586			
0.101	0.11799	0.68841	0.101	0.11799	0.52321			
0.102	0.11916	0.68841	0.102	0.11916	0.51899			
0.103	0.12033	0.68841	0.103	0.12033	0.51055			
0.104	0.12150	0.68841	0.104	0.12150	0.50633			
0.105	0.12266	0.68841	0.105	0.12266	0.50633			
0.106	0.12383	0.68116	0.106	0.12383	0.50633			
0.107	0.12500	0.68116	0.107	0.12500	0.50211			
0.108	0.12617	0.68116	0.108	0.12617	0.49367			
0.109	0.12734	0.68116	0.109	0.12734	0.48523			
0.11	0.12850	0.68116	0.11	0.12850	0.48523			
0.111	0.12967	0.68116	0.111	0.12967	0.48101			
0.112	0.13084	0.68116	0.112	0.13084	0.48101			
0.113	0.13201	0.68116	0.113	0.13201	0.47679			
0.114	0.13318	0.68116	0.114	0.13318	0.47679			

0.115	0.13435	0.68116	0.115	0.13435	0.47679			
0.116	0.13551	0.68116	0.116	0.13551	0.47257			
0.117	0.13668	0.68116	0.117	0.13668	0.47257			
0.118	0.13785	0.68116	0.118	0.13785	0.46835			
0.119	0.13902	0.68116	0.119	0.13902	0.46835			
0.12	0.14019	0.68116	0.12	0.14019	0.46414			
0.121	0.14136	0.68116	0.121	0.14136	0.46414			
0.122	0.14252	0.68116	0.122	0.14252	0.45992			
0.123	0.14369	0.67391	0.123	0.14369	0.45570			
0.124	0.14486	0.67391	0.124	0.14486	0.45148			
0.125	0.14603	0.67391	0.125	0.14603	0.44304			
0.126	0.14720	0.67391	0.126	0.14720	0.43038			
0.127	0.14836	0.67391	0.127	0.14836	0.42616			
0.128	0.14953	0.67391	0.128	0.14953	0.42616			
0.129	0.15070	0.66667	0.129	0.15070	0.42616			
0.13	0.15187	0.66667	0.13	0.15187	0.42616			
0.131	0.15304	0.66667	0.131	0.15304	0.42194			
0.132	0.15421	0.66667	0.132	0.15421	0.42194			
0.133	0.15537	0.66667	0.133	0.15537	0.42194			
0.134	0.15654	0.65942	0.134	0.15654	0.42194			
0.135	0.15771	0.65942	0.135	0.15771	0.42194			
0.136	0.15888	0.65942	0.136	0.15888	0.42194			
0.137	0.16005	0.65942	0.137	0.16005	0.42194			
0.138	0.16121	0.65942	0.138	0.16121	0.42194			
0.139	0.16238	0.65942	0.139	0.16238	0.42194			
0.14	0.16355	0.65942	0.14	0.16355	0.41772			
0.141	0.16472	0.65942	0.141	0.16472	0.40928			
0.142	0.16589	0.65942	0.142	0.16589	0.40928			
0.143	0.16706	0.65217	0.143	0.16706	0.40084			
0.144	0.16822	0.65217	0.144	0.16822	0.39662			
0.145	0.16939	0.65217	0.145	0.16939	0.39662			
0.146	0.17056	0.65217	0.146	0.17056	0.39662			
0.147	0.17173	0.65217	0.147	0.17173	0.39241			
0.148	0.17290	0.65217	0.148	0.17290	0.39241			
0.149	0.17407	0.65217	0.149	0.17407	0.38819			
0.15	0.17523	0.65217	0.15	0.17523	0.38819			
0.151	0.17640	0.65217	0.151	0.17640	0.37975			
0.152	0.17757	0.64493	0.152	0.17757	0.37131			
0.153	0.17874	0.64493	0.153	0.17874	0.37131			
0.154	0.17991	0.64493	0.154	0.17991	0.37131			
0.155	0.18107	0.63768	0.155	0.18107	0.37131			

0.156	0.18224	0.63768	0.156	0.18224	0.35443			
0.157	0.18341	0.63768	0.157	0.18341	0.35443			
0.158	0.18458	0.63043	0.158	0.18458	0.35443			
0.159	0.18575	0.63043	0.159	0.18575	0.35443			
0.16	0.18692	0.63043	0.16	0.18692	0.35443			
0.161	0.18808	0.62319	0.161	0.18808	0.35443			
0.162	0.18925	0.62319	0.162	0.18925	0.35443			
0.163	0.19042	0.62319	0.163	0.19042	0.35443			
0.164	0.19159	0.62319	0.164	0.19159	0.35443			
0.165	0.19276	0.61594	0.165	0.19276	0.35443			
0.166	0.19393	0.61594	0.166	0.19393	0.35443			
0.167	0.19509	0.60870	0.167	0.19509	0.35021			
0.168	0.19626	0.60870	0.168	0.19626	0.35021			
0.169	0.19743	0.60870	0.169	0.19743	0.35021			
0.17	0.19860	0.60870	0.17	0.19860	0.35021			
0.171	0.19977	0.60870	0.171	0.19977	0.34599			
0.172	0.20093	0.60870	0.172	0.20093	0.34599			
0.173	0.20210	0.60870	0.173	0.20210	0.34599			
0.174	0.20327	0.60870	0.174	0.20327	0.34599			
0.175	0.20444	0.60870	0.175	0.20444	0.34599			
0.176	0.20561	0.60870	0.176	0.20561	0.34599			
0.177	0.20678	0.60870	0.177	0.20678	0.34599			
0.178	0.20794	0.60870	0.178	0.20794	0.34177			
0.179	0.20911	0.60870	0.179	0.20911	0.34177			
0.18	0.21028	0.60145	0.18	0.21028	0.34177			
0.181	0.21145	0.60145	0.181	0.21145	0.34177			
0.182	0.21262	0.60145	0.182	0.21262	0.34177			
0.183	0.21379	0.60145	0.183	0.21379	0.34177			
0.184	0.21495	0.60145	0.184	0.21495	0.33755			
0.185	0.21612	0.60145	0.185	0.21612	0.33755			
0.186	0.21729	0.60145	0.186	0.21729	0.33755			
0.187	0.21846	0.60145	0.187	0.21846	0.33755			
0.188	0.21963	0.59420	0.188	0.21963	0.33755			
0.189	0.22079	0.59420	0.189	0.22079	0.33755			
0.19	0.22196	0.59420	0.19	0.22196	0.33333			
0.191	0.22313	0.59420	0.191	0.22313	0.33333			
0.192	0.22430	0.59420	0.192	0.22430	0.33333			
0.193	0.22547	0.59420	0.193	0.22547	0.33333			
0.194	0.22664	0.58696	0.194	0.22664	0.33333			
0.195	0.22780	0.58696	0.195	0.22780	0.33333			
0.196	0.22897	0.58696	0.196	0.22897	0.33333			

0.197	0.23014	0.56522	0.197	0.23014	0.33333			
0.198	0.23131	0.56522	0.198	0.23131	0.33333			
0.199	0.23248	0.55797	0.199	0.23248	0.33333			
0.2	0.23364	0.55072	0.2	0.23364	0.33333			
0.201	0.23481	0.54348	0.201	0.23481	0.33333			
0.202	0.23598	0.52899	0.202	0.23598	0.33333			
0.203	0.23715	0.51449	0.203	0.23715	0.33333			
0.204	0.23832	0.50000	0.204	0.23832	0.33333			
0.205	0.23949	0.50000	0.205	0.23949	0.33333			
0.206	0.24065	0.49275	0.206	0.24065	0.33333			
0.207	0.24182	0.47101	0.207	0.24182	0.33333			
0.208	0.24299	0.44928	0.208	0.24299	0.33333			
0.209	0.24416	0.44928	0.209	0.24416	0.33333			
0.21	0.24533	0.44203	0.21	0.24533	0.33333			
0.211	0.24650	0.43478	0.211	0.24650	0.33333			
0.212	0.24766	0.43478	0.212	0.24766	0.33333			
0.213	0.24883	0.42754	0.213	0.24883	0.33333			
0.214	0.25000	0.42754	0.214	0.25000	0.33333			
0.215	0.25117	0.42754	0.215	0.25117	0.33333			
0.216	0.25234	0.42754	0.216	0.25234	0.33333			
0.217	0.25350	0.42754	0.217	0.25350	0.33333			
0.218	0.25467	0.42029	0.218	0.25467	0.33333			
0.219	0.25584	0.39855	0.219	0.25584	0.33333			
0.22	0.25701	0.39855	0.22	0.25701	0.33333			
0.221	0.25818	0.39130	0.221	0.25818	0.33333			
0.222	0.25935	0.38406	0.222	0.25935	0.33333			
0.223	0.26051	0.38406	0.223	0.26051	0.33333			
0.224	0.26168	0.37681	0.224	0.26168	0.33333			
0.225	0.26285	0.37681	0.225	0.26285	0.33333			
0.226	0.26402	0.36957	0.226	0.26402	0.33333			
0.227	0.26519	0.36957	0.227	0.26519	0.33333			
0.228	0.26636	0.36957	0.228	0.26636	0.33333			
0.229	0.26752	0.36957	0.229	0.26752	0.33333			
0.23	0.26869	0.36957	0.23	0.26869	0.33333			
0.231	0.26986	0.36957	0.231	0.26986	0.33333			
0.232	0.27103	0.36957	0.232	0.27103	0.33333			
0.233	0.27220	0.36957	0.233	0.27220	0.33333			
0.234	0.27336	0.36957	0.234	0.27336	0.33333			
0.235	0.27453	0.36957	0.235	0.27453	0.33333			
0.236	0.27570	0.36957	0.236	0.27570	0.33333			
0.237	0.27687	0.36957	0.237	0.27687	0.33333			

0.238	0.27804	0.36957	0.238	0.27804	0.33333			
0.239	0.27921	0.36957	0.239	0.27921	0.33333			
0.24	0.28037	0.36957	0.24	0.28037	0.33333			
0.241	0.28154	0.36957	0.241	0.28154	0.33333			
0.242	0.28271	0.36957	0.242	0.28271	0.33333			
0.243	0.28388	0.36957	0.243	0.28388	0.33333			
0.244	0.28505	0.36957	0.244	0.28505	0.33333			
0.245	0.28621	0.36957	0.245	0.28621	0.33333			
0.246	0.28738	0.36957	0.246	0.28738	0.33333			
0.247	0.28855	0.36957	0.247	0.28855	0.33333			
0.248	0.28972	0.36957	0.248	0.28972	0.33333			
0.249	0.29089	0.36957	0.249	0.29089	0.33333			
0.25	0.29206	0.36957	0.25	0.29206	0.33333			
0.251	0.29322	0.36957	0.251	0.29322	0.33333			
0.252	0.29439	0.36957	0.252	0.29439	0.33333			
0.253	0.29556	0.36957	0.253	0.29556	0.33333			
0.254	0.29673	0.36957	0.254	0.29673	0.33333			
0.255	0.29790	0.36957	0.255	0.29790	0.33333			
0.256	0.29907	0.36957	0.256	0.29907	0.33333			
0.257	0.30023	0.36957	0.257	0.30023	0.33333			
0.258	0.30140	0.36957	0.258	0.30140	0.33333			
0.259	0.30257	0.35507	0.259	0.30257	0.33333			
0.26	0.30374	0.35507	0.26	0.30374	0.33333			
0.261	0.30491	0.33333	0.261	0.30491	0.33333			
0.262	0.30607	0.32609	0.262	0.30607	0.33333			
0.263	0.30724	0.32609	0.263	0.30724	0.33333			
0.264	0.30841	0.31884	0.264	0.30841	0.32911			
0.265	0.30958	0.30435	0.265	0.30958	0.32911			
0.266	0.31075	0.28986	0.266	0.31075	0.32911			
0.267	0.31192	0.28261	0.267	0.31192	0.32911			
0.268	0.31308	0.25362	0.268	0.31308	0.32911			
0.269	0.31425	0.24638	0.269	0.31425	0.32489			
0.27	0.31542	0.23913	0.27	0.31542	0.32489			
0.271	0.31659	0.23913	0.271	0.31659	0.32489			
0.272	0.31776	0.23188	0.272	0.31776	0.32489			
0.273	0.31893	0.21739	0.273	0.31893	0.32489			
0.274	0.32009	0.21014	0.274	0.32009	0.32068			
0.275	0.32126	0.19565	0.275	0.32126	0.31646			
0.276	0.32243	0.18841	0.276	0.32243	0.31224			
0.277	0.32360	0.17391	0.277	0.32360	0.31224			
0.278	0.32477	0.17391	0.278	0.32477	0.30802			

0.279	0.32593	0.16667	0.279	0.32593	0.30802			
0.28	0.32710	0.15942	0.28	0.32710	0.30802			
0.281	0.32827	0.15942	0.281	0.32827	0.29958			
0.282	0.32944	0.15217	0.282	0.32944	0.28270			
0.283	0.33061	0.14493	0.283	0.33061	0.27848			
0.284	0.33178	0.13043	0.284	0.33178	0.27848			
0.285	0.33294	0.12319	0.285	0.33294	0.27848			
0.286	0.33411	0.12319	0.286	0.33411	0.27004			
0.287	0.33528	0.12319	0.287	0.33528	0.27004			
0.288	0.33645	0.12319	0.288	0.33645	0.27004			
0.289	0.33762	0.12319	0.289	0.33762	0.26160			
0.29	0.33879	0.12319	0.29	0.33879	0.25738			
0.291	0.33995	0.12319	0.291	0.33995	0.25738			
0.292	0.34112	0.12319	0.292	0.34112	0.25738			
0.293	0.34229	0.12319	0.293	0.34229	0.25316			
0.294	0.34346	0.12319	0.294	0.34346	0.25316			
0.295	0.34463	0.12319	0.295	0.34463	0.25316			
0.296	0.34579	0.11594	0.296	0.34579	0.25316			
0.297	0.34696	0.11594	0.297	0.34696	0.25316			
0.298	0.34813	0.11594	0.298	0.34813	0.25316			
0.299	0.34930	0.09420	0.299	0.34930	0.25316			
0.3	0.35047	0.08696	0.3	0.35047	0.25316			
0.301	0.35164	0.08696	0.301	0.35164	0.24895			
0.302	0.35280	0.08696	0.302	0.35280	0.24473			
0.303	0.35397	0.08696	0.303	0.35397	0.24473			
0.304	0.35514	0.08696	0.304	0.35514	0.24051			
0.305	0.35631	0.08696	0.305	0.35631	0.24051			
0.306	0.35748	0.08696	0.306	0.35748	0.24051			
0.307	0.35864	0.08696	0.307	0.35864	0.22785			
0.308	0.35981	0.08696	0.308	0.35981	0.22785			
0.309	0.36098	0.08696	0.309	0.36098	0.22785			
0.31	0.36215	0.07971	0.31	0.36215	0.22785			
0.311	0.36332	0.07246	0.311	0.36332	0.22785			
0.312	0.36449	0.06522	0.312	0.36449	0.22785			
0.313	0.36565	0.05797	0.313	0.36565	0.22785			
0.314	0.36682	0.05072	0.314	0.36682	0.22785			
0.315	0.36799	0.05072	0.315	0.36799	0.22363			
0.316	0.36916	0.05072	0.316	0.36916	0.21941			
0.317	0.37033	0.04348	0.317	0.37033	0.21941			
0.318	0.37150	0.04348	0.318	0.37150	0.21097			
0.319	0.37266	0.04348	0.319	0.37266	0.21097			

0.32	0.37383	0.02174	0.32	0.37383	0.21097			
0.321	0.37500	0.02174	0.321	0.37500	0.21097			
0.322	0.37617	0.02174	0.322	0.37617	0.21097			
0.323	0.37734	0.02174	0.323	0.37734	0.20675			
0.324	0.37850	0.01449	0.324	0.37850	0.20675			
0.325	0.37967	0.01449	0.325	0.37967	0.20675			
0.326	0.38084	0.00725	0.326	0.38084	0.20675			
0.327	0.38201	0.00725	0.327	0.38201	0.20675			
0.328	0.38318	0.00725	0.328	0.38318	0.20675			
0.329	0.38435	0.00725	0.329	0.38435	0.20253			
			0.33	0.38551	0.19409			
			0.331	0.38668	0.18987			
			0.332	0.38785	0.18987			
			0.333	0.38902	0.18987			
			0.334	0.39019	0.18987			
			0.335	0.39136	0.18987			
			0.336	0.39252	0.18565			
			0.337	0.39369	0.17722			
			0.338	0.39486	0.17722			
			0.339	0.39603	0.17300			
			0.34	0.39720	0.16456			
			0.341	0.39836	0.16034			
			0.342	0.39953	0.16034			
			0.343	0.40070	0.15190			
			0.344	0.40187	0.14768			
			0.345	0.40304	0.14346			
			0.346	0.40421	0.14346			
			0.347	0.40537	0.13924			
			0.348	0.40654	0.13502			
			0.349	0.40771	0.12658			
			0.35	0.40888	0.11392			
			0.351	0.41005	0.09283			
			0.352	0.41121	0.08439			
			0.353	0.41238	0.07595			
			0.354	0.41355	0.06751			
			0.355	0.41472	0.06329			
			0.356	0.41589	0.06329			
			0.357	0.41706	0.05907			
			0.358	0.41822	0.05063			
			0.359	0.41939	0.04641			
			0.36	0.42056	0.03797			

			0.361	0.42173	0.02532			
			0.362	0.42290	0.01688			
			0.363	0.42407	0.00844			
			0.364	0.42523	0.00422			
			0.365	0.42640	0.00422			

Table G-19. 80/20 Long AML neo-sinus particle tracking results for 6.5 L/min.

0% LAMPOON			50% LAMPOON			100% LAMPOON		
Time (s)	Cycle (#)	Particle Density (%)	Time (s)	Cycle (#)	Particle Density (%)	Time (s)	Cycle (#)	Particle Density (%)
0	0	1	0	0	1	0	0	1
0.001	0.00117	1	0.001	0.00117	1	0.001	0.00117	1
0.002	0.00234	1	0.002	0.00234	1	0.002	0.00234	1
0.003	0.00350	1	0.003	0.00350	1	0.003	0.00350	0.97429
0.004	0.00467	1	0.004	0.00467	1	0.004	0.00467	0.95429
0.005	0.00584	0.97101	0.005	0.00584	1	0.005	0.00584	0.92571
0.006	0.00701	0.95652	0.006	0.00701	1	0.006	0.00701	0.90857
0.007	0.00818	0.94928	0.007	0.00818	0.99578	0.007	0.00818	0.88857
0.008	0.00935	0.94203	0.008	0.00935	0.97890	0.008	0.00935	0.84000
0.009	0.01051	0.93478	0.009	0.01051	0.96624	0.009	0.01051	0.82000
0.01	0.01168	0.93478	0.01	0.01168	0.95781	0.01	0.01168	0.78571
0.011	0.01285	0.92754	0.011	0.01285	0.94937	0.011	0.01285	0.74000
0.012	0.01402	0.92029	0.012	0.01402	0.93671	0.012	0.01402	0.72000
0.013	0.01519	0.91304	0.013	0.01519	0.92827	0.013	0.01519	0.68571
0.014	0.01636	0.89855	0.014	0.01636	0.91983	0.014	0.01636	0.63429
0.015	0.01752	0.89130	0.015	0.01752	0.91139	0.015	0.01752	0.60000
0.016	0.01869	0.89130	0.016	0.01869	0.90717	0.016	0.01869	0.57714
0.017	0.01986	0.89130	0.017	0.01986	0.90295	0.017	0.01986	0.53429
0.018	0.02103	0.88406	0.018	0.02103	0.89873	0.018	0.02103	0.48571
0.019	0.02220	0.87681	0.019	0.02220	0.88608	0.019	0.02220	0.45714
0.02	0.02336	0.87681	0.02	0.02336	0.87342	0.02	0.02336	0.40857
0.021	0.02453	0.87681	0.021	0.02453	0.87342	0.021	0.02453	0.35429
0.022	0.02570	0.86957	0.022	0.02570	0.86920	0.022	0.02570	0.31429
0.023	0.02687	0.86232	0.023	0.02687	0.85232	0.023	0.02687	0.26857

0.024	0.02804	0.86232	0.024	0.02804	0.85232	0.024	0.02804	0.22286
0.025	0.02921	0.85507	0.025	0.02921	0.84810	0.025	0.02921	0.19429
0.026	0.03037	0.84783	0.026	0.03037	0.84810	0.026	0.03037	0.15429
0.027	0.03154	0.84058	0.027	0.03154	0.83966	0.027	0.03154	0.11714
0.028	0.03271	0.83333	0.028	0.03271	0.83966	0.028	0.03271	0.09714
0.029	0.03388	0.82609	0.029	0.03388	0.83966	0.029	0.03388	0.07143
0.03	0.03505	0.82609	0.03	0.03505	0.83544	0.03	0.03505	0.06286
0.031	0.03621	0.81159	0.031	0.03621	0.82700	0.031	0.03621	0.05143
0.032	0.03738	0.81159	0.032	0.03738	0.82278	0.032	0.03738	0.03429
0.033	0.03855	0.81159	0.033	0.03855	0.80591	0.033	0.03855	0.03429
0.034	0.03972	0.81159	0.034	0.03972	0.80591	0.034	0.03972	0.02571
0.035	0.04089	0.79710	0.035	0.04089	0.80169	0.035	0.04089	0.01714
0.036	0.04206	0.79710	0.036	0.04206	0.80169	0.036	0.04206	0.01429
0.037	0.04322	0.79710	0.037	0.04322	0.79325	0.037	0.04322	0.01143
0.038	0.04439	0.79710	0.038	0.04439	0.78481	0.038	0.04439	0.01143
0.039	0.04556	0.79710	0.039	0.04556	0.77637	0.039	0.04556	0.00571
0.04	0.04673	0.77536	0.04	0.04673	0.76793	0.04	0.04673	0.00286
0.041	0.04790	0.76087	0.041	0.04790	0.75949	0.041	0.04790	0.00286
0.042	0.04907	0.75362	0.042	0.04907	0.75949	0.042	0.04907	0.00286
0.043	0.05023	0.75362	0.043	0.05023	0.75527			
0.044	0.05140	0.74638	0.044	0.05140	0.75105			
0.045	0.05257	0.74638	0.045	0.05257	0.75105			
0.046	0.05374	0.74638	0.046	0.05374	0.75105			
0.047	0.05491	0.74638	0.047	0.05491	0.75105			
0.048	0.05607	0.73913	0.048	0.05607	0.74684			
0.049	0.05724	0.73188	0.049	0.05724	0.74684			
0.05	0.05841	0.73188	0.05	0.05841	0.74684			
0.051	0.05958	0.73188	0.051	0.05958	0.74684			
0.052	0.06075	0.73188	0.052	0.06075	0.73840			
0.053	0.06192	0.73188	0.053	0.06192	0.72996			
0.054	0.06308	0.72464	0.054	0.06308	0.72574			
0.055	0.06425	0.71739	0.055	0.06425	0.72152			
0.056	0.06542	0.71014	0.056	0.06542	0.72152			
0.057	0.06659	0.71014	0.057	0.06659	0.71308			
0.058	0.06776	0.71014	0.058	0.06776	0.71308			
0.059	0.06893	0.71014	0.059	0.06893	0.71308			
0.06	0.07009	0.71014	0.06	0.07009	0.71308			
0.061	0.07126	0.69565	0.061	0.07126	0.70886			
0.062	0.07243	0.68841	0.062	0.07243	0.70886			
0.063	0.07360	0.68841	0.063	0.07360	0.70464			
0.064	0.07477	0.68841	0.064	0.07477	0.70042			

0.065	0.07593	0.67391	0.065	0.07593	0.69620			
0.066	0.07710	0.65942	0.066	0.07710	0.68776			
0.067	0.07827	0.65942	0.067	0.07827	0.68354			
0.068	0.07944	0.65942	0.068	0.07944	0.68354			
0.069	0.08061	0.64493	0.069	0.08061	0.67932			
0.07	0.08178	0.63768	0.07	0.08178	0.67932			
0.071	0.08294	0.63043	0.071	0.08294	0.67932			
0.072	0.08411	0.63043	0.072	0.08411	0.67089			
0.073	0.08528	0.62319	0.073	0.08528	0.67089			
0.074	0.08645	0.60870	0.074	0.08645	0.66245			
0.075	0.08762	0.58696	0.075	0.08762	0.64979			
0.076	0.08879	0.57971	0.076	0.08879	0.64557			
0.077	0.08995	0.57246	0.077	0.08995	0.64557			
0.078	0.09112	0.55072	0.078	0.09112	0.64135			
0.079	0.09229	0.53623	0.079	0.09229	0.63713			
0.08	0.09346	0.52174	0.08	0.09346	0.63713			
0.081	0.09463	0.50000	0.081	0.09463	0.63291			
0.082	0.09579	0.50000	0.082	0.09579	0.63291			
0.083	0.09696	0.47101	0.083	0.09696	0.63291			
0.084	0.09813	0.45652	0.084	0.09813	0.62869			
0.085	0.09930	0.45652	0.085	0.09930	0.62869			
0.086	0.10047	0.42029	0.086	0.10047	0.62869			
0.087	0.10164	0.41304	0.087	0.10164	0.62447			
0.088	0.10280	0.39855	0.088	0.10280	0.62447			
0.089	0.10397	0.37681	0.089	0.10397	0.62447			
0.09	0.10514	0.35507	0.09	0.10514	0.62447			
0.091	0.10631	0.34783	0.091	0.10631	0.62025			
0.092	0.10748	0.32609	0.092	0.10748	0.61603			
0.093	0.10864	0.31159	0.093	0.10864	0.61181			
0.094	0.10981	0.29710	0.094	0.10981	0.61181			
0.095	0.11098	0.28986	0.095	0.11098	0.59072			
0.096	0.11215	0.28986	0.096	0.11215	0.57384			
0.097	0.11332	0.27536	0.097	0.11332	0.56962			
0.098	0.11449	0.26087	0.098	0.11449	0.56540			
0.099	0.11565	0.26087	0.099	0.11565	0.56118			
0.1	0.11682	0.25362	0.1	0.11682	0.56118			
0.101	0.11799	0.23913	0.101	0.11799	0.55696			
0.102	0.11916	0.23913	0.102	0.11916	0.55696			
0.103	0.12033	0.23913	0.103	0.12033	0.55696			
0.104	0.12150	0.23188	0.104	0.12150	0.55696			
0.105	0.12266	0.22464	0.105	0.12266	0.55696			

0.106	0.12383	0.22464	0.106	0.12383	0.55696			
0.107	0.12500	0.21739	0.107	0.12500	0.55274			
0.108	0.12617	0.21739	0.108	0.12617	0.54852			
0.109	0.12734	0.21739	0.109	0.12734	0.54852			
0.11	0.12850	0.21739	0.11	0.12850	0.54430			
0.111	0.12967	0.21014	0.111	0.12967	0.53165			
0.112	0.13084	0.19565	0.112	0.13084	0.53165			
0.113	0.13201	0.19565	0.113	0.13201	0.52321			
0.114	0.13318	0.19565	0.114	0.13318	0.52321			
0.115	0.13435	0.18841	0.115	0.13435	0.51477			
0.116	0.13551	0.18116	0.116	0.13551	0.51055			
0.117	0.13668	0.18116	0.117	0.13668	0.51055			
0.118	0.13785	0.18116	0.118	0.13785	0.51055			
0.119	0.13902	0.18116	0.119	0.13902	0.51055			
0.12	0.14019	0.18116	0.12	0.14019	0.51055			
0.121	0.14136	0.18116	0.121	0.14136	0.50633			
0.122	0.14252	0.17391	0.122	0.14252	0.50633			
0.123	0.14369	0.17391	0.123	0.14369	0.50211			
0.124	0.14486	0.16667	0.124	0.14486	0.49789			
0.125	0.14603	0.15942	0.125	0.14603	0.49367			
0.126	0.14720	0.15942	0.126	0.14720	0.49367			
0.127	0.14836	0.15217	0.127	0.14836	0.48945			
0.128	0.14953	0.15217	0.128	0.14953	0.48523			
0.129	0.15070	0.13768	0.129	0.15070	0.48523			
0.13	0.15187	0.13043	0.13	0.15187	0.47257			
0.131	0.15304	0.13043	0.131	0.15304	0.47257			
0.132	0.15421	0.13043	0.132	0.15421	0.46835			
0.133	0.15537	0.13043	0.133	0.15537	0.46414			
0.134	0.15654	0.12319	0.134	0.15654	0.46414			
0.135	0.15771	0.12319	0.135	0.15771	0.45992			
0.136	0.15888	0.12319	0.136	0.15888	0.45992			
0.137	0.16005	0.12319	0.137	0.16005	0.45992			
0.138	0.16121	0.12319	0.138	0.16121	0.45992			
0.139	0.16238	0.12319	0.139	0.16238	0.45570			
0.14	0.16355	0.12319	0.14	0.16355	0.45148			
0.141	0.16472	0.12319	0.141	0.16472	0.45148			
0.142	0.16589	0.12319	0.142	0.16589	0.45148			
0.143	0.16706	0.12319	0.143	0.16706	0.44304			
0.144	0.16822	0.12319	0.144	0.16822	0.44304			
0.145	0.16939	0.12319	0.145	0.16939	0.43460			
0.146	0.17056	0.11594	0.146	0.17056	0.41772			

0.147	0.17173	0.11594	0.147	0.17173	0.39241			
0.148	0.17290	0.10145	0.148	0.17290	0.38397			
0.149	0.17407	0.09420	0.149	0.17407	0.38397			
0.15	0.17523	0.09420	0.15	0.17523	0.37975			
0.151	0.17640	0.09420	0.151	0.17640	0.37553			
0.152	0.17757	0.09420	0.152	0.17757	0.37553			
0.153	0.17874	0.09420	0.153	0.17874	0.37553			
0.154	0.17991	0.09420	0.154	0.17991	0.37553			
0.155	0.18107	0.09420	0.155	0.18107	0.37553			
0.156	0.18224	0.08696	0.156	0.18224	0.37553			
0.157	0.18341	0.08696	0.157	0.18341	0.37131			
0.158	0.18458	0.08696	0.158	0.18458	0.37131			
0.159	0.18575	0.08696	0.159	0.18575	0.37131			
0.16	0.18692	0.08696	0.16	0.18692	0.36709			
0.161	0.18808	0.08696	0.161	0.18808	0.36287			
0.162	0.18925	0.08696	0.162	0.18925	0.36287			
0.163	0.19042	0.08696	0.163	0.19042	0.36287			
0.164	0.19159	0.08696	0.164	0.19159	0.35865			
0.165	0.19276	0.08696	0.165	0.19276	0.35865			
0.166	0.19393	0.07971	0.166	0.19393	0.35865			
0.167	0.19509	0.07971	0.167	0.19509	0.35021			
0.168	0.19626	0.07971	0.168	0.19626	0.34599			
0.169	0.19743	0.07971	0.169	0.19743	0.34599			
0.17	0.19860	0.07971	0.17	0.19860	0.34177			
0.171	0.19977	0.07971	0.171	0.19977	0.33333			
0.172	0.20093	0.07971	0.172	0.20093	0.33333			
0.173	0.20210	0.07971	0.173	0.20210	0.32489			
0.174	0.20327	0.07971	0.174	0.20327	0.32068			
0.175	0.20444	0.07971	0.175	0.20444	0.31224			
0.176	0.20561	0.07971	0.176	0.20561	0.31224			
0.177	0.20678	0.07971	0.177	0.20678	0.31224			
0.178	0.20794	0.07246	0.178	0.20794	0.31224			
0.179	0.20911	0.07246	0.179	0.20911	0.30802			
0.18	0.21028	0.07246	0.18	0.21028	0.30802			
0.181	0.21145	0.07246	0.181	0.21145	0.30802			
0.182	0.21262	0.07246	0.182	0.21262	0.30802			
0.183	0.21379	0.07246	0.183	0.21379	0.30380			
0.184	0.21495	0.07246	0.184	0.21495	0.30380			
0.185	0.21612	0.07246	0.185	0.21612	0.29958			
0.186	0.21729	0.06522	0.186	0.21729	0.29536			
0.187	0.21846	0.06522	0.187	0.21846	0.29536			

0.188	0.21963	0.06522	0.188	0.21963	0.29536			
0.189	0.22079	0.05797	0.189	0.22079	0.29536			
0.19	0.22196	0.05072	0.19	0.22196	0.29536			
0.191	0.22313	0.05072	0.191	0.22313	0.29114			
0.192	0.22430	0.05072	0.192	0.22430	0.28692			
0.193	0.22547	0.05072	0.193	0.22547	0.28692			
0.194	0.22664	0.03623	0.194	0.22664	0.28270			
0.195	0.22780	0.03623	0.195	0.22780	0.27004			
0.196	0.22897	0.03623	0.196	0.22897	0.26582			
0.197	0.23014	0.03623	0.197	0.23014	0.26582			
0.198	0.23131	0.03623	0.198	0.23131	0.26582			
0.199	0.23248	0.03623	0.199	0.23248	0.26582			
0.2	0.23364	0.03623	0.2	0.23364	0.26160			
0.201	0.23481	0.03623	0.201	0.23481	0.26160			
0.202	0.23598	0.03623	0.202	0.23598	0.26160			
0.203	0.23715	0.03623	0.203	0.23715	0.25738			
0.204	0.23832	0.03623	0.204	0.23832	0.25738			
0.205	0.23949	0.02899	0.205	0.23949	0.25738			
0.206	0.24065	0.01449	0.206	0.24065	0.25738			
0.207	0.24182	0.01449	0.207	0.24182	0.25738			
0.208	0.24299	0.01449	0.208	0.24299	0.25738			
0.209	0.24416	0.01449	0.209	0.24416	0.25316			
0.21	0.24533	0.01449	0.21	0.24533	0.25316			
0.211	0.24650	0.01449	0.211	0.24650	0.25316			
0.212	0.24766	0.01449	0.212	0.24766	0.25316			
0.213	0.24883	0.01449	0.213	0.24883	0.25316			
0.214	0.25000	0.01449	0.214	0.25000	0.25316			
0.215	0.25117	0.01449	0.215	0.25117	0.25316			
0.216	0.25234	0.01449	0.216	0.25234	0.25316			
0.217	0.25350	0.01449	0.217	0.25350	0.25316			
0.218	0.25467	0.01449	0.218	0.25467	0.25316			
0.219	0.25584	0.01449	0.219	0.25584	0.25316			
0.22	0.25701	0.00725	0.22	0.25701	0.25316			
0.221	0.25818	0.00725	0.221	0.25818	0.25316			
0.222	0.25935	0.00725	0.222	0.25935	0.25316			
			0.223	0.26051	0.25316			
			0.224	0.26168	0.25316			
			0.225	0.26285	0.25316			
			0.226	0.26402	0.25316			
			0.227	0.26519	0.25316			
			0.228	0.26636	0.25316			

			0.229	0.26752	0.25316			
			0.23	0.26869	0.25316			
			0.231	0.26986	0.25316			
			0.232	0.27103	0.25316			
			0.233	0.27220	0.25316			
			0.234	0.27336	0.25316			
			0.235	0.27453	0.25316			
			0.236	0.27570	0.25316			
			0.237	0.27687	0.25316			
			0.238	0.27804	0.25316			
			0.239	0.27921	0.25316			
			0.24	0.28037	0.25316			
			0.241	0.28154	0.25316			
			0.242	0.28271	0.25316			
			0.243	0.28388	0.25316			
			0.244	0.28505	0.25316			
			0.245	0.28621	0.25316			
			0.246	0.28738	0.25316			
			0.247	0.28855	0.25316			
			0.248	0.28972	0.25316			
			0.249	0.29089	0.25316			
			0.25	0.29206	0.25316			
			0.251	0.29322	0.25316			
			0.252	0.29439	0.25316			
			0.253	0.29556	0.25316			
			0.254	0.29673	0.25316			
			0.255	0.29790	0.25316			
			0.256	0.29907	0.25316			
			0.257	0.30023	0.25316			
			0.258	0.30140	0.25316			
			0.259	0.30257	0.25316			
			0.26	0.30374	0.25316			
			0.261	0.30491	0.25316			
			0.262	0.30607	0.25316			
			0.263	0.30724	0.25316			
			0.264	0.30841	0.25316			
			0.265	0.30958	0.25316			
			0.266	0.31075	0.25316			
			0.267	0.31192	0.25316			
			0.268	0.31308	0.25316			
			0.269	0.31425	0.25316			

			0.27	0.31542	0.25316			
			0.271	0.31659	0.25316			
			0.272	0.31776	0.25316			
			0.273	0.31893	0.25316			
			0.274	0.32009	0.25316			
			0.275	0.32126	0.25316			
			0.276	0.32243	0.25316			
			0.277	0.32360	0.25316			
			0.278	0.32477	0.25316			
			0.279	0.32593	0.25316			
			0.28	0.32710	0.25316			
			0.281	0.32827	0.25316			
			0.282	0.32944	0.25316			
			0.283	0.33061	0.25316			
			0.284	0.33178	0.25316			
			0.285	0.33294	0.25316			
			0.286	0.33411	0.25316			
			0.287	0.33528	0.25316			
			0.288	0.33645	0.25316			
			0.289	0.33762	0.25316			
			0.29	0.33879	0.24895			
			0.291	0.33995	0.24895			
			0.292	0.34112	0.24895			
			0.293	0.34229	0.24895			
			0.294	0.34346	0.24895			
			0.295	0.34463	0.24895			
			0.296	0.34579	0.24895			
			0.297	0.34696	0.24895			
			0.298	0.34813	0.24895			
			0.299	0.34930	0.24895			
			0.3	0.35047	0.24895			
			0.301	0.35164	0.24895			
			0.302	0.35280	0.24895			
			0.303	0.35397	0.24895			
			0.304	0.35514	0.24895			
			0.305	0.35631	0.24895			
			0.306	0.35748	0.24895			
			0.307	0.35864	0.24895			
			0.308	0.35981	0.24895			
			0.309	0.36098	0.24895			
			0.31	0.36215	0.24895			

			0.311	0.36332	0.24895			
			0.312	0.36449	0.24895			
			0.313	0.36565	0.24895			
			0.314	0.36682	0.24895			
			0.315	0.36799	0.24895			
			0.316	0.36916	0.24895			
			0.317	0.37033	0.24895			
			0.318	0.37150	0.24895			
			0.319	0.37266	0.24895			
			0.32	0.37383	0.24895			
			0.321	0.37500	0.24895			
			0.322	0.37617	0.24895			
			0.323	0.37734	0.24895			
			0.324	0.37850	0.24473			
			0.325	0.37967	0.24473			
			0.326	0.38084	0.24473			
			0.327	0.38201	0.24473			
			0.328	0.38318	0.24473			
			0.329	0.38435	0.24473			
			0.33	0.38551	0.24473			
			0.331	0.38668	0.24473			
			0.332	0.38785	0.24473			
			0.333	0.38902	0.24473			
			0.334	0.39019	0.24051			
			0.335	0.39136	0.23629			
			0.336	0.39252	0.23629			
			0.337	0.39369	0.23629			
			0.338	0.39486	0.22785			
			0.339	0.39603	0.22785			
			0.34	0.39720	0.22785			
			0.341	0.39836	0.22785			
			0.342	0.39953	0.22363			
			0.343	0.40070	0.21941			
			0.344	0.40187	0.21941			
			0.345	0.40304	0.21941			
			0.346	0.40421	0.21941			
			0.347	0.40537	0.21941			
			0.348	0.40654	0.21941			
			0.349	0.40771	0.21941			
			0.35	0.40888	0.21519			
			0.351	0.41005	0.21097			

			0.352	0.41121	0.21097			
			0.353	0.41238	0.21097			
			0.354	0.41355	0.21097			
			0.355	0.41472	0.20675			
			0.356	0.41589	0.20675			
			0.357	0.41706	0.20675			
			0.358	0.41822	0.19409			
			0.359	0.41939	0.18565			
			0.36	0.42056	0.18143			
			0.361	0.42173	0.17722			
			0.362	0.42290	0.17300			
			0.363	0.42407	0.16456			
			0.364	0.42523	0.16456			
			0.365	0.42640	0.16034			
			0.366	0.42757	0.16034			
			0.367	0.42874	0.14768			
			0.368	0.42991	0.13080			
			0.369	0.43107	0.10970			
			0.37	0.43224	0.10127			
			0.371	0.43341	0.09283			
			0.372	0.43458	0.08017			
			0.373	0.43575	0.05907			
			0.374	0.43692	0.05063			
			0.375	0.43808	0.05063			
			0.376	0.43925	0.05063			
			0.377	0.44042	0.05063			
			0.378	0.44159	0.05063			
			0.379	0.44276	0.04219			
			0.38	0.44393	0.04219			
			0.381	0.44509	0.04219			
			0.382	0.44626	0.03376			
			0.383	0.44743	0.02954			
			0.384	0.44860	0.02954			
			0.385	0.44977	0.02110			
			0.386	0.45093	0.02110			
			0.387	0.45210	0.01688			
			0.388	0.45327	0.01688			
			0.389	0.45444	0.01266			
			0.39	0.45561	0.00844			
			0.391	0.45678	0.00422			
			0.392	0.45794	0.00422			

APPENDIX H. DRAWINGS AND PARTS – SPECIFIC AIM 1

H.1 Specific Aim 1 – Experiment A

Table H-1. List of parts to make dynamically contracting annulus (DCA) for the box left heart chamber.

Item	Vendor	Item#	Description
Wire	McMaster	3461T63	Used for the contraction; embedded in the annulus cuff
Cam Lever	McMaster	5720K17	Used to hold wires in place on motors
Spring	McMaster	9663K16	Embedded in the annulus cuff to provide relaxation
Screws	McMaster	99477A620	Secures top plate onto bottom plate of DCA
Nylon	McMaster		Shell of annulus cuff
Silicone	McMaster		Fills the annulus cuff for suturing

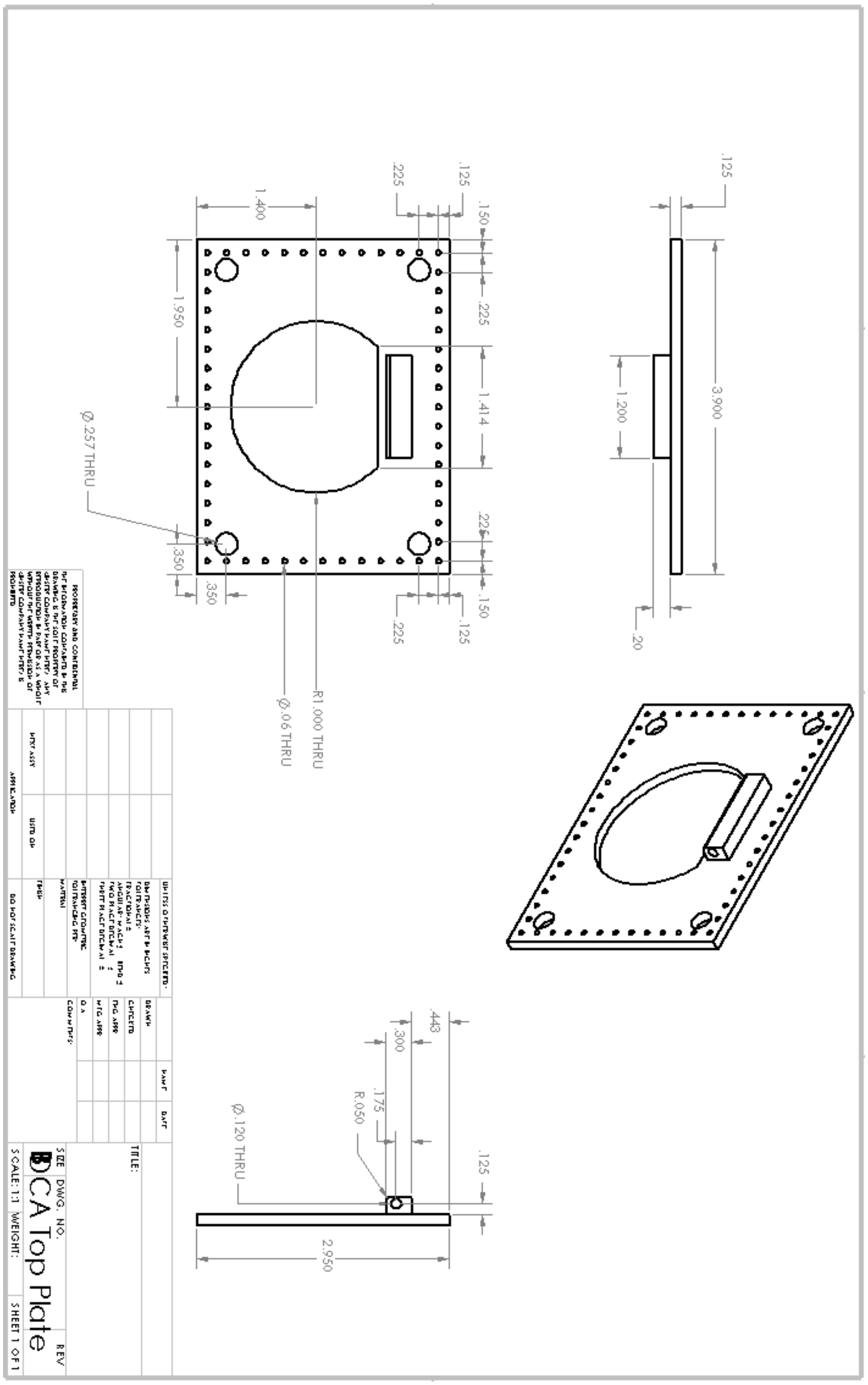

Figure H-1. Drawing of the top plate of the dynamically contracting annulus (DCA) for the box left heart chamber.

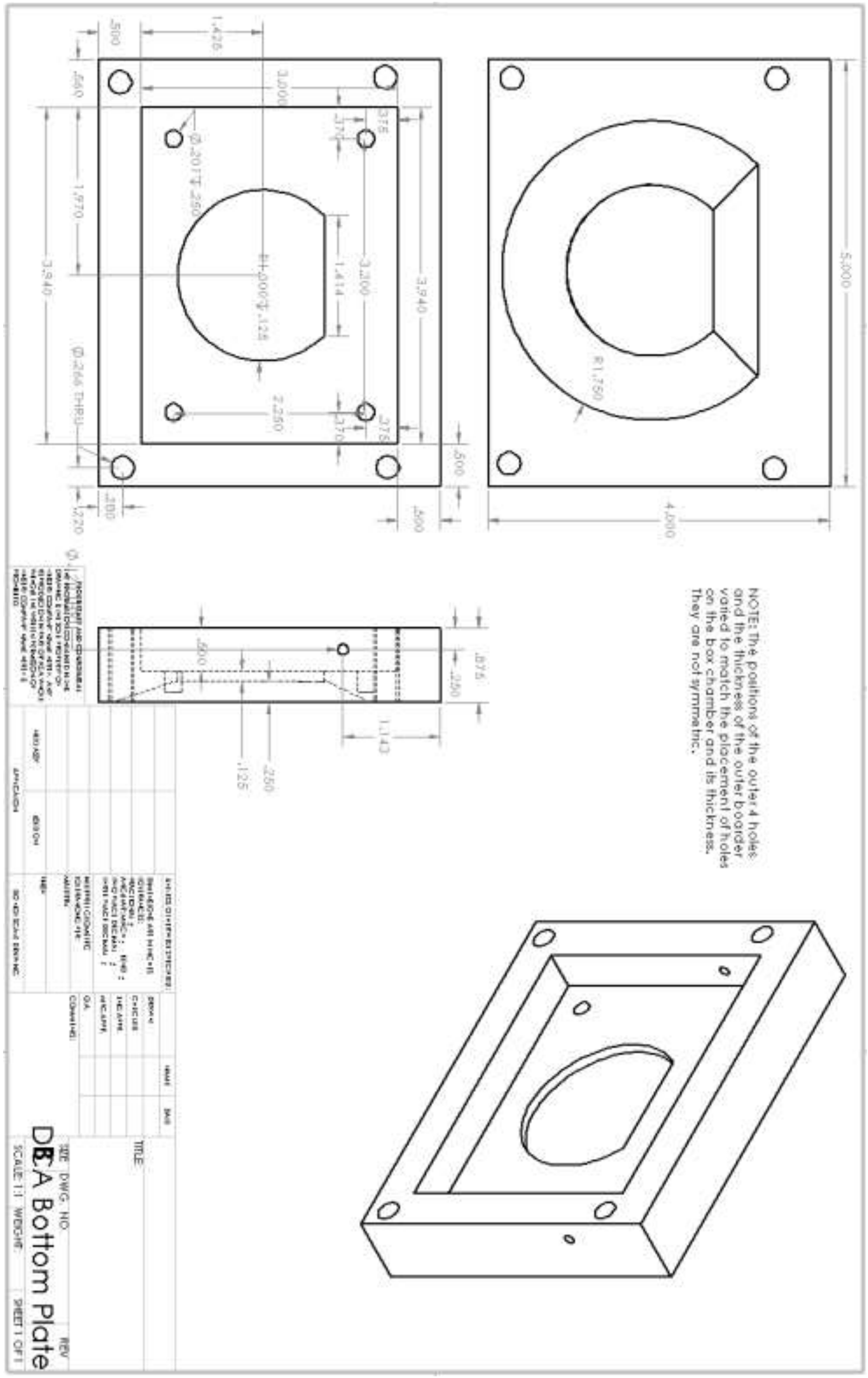

Figure H-2. Drawing of the bottom plate of the dynamically contracting annulus (DCA) for the box left heart chamber.

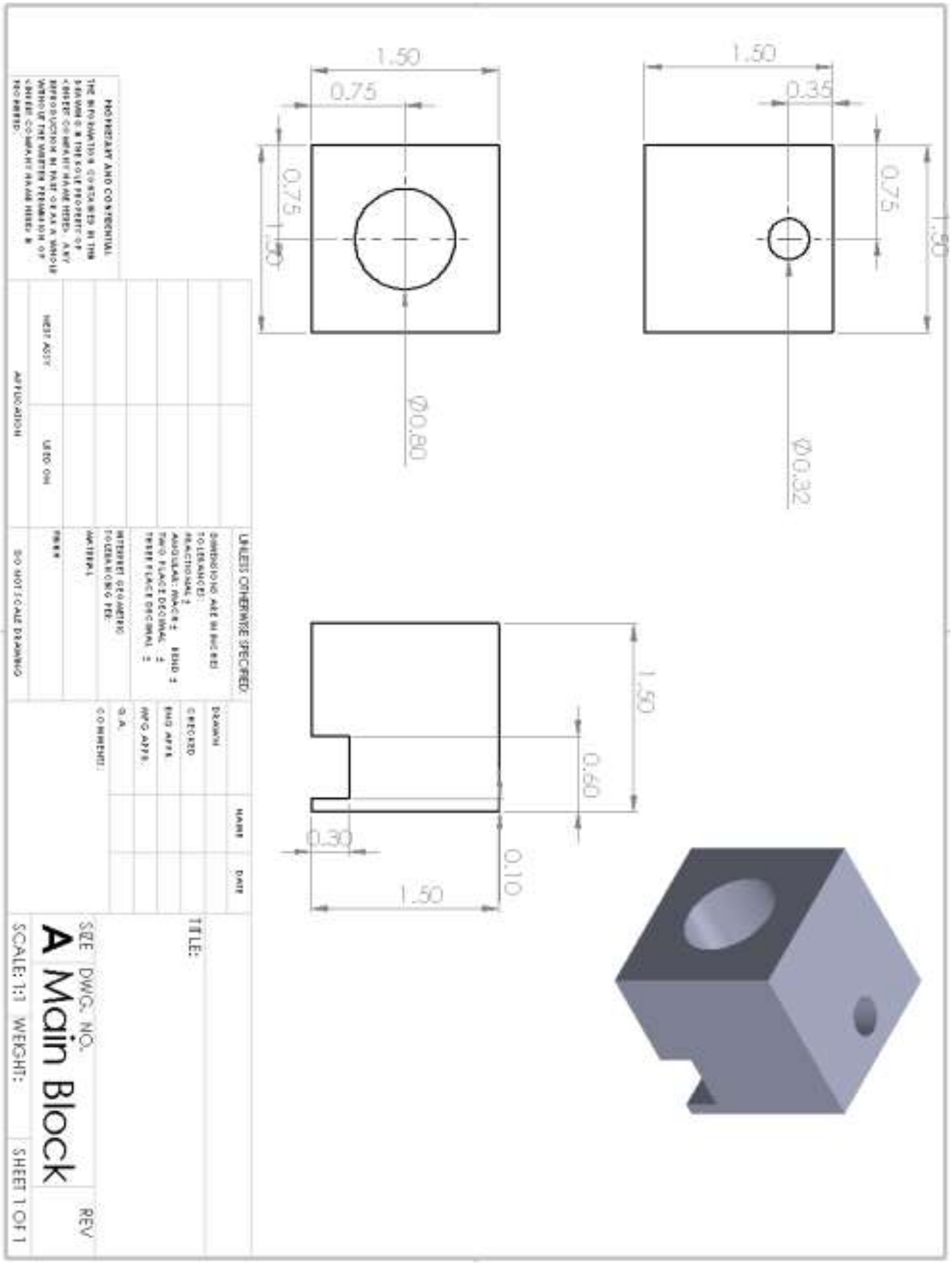

Figure H-3. Motor block for attaching the wire via a cam lever.

H.2 Specific Aim 2 – Experiment B

Table H-2. List of parts to make dynamically contracting annulus (DCA) for the cylindrical left heart chamber.

Item	**Vendor**	**Item#**	**Description**
Screws	McMaster	92185A992	Secures top plate onto bottom plate of DCA
Gasket	McMaster	4061T14	Put between top and bottom plates to increase seal
Spring	McMaster	9663K16	Embedded in the annulus cuff to provide relaxation
Nylon	McMaster		Shell of annulus cuff
Silicone	McMaster		Fills the annulus cuff for suturing

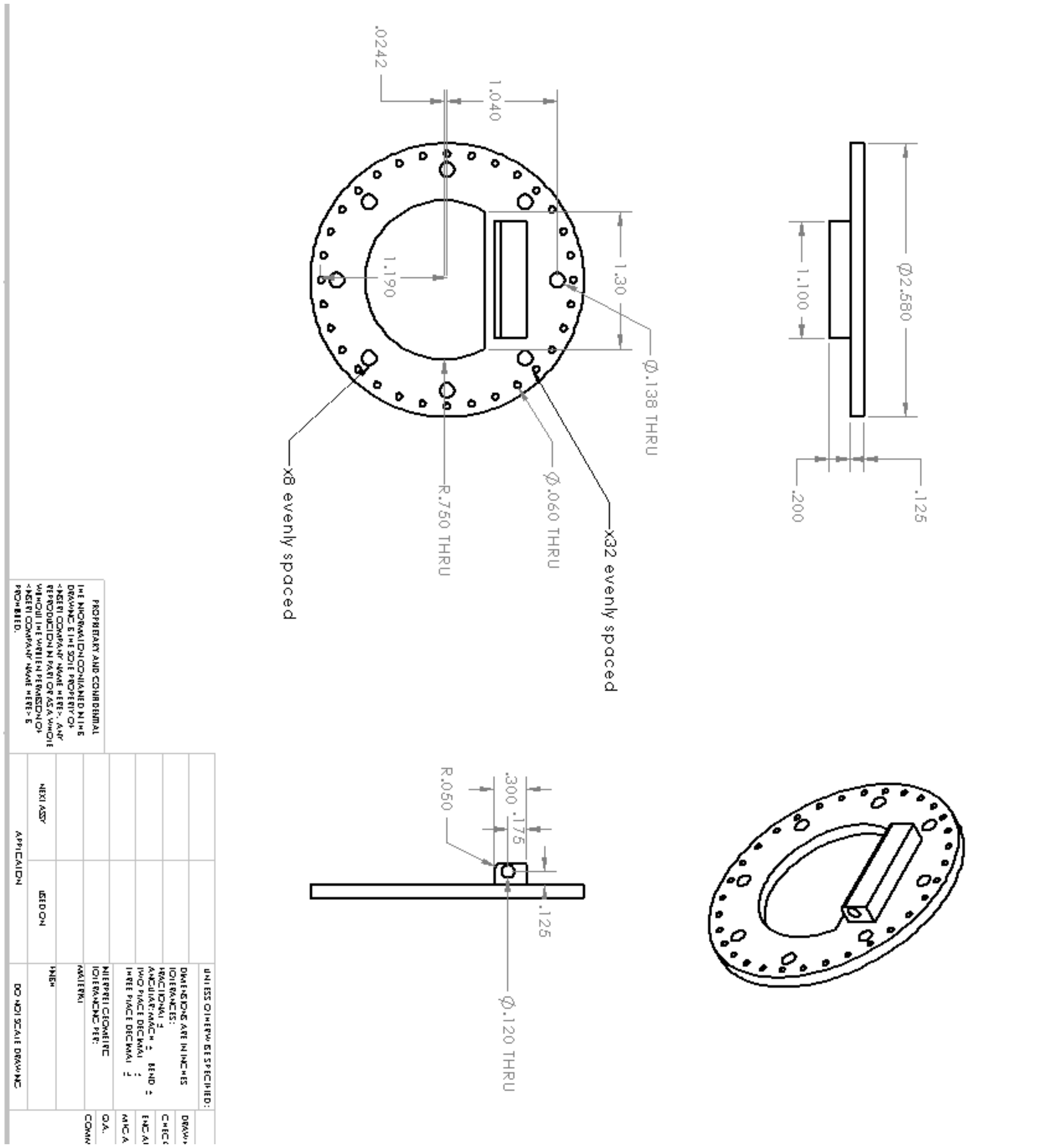

Figure H-4. Drawing of the top plate of the dynamically contracting annulus (DCA) for the cylinder left heart chamber.

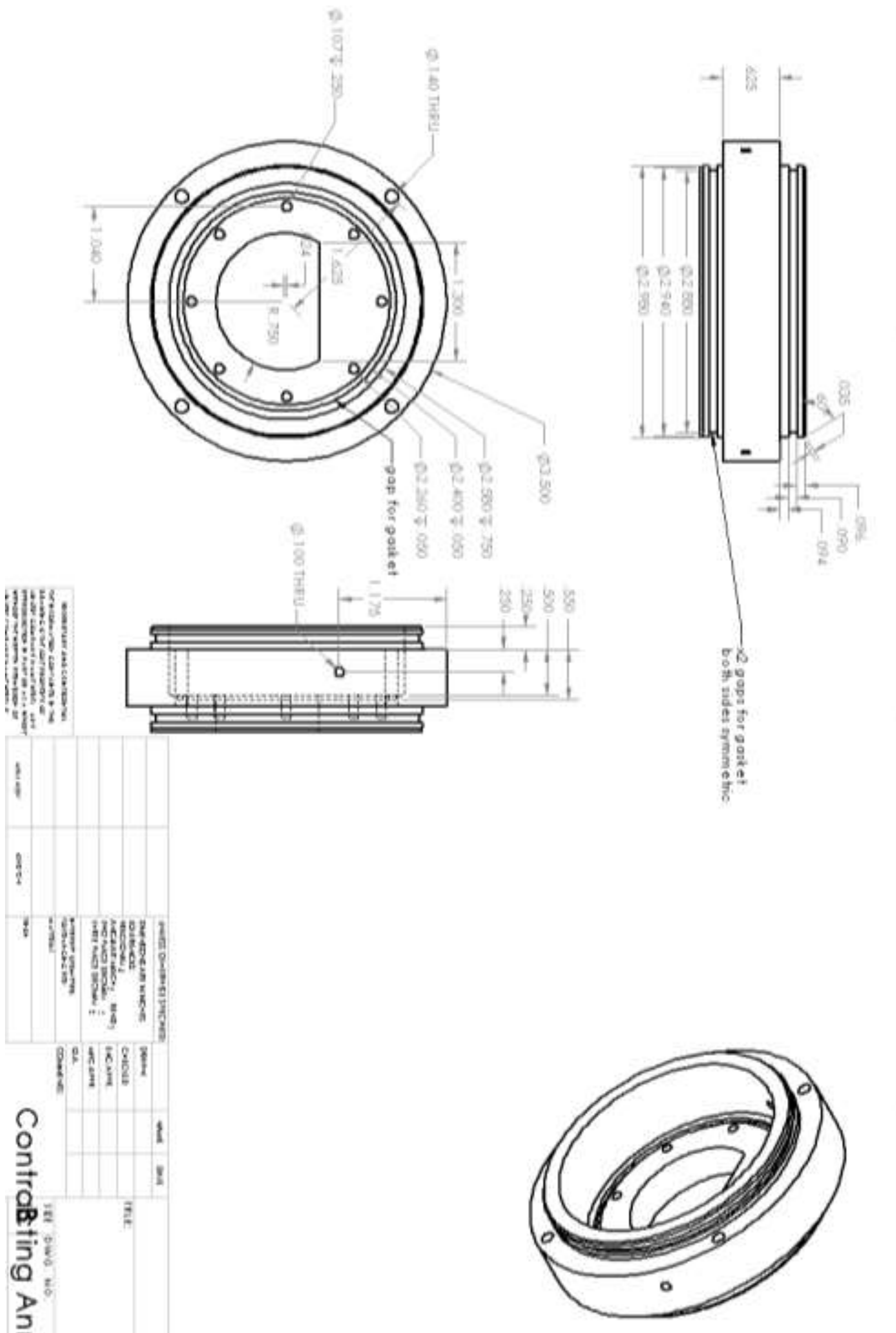

Figure H-5. Drawing of the bottom plate of the dynamically contracting annulus (DCA) for the cylinder left heart chamber.

APPENDIX I. DRAWINGS AND PARTS – SPECIFIC AIM 2

I.1 Left Ventricle Box Chamber

Table I-1. List of parts to make left ventricle box chamber.

Item	Vendor	Item#	Description
Acrylic	McMaster	8560K361 8560K359 8560K363 8560K321	Chamber material: LV Box Parts 1 and 2; Parts 10 and 11; Parts 5, 5-2, 6, 7, and 8; Parts 3 and 4, respectively
Tap Inserts	McMaster	99362A700 99362A600	Brass tap inserts for acylic assembly
Screws	McMaster	93465A540 93465A541 93465A324 97595A236	Brass screws for assembly

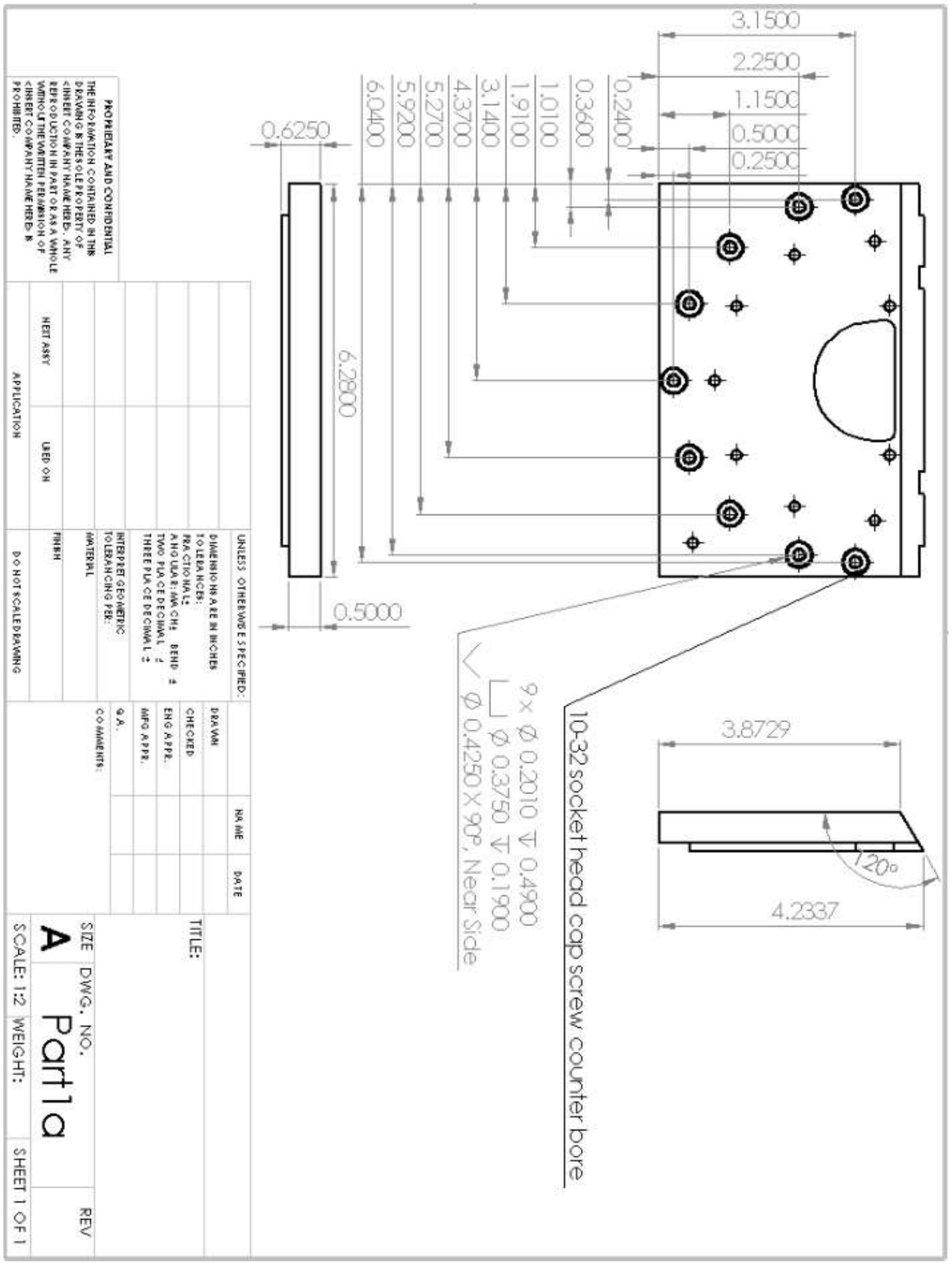

Figure I-1. Part 1-a drawing.

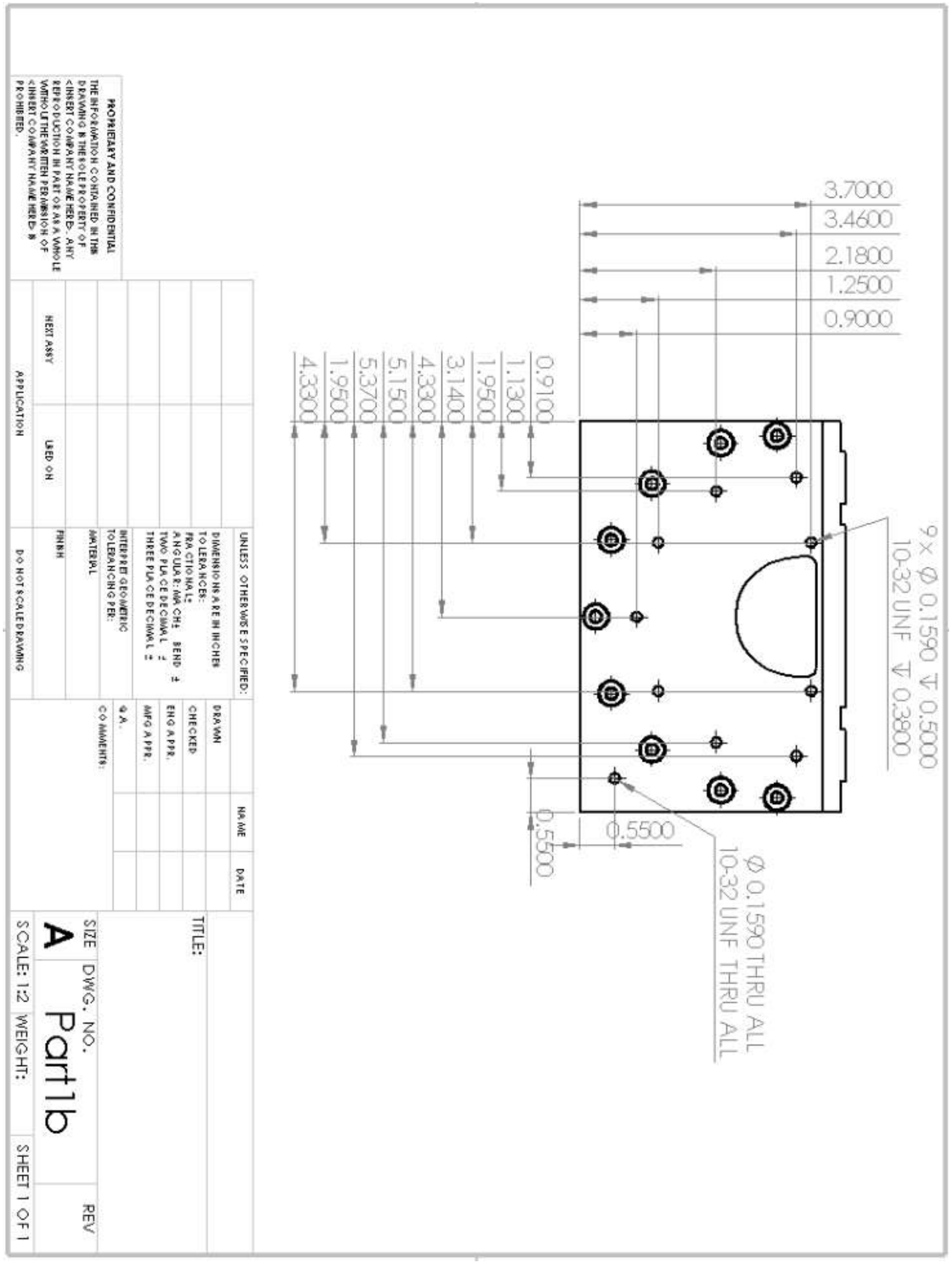

Figure I-2. **Part 1-b drawing.**

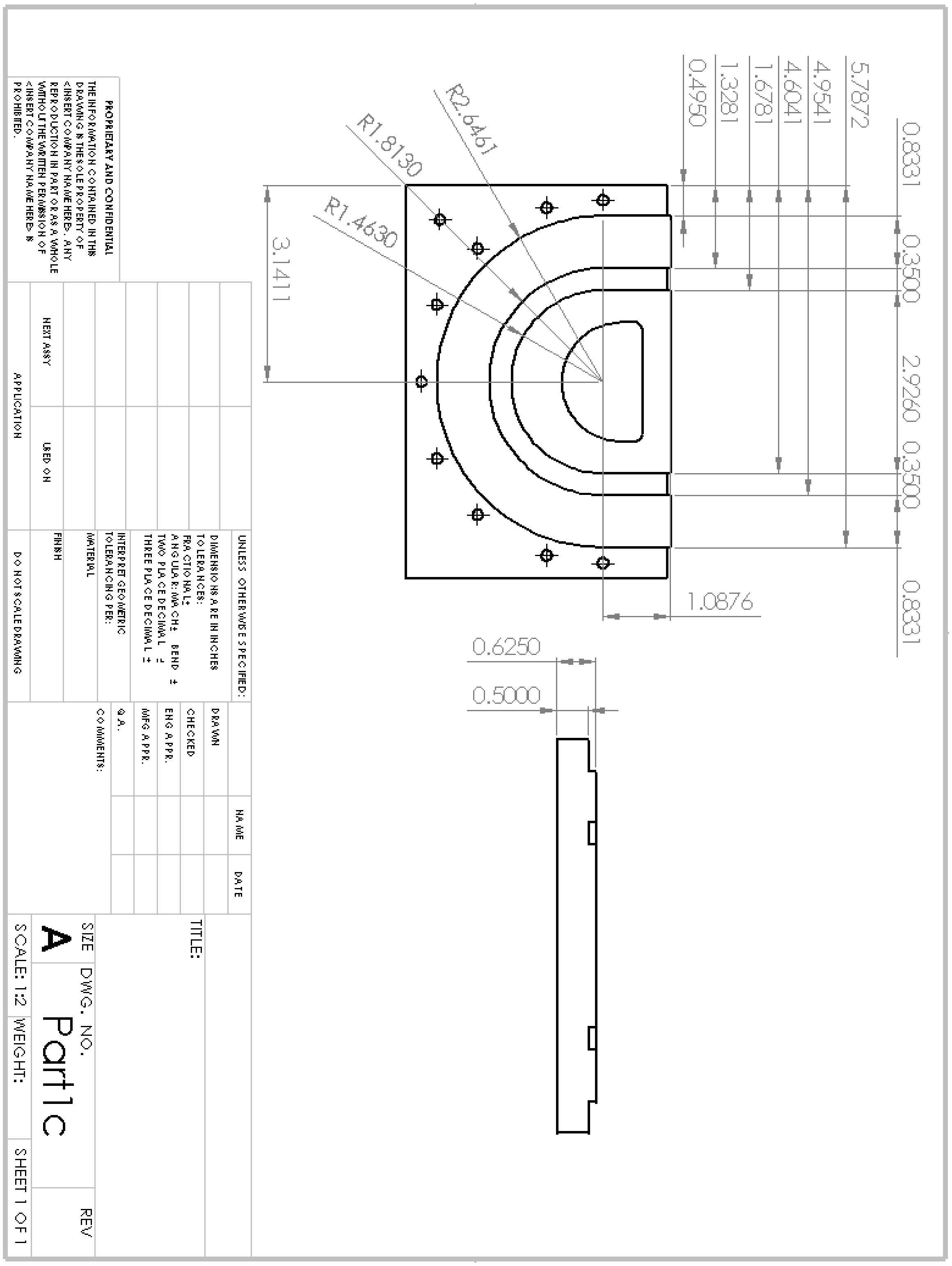

Figure I-3. **Part 1-c drawing.**

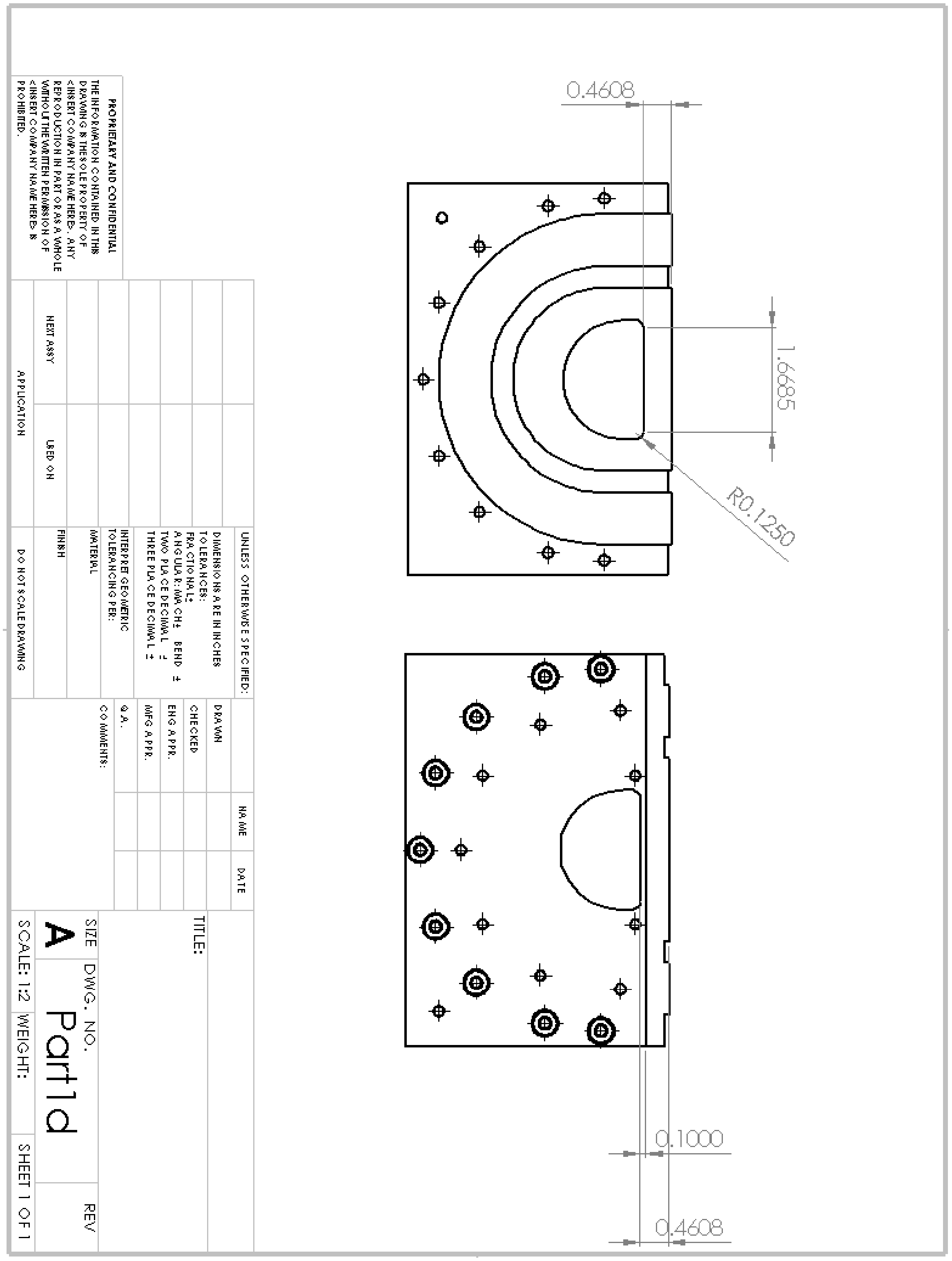

Figure I-4. **Part 1-d drawing.**

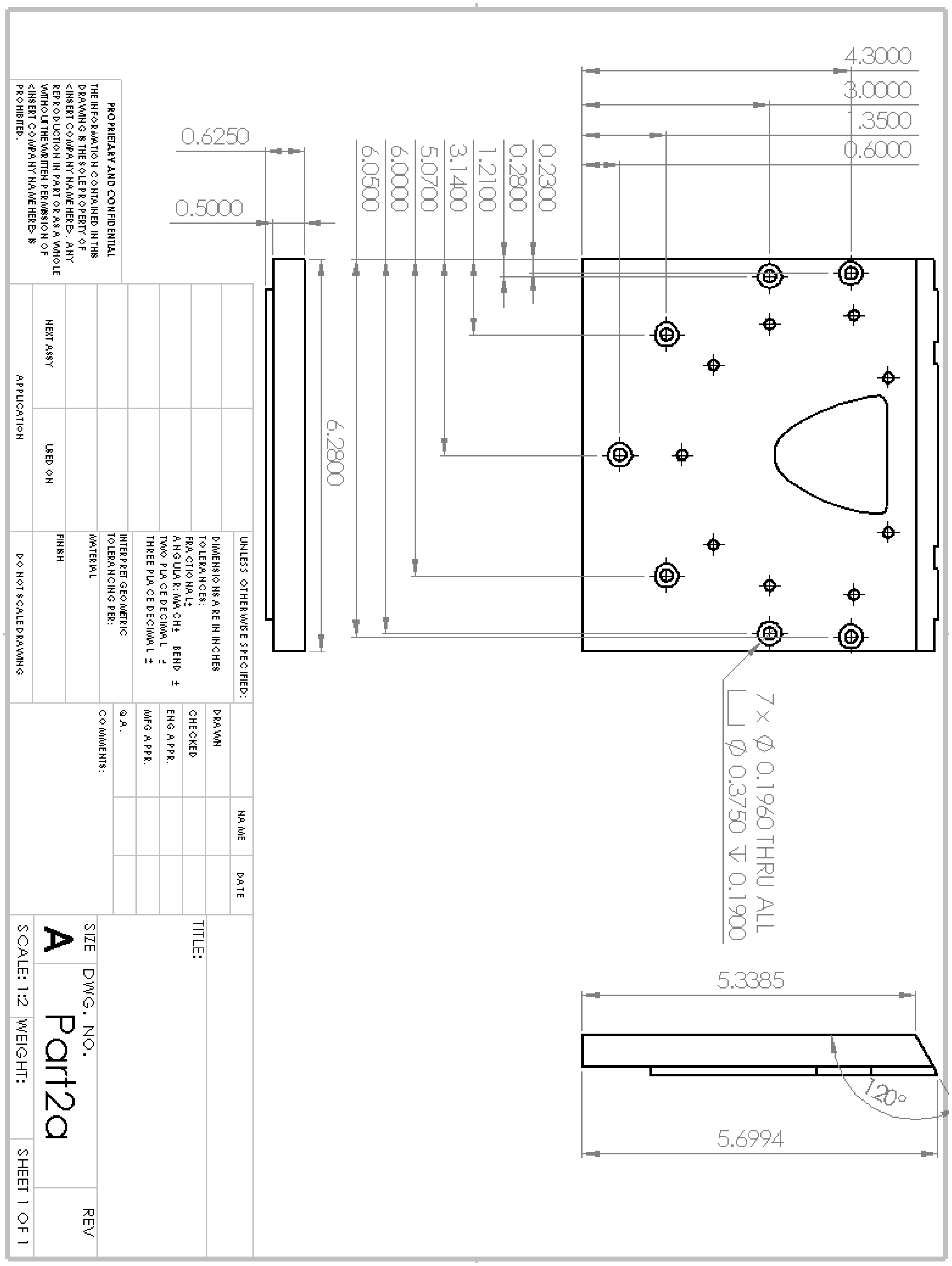

Figure I-5. **Part 2-a drawing.**

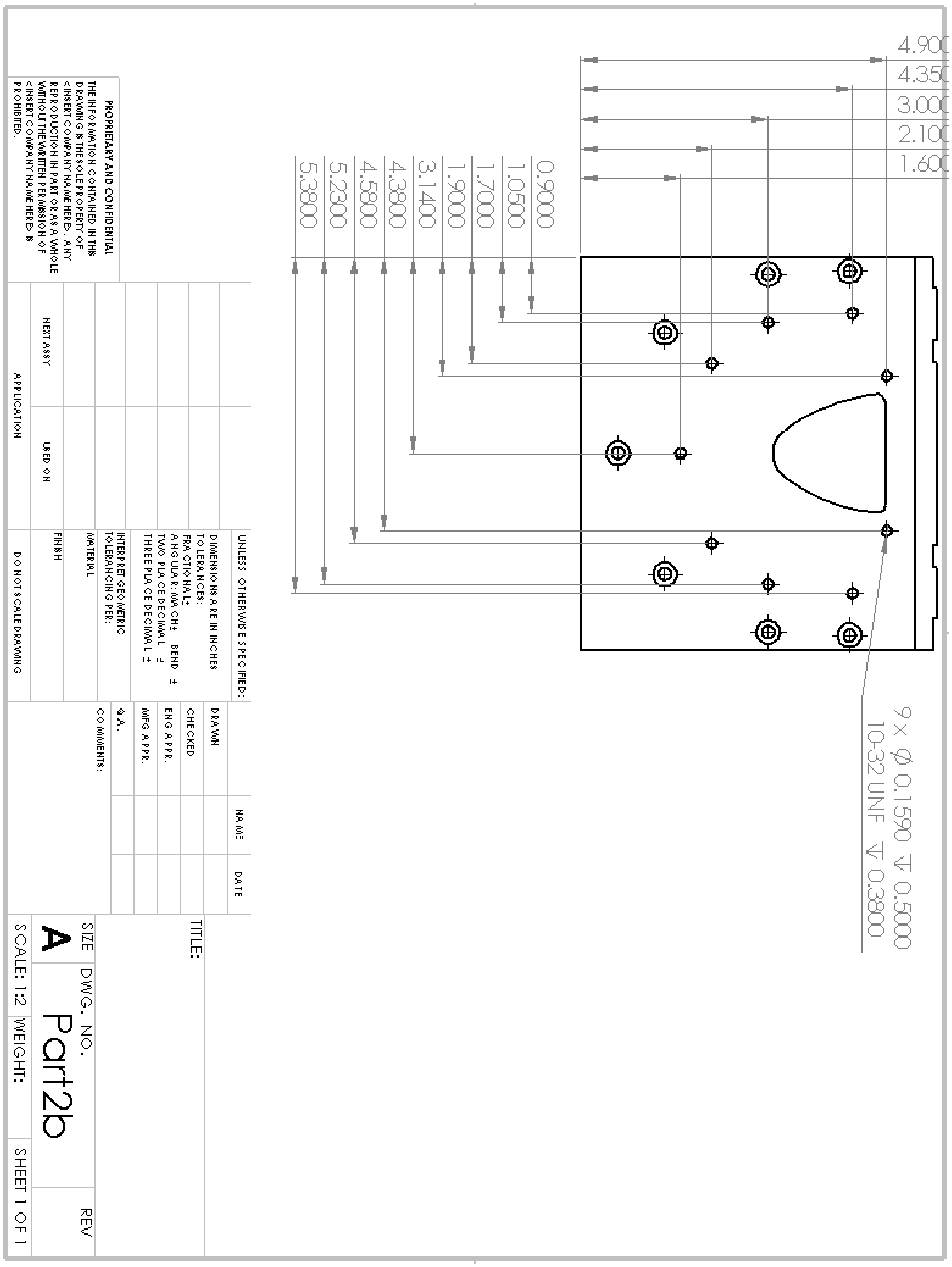

Figure I-6. **Part 2-b drawing.**

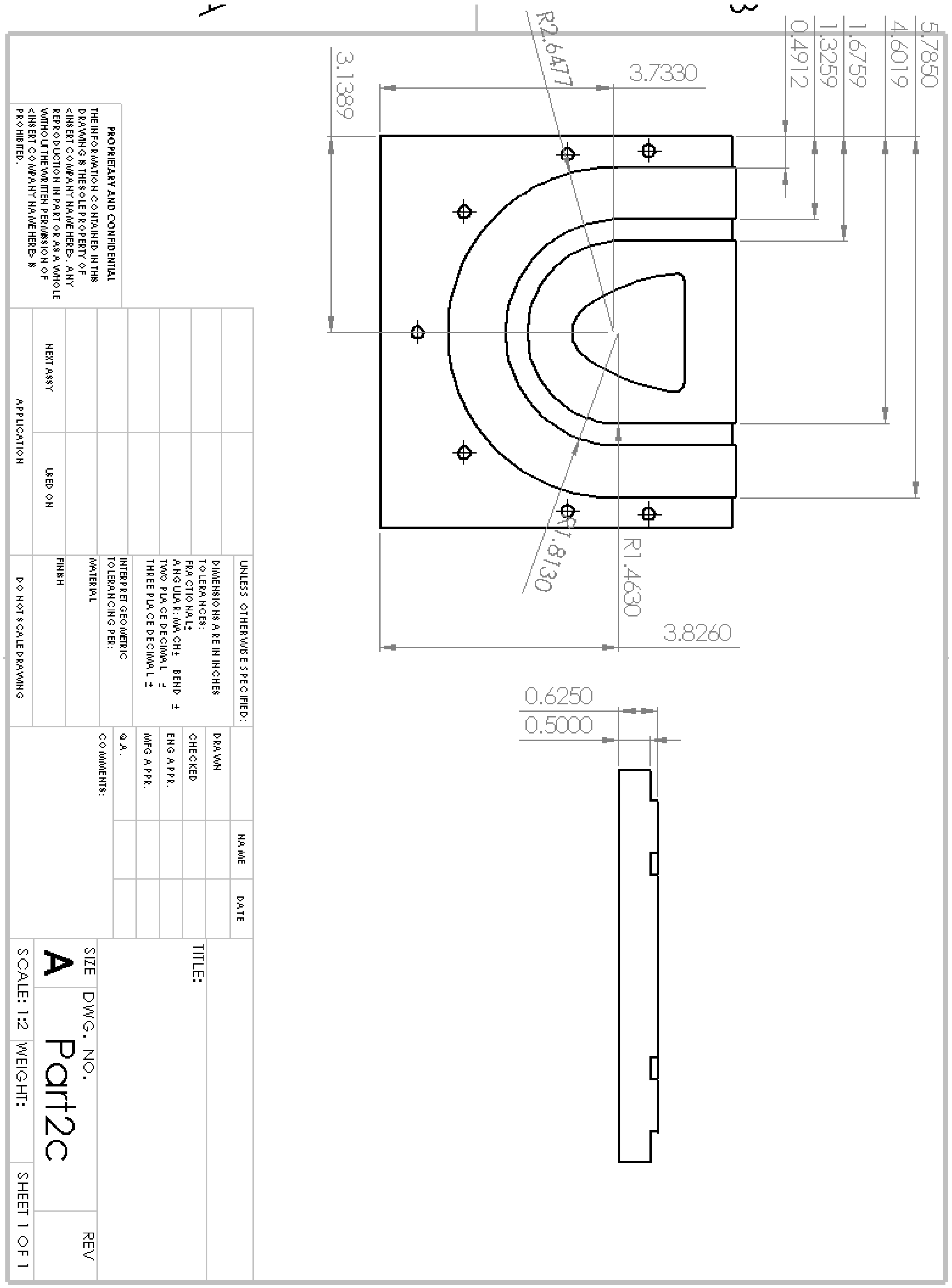

Figure I-7. Part 2-c drawing.

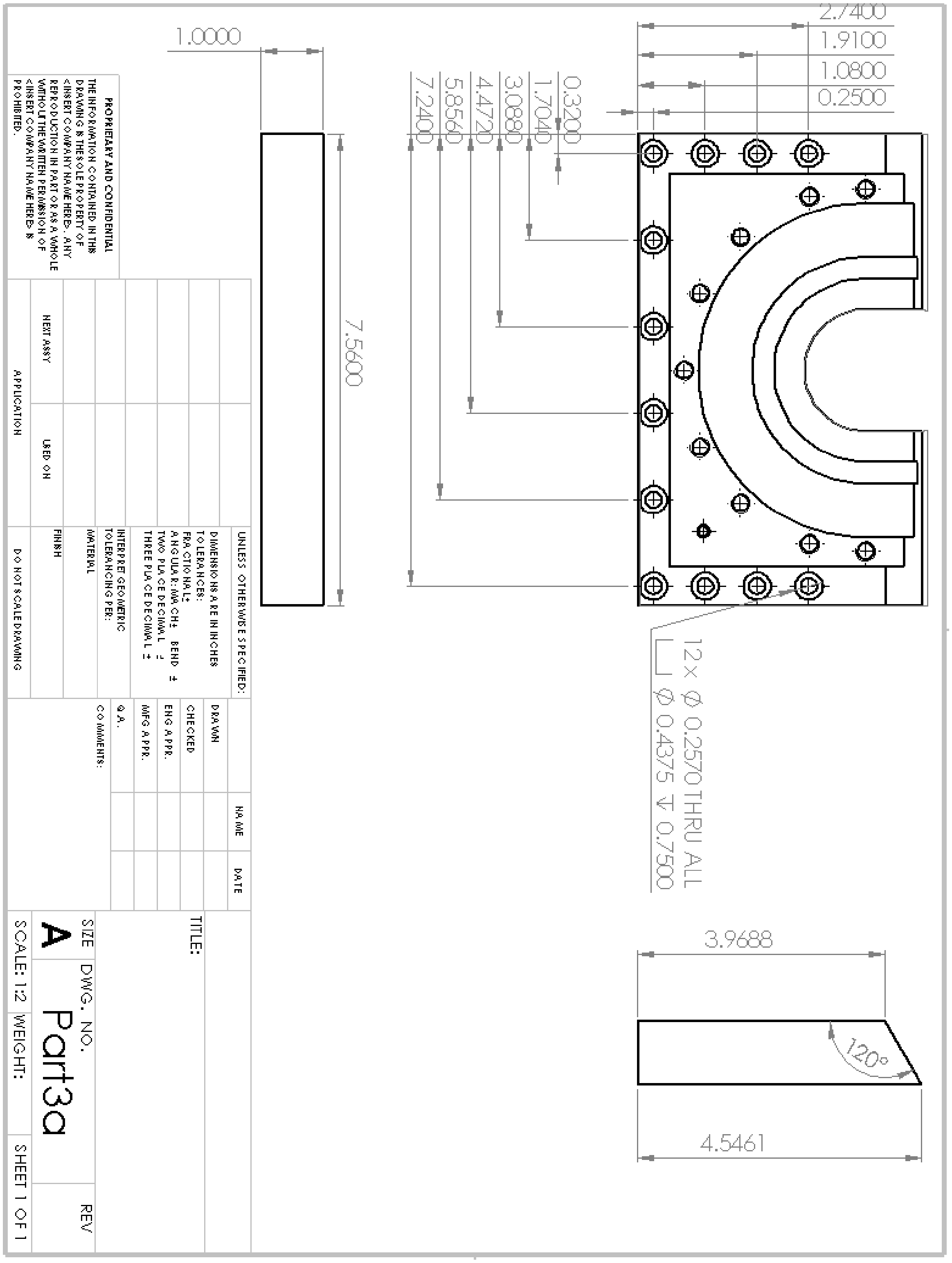

Figure I-8. **Part 3-a drawing.**

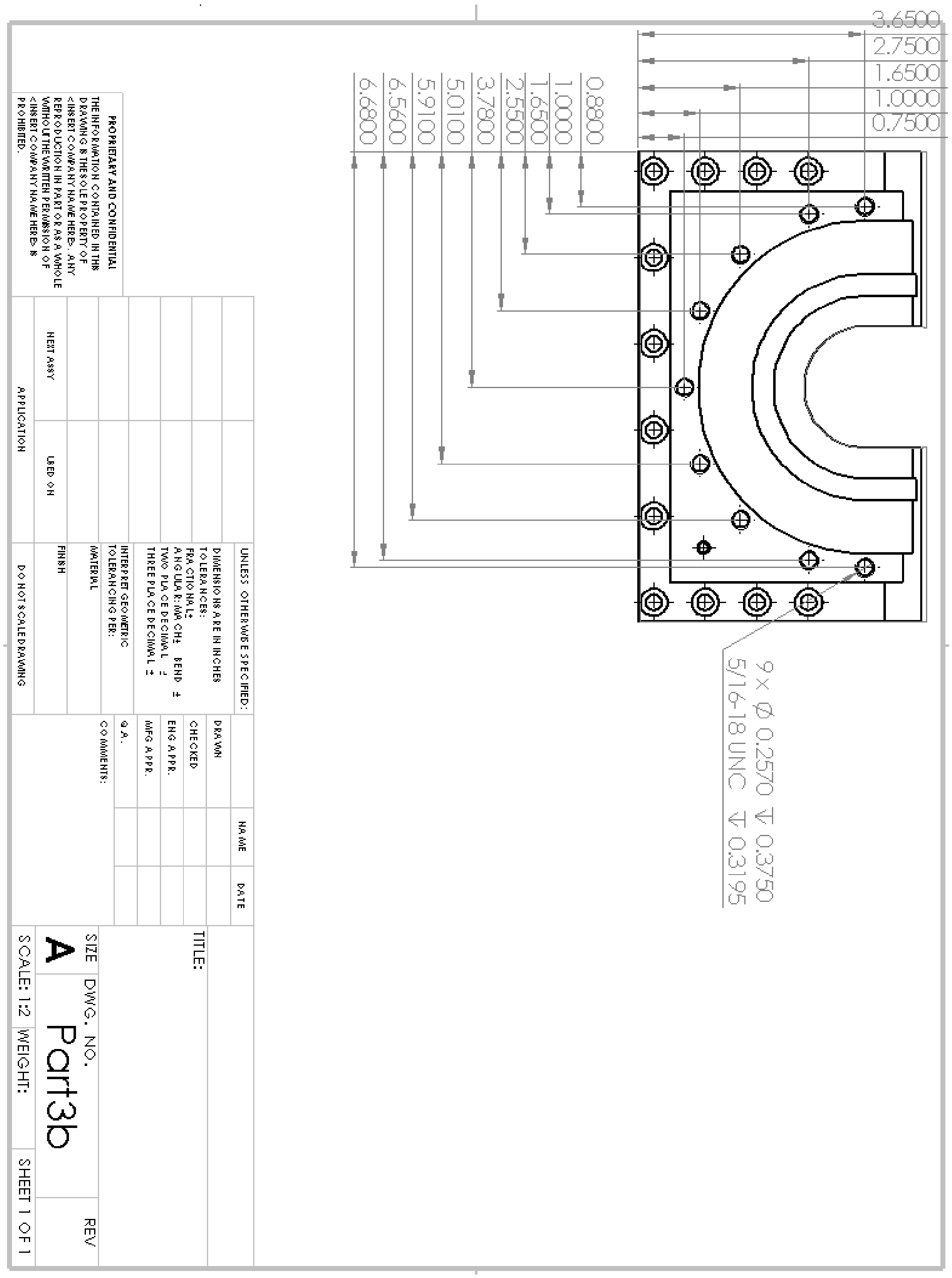

Figure I-9. Part 3-b drawing.

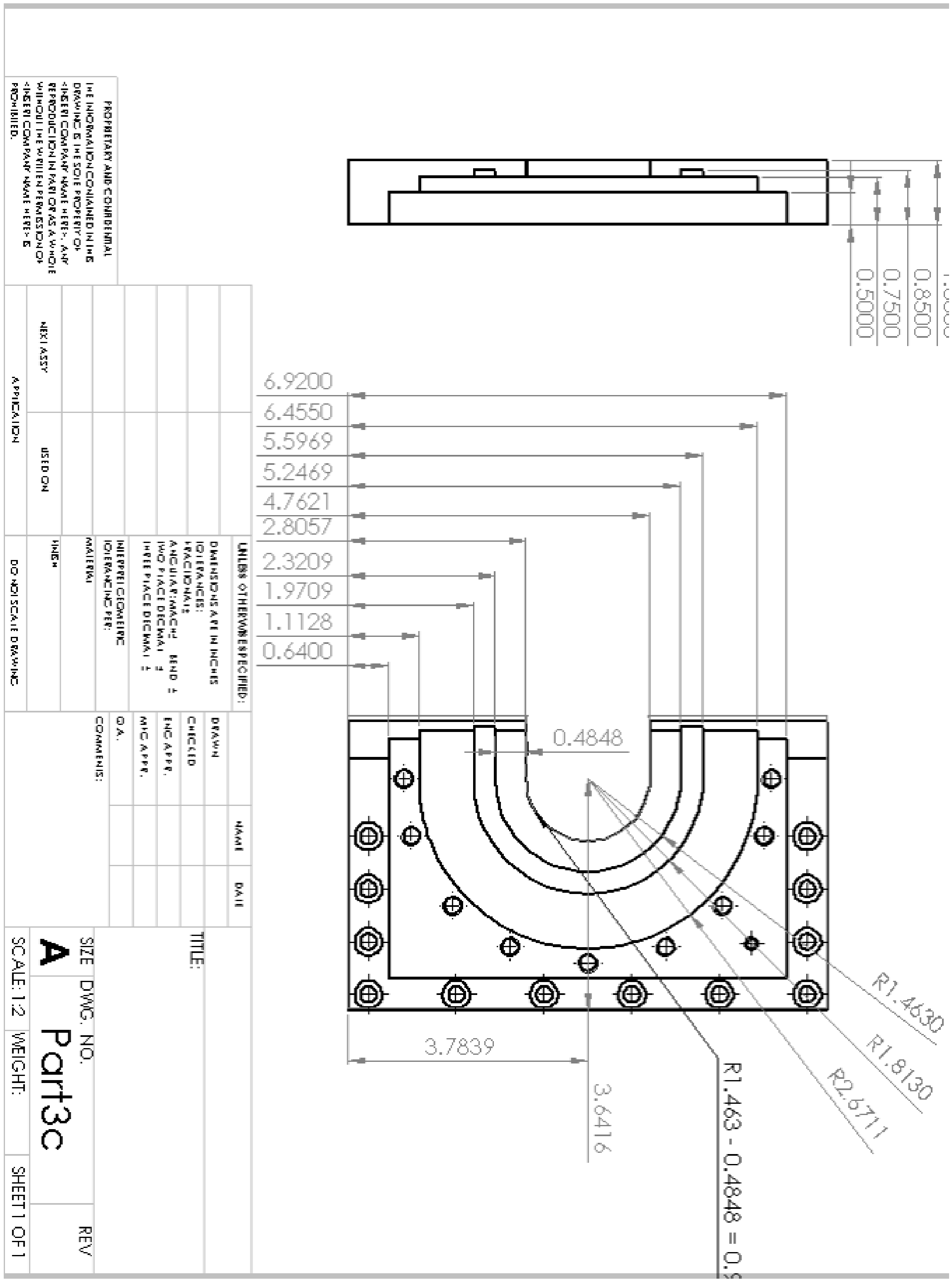

Figure I-10. Part 3-c drawing.

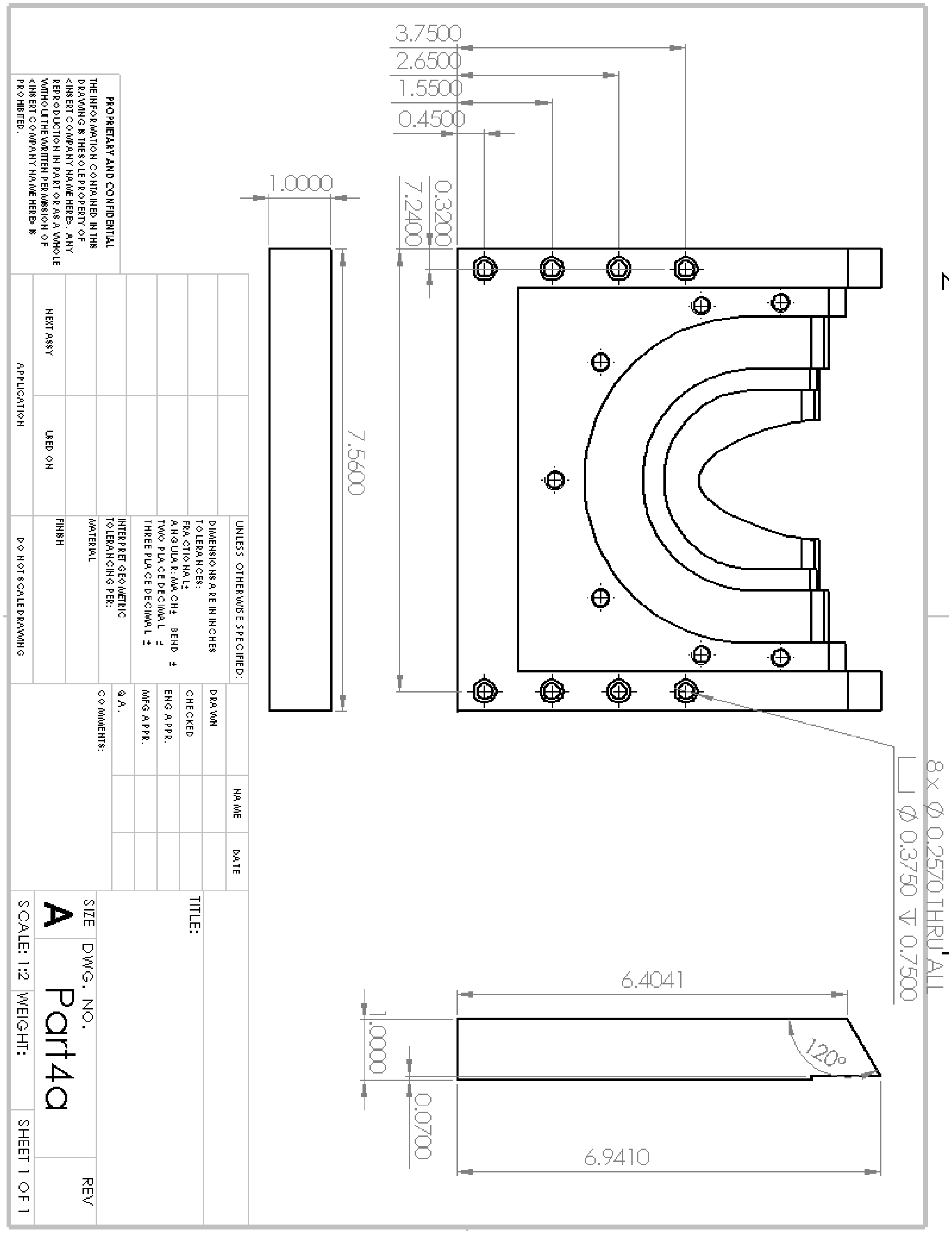

Figure I-11. Part 4-a drawing.

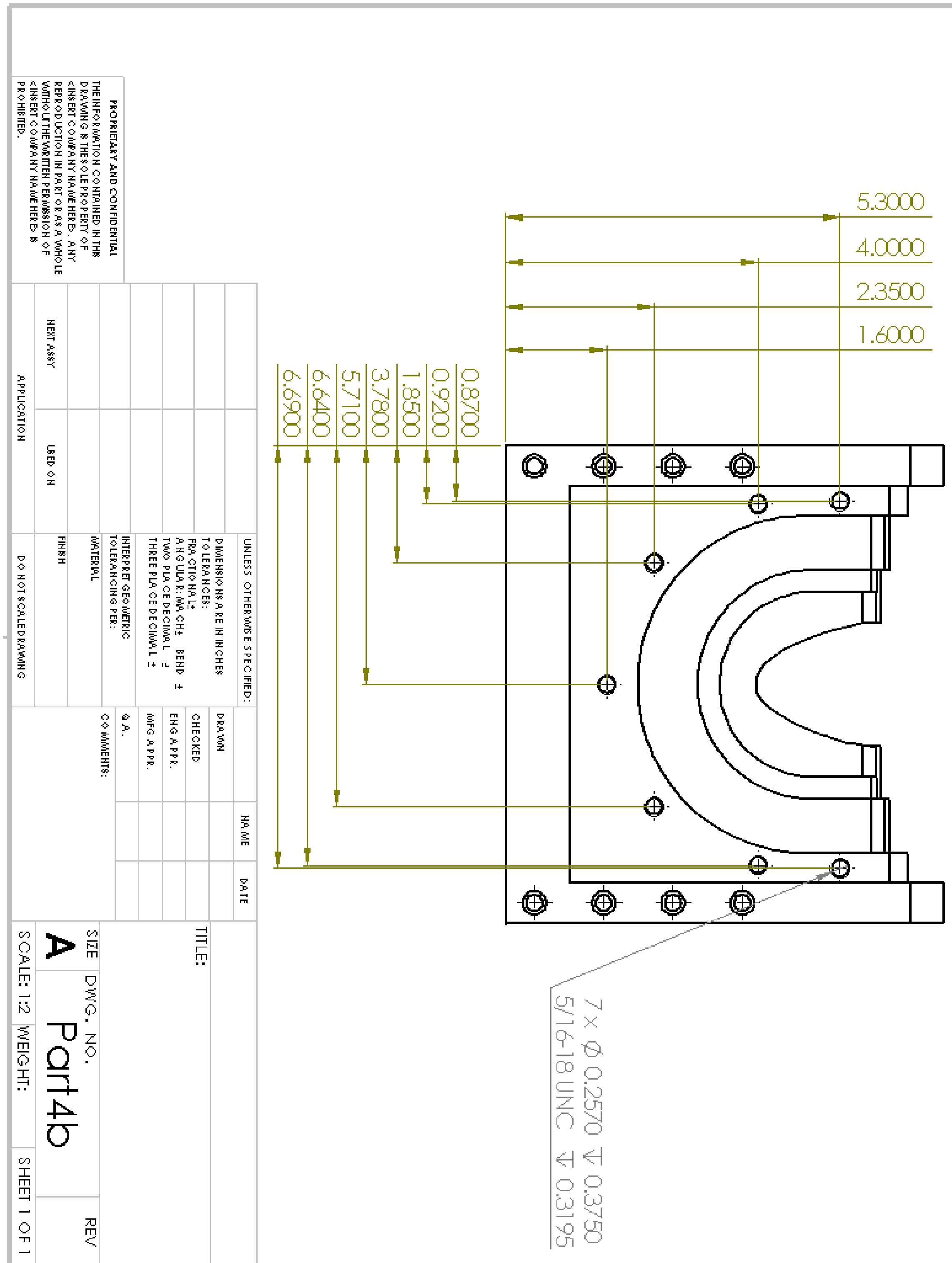

Figure I-12. Part 4-b drawing.

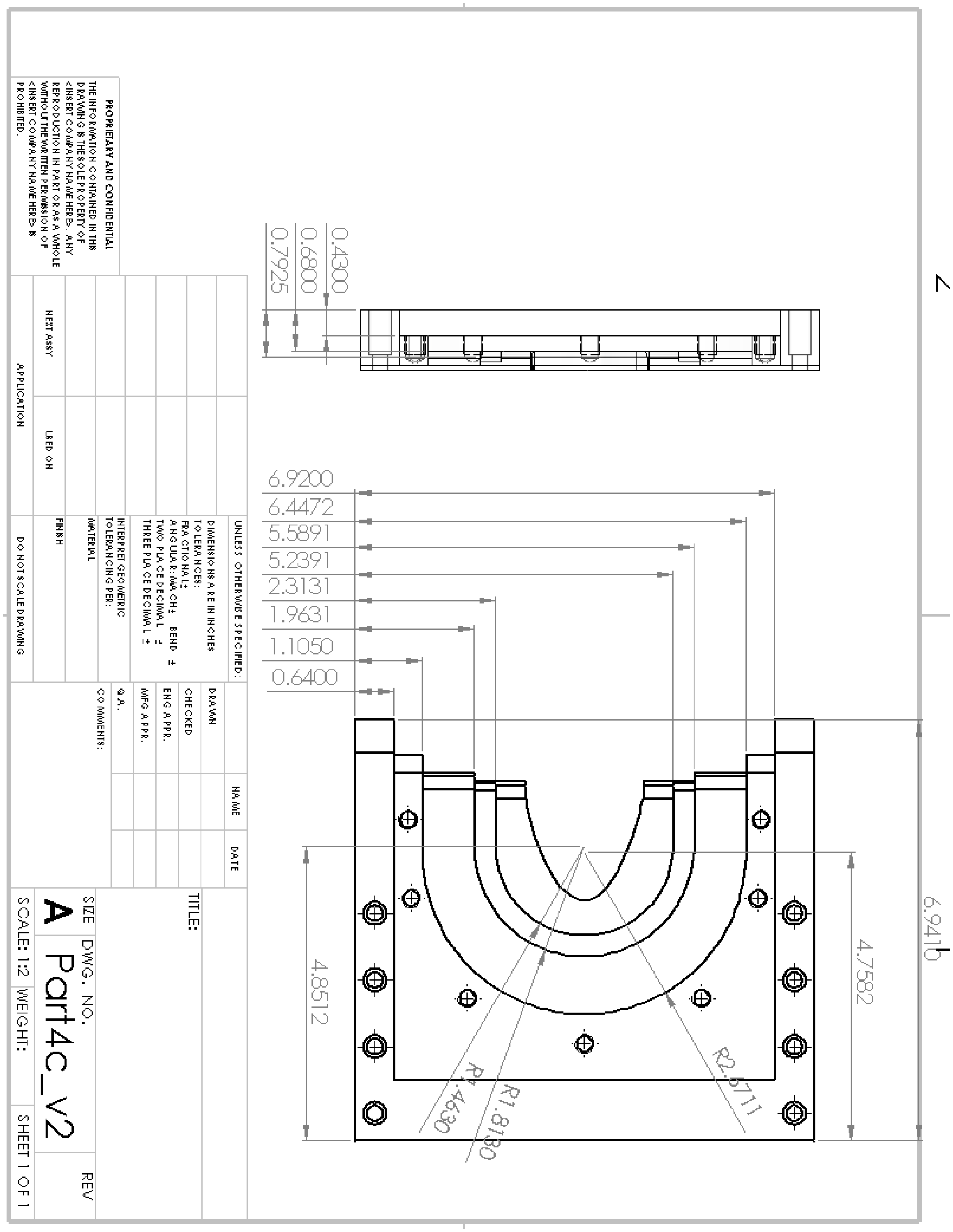

Figure I-13. Part 4-c drawing.

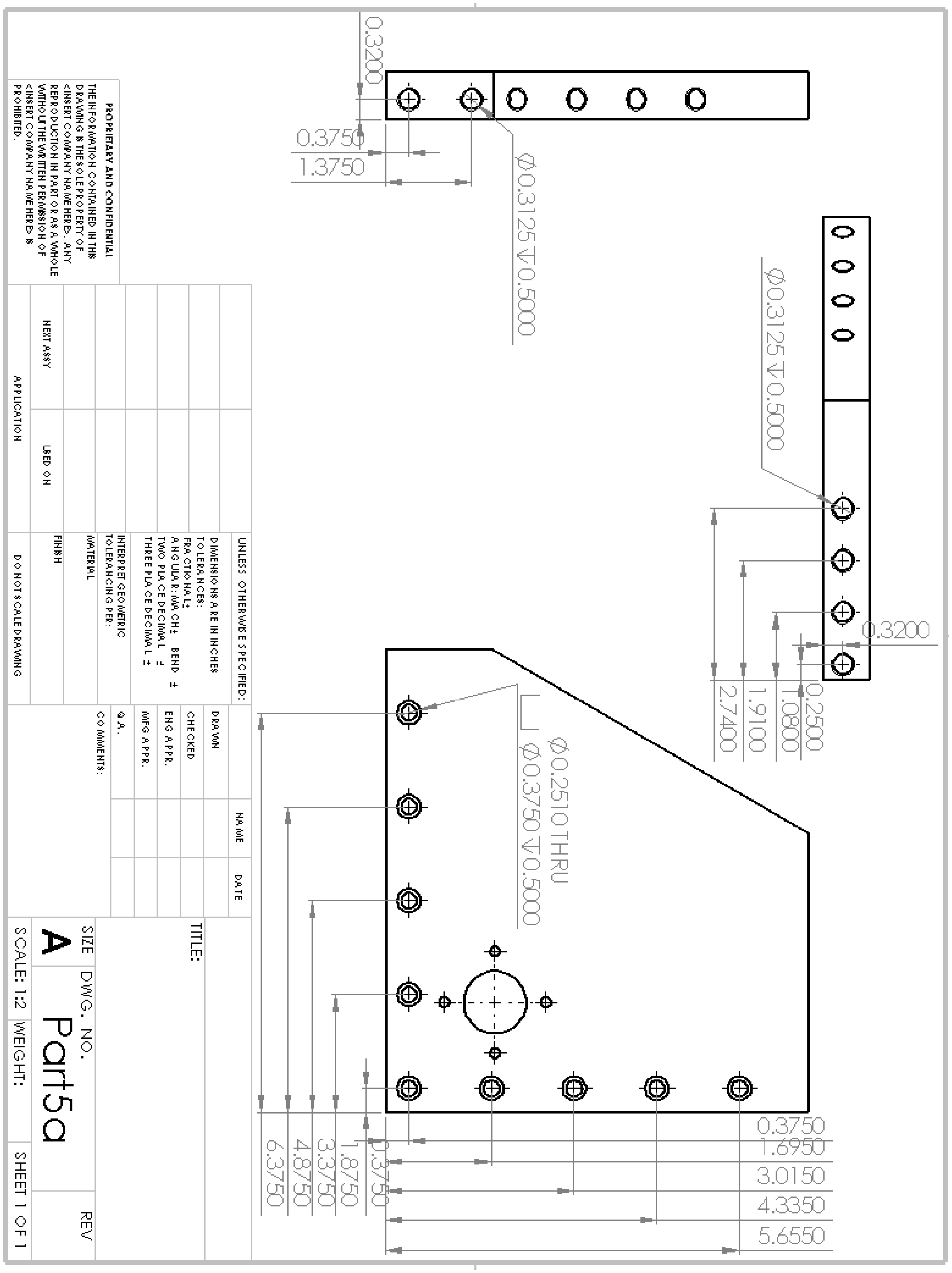

Figure I-14.   Part 5-a drawing.

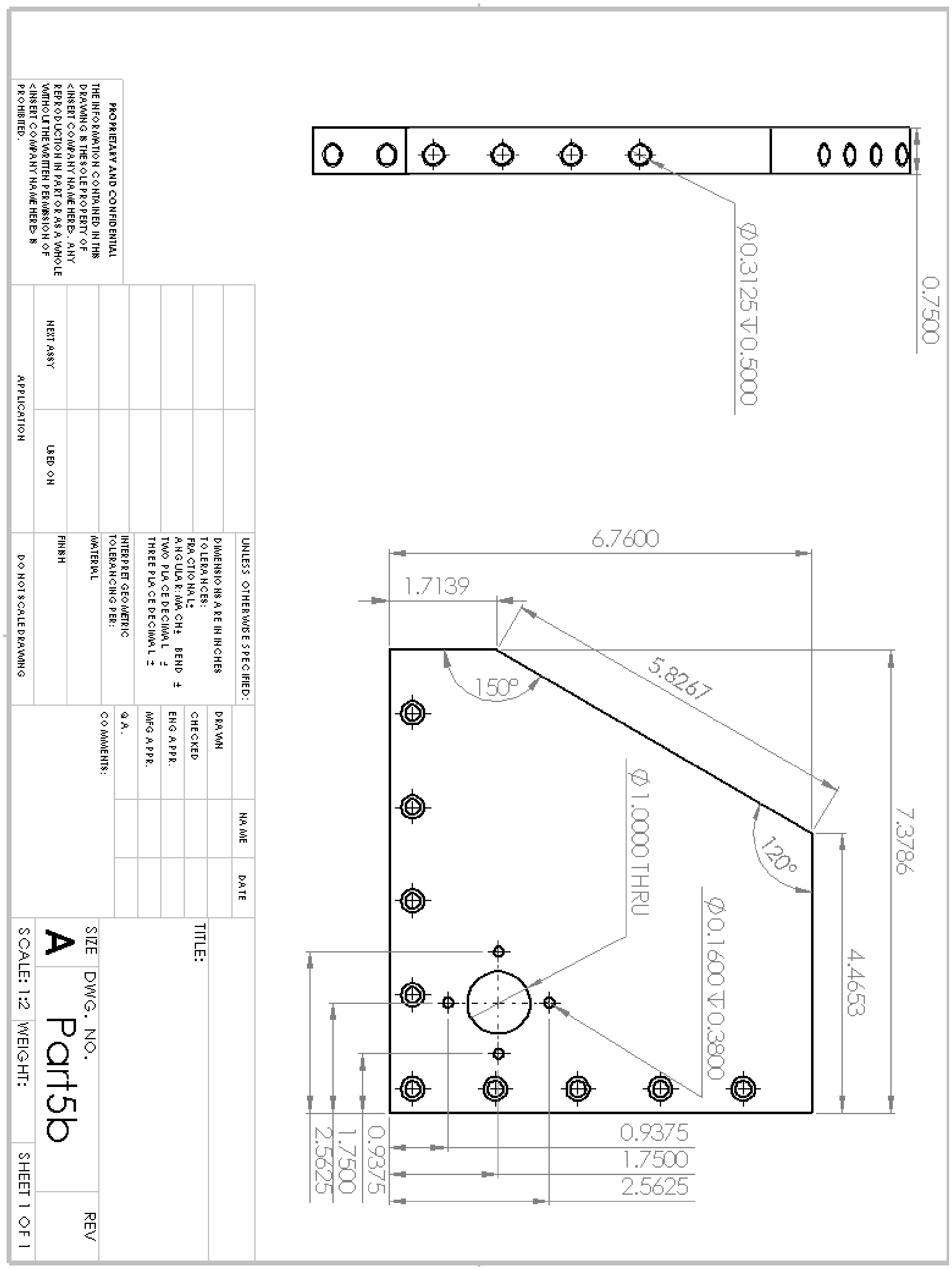

Figure I-15. Part 5-b drawing.

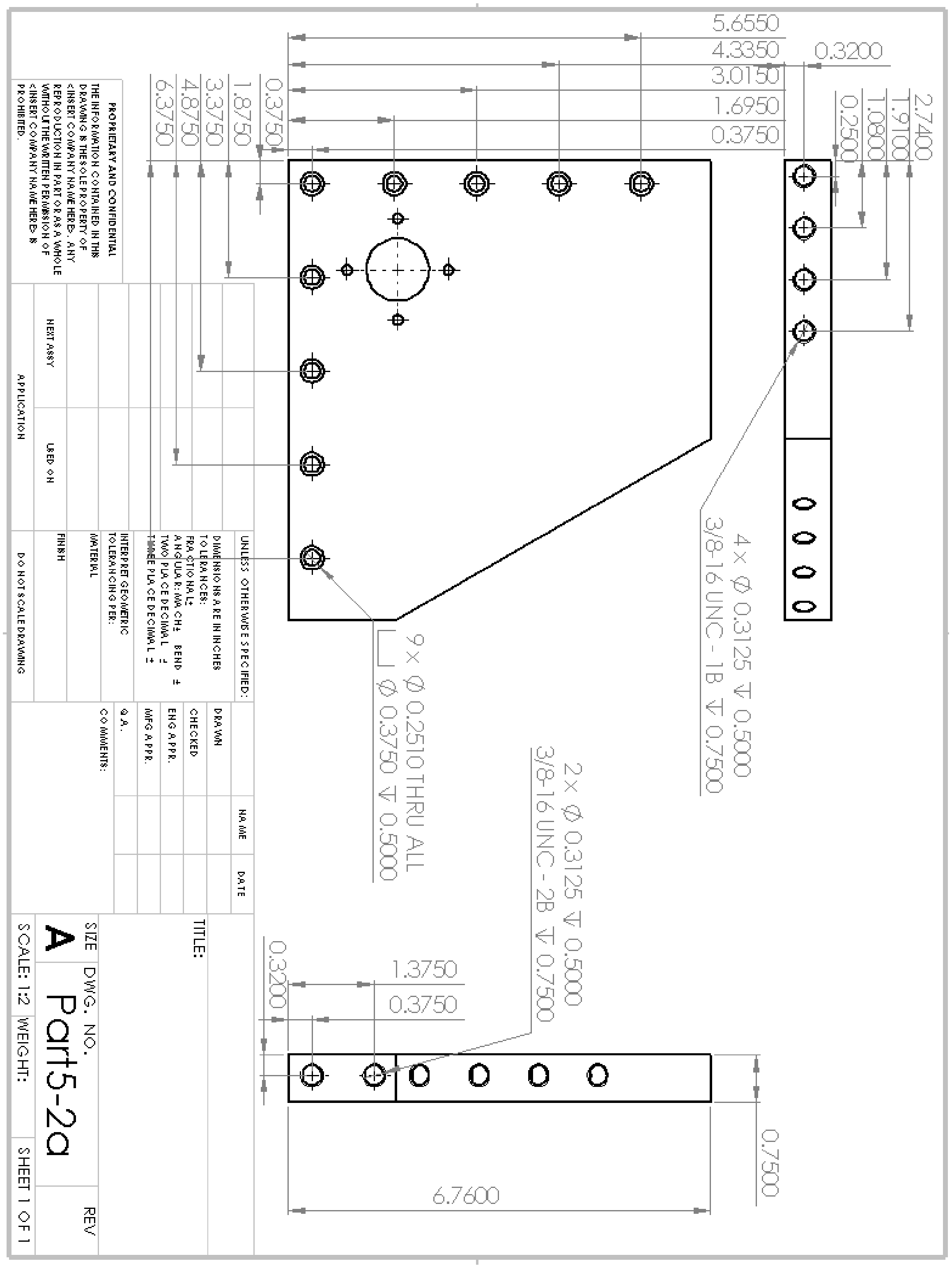

Figure I-16. Part 5-2a drawing.

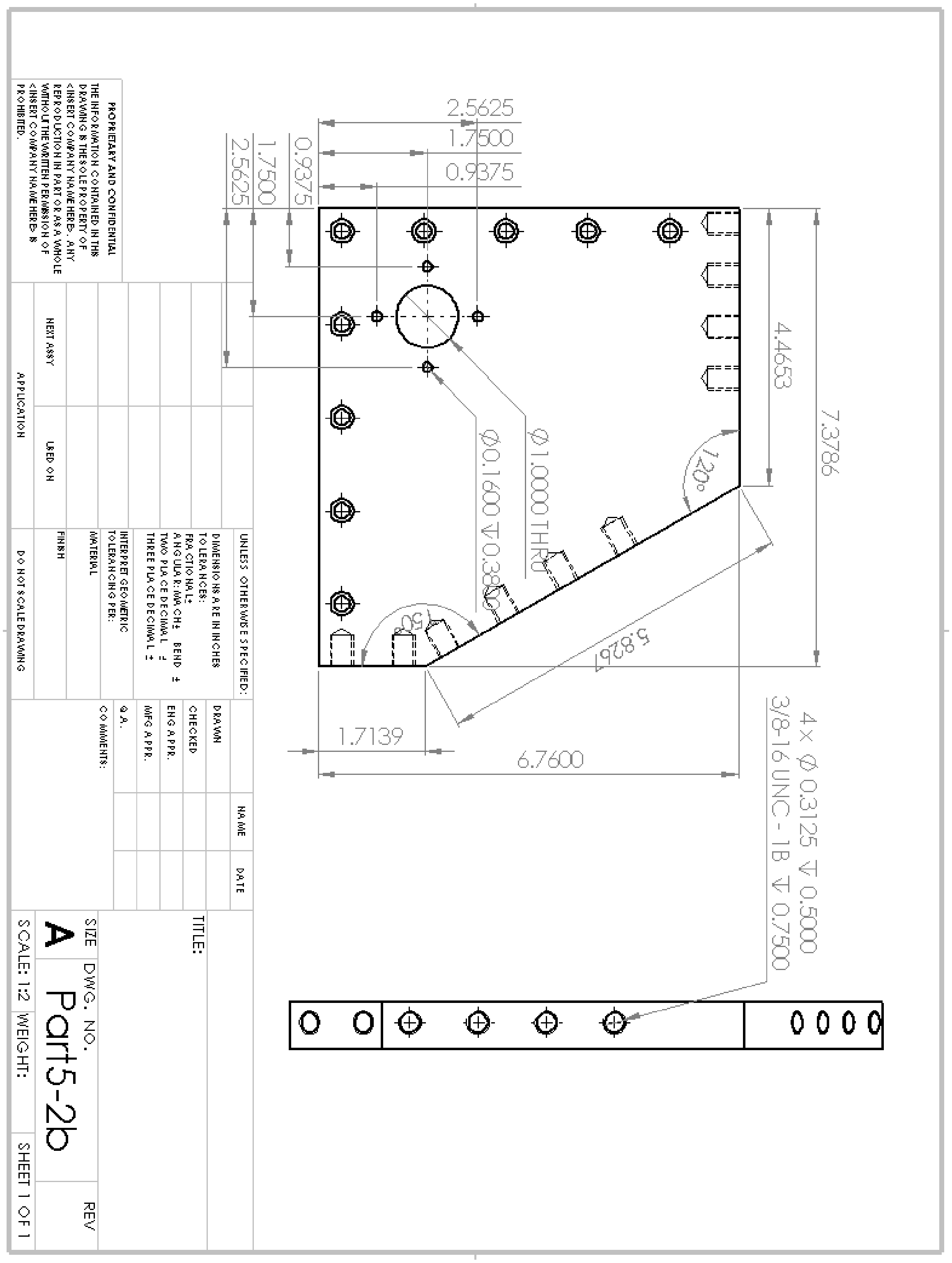

Figure I-17. Part 5-2b drawing.

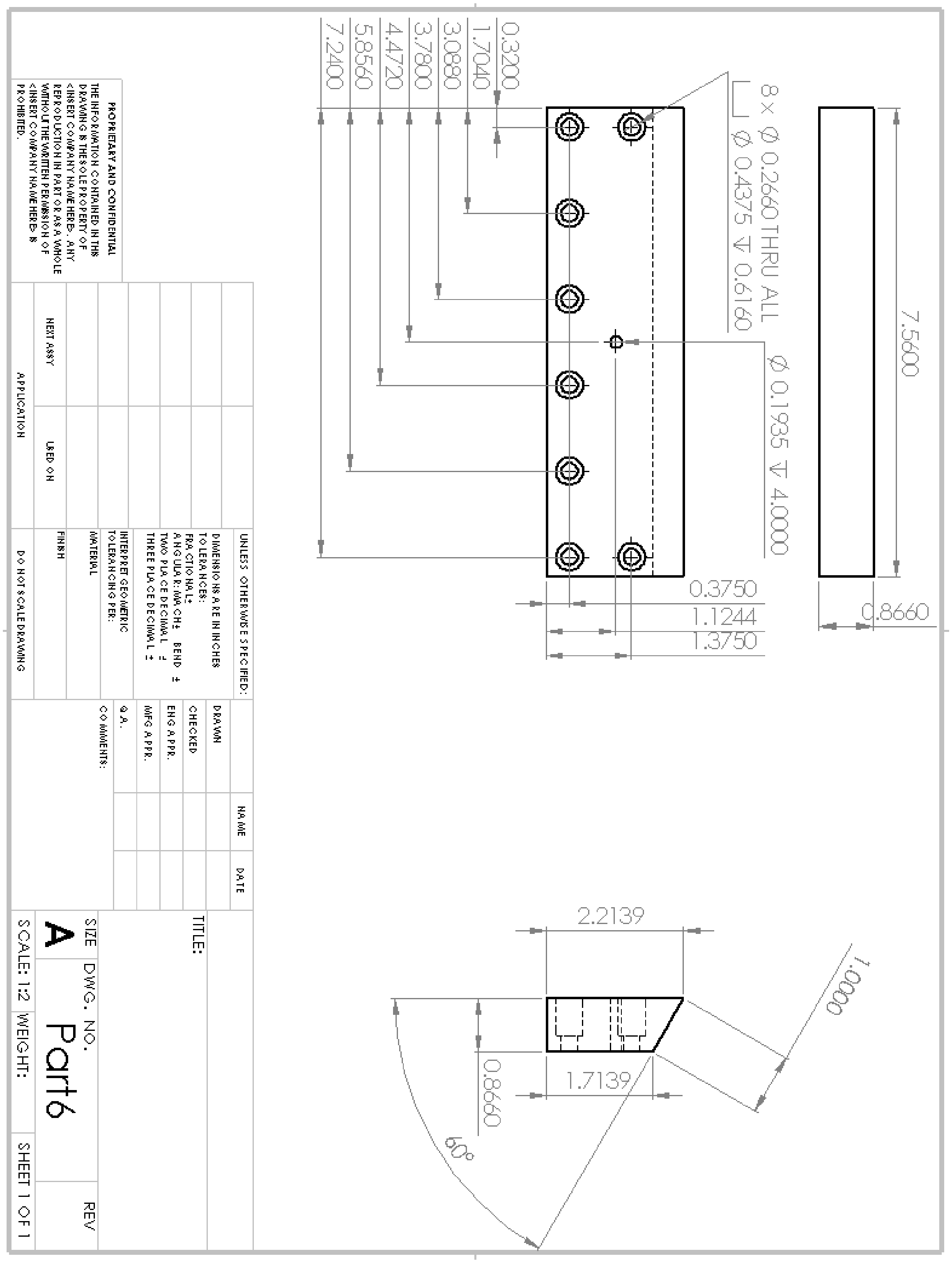

Figure I-18. Part 6 drawing.

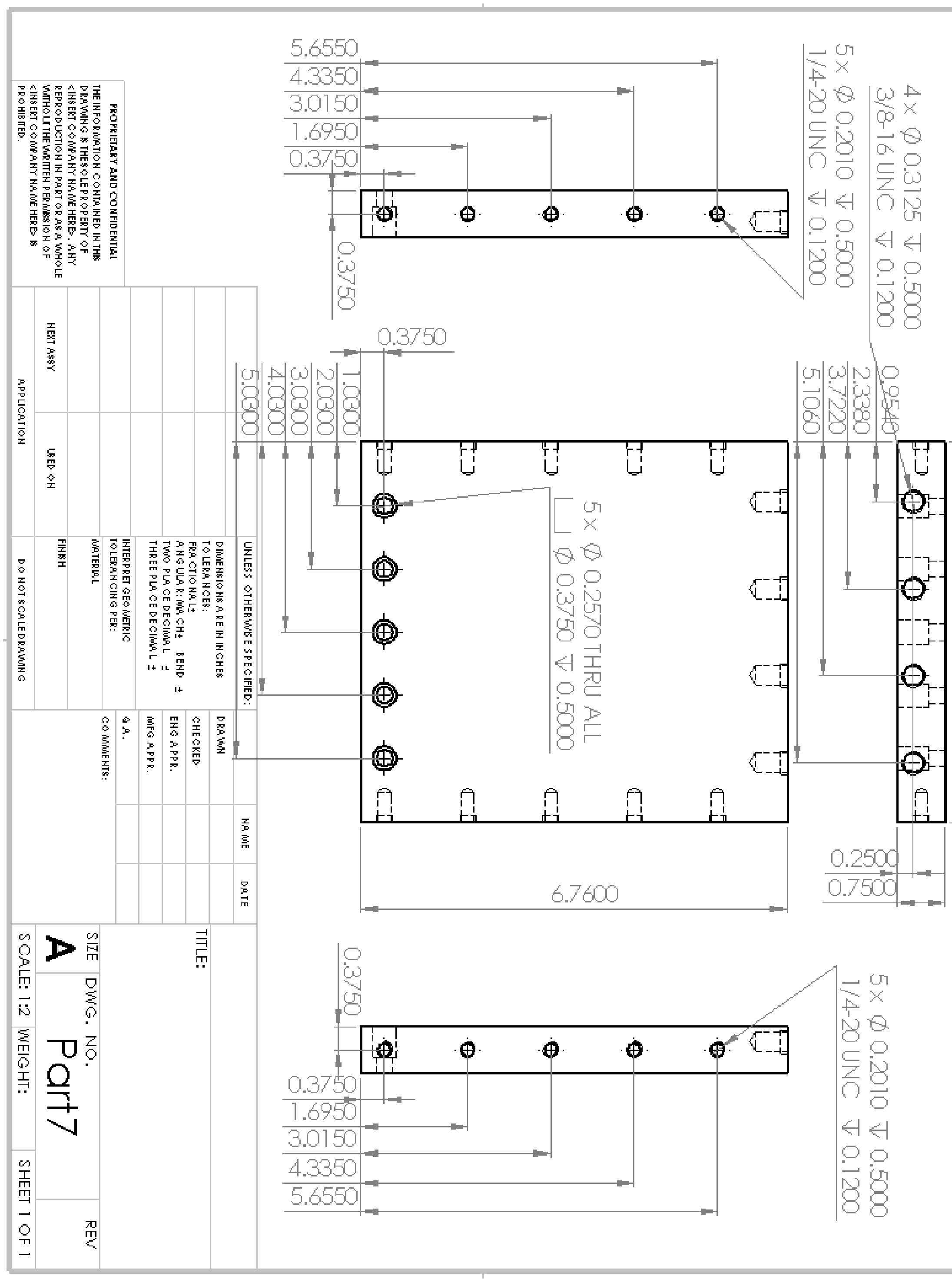

Figure I-19. Part 7 drawing.

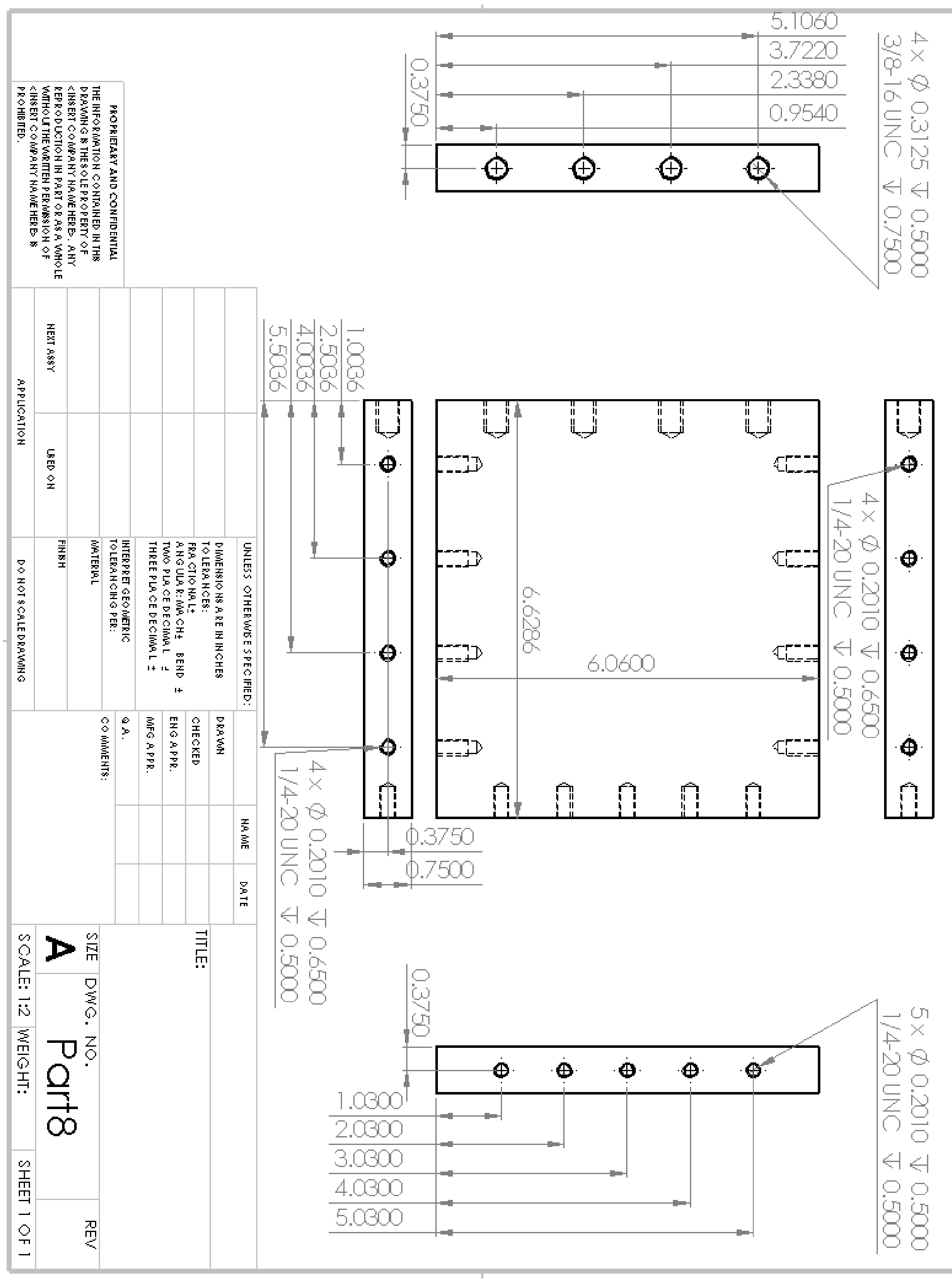

Figure I-20. Part 8 drawing.

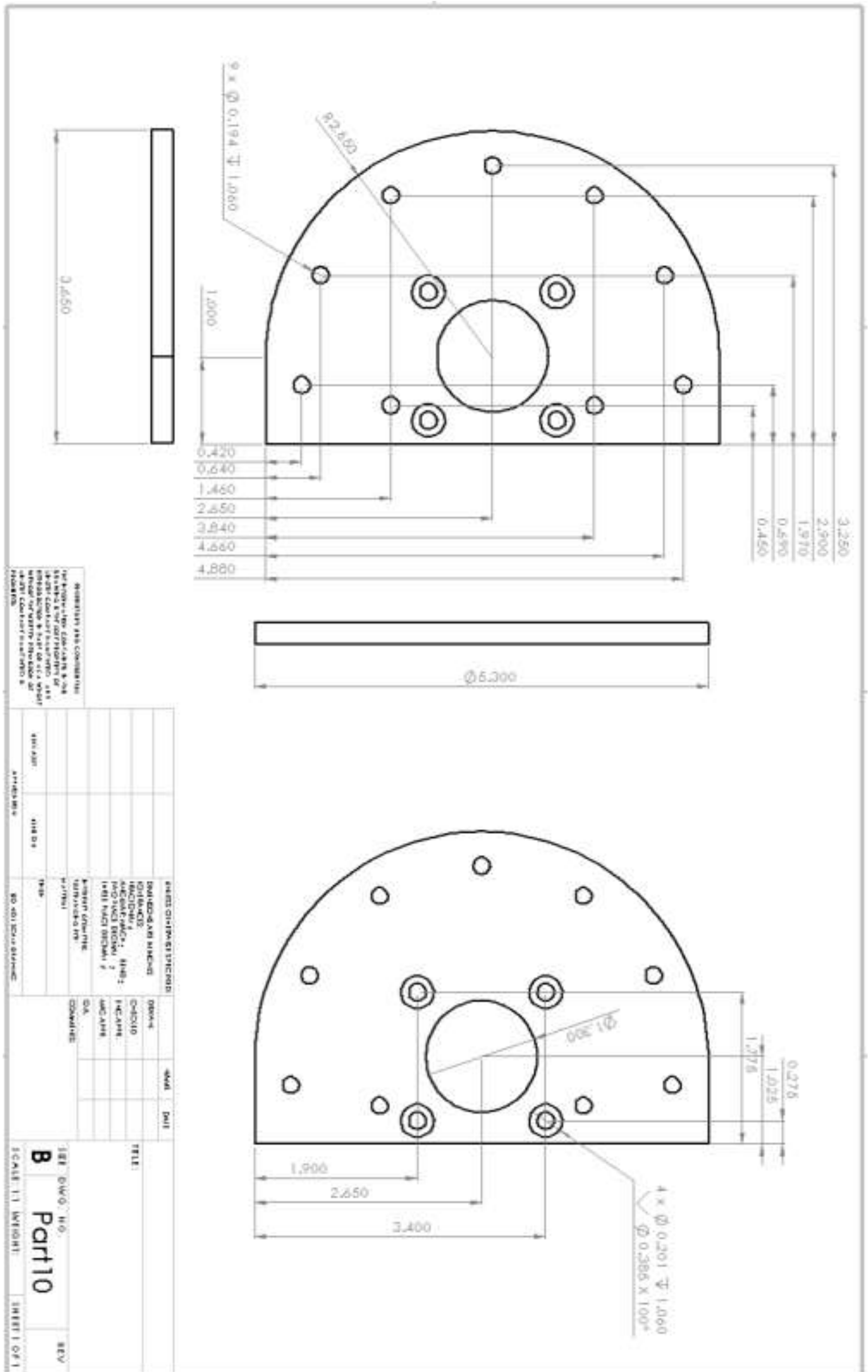

Figure I-21.   Part 10 drawing.

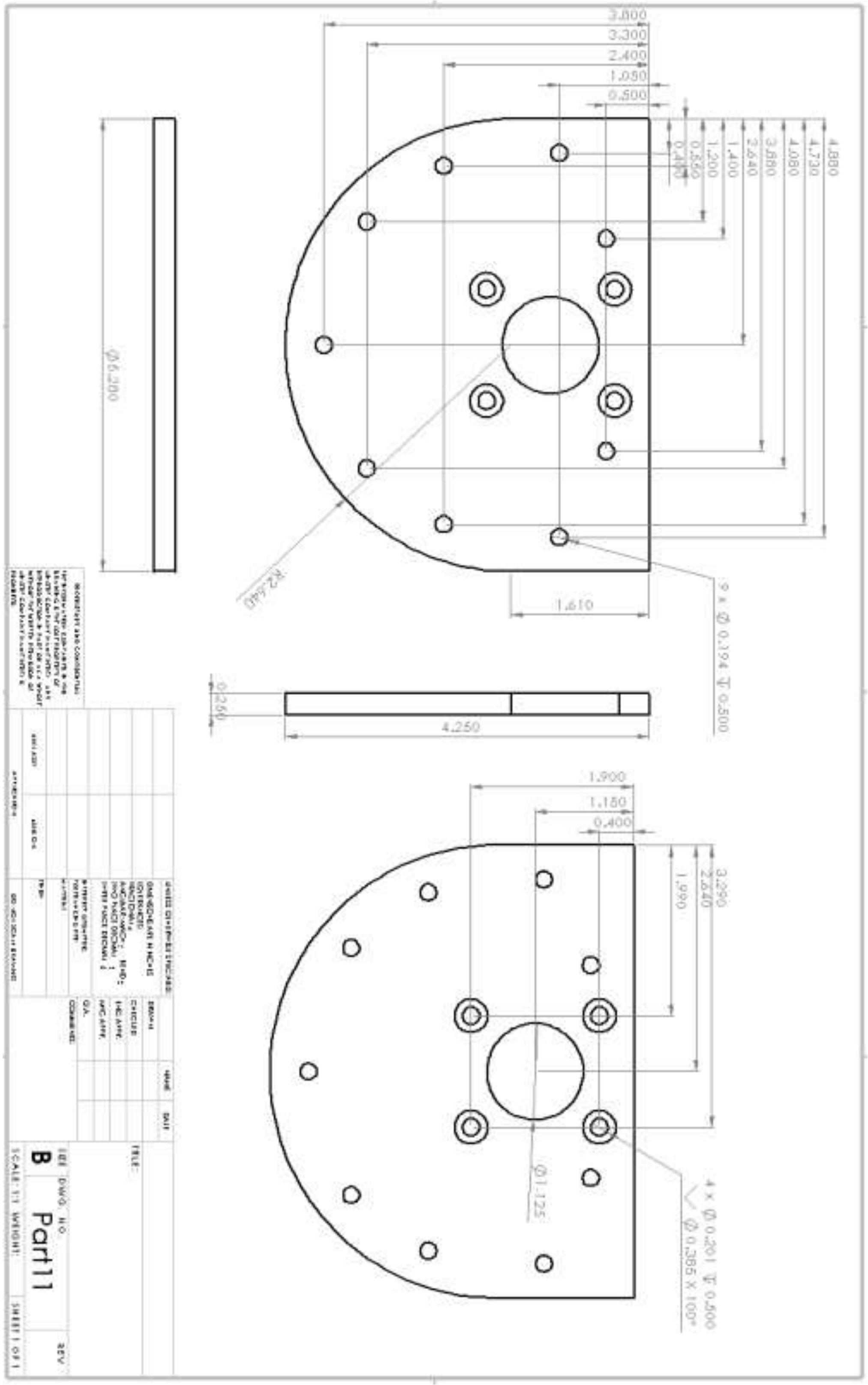

Figure I-22. Part 11 drawing.

I.2 Left Ventricle Aorto-Mitral Insert

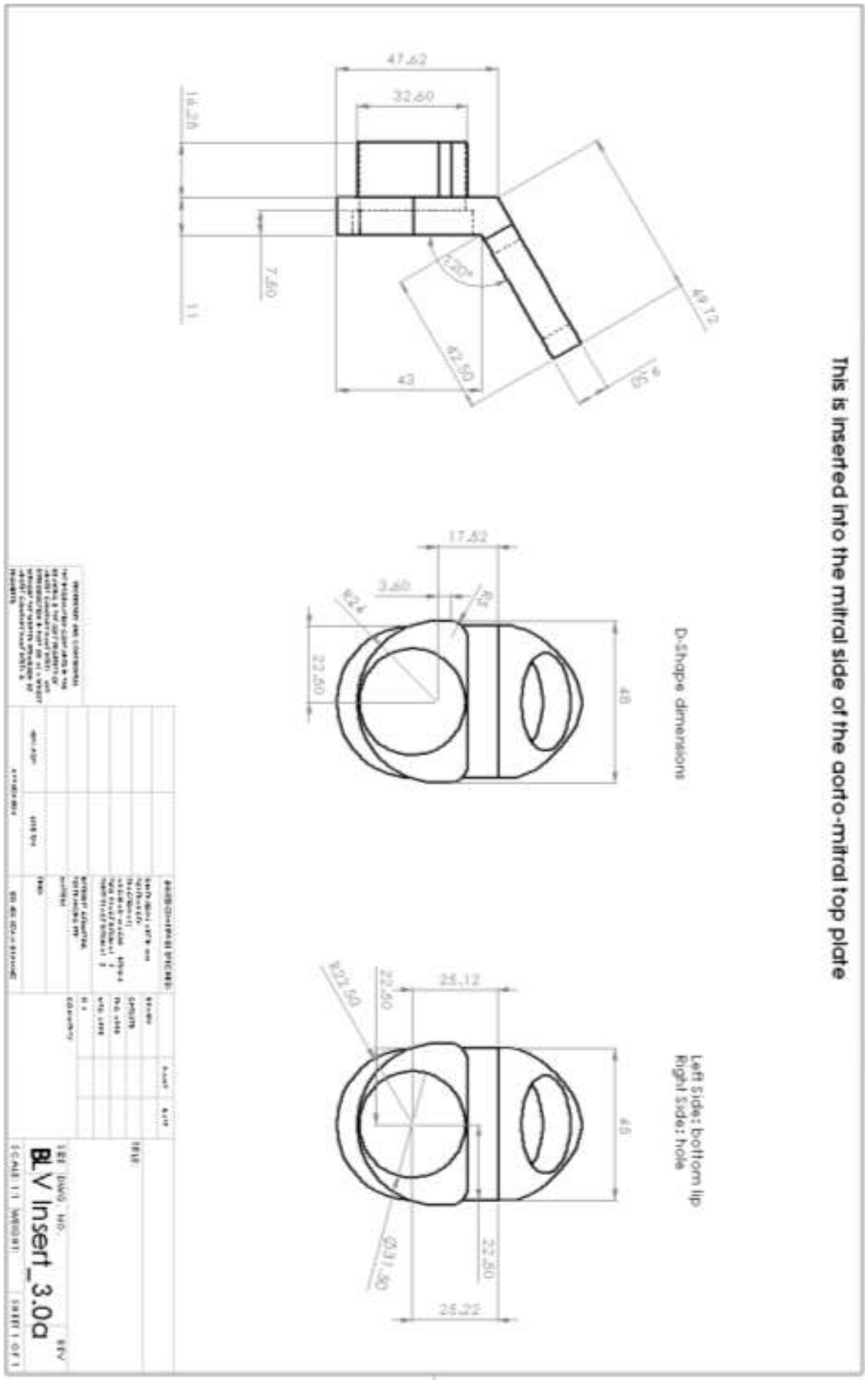

Figure I-23.   LV Insert 1a drawing.

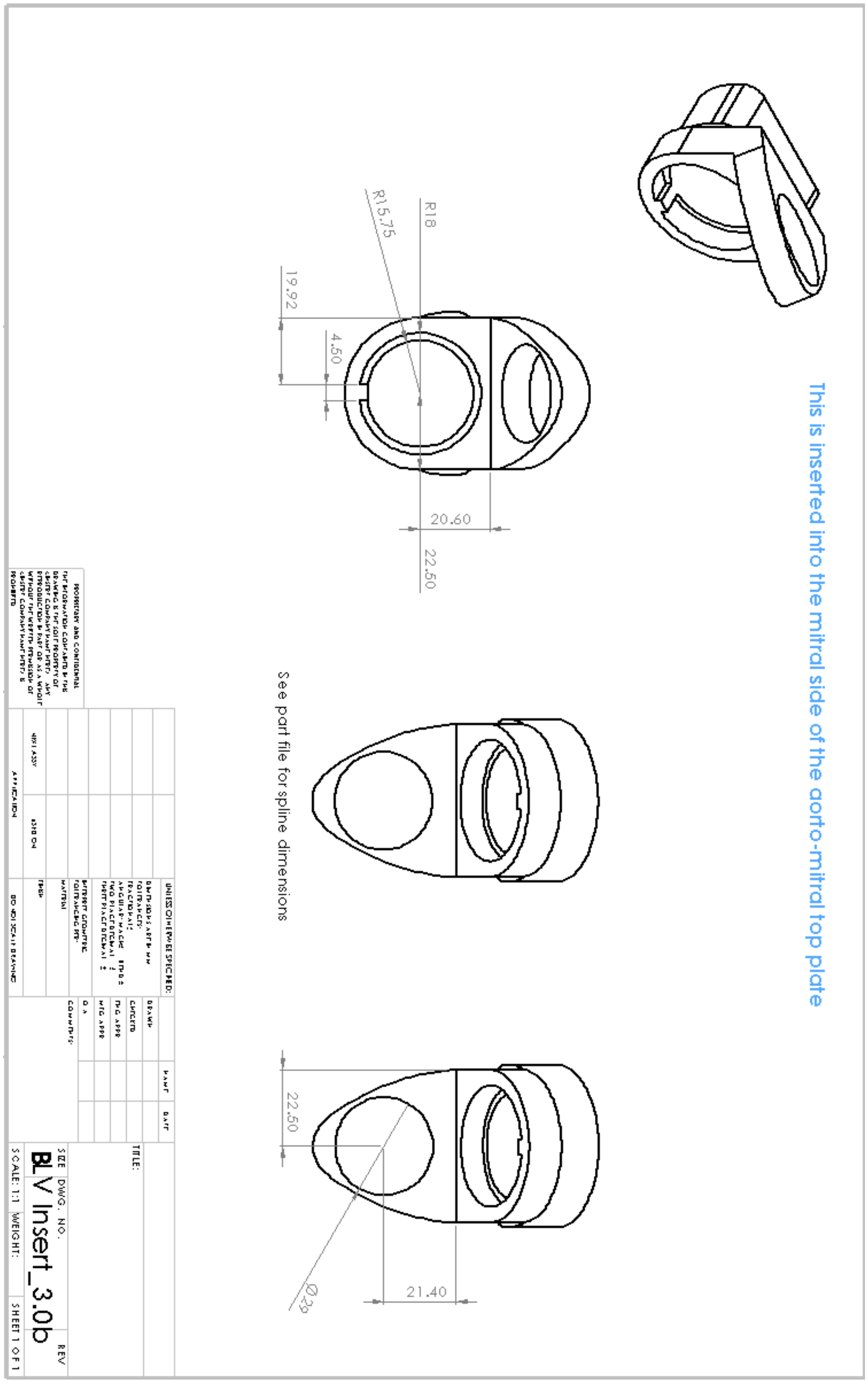

Figure I-24. LV Insert 1b drawing.

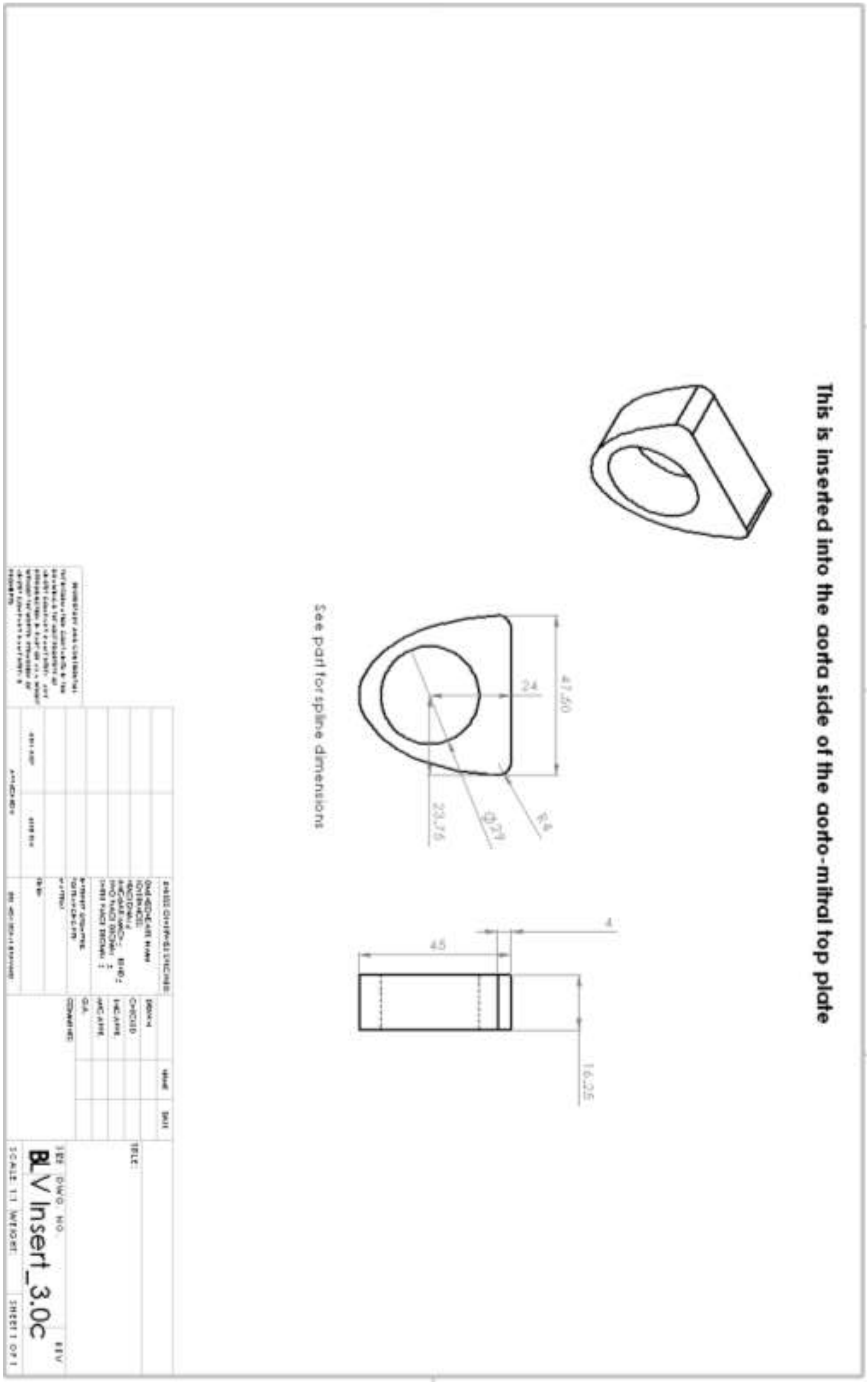

Figure I-25.   LV Insert 2 drawing.

I.3 Georgia Tech – Transcatheter Aortic Valve

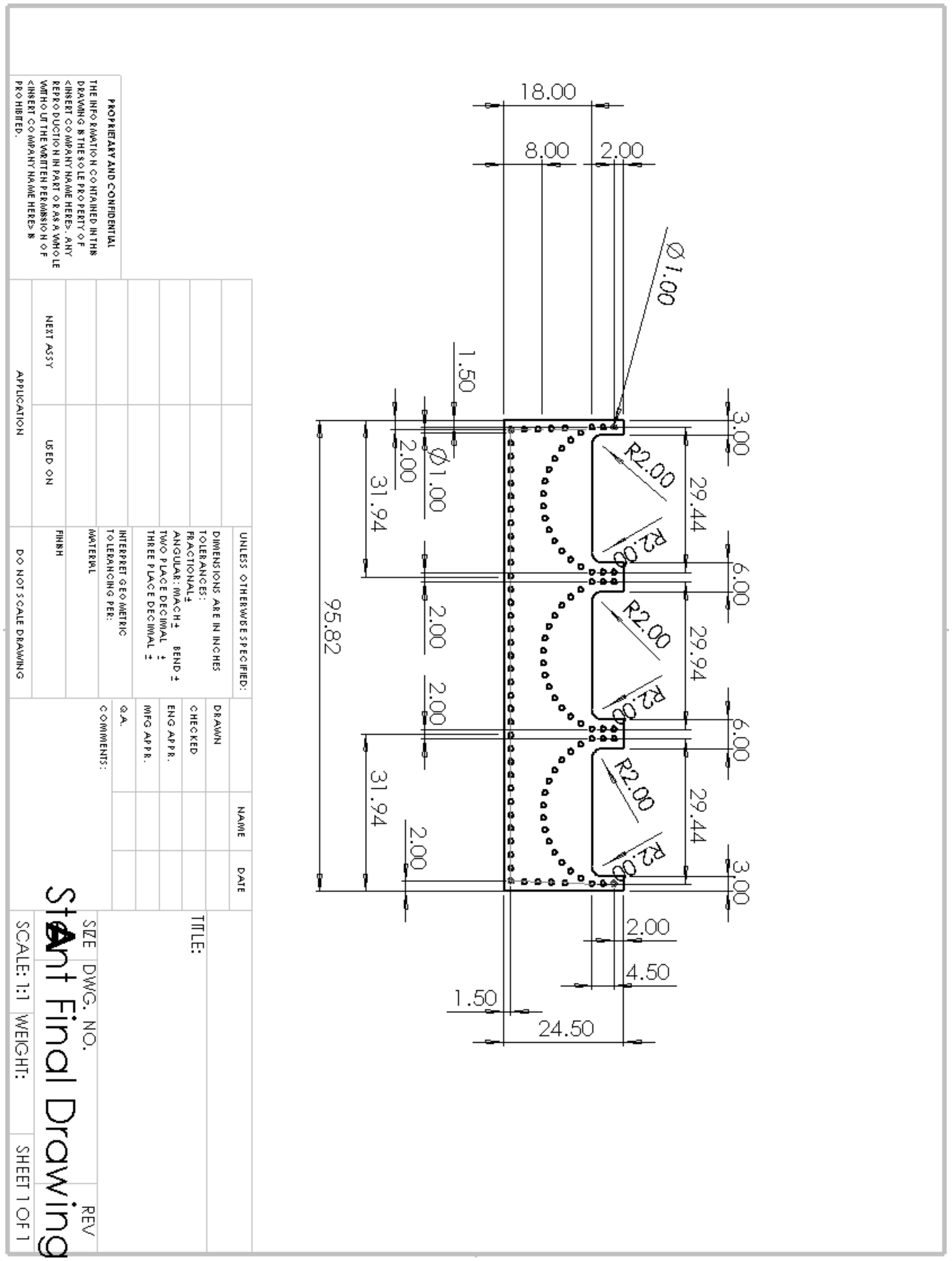

Figure I-26. 29 mm GT-TAV stent frame drawing.

APPENDIX J. LABVIEW CODES – SPECIFIC AIM 1

J.1 Dynamically Contracting Annulus.vi

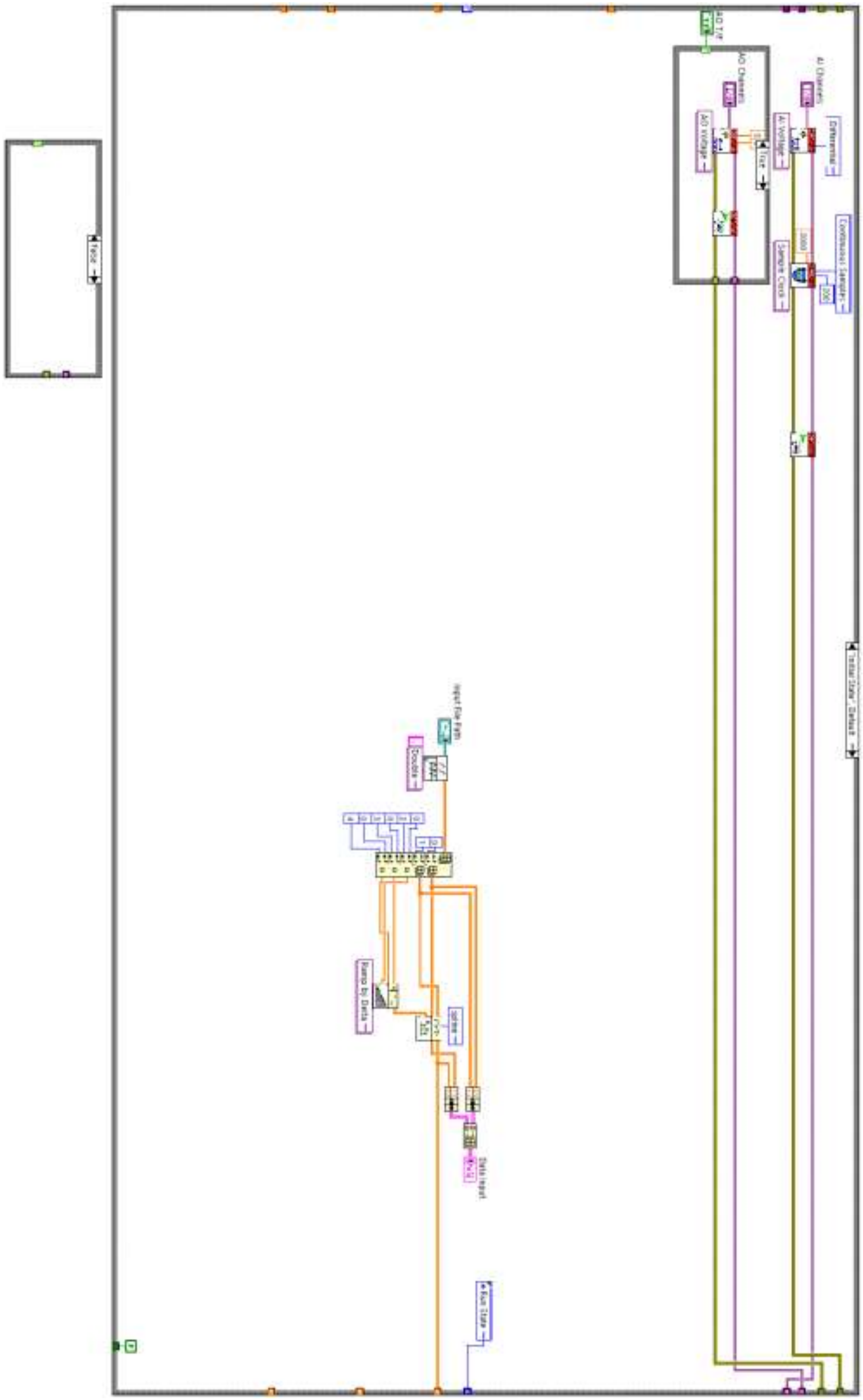

Figure J-1. Initial State of DCA LabVIEW code.

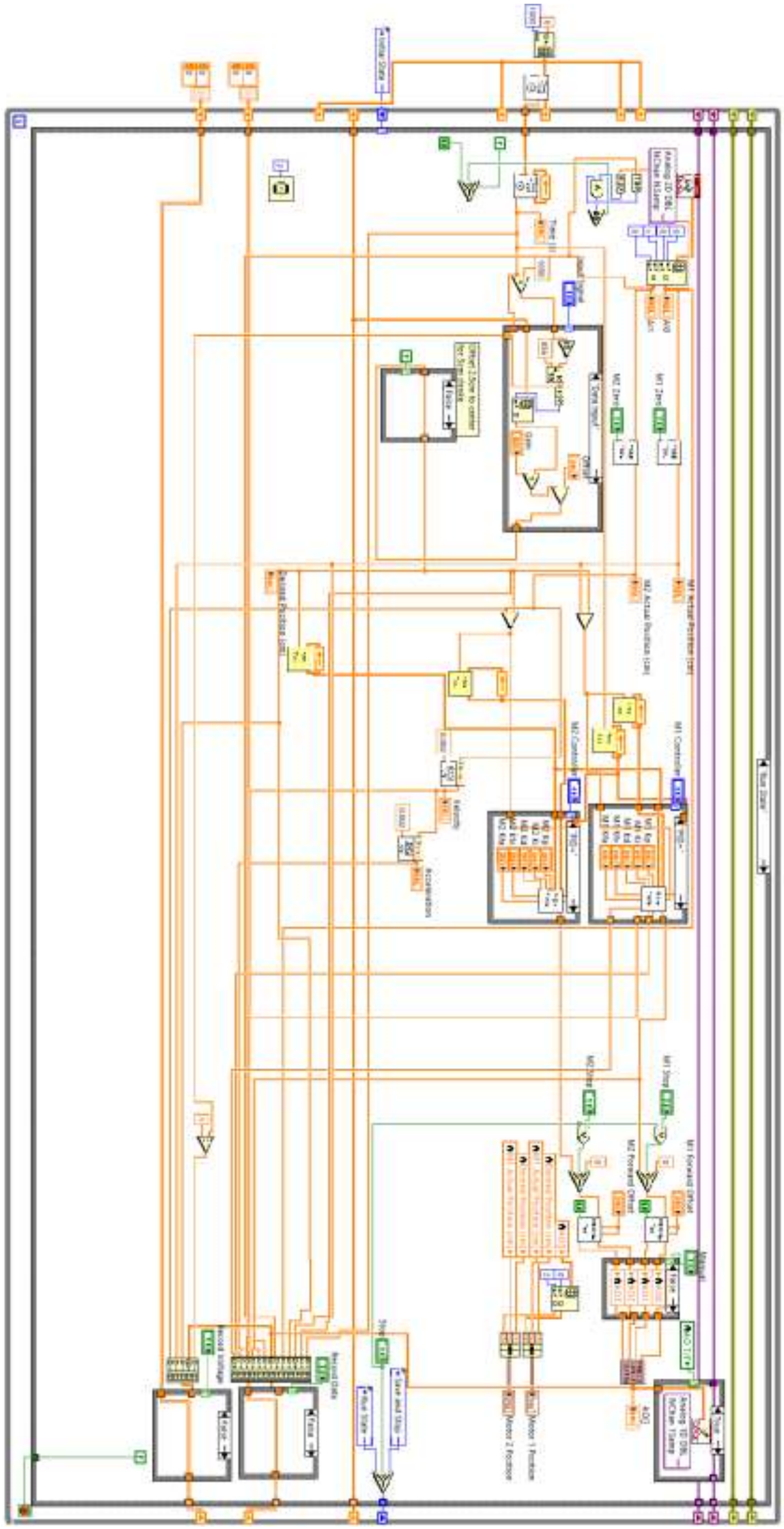

Figure J-2. Run State of DCA LabVIEW code.

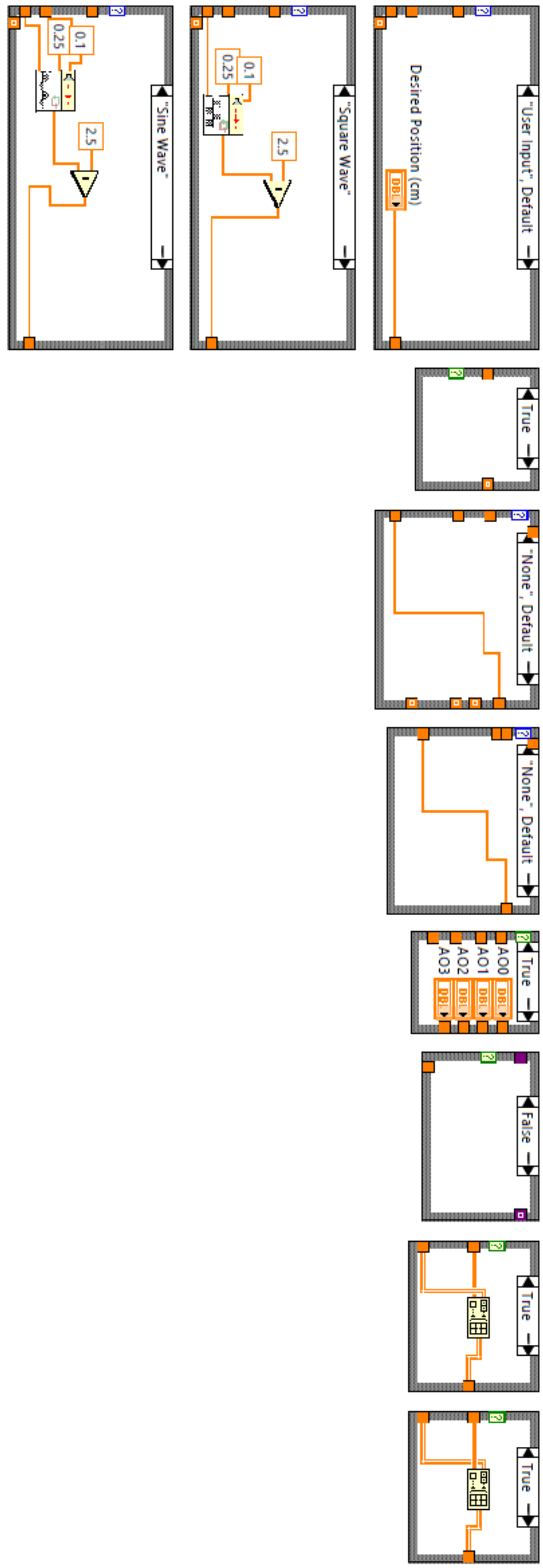

Figure J-3. Blocks within the Run State of DCA LabVIEW code.

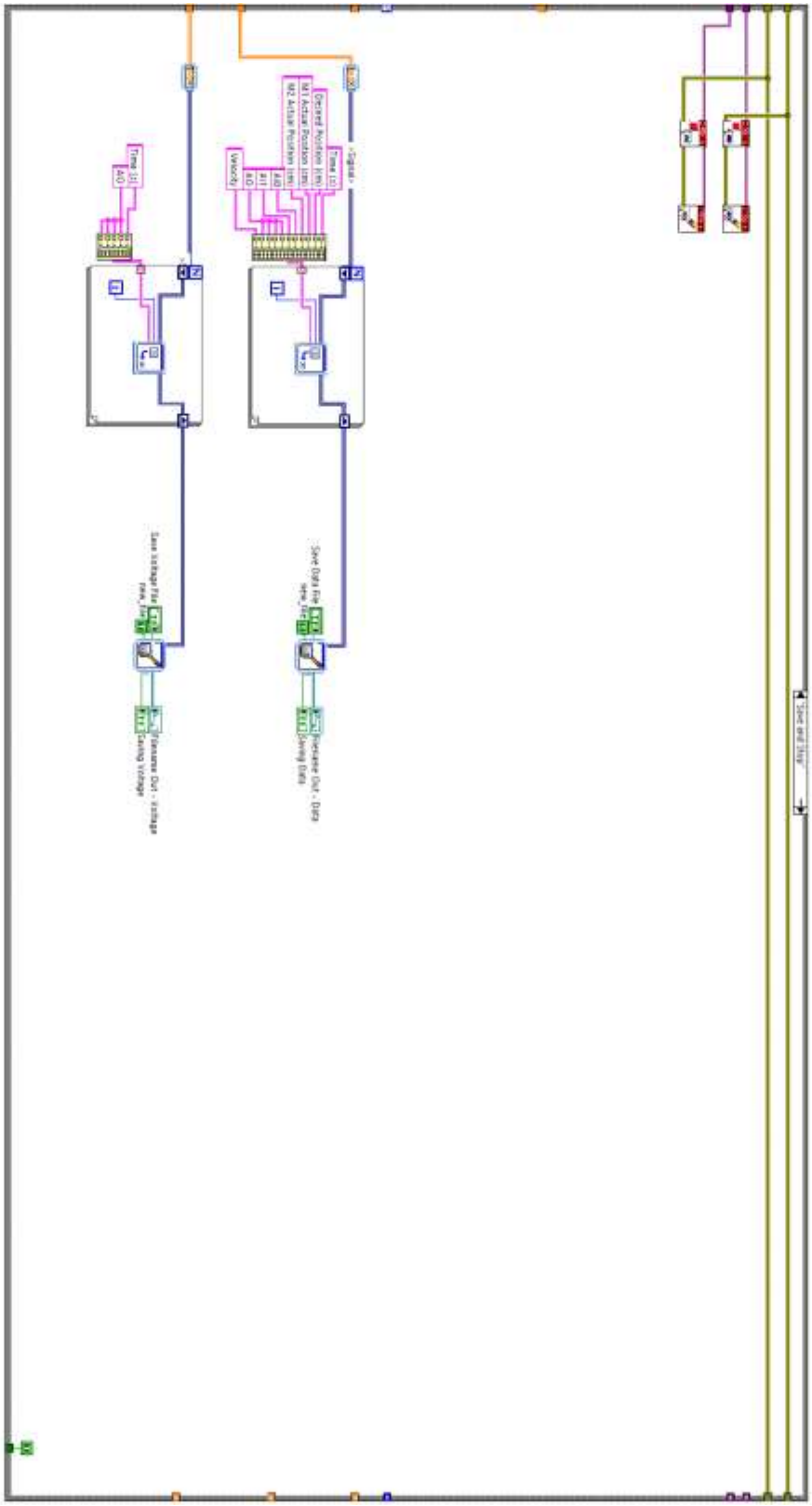

Figure J-4. Save and Stop state of the DCA LabVIEW code.

APPENDIX K. MATLAB CODES – SPECIFIC AIM 1

K.1 Datasnatch.m

```
function datasnatch
clc
clear all
close all

%Read in the file in gray scale with pixel information
img = imread('W:\Work\Work - Graduate\Work - Contracting Annulus\Input
Graphs\Gorman\Annular Area.PNG');
info = imfinfo('W:\Work\Work - Graduate\Work - Contracting
Annulus\Input Graphs\Gorman\Annular Area.PNG');
figure(1)
imshow(img);
hold on
grid on

%Input image axis' scale difference
X = 100;                                %X-scale difference
Y = 0.30;                               %Y-scale difference

%Input points of interest from image using mouse
%MATLAB reads (0,0) as the top left corner for pixels
%Click Order: xmin, xmax, ymax, ymin
[xl,y1] = ginput(2)                %Inputting x-scale
[x2,y2] = ginput(2)                %Inputting y-scale
a = 0;                             %Graph value for x1(1)
b = 0.9;                           %Graph value for y2(1)
c = xl(1)                          %x-axis pixel offset
d = y2(1)                          %y-axis pixel offset
x = X/(xl(2)-xl(1))                %cycle/pixel
y = Y/(y2(2)-y2(1))                %(cm/s)/pixel
[Px,Py] = ginput();                %Inputting graph data points
Dx = (Px*x)-(c*x)+a;
Dy = (d*y)-(Py*y)+b+Y;
Data = [Dx,Dy];                    %Snatched data
n = size(Dx)
xx = Dx(1):((Dx(n)-Dx(1))/40):Dx(n);
yy = spline(Dx,Dy,xx);
%M = mean(yy)
hold on
plot(Px,Py)
figure
plot(Dx,Dy,'o',xx,yy)

%Export data array "Data" to excel spreadsheet
filename = 'ischemic area.xlsx';
xlswrite(filename,Data,'Raw Data','B2')
warning('off','MATLAB:xlswrite:Addsheet')
```

```
hold on
```

APPENDIX L. MATLAB CODES – SPECIFIC AIM 2

L.1 BinAVG.m

```
% This code bins each cardiac cycle into 5-frame bins
% Updated by Thomas Easley on 2018/12/03 to bin average data for 20
% continuos cycles rather than 5 cycles of 4 cycles, 3 times

close all
clc

% File containing list of input files for processing
infile = 'input.txt';
fid_inp = fopen(infile,'r');

TrueImagesPerCycle = 602;
NumCyclesAcquired = 20;
BinWidth = 5;
ImagesPerCycle = floor(TrueImagesPerCycle/BinWidth)*BinWidth;

CardiacCycleLength = 0.856;
TimeStep = CardiacCycleLength/(ImagesPerCycle/BinWidth);

while ~feof(fid_inp)
    folder0 = fgetl(fid_inp);
%    folder1 = fgetl(fid_inp);
%    folder2 = fgetl(fid_inp);
%    folder3 = fgetl(fid_inp);


    cd(folder0)
    %%% Seperate 20 cycles individually. Since one cycle is 600 frames,
    %%% cycle 1= the first 600 vc7 files, the cycle two is the next and
so
    %%% forth
    VelField1 = loadvec(sprintf('B[%d:%d]*.vc7', 1, ImagesPerCycle));
    VelField2 = loadvec(sprintf('B[%d:%d]*.vc7',
(TrueImagesPerCycle+1), TrueImagesPerCycle+ImagesPerCycle));
    VelField3 = loadvec(sprintf('B[%d:%d]*.vc7',
(2*TrueImagesPerCycle+1), (2*TrueImagesPerCycle)+ImagesPerCycle));
    VelField4 = loadvec(sprintf('B[%d:%d]*.vc7',
(3*TrueImagesPerCycle+1), (3*TrueImagesPerCycle)+ImagesPerCycle));
    VelField5 = loadvec(sprintf('B[%d:%d]*.vc7',
(4*TrueImagesPerCycle+1), (4*TrueImagesPerCycle)+ImagesPerCycle));
    VelField6 = loadvec(sprintf('B[%d:%d]*.vc7',
(5*TrueImagesPerCycle+1), (5*TrueImagesPerCycle)+ImagesPerCycle));
    VelField7 = loadvec(sprintf('B[%d:%d]*.vc7',
(6*TrueImagesPerCycle+1), (6*TrueImagesPerCycle)+ImagesPerCycle));
    VelField8 = loadvec(sprintf('B[%d:%d]*.vc7',
(7*TrueImagesPerCycle+1), (7*TrueImagesPerCycle)+ImagesPerCycle));
```

```
    VelField9 = loadvec(sprintf('B[%d:%d]*.vc7',
(8*TrueImagesPerCycle+1), (8*TrueImagesPerCycle)+ImagesPerCycle));
    VelField10 = loadvec(sprintf('B[%d:%d]*.vc7',
(9*TrueImagesPerCycle+1), (9*TrueImagesPerCycle)+ImagesPerCycle));
    VelField11 = loadvec(sprintf('B[%d:%d]*.vc7',
(10*TrueImagesPerCycle+1), (10*TrueImagesPerCycle)+ImagesPerCycle));
    VelField12 = loadvec(sprintf('B[%d:%d]*.vc7',
(11*TrueImagesPerCycle+1), (11*TrueImagesPerCycle)+ImagesPerCycle));
    VelField13 = loadvec(sprintf('B[%d:%d]*.vc7',
(12*TrueImagesPerCycle+1), (12*TrueImagesPerCycle)+ImagesPerCycle));
    VelField14 = loadvec(sprintf('B[%d:%d]*.vc7',
(13*TrueImagesPerCycle+1), (13*TrueImagesPerCycle)+ImagesPerCycle));
    VelField15 = loadvec(sprintf('B[%d:%d]*.vc7',
(14*TrueImagesPerCycle+1), (14*TrueImagesPerCycle)+ImagesPerCycle));
    VelField16 = loadvec(sprintf('B[%d:%d]*.vc7',
(15*TrueImagesPerCycle+1), (15*TrueImagesPerCycle)+ImagesPerCycle));
    VelField17 = loadvec(sprintf('B[%d:%d]*.vc7',
(16*TrueImagesPerCycle+1), (16*TrueImagesPerCycle)+ImagesPerCycle));
    VelField18 = loadvec(sprintf('B[%d:%d]*.vc7',
(17*TrueImagesPerCycle+1), (17*TrueImagesPerCycle)+ImagesPerCycle));
    VelField19 = loadvec(sprintf('B[%d:%d]*.vc7',
(18*TrueImagesPerCycle+1), (18*TrueImagesPerCycle)+ImagesPerCycle));
    VelField20 = loadvec(sprintf('B[%d:%d]*.vc7',
(19*TrueImagesPerCycle+1), (19*TrueImagesPerCycle)+ImagesPerCycle));

%     cd(folder2)
%     VelField4 = loadvec(sprintf('B[%d:%d]*.vc7', 1, ImagesPerCycle));
%     VelField5 = loadvec(sprintf('B[%d:%d]*.vc7',
(TrueImagesPerCycle+1), TrueImagesPerCycle+ImagesPerCycle));
%     VelField6 = loadvec(sprintf('B[%d:%d]*.vc7',
(2*TrueImagesPerCycle+1), (2*TrueImagesPerCycle)+ImagesPerCycle));
%
%     cd(folder3)
%     VelField7 = loadvec(sprintf('B[%d:%d]*.vc7', 1, ImagesPerCycle));
%     VelField8 = loadvec(sprintf('B[%d:%d]*.vc7',
(TrueImagesPerCycle+1), TrueImagesPerCycle+ImagesPerCycle));
%     VelField9 = loadvec(sprintf('B[%d:%d]*.vc7',
(2*TrueImagesPerCycle+1), (2*TrueImagesPerCycle)+ImagesPerCycle));

%     VelField1 = loadvec(sprintf('%s/B[%d:%d]*.vc7',folder1, 1,
ImagesPerCycle));
%     VelField2 = loadvec(sprintf('%s/B[%d:%d]*.vc7',folder1,
(TrueImagesPerCycle+1), TrueImagesPerCycle+ImagesPerCycle));
%     VelField3 = loadvec(sprintf('%s/B[%d:%d]*.vc7',folder1,
(2*TrueImagesPerCycle+1), (2*TrueImagesPerCycle)+ImagesPerCycle));
%     VelField4 = loadvec(sprintf('%s/B[%d:%d]*.vc7',folder2, 1,
ImagesPerCycle));
%     VelField5 = loadvec(sprintf('%s/B[%d:%d]*.vc7',folder2,
(TrueImagesPerCycle+1), TrueImagesPerCycle+ImagesPerCycle));
%     VelField6 = loadvec(sprintf('%s/B[%d:%d]*.vc7',folder2,
(2*TrueImagesPerCycle+1), (2*TrueImagesPerCycle)+ImagesPerCycle));
%     VelField7 = loadvec(sprintf('%s/B[%d:%d]*.vc7',folder3, 1,
ImagesPerCycle));
%     VelField8 = loadvec(sprintf('%s/B[%d:%d]*.vc7',folder3,
(TrueImagesPerCycle+1), TrueImagesPerCycle+ImagesPerCycle));
```

```
%     VelField9 = loadvec(sprintf('%s/B[%d:%d]*.vc7',folder3,
(2*TrueImagesPerCycle+1), (2*TrueImagesPerCycle)+ImagesPerCycle));
%
    NumBins = length(VelField1)/BinWidth;
    NumBins20 = length(VelField20)/BinWidth;

    %Initializing BinAvg Fields
    BinAvg1 = VelField1(1:NumBins);
    BinAvg2 = VelField2(1:NumBins);
    BinAvg3 = VelField3(1:NumBins);
    BinAvg4 = VelField4(1:NumBins);
    BinAvg5 = VelField5(1:NumBins);
    BinAvg6 = VelField6(1:NumBins);
    BinAvg7 = VelField7(1:NumBins);
    BinAvg8 = VelField8(1:NumBins);
    BinAvg9 = VelField9(1:NumBins);
    BinAvg10 = VelField10(1:NumBins);
    BinAvg11 = VelField11(1:NumBins);
    BinAvg12 = VelField12(1:NumBins);
    BinAvg13 = VelField13(1:NumBins);
    BinAvg14 = VelField14(1:NumBins);
    BinAvg15 = VelField15(1:NumBins);
    BinAvg16 = VelField16(1:NumBins);
    BinAvg17 = VelField17(1:NumBins);
    BinAvg18 = VelField18(1:NumBins);
    BinAvg19 = VelField19(1:NumBins);
    BinAvg20 = VelField20(1:NumBins);

    %Initializing PhaseAvg matrix

    for i = 1:NumBins
        BinAvg1(i) = averf(VelField1(((BinWidth*i-(BinWidth-
1)):(BinWidth*i))));
        BinAvg2(i) = averf(VelField2(((BinWidth*i-(BinWidth-
1)):(BinWidth*i))));
        BinAvg3(i) = averf(VelField3(((BinWidth*i-(BinWidth-
1)):(BinWidth*i))));
        BinAvg4(i) = averf(VelField4(((BinWidth*i-(BinWidth-
1)):(BinWidth*i))));
        BinAvg5(i) = averf(VelField5(((BinWidth*i-(BinWidth-
1)):(BinWidth*i))));
        BinAvg6(i) = averf(VelField6(((BinWidth*i-(BinWidth-
1)):(BinWidth*i))));
        BinAvg7(i) = averf(VelField7(((BinWidth*i-(BinWidth-
1)):(BinWidth*i))));
        BinAvg8(i) = averf(VelField8(((BinWidth*i-(BinWidth-
1)):(BinWidth*i))));
        BinAvg9(i) = averf(VelField9(((BinWidth*i-(BinWidth-
1)):(BinWidth*i))));
        BinAvg10(i) = averf(VelField10(((BinWidth*i-(BinWidth-
1)):(BinWidth*i))));
        BinAvg11(i) = averf(VelField11(((BinWidth*i-(BinWidth-
1)):(BinWidth*i))));
        BinAvg12(i) = averf(VelField12(((BinWidth*i-(BinWidth-
1)):(BinWidth*i))));
```

```
        BinAvg13(i) = averf(VelField13(((BinWidth*i-(BinWidth-
1)):(BinWidth*i))));
        BinAvg14(i) = averf(VelField14(((BinWidth*i-(BinWidth-
1)):(BinWidth*i))));
        BinAvg15(i) = averf(VelField15(((BinWidth*i-(BinWidth-
1)):(BinWidth*i))));
        BinAvg16(i) = averf(VelField16(((BinWidth*i-(BinWidth-
1)):(BinWidth*i))));
        BinAvg17(i) = averf(VelField17(((BinWidth*i-(BinWidth-
1)):(BinWidth*i))));
        BinAvg18(i) = averf(VelField18(((BinWidth*i-(BinWidth-
1)):(BinWidth*i))));
        BinAvg19(i) = averf(VelField19(((BinWidth*i-(BinWidth-
1)):(BinWidth*i))));
        BinAvg20(i) = averf(VelField20(((BinWidth*i-(BinWidth-
1)):(BinWidth*i))));

    end

    TotBinAvg = [BinAvg1, BinAvg2, BinAvg3, BinAvg4, BinAvg5, BinAvg6,
BinAvg7, BinAvg8, BinAvg9, BinAvg10, BinAvg11, BinAvg12, BinAvg13,
BinAvg14, BinAvg15, BinAvg16, BinAvg17, BinAvg18, BinAvg19, BinAvg20];


    [m,n] = size(TotBinAvg(1).vx);
    sz = m*n;
    DatExportX = zeros(sz,1);
    DatExportY = zeros(sz,1);
    DatExportVX = zeros(sz,1);
    DatExportVY = zeros(sz,1);


    %% EXPORT BIN AVERAGED DATA TO DAT

    h = waitbar(0);
    tic

    for t = 1:length(TotBinAvg)
        counter = 1;
        for j = 1:n
            for i = 1:m
                DatExportX(counter) = TotBinAvg(t).x(i);
                DatExportY(counter) = TotBinAvg(t).y(j);
                DatExportVX(counter) = TotBinAvg(t).vx(i,j);
                DatExportVY(counter) = TotBinAvg(t).vy(i,j);
                counter = counter + 1;
            end
        end

        %Export DatExport from (t*NumBins-NumBins+1):(t*NumBins)
        if isempty(dir(sprintf('%s/BinAVG',folder0)))         %if the
directory doesn't exist, make it
            mkdir(sprintf('%s/BinAVG',folder0));
        end
```

```
        fid2 = fopen(sprintf('%s/BinAVG\\T=%04d.dat',folder0,t),'w');
        fprintf(fid2,'%s %s %s\n','TITLE = "T =
',sprintf('%04d',t),'"');
        fprintf(fid2,'%s\n','VARIABLES = "X (m)", "Y (m)", "U (m/s)",
"V (m/s)"');
        fprintf(fid2,'%s %s %s %d %s %d\n','ZONE T="T =
',sprintf('%04d',t),'", I=',m, 'J=',n);
        tot = m*n;
        for l = 1:tot
            fprintf(fid2,'%8.6f %8.6f %8.6f
%8.6f\n',DatExportX(l)/1000,DatExportY(l)/1000,DatExportVX(l),DatExport
VY(l));
        end
        fclose(fid2);
        progress = (t/(length(TotBinAvg)));
        time_elapsed = toc;
        time_remaining = (1-progress)*(time_elapsed/progress)/60;
        waitbar(progress, h,['Time Remaining: ',
num2str(time_remaining),'min'], 'Name', num2str(progress*100));
    end
    close(h);
end
fclose(fid_inp);
```

L.2 ScalingData.m

```
%% Copies and organizes files: orders them by frame and puts all cycles
togethers

close all
clear
clc

%%
datafolder =
'I:\Data\SA2B\HSPIV\FLAIL8020\20181207_Flail8020_50Per_Neo\6.5_700hz\Ma
skOutImage_01\SubOverTimeMin_sL=5\TR_PIV_MPd(5x16x16_50%ov_ImgCorr)_GPU
\PostProc\BinAVG_703Hz'...
    ;                                              %folder containing PIV
data
outputfolder = '%s/Scaled';                        %folder containing
output folders
outputfolderroot = 'Scaled';                       %folder containing
output data
inroot = 'T=';                                     %input filename prefix
outroot = 'Ts=';                                   %output filename prefix
numformat = '%04d';                                %total digits in
numbering
fileextension = '.dat';                            %file type
firstf = 1;                                        %first file number
lastf = 2400;                                      %last file number
```

```
incrementf = 1;                                  %increments between
files
%xfactor = 0.9541985;                                     %0x-axis
scaling factor
%yfactor = 1.0087719;                                     %0y-axis
scaling factor
xfactor = 0.7668712;                                     %50x-axis
scaling factor
yfactor = 0.858209;                                      %50y-axis
scaling factor
%xfactor = 0.8081897;                                     %100x-axis
scaling factor
%yfactor = 1.124031;                                      %100y-axis
scaling factor
%%
cd(datafolder)
myfolder = sprintf(outputfolder,datafolder);
if isempty(dir(myfolder))          %if the directory doesn't exist, make
it
   mkdir(myfolder);
end

NumHeaderLines = 3;                              %number of headerlines
to skip
NumCols = 4;
initialize = 1;
lengthf = (lastf-firstf+1)/incrementf;

h = waitbar(0);
    tic

for FileNum = firstf:incrementf:lastf
    u = sprintf(numformat,FileNum);
    infilenumformat = strcat(inroot,u,fileextension);
    outfilenumformat =
strcat(outputfolderroot,'\\',outroot,u,fileextension);

    %open .dat file
    fid = fopen(infilenumformat,'r');

    InputText = textscan(fid,'%s',NumHeaderLines,'delimiter','\n');

    if initialize == 1;
        temp = InputText{1};
        RowThree = temp(3);
        SplitRow = strsplit(RowThree{1});
        m = str2num(SplitRow{7});
        n = str2num(SplitRow{9});
        DataLength = m*n;
        RawData = zeros(DataLength,NumCols);
        ScaledData = zeros(DataLength,NumCols);
        initialize = 0;
    end

    %Create format string based on parameter
```

```
    FormatString = repmat('%f',1,NumCols);

    %Read Original Data
    RawData(:,:) =
cell2mat(textscan(fid,FormatString,'delimiter',','));

    fclose(fid);

    %Scaled Data
    ScaledData(:,1) = RawData(:,1)*xfactor; %X
    ScaledData(:,2) = RawData(:,2)*yfactor; %Y
    ScaledData(:,3) = RawData(:,3)*xfactor; %VX
    ScaledData(:,4) = RawData(:,4)*yfactor; %VY


    %EXPORT TO DAT
    DatExportX = ScaledData(:,1);
    DatExportY = ScaledData(:,2);
    DatExportVX = ScaledData(:,3);
    DatExportVY = ScaledData(:,4);

    fid2 = fopen(outfilenumformat,'w');
    fprintf(fid2,'%s %s %s\n','TITLE = "T =
',sprintf('%04d',FileNum),'"');
    fprintf(fid2,'%s\n','VARIABLES = "X (m)", "Y (m)", "U (m/s)", "V
(m/s)"');
    fprintf(fid2,'%s %s %s %d %s %d\n','ZONE T="T =
',sprintf('%04d',FileNum),'", I=',m, 'J=',n);
    for L = 1:DataLength
        fprintf(fid2,'%8.6f %8.6f %8.6f
%8.6f\n',DatExportX(L),DatExportY(L),DatExportVX(L),DatExportVY(L));
    end
    fclose(fid2);

    %progress bar
    progress = (FileNum/lengthf);
    time_elapsed = toc;
    time_remaining = (1-progress)*(time_elapsed/progress)/60;
    waitbar(progress, h,['Time Remaining: ',
num2str(time_remaining),'min'], 'Name', num2str(progress*100));
end
close(h);
toc
```

L.3 PhaseAvgBinnedData.m

```
%% Input files for this script must be bin averaged .dat files
%% clear workspace
clear
clc
```

```matlab
%% input parameters
NumCycles = 20;
TotalBins = 2400;

%% Read Bin Averaged Data
NumBins = TotalBins/NumCycles;
NumHeaderLines = 3;
NumCols = 4;
initialize = 1;

for FileNum = 1:TotalBins
    fid = fopen(strcat('Ts=',sprintf('%04d',FileNum),'.dat'),'r');
    InputText = textscan(fid,'%s',NumHeaderLines,'delimiter','\n');

    if initialize == 1;
        temp = InputText{1};
        RowThree = temp(3);
        SplitRow = strsplit(RowThree{1});
        m = str2num(SplitRow{7});
        n = str2num(SplitRow{9});
        DataLength = m*n;
        BinnedData = zeros(DataLength, 4, TotalBins);
        PhaseAvgData = zeros(DataLength,4, NumBins);
        initialize = 0;
    end

    % Create format string based on parameter
    FormatString = repmat('%f',1,NumCols);

    % Read data block
    BinnedData(:,:,FileNum) =
cell2mat(textscan(fid,FormatString,'delimiter',','));

    % Close the file
    fclose(fid);
end

%% Phase Average Binned Data
for count = 1:NumBins
    for cycle = 1:NumCycles
        PhaseAvgData(:,:,count) = PhaseAvgData(:,:,count) +
BinnedData(:,:,(NumBins*(cycle-1))+count);
    end
end

PhaseAvgData(:,:,:) = PhaseAvgData(:,:,:)/NumCycles;

%% EXPORT TO DAT

DatExportX = zeros(DataLength);
DatExportY = zeros(DataLength);
DatExportVX = zeros(DataLength);
DatExportVY = zeros(DataLength);
```

```
for t = 1:NumBins
    DatExportX = PhaseAvgData(:,1,t);
    DatExportY = PhaseAvgData(:,2,t);
    DatExportVX = PhaseAvgData(:,3,t);
    DatExportVY = PhaseAvgData(:,4,t);

    if isempty(dir(sprintf('%s/BinPhaseAVG',pwd)))
        mkdir(sprintf('%s/BinPhaseAVG',pwd));
    end

    fid2 = fopen(sprintf('BinPhaseAVG\\T=%04d.dat',t),'w');
    fprintf(fid2,'%s %s %s\n','TITLE = "T = ',sprintf('%04d',t),'"');
    fprintf(fid2,'%s\n','VARIABLES = "X (m)", "Y (m)", "U (m/s)", "V
(m/s)"');
    fprintf(fid2,'%s %s %s %d %s %d\n','ZONE T="T =
',sprintf('%04d',t),'", I=',m, 'J=',n);
    tot = m*n;
    for l = 1:tot
        fprintf(fid2,'%8.6f %8.6f %8.6f
%8.6f\n',DatExportX(l),DatExportY(l),DatExportVX(l),DatExportVY(l));
    end
    fclose(fid2);
end

% Notify Me When Done By Playing Song
%load handel;
%player = audioplayer(y, Fs);
%play(player);
```

L.4 Extract_min_max_avg_vel_TFE.m

```
clear
close all


%*************CHANGE FILE PATH FOR EACH EXPERIMENT!******************
%                                                                  *
file_path='I:\Data\SA2B\HSPIV\FLAIL8020\20181207_Flail8020_50Per_Neo\6.
5_700hz\MaskOutImage_01\SubOverTimeMin_sL=5\TR_PIV_MPd(5x16x16_50%ov_Im
gCorr)_GPU\PostProc\BinAVG_703Hz\Scaled\BinPhaseAVG';
znam = '8020F_neo_0Per_6.5minmaxavg';
timepoints = 120;
sz = [112 118 timepoints]; %get from dat file header
%                                                                  *
%******************************************************************

listing = dir(file_path);
filenames = {listing.name};
dat1 = [];
```

```
for i  = 3:length(filenames) %loop through all time points
    file_1 = char(cellstr(filenames(i)));
    file = sprintf('%s\\%s',file_path,file_1);


    fid1 = fopen(file,'r');
    head = fgetl(fid1);
    fgetl(fid1);
    tem = fgetl(fid1);
    sz2 = sscanf(tem,['ZONE T="Frame 0", I=','%d',', J=','%d'],[1
Inf]);
    dat1(:,:,i-2) = fscanf(fid1,'%f %f %f %f\n',[4 inf]);
    fclose(fid1);

end

vel_mag = sqrt(dat1(3,:,:).^2+dat1(4,:,:).^2);
vel = reshape(vel_mag,sz(1)*sz(2),1,sz(3));
tpts = 0:((1/timepoints)*0.856):0.856;

% Initialize minimum array
minim = ones(sz(1)*sz(2),1)*1000;
maxim = zeros(sz(1)*sz(2),1);
min_ind = zeros(sz(1)*sz(2),1);
max_ind = zeros(sz(1)*sz(2),1);
add = zeros(sz(1)*sz(2),1);

for i = 1:(timepoints)
    minim = min(minim,vel(:,:,i));
    min_ind =
plus(times(tpts(i),ge(minim,vel(:,:,i))),times(min_ind,lt(minim,vel(:,:
,i))));
    maxim = max(maxim,vel(:,:,i));
    max_ind =
plus(times(tpts(i),le(maxim,vel(:,:,i))),times(max_ind,gt(maxim,vel(:,:
,i))));
    add = plus(add,vel(:,:,i));
end

avg = add/timepoints;

% Write out minimum and maximum fields
fid2 = fopen(strcat(file_path,'\',znam,'.dat'),'w');
fprintf(fid2,'%s\n',strcat('TITLE = "',znam,'"'));
fprintf(fid2,'%s\n','VARIABLES = "X (m)", "Y (m)", "Min (m/s)", "Min
Time (ms)", "Max (m/s)", "Max Time (ms)", "Average (m/s)"');
fprintf(fid2,'%s %s %s %d %s %d\n','ZONE T="',znam,' ", I=',sz(1),
'J=',sz(2));
for j=1:sz(1)*sz(2)
    fprintf(fid2,'%8.4f %8.4f %8.4f %8.4f %8.4f %8.4f
%8.4f\n',dat1(1,j),dat1(2,j),minim(j),min_ind(j),maxim(j),max_ind(j),av
g(j));
end
fclose(fid2);
```

```
clear all
close all
```

L.5 PIV_Renaming_v1.m

```
%% Copies and organizes files: orders them by frame and puts all cycles
togethers

close all
clear
clc

%%
datafolder = 'Z:\Work\Work - Graduate\Work - SA2\SA2b
Processed\Flail8020rescaled\50Per\6.5L_2\Cycle Averaged'...
    ;                                               %folder containing PIV
data
outputfolder = '%s/Reordered_200ms';                %folder containing
output folders
inroot = 'T=';                                      %input filename prefix
outroot = 'T=';                                     %output filename prefix
numformat = '%04d';                                 %total digits in
numbering
fileextension = '.dat';                             %file type
firstf = 1;                                         %number of old first
file
lastf = 120;                                        %number of old last
file
incrementf = 1;                                     %increments between
files
firstfin = 29;                                      %start number of old
file
firstfout = 1;                                      %start number of new
first file

%%

cd(datafolder)
myfolder = sprintf(outputfolder,datafolder);
if isempty(dir(myfolder))         %if the directory doesn't exist, make
it
   mkdir(myfolder);
end
length = ((lastf-firstf)+1)/incrementf;
h = waitbar(0);
    tic

for m = firstf:incrementf:lastf
    if m >= firstfin
        k = (m-firstfin)+1;
    elseif m < firstfin
```

```
        k = (m-firstfin)+1+lastf;
    end
    t = sprintf(numformat,m);                  %input file number
    u = sprintf(numformat,k);
    infilenumformat = strcat(inroot,t,fileextension);
    outfilenumformat =
strcat(outputfolder,'\\',outroot,u,fileextension);
    copyfile(infilenumformat,sprintf(outfilenumformat,datafolder));
%copies and renames file

    %progress bar
    progress = (m/length);
    time_elapsed = toc;
    time_remaining = (1-progress)*(time_elapsed/progress)/60;
    waitbar(progress, h,['Time Remaining: ',
num2str(time_remaining),'min'], 'Name', num2str(progress*100));
end
close(h);
```

L.6 PIV_Organizing_final_v1.m

```
%% Copies and organizes files: orders them by frame and puts all cycles
togethers

close all
clc

%%
datafolder =
'I:\Data\SA2A\HSPIV\FLAIL8020\20190206_Flail8020_0Per\5\MaskOutImage\Su
bOverTimeMin_sL=5\TR_SeqPIV_MP(2x32x32_50%ov)\PostProc\BinAVG_702Hz'...
    ;                                               %folder containing PIV
data
outputfolder = '%s/Frames';                         %folder containing
output folders
outputfolderroot = 'Frame';                         %folder containing
output data
inroot = 'T=';                                      %input filename prefix
outroot = 'Tr=';                                    %output filename prefix
numformat = '%04d';                                 %total digits in
numbering
fileextension = '.dat';                             %file type
firstf = 1;                                         %first frame number of
cycle
lastf = 120;                                        %last frame number of
cycle
incrementf = 1;                                     %increments between
frames
lengthc = 120;                                      %number of frames in a
cycle
firstc = 1;                                         %first cycle number
```

```
lastc = 20;                                     %last cycle number
incrementc = 1;                                 %increments between
cycles
cyclelength = 856;                              %(ms) length of cardiac
cycle
PIVoutfolder = 'Frames';                        %for syntax in PIV file
(same as outputfolder)
PIVfilename = 'PIVinput.txt';                   %list of folders used
for PIV processing
deltatfilename = 'dtinput.txt';                 %list of timepoints for
PIV processing

%%
dt = cyclelength/lengthc;

cd(datafolder)
myfolder = sprintf(outputfolder,datafolder);
if isempty(dir(myfolder))         %if the directory doesn't exist, make
it
   mkdir(myfolder);
end

FileArray = strings(lengthc,1);
FileArray2 = zeros(1,lengthc);
dirfilename = strcat(outputfolder,'\\',PIVfilename);
dtfilename = strcat(outputfolder,'\\',deltatfilename);

h = waitbar(0);
    tic

for m = firstf:incrementf:lastf
    %make folder for frame m
    s = sprintf(numformat,m);                   %folder number
    outputfolders = strcat(outputfolder,'\\',outputfolderroot,s);
    if isempty(dir(sprintf(outputfolders,datafolder)))         %if the
directory doesn't exist, make it
        mkdir(sprintf(outputfolders,datafolder));
    end
    %copy files to folder and renames to cycle n
    for n = firstc:incrementc:lastc
        k = (n-1)*lengthc+m;
        t = sprintf(numformat,k);               %input file number
        u = sprintf(numformat,n);
        infilenumformat = strcat(inroot,t,fileextension);
        outfilenumformat =
strcat(outputfolders,'\\',outroot,u,fileextension);
        copyfile(infilenumformat,sprintf(outfilenumformat,datafolder));
%copies and renames file
    end

    %Export folder names to .txt file
    diroutfolder = strcat(PIVoutfolder,'\',outputfolderroot,s);
    FileArray(m,1) = string(strcat(datafolder,'\',diroutfolder));
    fid2 = fopen(sprintf(dirfilename,datafolder),'w');
    fprintf(fid2,'%s\n',FileArray(:));
    fclose(fid2);
```

```
    %Export dt to .txt file
    diroutfolder = strcat(PIVoutfolder,'\',outputfolderroot,s);
    FileArray2(1,m) = dt*(m-1);
    fid3 = fopen(sprintf(dtfilename,datafolder),'w');
    fprintf(fid3,'%8.6f ',FileArray2(:));
    fclose(fid3);

    %progress bar
    progress = (m/lengthc);
    time_elapsed = toc;
    time_remaining = (1-progress)*(time_elapsed/progress)/60;
    waitbar(progress, h,['Time Remaining: ',
num2str(time_remaining),'min'], 'Name', num2str(progress*100));
end
close(h);
```

L.7 Master_PIV2_TFE_new.m

```
clear all
clc

tic
cd
'I:\Data\SA2A\HSPIV\Control\Thomas_LAMPOON_control_20180905\6.5lpm_cont
rol_1\MaskOutImage\SubOverTimeMin_sL=5\TR_SeqPIV_MP(2x32x32_50%ov)\Post
Proc\BinAVG_904Hz'
%%%%%%%%%%%%%%%%%%%%%%%%%%%%%%%%%%%%%%%%%%%%%%%%%%%%%%%%%%%%%%%%%%%%%%%
%%%
% MASTER PROGRAM FOR PIV PROCESSING
% CURRENT AS OF 06/02/2019
% ASSUME NUMBER OF FILES IS NFILE
% THIS PROGRAM CREATES TWO FILES:
% 1. B00001-NFILE.DAT
% 2. MEAN FILES CREATING FROM THE AVERAGING PROGRAM
% THE INPUT FILE FOR THIS PROGRAM IS input.txt
% input.txt - List of data folders, exported from Davis
% THIS PROGRAM ASSUMES THAT THE DATAFILES ARE STORED AS B*****.DAT,
WHERE
% ***** RANGES FROM 1-NFILE.
%%%%%%%%%%%%%%%%%%%%%%%%%%%%%%%%%%%%%%%%%%%%%%%%%%%%%%%%%%%%%%%%%%%%%%%
%%%
flow = 6.5; %lpm
plane = 'c';
% Time points of data acquisitions
dt =
'I:\Data\SA2A\HSPIV\Control\Thomas_LAMPOON_control_20180905\6.5lpm_cont
rol_1\MaskOutImage\SubOverTimeMin_sL=5\TR_SeqPIV_MP(2x32x32_50%ov)\Post
Proc\BinAVG_904Hz\Frames\dtinput.txt';

% % % % create input file
```

```
%     fidi = fopen('F:\BSCI_23mm_dat files\plan_a_5lpm -
Copy/input.txt','w');
%     for i=1:length(tp)
%         fprintf(fidi,'F:\BSCI_23mm_dat files\plan_a_5lpm -
Copy/T1=%d/\n',tp(i));
%     end
% % % % File containing the list of data directories
inpf =
'I:\Data\SA2A\HSPIV\Control\Thomas_LAMPOON_control_20180905\6.5lpm_cont
rol_1\MaskOutImage\SubOverTimeMin_sL=5\TR_SeqPIV_MP(2x32x32_50%ov)\Post
Proc\BinAVG_904Hz\Frames\PIVinput.txt';
% Directory for writing the output files
outdir =
['I:\Data\SA2A\HSPIV\Control\Thomas_LAMPOON_control_20180905\6.5lpm_con
trol_1\MaskOutImage\SubOverTimeMin_sL=5\TR_SeqPIV_MP(2x32x32_50%ov)\Pos
tProc\BinAVG_904Hz\Frames\' num2str(flow) 'lpm_' plane '/'];
% Number of data files
nfile = 16;
% Size of data array in one file
sz = [96 70];
% Density of solution in kg/m3
rho = 1091;
% Kinematic viscosity in m2/s
nu = 3.5E-6;
% z-location of plane of interest;
% For BAV, z=5.0 for pl1, z=0.0 for pl2 and z=2.5 for pl3
% For Normal, z=2.5 for pl1, z=0.0 for pl2 and z=5.0 for pl3
z = 0.0;
% Flag for coordinates
% Flag = 1, write out coordinates, use only for pl2 of all datasets
% Flag = 2, read coordinates
flag = 1;
% Path of coordinates file
coordfile = strcat(outdir,'coordfile.dat');
% Length of string for output files
lencur = 6;
% flag_del = 1 deletes the file named B00001-NFILE.DAT.
% Any other value keeps the file in the folder
flag_del = 0;
%%%%%%%%%%%%%%%%%%%%%%%%%%%%%%%%%%%%%%%%%%%%%%%%%%%%%%%%%%%%%%%%%%%%%%%
%%%
% Total number of elements
tot = sz(1)*sz(2);

% Open the file containing the list of dt value
fid0 = fopen(dt,'r');
tp = cell2mat(textscan(fid0,'%f','Delimiter',''));
tp = tp.';
fclose(fid0);

% Open the file containing the list of data directories
fid1 = fopen(inpf,'r');
dirs = textscan(fid1,'%s','Delimiter','\n');
dirs = dirs{1};
fclose(fid1);
```

```
% Create file for writing time points of measurements
A = exist(strcat(outdir,'Mean'));
if (A~=7)
    mkdir(outdir,'Mean');
end
outf = strcat(outdir,'Mean/tpts.txt');
fid5 = fopen(outf,'w');

h = waitbar(0);
    tic
lengthc = size(dirs,1);
% Scan through the list of directories
for i=1:size(dirs,1)
    curr = char(dirs(i));
    mean_term = zeros(8,tot);

    if (nfile>99)
        nfile_nam = num2str(nfile,'%3d');
    else if (nfile>9)
            nfile_nam = num2str(nfile,'%2d');
        else
            nfile_nam = num2str(nfile,'%1d');
        end
    end
% Create the output file name for writing
    outf = strcat(curr,'_Tr=0001-',nfile_nam,'.dat');
    fid3 = fopen(outf,'w');
    fprintf('%s%s\n','Writing file: ',outf);

    for l=1:nfile
        fprintf('%s%s\n','Processing file:
',strcat(curr,'\Tr=',sprintf('%04d\n',l),'.dat'));
%   CREATE FILENAME
        fnam = strcat(curr,'\Tr=',sprintf('%04d\n',l),'.dat');
%   OPEN FILE
        fid2 = fopen(fnam,'r');
%   READ HEADER
        head = fgetl(fid2);
        fgetl(fid2);
        tem = fgetl(fid2);
        %sz = sscanf(tem,['ZONE T="T= 0001", I=','%d','J=','%d'],[1
Inf]);
%   READ DATA
        dat = fscanf(fid2,'%f %f %f %f\n',[4 inf]);
        fclose(fid2);

%   VELOCITY MAGNITUDE
        vel_mag = sqrt(dat(3,:).^2+dat(4,:).^2);

%   RESHAPING DATA
        X = reshape(dat(1,:),sz(1),sz(2));
        Y = reshape(dat(2,:),sz(1),sz(2));
        U = reshape(dat(3,:),sz(1),sz(2));
        V = reshape(dat(4,:),sz(1),sz(2));

%   VECTOR SPACING
```

```
        dx = (X(2,1)-X(1,1));
        dy = (Y(1,1)-Y(1,2));

        dUdx = zeros(sz(1),sz(2));
        dUdy = zeros(sz(1),sz(2));
        dVdx = zeros(sz(1),sz(2));
        dVdy = zeros(sz(1),sz(2));
        tau_sumxy = zeros(sz(1),sz(2));

%   CALCULATING GRADIENTS AND WALL-NORMAL GRADIENTS
        for j=2:sz(1)-1
            for k=2:sz(2)-1
                dUdx(j,k)  = (U(j+1,k)-U(j-1,k))/(X(j+1,k)-X(j-1,k));
                dUdy(j,k)  = (U(j,k+1)-U(j,k-1))/(Y(j,k+1)-Y(j,k-1));
                dVdx(j,k)  = (V(j+1,k)-V(j-1,k))/(X(j+1,k)-X(j-1,k));
                dVdy(j,k)  = (V(j,k+1)-V(j,k-1))/(Y(j,k+1)-Y(j,k-1));
                tau_sumxy(j,k)  = dUdy(j,k)+dVdx(j,k);
            end
        end

        dUdx = reshape(dUdx,1,tot);
        dUdy = reshape(dUdy,1,tot);
        dVdx = reshape(dVdx,1,tot);
        dVdy = reshape(dVdy,1,tot);
        tau_sumxy = reshape(tau_sumxy,1,tot);

% If it is the first file, write the common header, else only write
zone
% header
        if (l==1)
            fprintf(fid3,'%s\n',head);
            fprintf(fid3,'%s\n','VARIABLES = "X (m)", "Y (m)", "U
(m/s)", "V (m/s)", "Vel (m/s)", "dUdX", "dUdY", "dVdX", "dVdY",
"dUdy+dVdx"');
        end
        fprintf(fid3,'%s%s%s%d%s%d%s\n','ZONE
T="',strcat('B',sprintf('%05d\n',i),'.dat'),'", I=',sz(1),'
J=',sz(2),',DATAPACKING=POINT');
        for j=1:tot
            fprintf(fid3,'%8.4f %8.4f %8.4f %8.4f %8.4f %8.4f %8.4f
%8.4f %8.4f
%8.4f\n',dat(1,j),dat(2,j),dat(3,j),dat(4,j),vel_mag(j),dUdx(j),dUdy(j)
,dVdx(j),dVdy(j),tau_sumxy(j));
        end
% Calculate mean quantities for the N files
        mean_term(1,:) = mean_term(1,:) + dat(3,:)/double(nfile);
        mean_term(2,:) = mean_term(2,:) + dat(4,:)/double(nfile);
        mean_term(3,:) = mean_term(3,:) + vel_mag/double(nfile);
        mean_term(4,:) = mean_term(4,:) + dUdx/double(nfile);
        mean_term(5,:) = mean_term(5,:) + dUdy/double(nfile);
        mean_term(6,:) = mean_term(6,:) + dVdx/double(nfile);
        mean_term(7,:) = mean_term(7,:) + dVdy/double(nfile);
        mean_term(8,:) = mean_term(8,:) + tau_sumxy/double(nfile);
    end
% Conversion of units from m/s/mm to 1/s
%     for j=4:8
```

```
%         mean_term(j,:) = mean_term(j,:)*1000;
%     end
    fclose(fid3);

% Open the newly created file for further calculations
    fid3 = fopen(outf,'r');
    fprintf('%s%s\n','Reading file for mean calculations: ',outf);
%   READ HEADER
    for l=1:2
        head = fgetl(fid3);
    end

    uu = zeros(1,tot);
    vv = zeros(1,tot);
    uv = zeros(1,tot);
    TKE = zeros(1,tot);
    pRSS = zeros(1,tot);
    VSS = zeros(1,tot);

% Calculation of quantities
    for l=1:nfile
        head = fgetl(fid3);
        dat = fscanf(fid3,'%f %f %f %f %f %f %f %f %f %f\n',[10,tot]);
        for j=1:tot
            uu(1,j) = uu(1,j) + (dat(3,j)-
mean_term(1,j))^2/double(nfile);
            vv(1,j) = vv(1,j) + (dat(4,j)-
mean_term(2,j))^2/double(nfile);
            uv(1,j) = uv(1,j) + (dat(4,j)-mean_term(2,j))*(dat(3,j)-
mean_term(1,j))/double(nfile);
        end
    end
% Calculation of TKE, Principle RSS, and VSS scalar shear components
    for j=1:tot
        TKE(1,j) = 0.5*(uu(1,j)+vv(1,j));
        pRSS(1,j) = rho*sqrt(((uu(1,j)-vv(1,j))/2)^2+(uv(1,j))^2);
        VSS(1,j) = nu*rho*mean_term(8,j);
    end
    fclose(fid3);

% Read or write coordinates file depending on flag
    if (flag==1)
        fid4 = fopen(coordfile,'w');
        for j=1:tot
            fprintf(fid4,'%8.4f %8.4f\n',dat(1,j),dat(2,j));
        end
        flag = 2;
        fclose(fid4);
    else
        fid4 = fopen(coordfile,'r');
        tem = fscanf(fid4,'%f %f\n',[1 inf]);
        fclose(fid4);
        dat(1,:) = tem(1:2:tot*2);
        dat(2,:) = tem(2:2:tot*2);
    end
```

```
% Write results of mean calculations
    slash = find(curr=='\');
    fnam = strcat(outdir,'Mean/T= ',sprintf('%f',tp(i)),'.dat');
    fid6 = fopen(fnam,'w');
    fprintf(fid5,'%s%s%s\n','T=',sprintf('%f',tp(i)),'.dat');
    fprintf('%s%s\n','Writing file: ',fnam);

    fprintf(fid6,'%s %s %s\n','TITLE = "T =
',sprintf('%f',tp(i)),'ms"');
    fprintf(fid6,'%s\n','VARIABLES = "X (m)", "Y (m)", "Z (m)", "U
(m/s)", "V (m/s)", "Vel (m/s)", "dU/dx (s<sup>-1</sup>)", "dU/dy
(s<sup>-1</sup>)", "dV/dx (s<sup>-1</sup>)", "dV/dy (s<sup>-1</sup>)",
"<b><greek>w</greek><sub>z</sub> (s<sup>-1</sup>)</b>",
"<greek>r</greek>u\''u\'' (N/m<sup>2</sup>)", "<greek>r</greek>v\''v\''
(N/m<sup>2</sup>)", "<greek>r</greek>u\''v\'' (N/m<sup>2</sup>)", "TKE
(m<sup>2</sup>/s<sup>2</sup>)", "RSS (N/m<sup>2</sup>)", "VSS
(N/m<sup>2</sup>)"');
    fprintf(fid6,'%s %s %s %d %s %d\n','ZONE T=" T =
',sprintf('%f',tp(i)),'ms", I=',sz(1), 'J=',sz(2));
    for j=1:tot
        fprintf(fid6,'%8.4f %8.4f %8.4f %8.4f %8.4f %8.4f %8.4f %8.4f
%8.4f %8.4f %8.4f %8.4f %8.4f %8.4f %8.4f %8.4f
%8.4f\n',dat(1,j),dat(2,j),z,mean_term(1,j),mean_term(2,j),mean_term(3,
j),mean_term(4,j),mean_term(5,j),mean_term(6,j),mean_term(7,j),mean_ter
m(8,j),uu(1,j),vv(1,j),uv(1,j),TKE(1,j),pRSS(1,j),VSS(1,j));
    end
    fclose(fid6);
    if (flag_del==1)
        delete(outf);
    end
    %progress bar
    progress = (i/lengthc);
    time_elapsed = toc;
    time_remaining = (1-progress)*(time_elapsed/progress)/60;
    waitbar(progress, h,['Time Remaining: ',
num2str(time_remaining),'min'], 'Name', num2str(progress*100));
end
close(h);
fclose(fid5);
toc
```

L.8 ParticleTrackingTecplotToExcelAndEPS_TFE.m

```
% clear stuff
clear
clc

% Input your file name WITHOUT FILE EXTENSION!
%[filename, pathname] = uigetfile({'*.txt*'},'Select Particle Path Text
File');
filename = '8020F_0Per_6.5pt_aa';
```

```
pathname = 'Z:\Work\Work - Graduate\Work - SA2\SA2a
Processed\Flail8020\0Per\6.5L\Cycle Averaged';
chdir(pathname);
%neo sinus axes
%user_axis = [-.011,.011,-.01,.01];  %0Per_neo 8020F
%user_axis = [-.01,.012,-.01,.01];  %50Per_neo 8020F
%user_axis = [-.017,.005,-.012,.008];  %100Per_neo 8020F
%LV axes
user_axis = [-.07,.03,-.05,.03];  %0Per 8020F
%user_axis = [-.01,.012,-.01,.01];  %50Per 8020F
%user_axis = [-.075,.025,-.055,.025];  %100Per 8020F

% Open text file
fid = fopen(strcat(filename,'.txt'),'r');

% Number of Header Lines
NumHeaderLines = 1;

%Read strings delimited by a carriage return
InputText = textscan(fid,'%s',NumHeaderLines,'delimiter','\n');

FileHeader = InputText{1};
%disp(FileHeader);

% Number of INTERNAL Header Lines
NumInternalHeaderLines = 1;

% Initialize block index
NumParticles = 1;

% Number of Columns of Data (X,Y,Z,etc)
NumCols = 2;

% For each block:
while (~feof(fid))

   % Display block number
   % disp(cellstr(['Particle ' num2str(NumParticles)]));

   % Read header lines
   InputText =
textscan(fid,'%s',NumInternalHeaderLines,'delimiter','\n');
   HeaderLines{NumParticles,1} = InputText{1};
   % disp(HeaderLines{NumParticles});

   % Create format string based on parameter
   FormatString = repmat('%f',1,NumCols);

   % Read data block
   InputText = textscan(fid,FormatString,'delimiter',',');

   % Convert to numerical array from cell
   ParticlePaths{NumParticles,1} = cell2mat(InputText);
```

```
    % Size of table
    [NumRows,NumCols] = size(ParticlePaths{NumParticles});
    % disp(cellstr(['Table data size: ' num2str(NumRows) ' x '
num2str(NumCols)]));

    % New line
    % disp('*****');

    % Increment block index
    NumParticles = NumParticles+1;
end

NumParticles = NumParticles - 1;

% Close the file
fclose(fid);



for i=1:NumParticles
%     LPP = length(ParticlePaths{i});
%     for j=1:LPP
%         if ParticlePaths{i}(j,1) == ParticlePaths{i}(LPP,1)
%             if ParticlePaths{i}(j,2) == ParticlePaths{i}(LPP,2)
%                 ParticlePaths{i}(j:end,:) = [];
%                 %break
%             end
%         end
%     end
    r = length(ParticlePaths{i}(:,1));
    FormatForExcel(1:r,2*i-1:2*i) = [ParticlePaths{i}(:,1),
ParticlePaths{i}(:,2)];
end
FormatForExcel(FormatForExcel == 0) = NaN;
csvwrite(strcat(filename,'.csv'),FormatForExcel);

%%

% Make directory for video frames
% if isempty(dir(sprintf('ParticleTrackingFrames')))
%     mkdir(sprintf('ParticleTrackingFrames'));
% end

v = VideoWriter(strcat(filename,'_particle_tracking.avi'));
v.FrameRate = 10;
v.Quality = 100;
open(v);

[m,n] = size(FormatForExcel);
h = waitbar(0);
tic
for t=1:10:m
    name = sprintf('ParticleTrackingFrames\\t=%04i',t);
    figure('Visible','off')
    for i=1:NumParticles
```

```
        plot(FormatForExcel(t,2*i-1),FormatForExcel(t,2*i),'.r');
        axis(user_axis)
        hold on
    end
    hold off
    F = getframe;
    writeVideo(v,F);
    %print(name,'-deps');  % writes EPS file
    close;
    clc;
    progress = (t/m);
    time_elapsed = toc;
    time_remaining = (1-progress)*(time_elapsed/progress)/60;
    waitbar(progress, h,['Time Remaining: ',
num2str(time_remaining),'min'], 'Name', num2str(progress*100));
end
close(h);
close(v);

%%

%Clear Workspace except for Particle Paths (not necessary)
clear ans fid FileHeader FormatString HeaderLines InputText ...
    NumHeaderLines NumInternalHeaderLines NumRows NumCols ...
    i r FormatForExcel;
```

L.9 ParticleTrackingWashout.m

```
%%[filename, pathname] = uigetfile({'*.csv*'},'Select Particle Path
Text File');
%%^had to comment out for Word
chdir(pathname);

A = importdata(filename);

[len, num] = size(A);

WashoutCurve = zeros(len,1);

for i = 1:2:num
    Var = A(:,i);
    Var(isnan(Var(:,1)),:)=[];
    Var(:)=1;
    dim = numel(Var);
    WashoutCurve(1:dim) = WashoutCurve(1:dim) + Var;
end

WashoutCurve = WashoutCurve/max(WashoutCurve);
Time = [0:0.001:(numel(WashoutCurve)-1)*0.001]';
CardiacCycles = Time/0.856;
```

```
plot(CardiacCycles,WashoutCurve);

data = [Time CardiacCycles WashoutCurve];
header = {'Time(s)','Cardiac Cycles', 'Particles Remaining (%)'};
Output = [header;num2cell(data)];

xlswrite(strcat(filename,'.xlsx'),data);
```

APPENDIX M. TECPLOT CODES – SPECIFIC AIM 2

M.1 neo_mma.m

```
#!MC 1410
$!FieldLayers ShowShade = No
$!FieldLayers ShowContour = Yes
$!ContourLevels New
  ContourGroup = 1
  RawData
14
0
0.02
0.04
0.06
0.08
0.1
0.12
0.14
0.16
0.18
0.2
0.22
0.24
0.26
$!SetContourVar
  Var = 5
  ContourGroup = 2
  LevelInitMode = ResetToNice
$!ContourLevels New
  ContourGroup = 2
  RawData
14
0
0.02
0.04
0.06
0.08
0.1
0.12
0.14
0.16
0.18
0.2
0.22
0.24
0.26
$!SetContourVar
  Var = 7
  ContourGroup = 3
  LevelInitMode = ResetToNice
$!ContourLevels New
```

```
  ContourGroup = 3
  RawData
14
0
0.02
0.04
0.06
0.08
0.1
0.12
0.14
0.16
0.18
0.2
0.22
0.24
0.26
$!GlobalContour 3  ColorMapName = 'Small Rainbow'
$!GlobalContour 3  ColorMapFilter{ColorMapDistribution = Continuous}
$!GlobalContour     3          ColorMapFilter{ContinuousColor{CMax     =
0.26000000000000001}}
$!GlobalContour 2  ColorMapFilter{ColorMapDistribution = Continuous}
$!GlobalContour     2          ColorMapFilter{ContinuousColor{CMax     =
0.26000000000000001}}
$!GlobalContour 1  ColorMapFilter{ColorMapDistribution = Continuous}
$!GlobalContour     1          ColorMapFilter{ContinuousColor{CMax     =
0.26000000000000001}}
$!GlobalContour 1  ColorMapName = 'Small Rainbow'
$!GlobalContour 2  ColorMapName = 'Small Rainbow'
$!Blanking Value{Constraint 1 {VarA = 7}}
$!Blanking Value{Constraint 1 {Include = Yes}}
$!Blanking Value{Include = Yes}
$!Blanking Value{Constraint 2 {VarA = 1}}
$!Blanking Value{Constraint 2 {VarA = 2}}
$!Blanking Value{Constraint 2 {RelOp = GreaterThanOrEqual}}
$!Blanking Value{Constraint 2 {ValueCutoff = 0.0050000000000000001}}
$!Blanking Value{Constraint 2 {Include = Yes}}
$!TwoDAxis YDetail{RangeMin = -0.01}
$!TwoDAxis YDetail{RangeMax = 0.01}
$!FrameLayout ShowBorder = No
$!FieldMap [1]  Contour{FloodColoring = Group3}
$!RedrawAll
```

M.2 neo_vel.m

```
#!MC 1410
$!FieldLayers ShowShade = No
$!GlobalRGB RedChannelVar = 3
$!GlobalRGB GreenChannelVar = 3
$!GlobalRGB BlueChannelVar = 3
$!SetContourVar
  Var = 3
  ContourGroup = 1
```

```
  LevelInitMode = ResetToNice
$!SetContourVar
  Var = 4
  ContourGroup = 2
  LevelInitMode = ResetToNice
$!SetContourVar
  Var = 3
  ContourGroup = 3
  LevelInitMode = ResetToNice
$!SetContourVar
  Var = 3
  ContourGroup = 4
  LevelInitMode = ResetToNice
$!SetContourVar
  Var = 3
  ContourGroup = 5
  LevelInitMode = ResetToNice
$!SetContourVar
  Var = 3
  ContourGroup = 6
  LevelInitMode = ResetToNice
$!SetContourVar
  Var = 3
  ContourGroup = 7
  LevelInitMode = ResetToNice
$!SetContourVar
  Var = 3
  ContourGroup = 8
  LevelInitMode = ResetToNice
$!FieldLayers ShowContour = Yes
$!ExtendedCommand
  CommandProcessorID = 'CFDAnalyzer4'
  Command  =  'SetFieldVariables  ConvectionVarsAreMomentum=\'F\'  UVar=3
VVar=4 WVar=0 ID1=\'NotUsed\' Variable1=0 ID2=\'NotUsed\' Variable2=0'
$!ExtendedCommand
  CommandProcessorID = 'CFDAnalyzer4'
  Command  =  'Calculate  Function=\'VELOCITYMAG\'  Normalization=\'None\'
ValueLocation=\'Nodal\'                         CalculateOnDemand=\'T\'
UseMorePointsForFEGradientCalculations=\'F\''
$!SetContourVar
  Var = 5
  ContourGroup = 1
  LevelInitMode = ResetToNice
$!ContourLevels New
  ContourGroup = 1
  RawData
14
0
0.02
0.04
0.06
0.08
0.1
0.12
0.14
0.16
0.18
```

```
0.2
0.22
0.24
0.26
$!GlobalContour 1  ColorMapName = 'Small Rainbow'
$!GlobalContour 1  ColorMapFilter{ColorMapDistribution = Continuous}
$!GlobalContour 1  ColorMapFilter{ContinuousColor{CMin = 0}}
$!GlobalContour     1          ColorMapFilter{ContinuousColor{CMax     =
0.26000000000000001}}
$!RedrawAll
$!Blanking Value{Constraint 2 {Include = Yes}}
$!Blanking Value{Constraint 2 {VarA = 5}}
$!Blanking Value{Include = Yes}
$!Blanking Value{Constraint 1 {VarA = 1}}
$!Blanking Value{Constraint 1 {VarA = 2}}
$!Blanking Value{Constraint 1 {RelOp = GreaterThanOrEqual}}
$!Blanking Value{Constraint 1 {ValueCutoff = 0.0050000000000000001}}
$!Blanking Value{Constraint 1 {Include = Yes}}
$!TwoDAxis YDetail{RangeMin = -0.01}
$!TwoDAxis YDetail{RangeMax = 0.01}
$!FrameLayout ShowBorder = No
$!RedrawAll
```

M.3 neo_fmech.m

```
#!MC 1410
$!FieldLayers ShowShade = No
$!GlobalRGB RedChannelVar = 17
$!GlobalRGB GreenChannelVar = 3
$!GlobalRGB BlueChannelVar = 3
$!SetContourVar
  Var = 3
  ContourGroup = 1
  LevelInitMode = ResetToNice
$!SetContourVar
  Var = 4
  ContourGroup = 2
  LevelInitMode = ResetToNice
$!SetContourVar
  Var = 5
  ContourGroup = 3
  LevelInitMode = ResetToNice
$!SetContourVar
  Var = 6
  ContourGroup = 4
  LevelInitMode = ResetToNice
$!SetContourVar
  Var = 7
  ContourGroup = 5
  LevelInitMode = ResetToNice
$!SetContourVar
  Var = 8
  ContourGroup = 6
```

```
  LevelInitMode = ResetToNice
$!SetContourVar
  Var = 9
  ContourGroup = 7
  LevelInitMode = ResetToNice
$!SetContourVar
  Var = 10
  ContourGroup = 8
  LevelInitMode = ResetToNice
$!FieldLayers ShowContour = Yes
$!SetContourVar
  Var = 6
  ContourGroup = 1
  LevelInitMode = ResetToNice
$!ContourLevels New
  ContourGroup = 1
  RawData
14
0
0.02
0.04
0.06
0.08
0.1
0.12
0.14
0.16
0.18
0.2
0.22
0.24
0.26
$!GlobalContour 1  ColorMapName = 'Small Rainbow'
$!GlobalContour 1  ColorMapFilter{ColorMapDistribution = Continuous}
$!GlobalContour     1          ColorMapFilter{ContinuousColor{CMax     =
0.25999999999999995}}
$!GlobalContour 2  ColorMapName = 'Small Rainbow'
$!GlobalContour 2  ColorMapFilter{ColorMapDistribution = Continuous}
$!SetContourVar
  Var = 12
  ContourGroup = 2
  LevelInitMode = ResetToNice
$!SetContourVar
  Var = 17
  ContourGroup = 3
  LevelInitMode = ResetToNice
$!SetContourVar
  Var = 16
  ContourGroup = 4
  LevelInitMode = ResetToNice
$!GlobalContour 3  ColorMapName = 'Small Rainbow'
$!GlobalContour 3  ColorMapFilter{ColorMapDistribution = Continuous}
$!GlobalContour 4  ColorMapName = 'Small Rainbow'
$!GlobalContour 4  ColorMapFilter{ColorMapDistribution = Continuous}
$!GlobalContour 2  ColorMapFilter{ContinuousColor{CMin = -2}}
$!GlobalContour 2  ColorMapFilter{ContinuousColor{CMax = 3.5}}
$!GlobalContour 3  ColorMapFilter{ContinuousColor{CMin = 1}}
```

```
$!GlobalContour 3  ColorMapFilter{ContinuousColor{CMax = 13}}
$!GlobalContour 4  ColorMapFilter{ContinuousColor{CMin = 2}}
$!GlobalContour 4  ColorMapFilter{ContinuousColor{CMax = 26}}
$!TwoDAxis YDetail{RangeMin = -0.01}
$!TwoDAxis YDetail{RangeMax = 0.01}
$!Blanking Value{Constraint 1 {VarA = 2}}
$!Blanking Value{Constraint 1 {RelOp = GreaterThanOrEqual}}
$!Blanking Value{Constraint 1 {ValueCutoff = 0.0050000000000000001}}
$!Blanking Value{Constraint 1 {Include = Yes}}
$!Blanking Value{Include = Yes}
$!Blanking Value{Constraint 2 {VarA = 1}}
$!Blanking Value{Constraint 2 {VarA = 6}}
$!Blanking Value{Constraint 2 {Include = Yes}}
$!Blanking Value{Constraint 3 {VarA = 1}}
$!RedrawAll
```

REFERENCES

1. McGee, E.C., et al., *Recurrent mitral regurgitation after annuloplasty for functional ischemic mitral regurgitation.* J Thorac Cardiovasc Surg, 2004. **128**(6): p. 916-24.

2. Flameng, W., P. Herijgers, and K. Bogaerts, *Recurrence of mitral valve regurgitation after mitral valve repair in degenerative valve disease.* Circulation, 2003. **107**(12): p. 1609-13.

3. Acker, M.A., et al., *Mitral-Valve Repair versus Replacement for Severe Ischemic Mitral Regurgitation.* New England Journal of Medicine, 2014. **370**(1): p. 23-32.

4. Himbert, D., et al., *Transcatheter valve replacement in patients with severe mitral valve disease and annular calcification.* J Am Coll Cardiol, 2014. **64**(23): p. 2557-8.

5. Nielsen, N.E., J. Baranowski, and H.C. Ahn, *Transvenous Implantation of a Stent Valve for Calcified Native Mitral Stenosis.* Ann Thorac Surg, 2015. **100**(1): p. e21-3.

6. Guerrero, M., et al., *1-Year Outcomes of Transcatheter Mitral Valve Replacement in Patients With Severe Mitral Annular Calcification.* J Am Coll Cardiol, 2018. **71**(17): p. 1841-1853.

7. Piazza, N., M. Pighi, and G. Martucci, *Transcatheter Aortic Valves for Failing Surgical Mitral Prostheses and Mitral Annular Calcification: Good From Far But Far From Good?* JACC Cardiovasc Interv, 2017. **10**(19): p. 1943-1945.

8. Webb, J.G., et al., *Transcatheter valve-in-valve implantation for failed bioprosthetic heart valves.* Circulation, 2010. **121**(16): p. 1848-57.

9. Guerrero, M., et al., *Transseptal transcatheter mitral valve-in-valve: A step by step guide from preprocedural planning to postprocedural care.* Catheter Cardiovasc Interv, 2018. **92**(3): p. E185-E196.

10. de Weger, A., et al., *First-in-man implantation of a trans-catheter aortic valve in a mitral annuloplasty ring: novel treatment modality for failed mitral valve repair.* Eur J Cardiothorac Surg, 2011. **39**(6): p. 1054-6.

11. Descoutures, F., et al., *Transcatheter valve-in-ring implantation after failure of surgical mitral repair*. Eur J Cardiothorac Surg, 2013. **44**(1): p. e8-15.

12. Pfeiffer, S., et al., *Transapical transcatheter valve-in-ring implantation following mitral annuloplasty*. J Card Surg, 2017. **32**(7): p. 407-409.

13. Wang, D.D., et al., *Predicting LVOT Obstruction After TMVR.* JACC Cardiovasc Imaging, 2016. **9**(11): p. 1349-1352.

14. Blanke, P., et al., *Predicting LVOT Obstruction in Transcatheter Mitral Valve Implantation: Concept of the Neo-LVOT.* JACC Cardiovasc Imaging, 2017. **10**(4): p. 482-485.

15. Akhras, N., et al., *Thrombolytic Therapy as the Management of Mitral Transcatheter Valve-in-Valve Implantation Early Thrombosis.* Heart, Lung and Circulation, 2015.

16. Beneduce, A., et al., *Subclinical Leaflet Thrombosis After Transcatheter Mitral Valve-in-Ring Implantation.* JACC Cardiovasc Interv, 2018. **11**(13): p. e105-e106.

17. Khan, J.M. and R.J. Lederman, *Unnatural milieu: Thrombus after transcatheter mitral valve replacement.* Catheter Cardiovasc Interv, 2017. **90**(2): p. 329-330.

18. David, T.E., *Ischemic Mitral Regurgitation: Chordal-Sparing Mitral Valve Replacement.* Operative Techniques in Thoracic and Cardiovascular Surgery, 2012. **17**(3): p. 194-203.

19. Babaliaros, V.C., et al., *Intentional Percutaneous Laceration of the Anterior Mitral Leaflet to Prevent Outflow Obstruction During Transcatheter Mitral Valve Replacement: First-in-Human Experience.* JACC Cardiovasc Interv, 2017. **10**(8): p. 798-809.

20. Iaizzo, P.A., *Handbook of cardiac anatomy, physiology, and devices*. 2009: Springer Science & Business Media.

21. Carpentier, A., D.H. Adams, and F. Filsoufi, *Carpentier's reconstructive valve surgery*. 2011: Elsevier Health Sciences.

22. Benjamin, E.J., et al., *Heart Disease and Stroke Statistics-2019 Update: A Report From the American Heart Association.* Circulation, 2019. **0**(0): p. CIR0000000000000659.

23. Rabbah, J.P., et al., *Mechanics of healthy and functionally diseased mitral valves: a critical review*. J Biomech Eng, 2013. **135**(2): p. 021007.

24. Toma, M., et al., *Fluid–structure interaction analysis of papillary muscle forces using a comprehensive mitral valve model with 3D chordal structure.* Annals of biomedical engineering, 2016. **44**(4): p. 942-953.

25. Levack, M.M., et al., *Three-dimensional echocardiographic analysis of mitral annular dynamics: implication for annuloplasty selection.* Circulation, 2012. **126**(11 Suppl 1): p. S183-8.

26. Rausch, M.K., et al., *Characterization of mitral valve annular dynamics in the beating heart.* Ann Biomed Eng, 2011. **39**(6): p. 1690-702.

27. Jolley, M.A., et al., *Three-Dimensional Mitral Valve Morphology and Age-Related Trends in Children and Young Adults with Structurally Normal Hearts Using Transthoracic Echocardiography.* Journal of the American Society of Echocardiography, 2017. **30**(6): p. 561-571.

28. Angelini, A., et al., *A histological study of the atrioventricular junction in hearts with normal and prolapsed leaflets of the mitral valve.* British Heart Journal, 1988. **59**(6): p. 712.

29. Stephens, E.H., et al., *Cellular and Extracellular Matrix Basis for Heterogeneity in Mitral Annular Contraction.* Cardiovascular Engineering and Technology, 2015. **6**(2): p. 151-159.

30. Nkomo, V.T., et al., *Burden of valvular heart diseases: a population-based study.* The Lancet, 2006. **368**(9540): p. 1005-1011.

31. Borger, M.A., et al., *Chronic ischemic mitral regurgitation: repair, replace or rethink?* The Annals of thoracic surgery, 2006. **81**(3): p. 1153-1161.

32. Pasca, I., et al., *Survival in Patients with Degenerative Mitral Stenosis: Results from a Large Retrospective Cohort Study.* Journal of the American Society of Echocardiography, 2016. **29**(5): p. 461-469.

33. Fox Caroline, S., et al., *Mitral Annular Calcification Predicts Cardiovascular Morbidity and Mortality.* Circulation, 2003. **107**(11): p. 1492-1496.

34. Adams, D.H., R. Rosenhek, and V. Falk, *Degenerative mitral valve regurgitation: best practice revolution.* European heart journal, 2010. **31**(16): p. 1958-1966.

35. Braun, J., et al., *Restrictive mitral annuloplasty cures ischemic mitral regurgitation and heart failure.* Ann Thorac Surg, 2008. **85**(2): p. 430-6; discussion 436-7.

36. Flameng, W., et al., *Durability of mitral valve repair in Barlow disease versus fibroelastic deficiency.* The Journal of thoracic and cardiovascular surgery, 2008. **135**(2): p. 274-282.

37. Gillinov, A. and D. Cosgrove, *Mitral valve repair for degenerative disease.* The Journal of heart valve disease, 2002. **11**: p. S15-20.

38. Kron, I.L., G.R. Green, and J.T. Cope, *Surgical relocation of the posterior papillary muscle in chronic ischemic mitral regurgitation.* The Annals of thoracic surgery, 2002. **74**(2): p. 600-601.

39. Salvador, L., et al., *A 20-year experience with mitral valve repair with artificial chordae in 608 patients.* The Journal of Thoracic and Cardiovascular Surgery, 2008. **135**(6): p. 1280-1287. e1.

40. Braun, J. and R.J. Klautz, *Mitral valve surgery in low ejection fraction, severe ischemic mitral regurgitation patients: should we repair them all?* Current opinion in cardiology, 2012. **27**(2): p. 111-117.

41. Harris, C., B. Croce, and C. Cao, *Tissue and mechanical heart valves.* Annals of cardiothoracic surgery, 2015. **4**(4): p. 399-399.

42. Yun Kwok, L., et al., *Randomized Trial of Partial Versus Complete Chordal Preservation Methods of Mitral Valve Replacement.* Circulation, 1999. **100**(suppl_2): p. II-90-Ii-94.

43. Mick, S.L., S. Keshavamurthy, and A.M. Gillinov, *Mitral valve repair versus replacement.* Annals of cardiothoracic surgery, 2015. **4**(3): p. 230-237.

44. Gammie, J.S., et al., *Trends in Mitral Valve Surgery in the United States: Results From The Society of Thoracic Surgeons Adult Cardiac Database.* The Annals of Thoracic Surgery, 2009. **87**(5): p. 1431-1439.

45. Enriquez-Sarano, M., et al., *Valve Repair Improves the Outcome of Surgery for Mitral Regurgitation.* Circulation, 1995. **91**(4): p. 1022-1028.

46. Gillinov, A.M., et al., *Valve repair versus valve replacement for degenerative mitral valve disease.* The Journal of Thoracic and Cardiovascular Surgery, 2008. **135**(4): p. 885-893.e2.

47. Suri, R.M., et al., *Survival Advantage and Improved Durability of Mitral Repair for Leaflet Prolapse Subsets in the Current Era.* The Annals of Thoracic Surgery, 2006. **82**(3): p. 819-826.

48. Zhou, Y.X., et al., *Long-Term Outcomes following Repair or Replacement in Degenerative Mitral Valve Disease.* Thorac cardiovasc Surg, 2010. **58**(07): p. 415-421.

49. LaPar, D.J., et al., *Does Urgent or Emergent Status Influence Choice in Mitral Valve Operations? An Analysis of Outcomes From the Virginia Cardiac Surgery Quality Initiative.* The Annals of Thoracic Surgery, 2010. **90**(1): p. 153-160.

50. Daneshmand, M.A., et al., *Mitral Valve Repair for Degenerative Disease: A 20-Year Experience.* The Annals of Thoracic Surgery, 2009. **88**(6): p. 1828-1837.

51. Akins, C.W., et al., *Mitral valve reconstruction versus replacement for degenerative or ischemic mitral regurgitation.* The Annals of Thoracic Surgery, 1994. **58**(3): p. 668-676.

52. Habib, G., F. Thuny, and J.-F. Avierinos, *Prosthetic Valve Endocarditis: Current Approach and Therapeutic Options.* Progress in Cardiovascular Diseases, 2008. **50**(4): p. 274-281.

53. Saccocci, M., M. Taramasso, and F. Maisano, *Mitral Valve Interventions in Structural Heart Disease.* Curr Cardiol Rep, 2018. **20**(6): p. 49.

54. Leon, M.B., et al., *Transcatheter Aortic-Valve Implantation for Aortic Stenosis in Patients Who Cannot Undergo Surgery.* New England Journal of Medicine, 2010. **363**(17): p. 1597-1607.

55. Smith, C.R., et al., *Transcatheter versus Surgical Aortic-Valve Replacement in High-Risk Patients.* New England Journal of Medicine, 2011. **364**(23): p. 2187-2198.

56. Adams, D.H., et al., *Transcatheter Aortic-Valve Replacement with a Self-Expanding Prosthesis.* New England Journal of Medicine, 2014. **370**(19): p. 1790-1798.

57. Leon, M.B., et al., *Transcatheter or Surgical Aortic-Valve Replacement in Intermediate-Risk Patients.* New England Journal of Medicine, 2016. **374**(17): p. 1609-1620.

58. Reardon, M.J., et al., *Surgical or Transcatheter Aortic-Valve Replacement in Intermediate-Risk Patients.* New England Journal of Medicine, 2017. **376**(14): p. 1321-1331.

59. Mack, M.J., et al., *Transcatheter Aortic-Valve Replacement with a Balloon-Expandable Valve in Low-Risk Patients.* New England Journal of Medicine, 2019. **380**(18): p. 1695-1705.

60. Popma, J.J., et al., *Transcatheter Aortic-Valve Replacement with a Self-Expanding Valve in Low-Risk Patients.* New England Journal of Medicine, 2019. **380**(18): p. 1706-1715.

61. Arnold, S.V., et al., *Health Status After Transcatheter Mitral-Valve Repair in Heart Failure and Secondary Mitral Regurgitation.* Journal of the American College of Cardiology, 2019. **73**(17): p. 2123.

62. Stone, G.W., et al., *Transcatheter Mitral-Valve Repair in Patients with Heart Failure.* New England Journal of Medicine, 2018. **379**(24): p. 2307-2318.

63. Nishimura, R.A. and R.O. Bonow, *Percutaneous Repair of Secondary Mitral Regurgitation — A Tale of Two Trials.* New England Journal of Medicine, 2018. **379**(24): p. 2374-2376.

64. Iung, B. and D. Messika-Zeitoun, *Transcatheter Mitral Valve Repair in Secondary MR.* Journal of the American College of Cardiology, 2019. **73**(17): p. 2133.

65. Beller, J.P., et al., *Early clinical results with the Tendyne transcatheter mitral valve replacement system.* Annals of Cardiothoracic Surgery, 2018. **7**(6): p. 776-779.

66. Sorajja, P., et al., *Initial Feasibility Study of a New Transcatheter Mitral Prosthesis.* Journal of the American College of Cardiology, 2019. **73**(11): p. 1250.

67. Sorajja, P. and V. Bapat, *Early experience with the Intrepid system for transcatheter mitral valve replacement.* Annals of Cardiothoracic Surgery, 2018. **7**(6): p. 792-798.

68. Anyanwu, A.C. and D.H. Adams, *Why Do Mitral Valve Repairs Fail?* Journal of the American Society of Echocardiography, 2009. **22**(11): p. 1265-1268.

69. Suri, R.M., et al., *Effect of Recurrent Mitral Regurgitation Following Degenerative Mitral Valve Repair.* Journal of the American College of Cardiology, 2016. **67**(5): p. 488.

70. Suri, R.M., et al., *Recurrent mitral regurgitation after repair: Should the mitral valve be re-repaired?* The Journal of Thoracic and Cardiovascular Surgery, 2006. **132**(6): p. 1390-1397.

71. Potter, D.D., et al., *Risk of repeat mitral valve replacement for failed mitral valve prostheses.* The Annals of thoracic surgery, 2004. **78**(1): p. 67-72.

72. Kohli, K., et al., *Transcatheter Mitral Valve Planning and the Neo-LVOT: Utilization of Virtual Simulation Models and 3D Printing.* Current Treatment Options in Cardiovascular Medicine, 2018. **20**(12): p. 99.

73. Seiffert, M., et al., *Transcatheter mitral valve-in-valve implantation in patients with degenerated bioprostheses.* JACC Cardiovasc Interv, 2012. **5**(3): p. 341-9.

74. Takagi, H., et al., *A meta-analysis of valve-in-valve and valve-in-ring transcatheter mitral valve implantation.* Journal of Interventional Cardiology, 2018. **31**(6): p. 899-906.

75. Long, A. and P. Mahoney, *Transcatheter Mitral Valve-in-Valve and Valve-in-Ring Replacement in High-Risk Surgical Patients: Feasibility, Safety, and Longitudinal Outcomes in a Single-Center Experience.* J Invasive Cardiol, 2018. **30**(9): p. 324-328.

76. Ando, T., et al., *A systematic review of reported cases of combined transcatheter aortic and mitral valve interventions.* Catheter Cardiovasc Interv, 2018. **91**(1): p. 124-134.

77. Nishimura, R.A., et al., *2014 AHA/ACC guideline for the management of patients with valvular heart disease: a report of the American College of Cardiology/American Heart Association Task Force on Practice Guidelines.* J Thorac Cardiovasc Surg, 2014. **148**(1): p. e1-e132.

78. Nishimura, R.A., et al., *2017 AHA/ACC Focused Update of the 2014 AHA/ACC Guideline for the Management of Patients With Valvular Heart Disease: A Report of the American College of Cardiology/American Heart Association Task Force on Clinical Practice Guidelines.* Circulation, 2017. **135**(25): p. e1159-e1195.

79. Mack, M.J., P.S. Douglas, and D.R. Holmes, *Shedding More Light on Valve Thrombosis After Transcatheter Aortic Valve Replacement.* J Am Coll Cardiol, 2016. **67**(6): p. 656-658.

80. Franzone, A., et al., *Transcatheter aortic valve thrombosis: incidence, clinical presentation and long-term outcomes.* Eur Heart J Cardiovasc Imaging, 2018. **19**(4): p. 398-404.

81. Basra, S.S., et al., *Clinical Leaflet Thrombosis in Transcatheter and Surgical Bioprosthetic Aortic Valves by Four-Dimensional Computed Tomography.* The Annals of Thoracic Surgery, 2018. **106**(6): p. 1716-1725.

82. De Backer, O., L. Søndergaard, and L. Rosseel, *Clinical valve thrombosis and subclinical leaflet thrombosis in transcatheter aortic heart valves: clinical manifestations, diagnosis, and treatment.* Precision Clinical Medicine, 2018. **1**(3): p. 111-117.

83. Midha Prem, A., et al., *The Fluid Mechanics of Transcatheter Heart Valve Leaflet Thrombosis in the Neosinus.* Circulation, 2017. **136**(17): p. 1598-1609.

84. Butnaru, A., et al., *Diagnosis and treatment of early bioprosthetic malfunction in the mitral valve position due to thrombus formation.* Am J Cardiol, 2013. **112**(9): p. 1439-44.

85. Jonveaux, M., et al., *Acute haemolysis after transcatheter mitral valve implantation.* European Heart Journal, 2018. **40**(5): p. 488-490.

86. Frigy, A., et al., *A CASE OF "BENIGN", RECURRENT, BIOPROSTHETIC MITRAL VALVE THROMBOSIS.* Acta Medica Transilvanica, 2017. **22**(4): p. 27-28.

87. Khan, J.M., et al., *Intentional Laceration of the Anterior Mitral Valve Leaflet to Prevent Left Ventricular Outflow Tract Obstruction During Transcatheter*

Mitral Valve Replacement: Pre-Clinical Findings. JACC: Cardiovascular Interventions, 2016. **9**(17): p. 1835-1843.

88. Khan, J.M., et al., *LAMPOON to Facilitate Tendyne Transcatheter Mitral Valve Replacement.* JACC. Cardiovascular interventions, 2018. **11**(19): p. 2014-2017.

89. Siefert, A.W. and R.L. Siskey, *Bench Models for Assessing the Mechanics of Mitral Valve Repair and Percutaneous Surgery.* Cardiovasc Eng Technol, 2015. **6**(2): p. 193-207.

90. Jensen, M.O., et al., *Measurement Technologies for Heart Valve Function*, in *Advances in Heart Valve Biomechanics: Valvular Physiology, Mechanobiology, and Bioengineering*, M.S. Sacks and J. Liao, Editors. 2018, Springer International Publishing: Cham. p. 115-149.

91. Okafor, I.U., et al., *Cardiovascular magnetic resonance compatible physical model of the left ventricle for multi-modality characterization of wall motion and hemodynamics.* J Cardiovasc Magn Reson, 2015. **17**(1): p. 51.

92. Easley, T., et al., *The Effects of Anterior Mitral Leaflet Resection on Left Ventricular Flow with Transcatheter Mitral Valves: An In Vitro Study.* Journal of the American College of Cardiology, 2019. **73**(9 Supplement 1): p. 1125.

93. Guerrero, M., A.B. Greenbaum, and W. O'Neill, *Early Experience with Transcatheter Mitral Valve Replacement.* Cardiac Interventions Today, 2015.

94. Schmidt, F.P., et al., *Usefulness of 3D-PISA as compared to guideline endorsed parameters for mitral regurgitation quantification.* Int J Cardiovasc Imaging, 2014. **30**(8): p. 1501-8.

95. Dvir, D., et al., *TCT-92 Transcatheter Mitral Valve-in-Valve/Valve-in-Ring Implantations for Degenerative Post Surgical Valves: Results from the Global Valve-in-Valve Registry.* Journal of the American College of Cardiology, 2013. **62**(18_S1): p. B30-B30.

96. Attizzani, G.F., C. Cheung Tam, and A. Markowitz, *Transcatheter mitral valve-in-ring implantation in prohibitive surgical risk patients: Single center initial experience in the United States.* Catheter Cardiovasc Interv, 2016. **88**(7): p. E233-E238.

97. Ghosh-Dastidar, M. and V. Bapat, *Transcatheter Valve Implantation in Mitral Annular Calcification During Open Surgery: Extended Collar Technique.* Ann Thorac Surg, 2017. **104**(3): p. e303-e305.

98. Bapat, V., et al., *Factors influencing left ventricular outflow tract obstruction following a mitral valve-in-valve or valve-in-ring procedure, part 1.* Catheter Cardiovasc Interv, 2015. **86**(4): p. 747-60.

99. Rabbah, J.P., N. Saikrishnan, and A.P. Yoganathan, *A novel left heart simulator for the multi-modality characterization of native mitral valve geometry and fluid mechanics.* Ann Biomed Eng, 2013. **41**(2): p. 305-15.

100. Bloodworth, C.H.t., et al., *Ex Vivo Methods for Informing Computational Models of the Mitral Valve.* Ann Biomed Eng, 2017. **45**(2): p. 496-507.

101. Siefert, A.W., et al., *In vitro mitral valve simulator mimics systolic valvular function of chronic ischemic mitral regurgitation ovine model.* Ann Thorac Surg, 2013. **95**(3): p. 825-30.

102. Okafor, I., et al., *Aortic Regurgitation Generates a Kinematic Obstruction Which Hinders Left Ventricular Filling.* Annals of Biomedical Engineering, 2017. **45**(5): p. 1305-1314.

103. Okafor, I.U., *Parametric evaluation of the effect of aortic regurgitation on ventricular performance*, in *School of Chemical and Biomolecular Engineering*. 2016, Georgia Institute of Technology: Georgia Tech Theses and Dissertations.

104. Rausch, M.K., et al., *In vivo dynamic strains of the ovine anterior mitral valve leaflet.* J Biomech, 2011. **44**(6): p. 1149-57.

105. Sacks, M.S., et al., *Surface strains in the anterior leaflet of the functioning mitral valve.* Ann Biomed Eng, 2002. **30**(10): p. 1281-90.

106. Bothe, W., et al., *Rigid, complete annuloplasty rings increase anterior mitral leaflet strains in the normal beating ovine heart.* Circulation, 2011. **124**(11 Suppl): p. S81-96.

107. Amini, R., et al., *On the in vivo deformation of the mitral valve anterior leaflet: effects of annular geometry and referential configuration.* Ann Biomed Eng, 2012. **40**(7): p. 1455-67.

108. He, S.Q., et al., *Mitral valve compensation for annular dilatation: In vitro study into the mechanisms of functional mitral regurgitation with an adjustable annulus model.* Journal of Heart Valve Disease, 1999. **8**(3): p. 294-302.

109. Rabbah, J.P., et al., *Effects of targeted papillary muscle relocation on mitral leaflet tenting and coaptation.* Ann Thorac Surg, 2013. **95**(2): p. 621-8.

110. Jimenez, J.H., et al., *A saddle-shaped annulus reduces systolic strain on the central region of the mitral valve anterior leaflet.* J Thorac Cardiovasc Surg, 2007. **134**(6): p. 1562-8.

111. Hanson, R., et al., *Identifying Patients at Risk for LVOT Obstruction in Mitral Valve-in-Valve Implantation.* JACC: Cardiovascular Imaging, 2016.

112. Kamioka, N., et al., *LAMPOON transseptal mitral valve in ring.* Annals of cardiothoracic surgery, 2018. **7**(6): p. 834-836.

113. Khan, J.M., et al., *Anterior Leaflet Laceration to Prevent Ventricular Outflow Tract Obstruction During Transcatheter Mitral Valve Replacement.* Journal of the American College of Cardiology, 2019. **73**(20): p. 2521.

114. Wurzinger, L.J., et al., *Platelet and Coagulation Parameters Following Millisecond Exposure to Laminar Shear Stress.* Thromb Haemost, 1985. **53**(02): p. 381-386.

115. Sakariassen, K.S., et al., *Shear-induced platelet activation and platelet microparticle formation in native human blood.* Thrombosis Research, 1998. **92**(6): p. S33-S41.

116. Fraser, K.H., et al., *A quantitative comparison of mechanical blood damage parameters in rotary ventricular assist devices: shear stress, exposure time and hemolysis index.* Journal of biomechanical engineering, 2012. **134**(8): p. 081002-081002.

117. Lu, P.C., H.C. Lai, and J.S. Liu, *A reevaluation and discussion on the threshold limit for hemolysis in a turbulent shear flow.* Journal of Biomechanics, 2001. **34**(10): p. 1361-1364.

118. Sallam, A.M. and N.H. Hwang, *Human red blood cell hemolysis in a turbulent shear flow: contribution of Reynolds shear stresses.* Biorheology, 1984. **21**(6): p. 783-797.

119. Gunning, P.S., et al., *An in vitro evaluation of the impact of eccentric deployment on transcatheter aortic valve hemodynamics.* Ann Biomed Eng, 2014. **42**(6): p. 1195-206.

120. Saikrishnan, N., et al., *In Vitro Characterization of Bicuspid Aortic Valve Hemodynamics Using Particle Image Velocimetry.* Annals of Biomedical Engineering, 2012. **40**(8): p. 1760-1775.

121. Chakravarty, T., et al., *Subclinical leaflet thrombosis in surgical and transcatheter bioprosthetic aortic valves: an observational study.* Lancet, 2017. **389**(10087): p. 2383-2392.

122. Makkar, R.R., et al., *Possible Subclinical Leaflet Thrombosis in Bioprosthetic Aortic Valves.* New England Journal of Medicine, 2015. **373**(21): p. 2015-2024.

123. De Marchena, E., et al., *Thrombus Formation Following Transcatheter Aortic Valve Replacement.* JACC: Cardiovascular Interventions, 2015. **8**(5): p. 728.

124. Hafiz, A.M., et al., *Clinical or Symptomatic Leaflet Thrombosis Following Transcatheter Aortic Valve Replacement: Insights from the U.S. FDA MAUDE Database.* Structural Heart, 2017. **1**(5-6): p. 256-264.

125. Midha, P.A., *A parametric investigation of transcatheter aortic valve replacement performance*, in *Mechanical Engineeirng*. 2017, Georgia Institute of Technology: Georgia Institute of Technology.

126. Raghav, V., et al., *Three-dimensional extent of flow stagnation in transcatheter heart valves.* Journal of The Royal Society Interface, 2019. **16**(154): p. 20190063.

127. Midha Prem, A., et al., *Abstract 19038: Neo-Sinus Washout is Faster in Supra-Annular Transcatheter Heart Valves.* Circulation, 2017. **136**(suppl_1): p. A19038-A19038.

128. Capretti, G., et al., *Valve Thrombosis After Transcatheter Mitral Valve Replacement.* Journal of the American College of Cardiology, 2016. **68**(16): p. 1814.

129. Quick, S., et al., *First Bioprosthesis Thrombosis After Transcatheter Mitral Valve-in-Valve Implantation: Diagnosis and Treatment.* Journal of the American College of Cardiology, 2014. **63**(18): p. e49.

130. Núñez, J.C., et al., *Repeat Fibrinolysis to Treat Thrombotic Dysfunction of a Mitral Valve-in-valve Prosthesis.* Revista Española de Cardiología (English Edition), 2018. **71**(02): p. 117-118.

131. Eng, M.H., et al., *Thrombotic valvular dysfunction with transcatheter mitral interventions for postsurgical failures.* Catheter Cardiovasc Interv, 2017. **90**(2): p. 321-328.

132. Roosen, J., et al., *Low-Dose and Slow-Infusion Thrombolysis for Prosthetic Valve Thrombosis After a Transcatheter Valve in the Mitral Position.* JACC Cardiovasc Interv, 2017. **10**(7): p. 738-739.

133. Thubrikar, M.J., *The Aortic Valve*. 1989: CRC Press.

134. Jatene, M.B., et al., *Aortic valve assessment. Anatomical study of 100 healthy human hearts.* Arquivos Brasileiros de Cardiologia, 1999. **73**: p. 81-86.

135. Swanson W, M. and E. Clark Richard, *Dimensions and Geometric Relationships of the Human Aortic Value as a Function of Pressure.* Circulation Research, 1974. **35**(6): p. 871-882.

136. Sim, E.K.W., et al., *Comparison of human and porcine aortic valves.* Clinical Anatomy, 2003. **16**(3): p. 193-196.

137. Sands, M.P., et al., *An Anatomical Comparison of Human, Pig, Calf, and Sheep Aortic Valves.* The Annals of Thoracic Surgery, 1969. **8**(5): p. 407-414.

138. Thubrikar, M.J., et al., *Aortic root dilatation may alter the dimensions of the valve leaflets.* European Journal of Cardio-Thoracic Surgery, 2005. **28**(6): p. 850-855.

139. Bonhoeffer, P., et al., *Transcatheter Implantation of a Bovine Valve in Pulmonary Position.* Circulation, 2000. **102**(7): p. 813-816.

140. Duncan, A.C. and D. Boughner, *Effect of dynamic glutaraldehyde fixation on the viscoelastic properties of bovine pericardial tissue.* Biomaterials, 1998. **19**(7): p. 777-783.

141. Aguiari, P., et al., *Mechanical testing of pericardium for manufacturing prosthetic heart valves.* Interactive CardioVascular and Thoracic Surgery, 2015. **22**(1): p. 72-84.

142. Vyavahare, N., et al., *Prevention of Bioprosthetic Heart Valve Calcification by Ethanol Preincubation.* Circulation, 1997. **95**(2): p. 479-488.